Performance of Retaining Walls with Reinforced Granular and Fly Ash Backfill

A Thesis Submitted in the Partial Fulfillment of the
Requirements for the Degree of

MASTER OF TECHNOLOGY

By

SUTAPA HAZRA

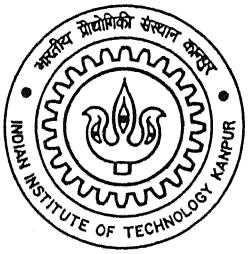

To the

DEPARTMENT OF CIVIL ENGINEERING
INDIAN INSTITUTE OF TECHNOLOGY
KANPUR
JUNE, 2005

Dedicated
To
My Parents
&
Brothers

CERTIFICATE

It is certified that the work contained in the thesis titled **"Performance of Retaining Walls with Reinforced Granular and Fly Ash Backfill"** by **Sutapa Hazra** (Y3103054), has been carried out under my supervision and that this work has not been submitted elsewhere for a degree.

Nihar Ranjan Patra 01/06/2005

Dr. N.R. Patra
Lecturer
Department of Civil Engineering
Indian Institute of Technology, Kanpur
Kanpur – 208016, India

ABSTRACT

Experimental investigations on model cantilever, counterfort and counterfort with shelves retaining walls have been carried out to study the lateral movement of the wall and the nature of the failure modes. Mild steel plates of size 1000 X 900 X 8mm used as model retaining wall are placed in a tank of size 900 X 900 X 670mm. Ennore sand, obtained from Madras India, and Fly ash, obtained from Panki Thermal Power Plant, India have been used as backfill material. These tests are carried out both with and without reinforced backfill. Two types of loading conditions such as line load and uniform surcharge are applied. The shape and size of the failure wedge is studied through the breaks visible through the bands of colour observed through the Perspex plate, fixed on one side of the tank. Plots of overturning moment against the rotation of wall top show that with the increase in rotation of wall, the overturning moment decreases. The minimum value of overturning moment is taken as the limiting value. The failure surfaces obtained in different cases are planar and parabolic in shape. An analytical method based on observed planar and parabolic failure surfaces, has been proposed to predict the lateral earth pressure and overturning moments on the wall. Validation of analysis has been done by comparing the present analytical method with the work reported by Saran et al (1992). Comparisons have been made between experimental results and the predicted values obtained from the analysis. The predicated values, in general, are about -36 to 41% and 28 to 44% higher than the observed values for sand and fly ash backfill respectively.

Key words: Lateral movement, failure mode, overturning moment, analytical method.

ACKNOWLEDGEMENT

During the journey towards the completion of this thesis work, many people have contributed directly or indirectly. I take this opportunity to thank all of them.

I take this opportunity to express my sincere gratitude to Dr. N. R. Patra for his involvement, motivation and encouragement throughout and beyond the thesis work. His patient hearing, critical comments and approach to the research problem made me do better every time. I express my sincere respect to him for his guidance throughout my period of stay at IIT Kanpur.

I would like to express my deep sense of gratitude and thanks to Prof. P.K. Basudhar and Prof. S. Chandra for the overall guidance and for enriching my understanding of geotechnical engineering and also for the kind co-operation that I received throughout my degree program.

I am also gratefully acknowledges the cooperation of staff of Geotechnical Engineering Laboratory of Civil Engineering Department, IIT Kanpur, particularly Srivastav ji, Gulab ji, Parasuram ji and Yadav ji.

I would like to thank all my friends, especially Paritosh, Arindam, Abhik, Pradipta, Bappaditya, Shyam, Meera, Trishikhi, Antara, Shahana, Mita, Kingshuk, Sudipto, Col. Saxena, and all others who made my stay a very joyous, pleasant and memorable one and made me feel to be within a family. I would also like to express special thanks to Kousik da and Shanker da for their immense help throughout and beyond my thesis work

Last but not the least, I would like to offer my cordial homage to my Baba and Ma for all the hardships and sufferings they had to bear during my distant stay from home. I like to pay my tribute to them for their blessings, encouragement and motivation throughout my academic career. I would like to deeply thank my elder brothers for their immense and unlimited moral support and encouragement which helped me keep up my stamina and will power throughout my stay at IIT Kanpur and throughout my academic career.

Sutapa Hazra
02/06/2005

Sutapa Hazra

CONTENTS

IV. EXPERIMENTAL RESULTS AND DISCUSSION

LIST OF FIGURES

LIST OF PLATES

LIST OF TABLES

LIST OF SYMBOLS

Following symbols are used throughout this thesis unless otherwise specified.

A	Constant depending upon θ
B	Constant depending upon θ
c	Shear stress
C_1, C_2, C_3	Constants depending upon θ, ϕ and δ
C_4, C_5, C_6	Constants depending upon θ, ϕ and δ
c_s	Cohesion of the soil
c_w	Adhesion between the soil and wall
c_r	Adhesion due to reinforcement
C_u	Uniformity coefficient
D_c	Non-dimensional coefficient for adhesion with reinforcement
D_p	Non-dimensional spacing coefficient
D_r	Relative density
D_1	Constant
f^*	Coefficient of soil-reinforcement friction
H	Height of wall
K_a	Coefficient of active earth pressure
K_o	Coefficient of earth pressure at rest
L	Total length of reinforcing strip
l	Length of strip in resistant zone; effective length of strip
M	Overturning moment
p	Lateral earth pressure intensity
R'	Intensity of reaction along failure surface
Q	Intensity of line load surcharge
q	Intensity of surcharge loading
S_1, S_2, S_3, S_4	Constants depending upon θ, ϕ and δ
S_x	Horizontal spacing of reinforcement

S_z	Vertical spacing of reinforcement
T	Tensile force in strip
T_1	Constant depending upon D_p
T_2	Constant depending upon D_c
T_3	Constant depending upon θ
U_1	Constant
w	Width of reinforcing strip
W	Weight of a slice or element of soil
W_c	Weight of countefort
x	Distance of line load surcharge from back face of the wall
y	Distance along the wall from top
Z_1, Z_2, Z_3	Depth from top wall
γ	Unit weight of soil
γ_c	Unit weight of mild steel
δ	Angle of wall friction
δ_s	Angle of wall friction between steel side of tank and soil
δ_p	Angle of wall friction between perspex sheet and soil
θ	Wedge angle with vertical
μ	Lateral force due to backfill
σ_y	Pressure intensity in vertical direction
ϕ	Angle of internal friction of soil

CHAPTER I

Introduction

1.1 General

A retaining wall is a structure designed to sustain the lateral pressure of earth or other material (grain, ore, liquids for example) and to retain behind it a steep-faced slope of an earth mass against rupture of slopes in cuts and fills and against sliding down. There are different kinds of retaining wall, such as, cantilever retaining wall, counterfort retaining wall, counterfort with shelves type retaining wall etc. Generally cantilever walls are designed in reinforced concrete for heights up to about 25 to 35 ft. Above these heights counterfort walls are more economical. A counterfort retaining wall is a retaining structure strengthened on the backfill side by a vertical slab of a wedge shape. These walls are suitable for heavy surcharge, resulting in a statically very stable structure. The stability of these walls can be considerably increased by providing in the cross section of such a wall one or more relief platforms or shelves, extending them to the rupture surface. These have the advantage of decreasing the total lateral earth pressure on the wall and increasing the overall stability of the structure. This results in an economical design.

The concept of soil reinforcement is not new and in its crude form it has been in practice since ancient times. Since long, engineers have been attempting to improve the mechanical properties of soil. Henry Vidal (1966), a French engineer, presented the concept of reinforced earth. The first reinforced earth retaining wall constructed in the United States used metallic strips for reinforcement and was completed in 1972 (Mitchel

and Christopher,1990).Henry Vidal investigated the frictional effects of reinforcement in soil with the aim of improving the mechanical properties of the soil in the direction in which soil is subjected to tensile strain. Reinforced earth is a composite material where in soils is reinforced by elements which can take tension. These reinforcing elements may be in different form, e.g., metal sheets, strips, nets, mats, synthetic fabrics or fiber reinforced plastics etc. Their incorporation in the soil mass is aimed at either reducing or suppressing the tensile strain which might develop under gravity and boundary forces. In general soils possess very low tensile strength which may be improved significantly by providing reinforcement in the direction of tensile strains.

Since its inception, reinforced earth has found a wide use in different areas of civil engineering, notably in retaining walls, sea walls, dams, bridge abutments and foundation slabs. The qualities of reinforced earth are its flexibility, which enable it to be used on poor foundation soils, quickness in construction, simplicity in construction and finally a low cost. A good number of reinforced earth structures have been constructed all over world after its invention. It has been found that many structures workout at only half of the cost of conventional earth structures. The other advantage in these types of construction is that they require neither specialized skill nor sophisticated construction machinery.

Most popular use of this technology has been made in retaining wall construction. Thousands of retaining walls have been constructed all over the world. The other advantage of this technology is that there is no restriction of height of wall. Many special structures, e.g., coal storage slots, rock crushers, ore transfer infrastructure etc. have been constructed by using this technique (Vidal, 1978). Also large lateral loads act on the

counterfort retaining wall due to lateral spreading and earthquake. The earth reinforcement increases the overall stability of the wall.

1.2 Brief review of available investigations

Since the invention of reinforced earth (Vidal, 1969), intensive world wide research is being made with particular emphasis on the performance of model and full scale retaining walls. In wall with reinforced backfill, the lateral pressure on wall is reduced by reinforcing the backfill with unattached horizontal strips or sheets. Broms (1977) was the first to report this concept.

Hausmann & Lee (1978) conducted small scale model tests to investigate the behaviour of rigid walls with reinforced backfill to establish effectiveness of unattached reinforcement in the fill.

Talwar (1981) observed that substantial reduction in the magnitude of active earth pressure on the wall can be affected by reinforcing its backfill. The investigator developed theoretical analysis for computing earth pressure distribution, total pressure and its point of application behind a retaining wall with a vertical back and retaining cohesionless backfill reinforced with unattached strips and no surcharge load. Saran et el (1992) extended the work of Talwar (1981) considering the uniformly distributed surcharge load on the reinforced cohesionless backfill and prepared non-dimensional design curves to calculate the resultant active earth pressure and the height of its point of application above the base of a wall retaining a reinforced cohesionless fill. Wong and Broms (1994) conducted a series of model tests to study the failure modes of a geotextile reinforced soil wall. Pinto and Cousens (1996) described a new method of retaining wall construction that combines the reinforced earth technique with a conventional brick wall.

The results showed that even short length of reinforcement could significantly increase the load capacity of a brick retaining wall. Mittal et al (2001) studied the performance of a retaining wall with cohesionless backfill (bottom ash) reinforced with geogrid. This study had shown that there is a considerable saving in cost, space and construction time and also bottom ash which is a waste material can be used as the backfill material. Garg et al (2002) studied two instrumented prototype rigid walls, retaining geogrid reinforced cohesionless earthfill in the field to establish the validity of the analytical approach reported by Saran et al. (1992).

1.3 Need for experimental investigation

On the basis of the review of the available literature, it can be concluded that the studies made so far are for mainly cantilever retaining walls. Again, very few data is available for design of counterfort retaining walls and retaining walls with shelves. The observed failure surfaces are not assumed as parabolic. Also fly ash is a waste material from thermal power stations. The disposal of fly ash poses a serious problem. So, fly ash can be used as the backfill material for retaining walls instead of using granular material. Field test results could yield the most rational approach for understanding the performance of retaining wall. However, the high cost measured both in time and money of obtaining high quality data from full-scale field tests led to determine if accurate data could be obtained by conducting model tests in controlled soil condition in the laboratory. In the absence of resources and scope of testing prototype, small-scale laboratory tests can substantiate the effects of above variables qualitatively on the performance of retaining wall. The results thus obtained could also be utilized for checking the validity of

the proposed theories and enriching the profession with data where limited information is available.

1.4 Need for analytical investigation

Analytical approaches based on the experimental observations would be helpful for predicting the active earth pressure and hence the overturning moment of the retaining walls with granular and fly ash backfill. These approaches should reflect the effects of the variables such as loading conditions, properties of backfill material and properties of reinforcing material.

1.5 Scope of the present study

The basic objectives of the present investigation can be summarized as follows:

(a) Fabrication of experimental set up for laboratory model tests.

(b) Laboratory model tests on the following retaining walls with and without reinforced sand and fly ash backfill with different loading conditions(uniform surcharge, line load, without any surcharge)

  (i) Rigid cantilever retaining wall.

  (ii) Counterfort retaining wall.

  (iii) Counterfort retaining wall with shelves.

(c) To study the failure modes and overturning moments of retaining walls under different loading conditions.

(d) To develop analytical models based on limit equilibrium method considering planar and observed parabolic failure surfaces.

(e) To compare the analytical results with observed experimental data.

Chapter II

Review of Literature

2.1. General

During the past few decades a large number of investigations on the behaviour of the retaining walls with reinforced backfill under different conditions of loading have been reported by many researchers. An attempt has been made in this chapter to review the available literature on analytical and experimental studies on the performance of the retaining walls with reinforced backfill.

Broms (1977) studied the effectiveness of fabric reinforcement, not attached to the wall, in reducing the magnitude of the lateral earth pressure on the wall. Fabric reinforcement was led horizontally in the backfill. According to his findings

(a) reinforcement anchor zone sufficient enough to transfer the force more than the allowable tension in the fabric is needed just behind the wall elements,

(b) the lateral earth pressure at any distance away from the wall face could also be computed.

The reinforcement thus provided will behave as if it was attached to the wall facing. Length of anchor zone would be equal to the width of wall elements.

Hausmann and Lee (1978) have reported the results of model tests on rigid wall having backfill reinforced with unattached Mylar strips. The experiments were carried out with a 0.61 m high rigid model wall designed to rotate about the knife edge support attached to the base of the box containing the sand backfill. A LVDT and eight simple

beams with strain gauges were incorporated in the test set up to record the rotation of the wall and the tie forces at the face of wall respectively. The model tests were carried out with unreinforced and reinforced backfill. The overturning moment for active state of failure was reduced by about 40% in this case.

Talwar (1981) developed theoretical analysis for computing earth pressure distribution, total pressure and its point of application behind a retaining wall with a vertical back and retaining cohesionless backfill reinforced with unattached strips. Reinforcement properties were taken into analysis in terms of a non-dimensional parameter D_p and L/H ratio. Here L is the length of reinforcing strip and D_p is defined by an expression given as $D_p = w*H/S_xS_z$ where w = width of strip, H = Height of wall and S_x and S_z represent horizontal and vertical spacings of reinforcing strips respectively. He developed two typical non-dimensional charts. According to his findings unattached reinforcing strips reduced the lateral earth pressure on the wall. The investigator had also concentrated on small-scale model tests on rigid wall retaining reinforced backfill with no surcharge load. From these tests overturning moments acting on the wall were measured and plotted against the rotation of wall.

Garg (1988) extended the work of Talwar (1981) considering the uniformly distributed surcharge load on the reinforced cohesionless backfill. He also developed a concept of economical placement of reinforcement in the backfill. He presented theoretical analysis for determining pressure distribution and total pressure acting on the wall. In addition to it, he developed an expression for determining point of application of total pressure above the base of the wall and presented the results in the form of non-dimensional charts for designing. Main findings of his work are as follows:

(a) Unattached reinforcing strips are quite effective in reducing the lateral earth pressure on the wall both due to backfill earth and surcharge loading.

(b) The extent of reduction in resultant pressure will depend on the amount of reinforcement, i.e., the length of reinforcing element L and non-dimensional parameter D_p.

Khan (1991) studied the case of wall with inclined back face retaining reinforced frictional soil supporting the uniformly distributed load and developed non-dimensional charts to determine total pressure and its moment acting on the wall. Bamboo strips, aluminium strips, nylon niwar, woven geotextiles and Nelton geogrids were chosen as the reinforcing materials and dry sand as backfill soil in the experimental work conducted on vertical wall. The pressure intensity curves were also drawn by him for reinforced and unreinforced cases. The conclusions drawn from his analytical study on the wall with inclined back face with reinforced backfill are:

(a) Unattached reinforcing strips considerably reduce the lateral pressure intensity on the wall.

(b) The resultant earth pressure and the resultant overturning moment are function of the length of reinforcement and non-dimensional parameter D_p and they reduce as the latter two increases. It is found that the decrease in the earth pressure becomes insignificant when $L/H>0.6$ and $D_p>1.0$.

(c) The value of $L/H = 0.6$ and $D_p = 1.0$ can be adopted for economic design of retaining wall with reinforced backfill.

Juran and Christopher (1992) described the results of a laboratory model study on the performance, behaviour and failure mechanisms of reinforced soil retaining walls using different reinforcing materials. The model walls were instrumented to obtain measurement of stresses in the reinforcements, displacements at different points along the reinforcements, displacements of the facing and to identify the failure surface in the soil. Experimental results indicate that the confinement of the reinforcement has a major effect on the structure performance.

Karpurapu and Bathurst (1992) used geosynthetic materials, a compressible layer against rigid wall structures, to induce controlled yielding of the retained soil backfill during construction and thereby ensured minimum lateral earth pressures on the structure. Two sets of numerical simulations were carried out to model the controlled yielding concept. The simulations used a finite element method together with a hyperbolic constitutive soil model. For finite element analysis they had used a software package known as GEOFEM.

Saran et al (1992) analyzed a rigid wall retaining a reinforced cohesionless fill that carries a uniform surcharge load based on the limit equilibrium approach. The reinforcement is not connected to the wall. The stability of an element of the failure edge, which is assumed to develop in the reinforced earth mass adjoining the back face of the wall, was considered in the study. Non dimensional design charts had been developed for computing the resulting lateral earth pressure on the wall and the height of its point of application above the base of the wall. They further compared the theoretical findings

with results obtained from two different sets of model tests on a rigid wall retaining dry sand fill reinforced with aluminium and bamboo strips and observed good agreement between the predicted and experimental values.

Singh and Basudhar (1993) had demonstrated the application of a generalized approach to the estimation of the lower-bound-bearing capacity of reinforced soil-retaining walls by using the finite element technique in conjunction with non-linear programming to isolate the optimal solution. The analysis was based on a rigid-plastic model for reinforced soil, treating it as a macroscopically homogeneous anisotropic material. The results obtained were found to be in good agreement with the theoretical and experimental data reported in the literature.

Palmeira and Lanz (1994) presented a study of geotextile reinforced model walls subjected to vertical surcharge. Different layouts were tested. Vertical stress distributions were measured at the base of the walls as well as internal displacements and horizontal displacements at the face of the wall. Comparisons between predictions and measurements were also made. The results showed that the reinforcement arrangement used in the wall could significantly affect its face displacements and the stresses at its base.

Wong and Broms (1994) conducted a series of model tests to study the failure modes of a geotextile reinforced soil wall. The backfill was uniform sand. Uniform surcharge was applied on the top of the model. The observed failure modes were block sliding and

slip failure. Other potential modes of failure were rupture of the reinforcements, bearing capacity and overall stability. The results did not support the pullout and the overturning modes of failure.

Pinto and Cousens (1996) described a new method of retaining wall construction that combines the reinforced earth technique with a conventional brick wall. The behaviour of geotextile reinforced brick faced retaining walls were investigated using model walls which were built, backfilled and then surcharged. The results showed that even short length of reinforcement could significantly increase the load capacity of a brick retaining wall. A visible front face crack at about mid-height developed during surcharging prior to collapse which always occurred far less quickly than on unreinforced walls.

Porbaha (1996) investigated the behaviour of geotextile reinforced retaining walls backfilled with lime treated cohesive soil using reduced-scale physical models tested to failure under self-weight in a geotechnical centrifuge. The author had identified three modes of in this study for untreated and lime treated cohesive soil walls such as overturning, rotational sliding and planar sliding. He had also analyzed the behaviour of the wall by a limit equilibrium analysis incorporating the horizontal and tangential effects of geotextile reinforcement. The results showed that the analysis was a good predictor of the wall behaviour.

Ho and Rowe (1997) examined the effect of geometric parameters such as reinforcement length, number of layers of reinforcement, distribution of reinforcement and wall height on the forces developed in the reinforcement.

Garg (1998) had done the design, construction and cost economics of a 11 m high and 19.50 m long random rubble stone masonry wall retaining reinforced earth fill. The cohesionless earth fill was reinforced by geogrids that were not attached to the wall back face. This technique of building rigid walls with reinforced earth backfill provides earth-retaining structures at lesser costs than the conventional rigid retaining walls.

Helwany et al (1999) had validated a finite element program by comparing its analytical results with the results of a well-instrumented large-scale laboratory test conducted on a geosynthetic reinforced soil (GRS) retaining wall under well-controlled test conditions. The authors had also used the validated computer program to investigate the effects of backfill type on the behaviour of GRS retaining wall. Three different geosynthetic reinforcements and sixteen different backfills were implemented in the analysis of three different wall configurations to produce 144 analysis combinations. They had shown that the type of backfill had the most profound effect on the behaviour of the GRS retaining wall and the stiffness of the geosynthetic reinforcement had a considerable effect on the behaviour of the GRS retaining wall when the backfill was of lower stiffness and shear strength. Also the authors had performed a parametric study on GRS retaining walls based on the finite element analyses to assist the design engineer in choosing the appropriate backfill and the appropriate geosynthetic reinforcement for GRS

retaining walls in order to satisfy the prescribed requirements of maximum lateral, maximum axial strain in the reinforcements and average safety factors.

Sawicki (1999) had presented a technique for performing the creep analysis of geosynthetic reinforced retaining walls and a method for estimating the initial stresses in reinforcement. This approach was based on the assumption that the creep of the structure takes place in the active zone, in which the soil was in the plastic state and the reinforcement was visco-elastic. The author had presented some experimental results relating to the creep of a model reinforced retaining wall and shown that there was a encouraging agreement between the theory and the observation.

Tsukamoto et al (1999) carried out large-scale model retaining wall tests using reinforced and unreinforced granular backfill and geogrid layers that were not attached to the wall facing. The objective of this study was to observe the lateral earth pressures on the model retaining walls under a range of surcharge pressures, which ranged from an at-rest to active-state condition. Interface shear stresses induced along the geogrid layers were also examined under different surcharge pressures. An apparent coefficient of lateral stress for the geogrid reinforcement was defined and compared with the corresponding coefficient of earth pressure. In addition, by measuring lateral stresses at several locations on the sidewalls of the model soil container, the changes in the out-of-plane stresses were examined.

Ling et al (2000) had done a finite element model of a full-scale, concrete-block, geosynthetic-reinforced soil retaining wall constructed at the Public Works research Institute in Japan. A nonlinear hyperbolic geosynthetic model was incorporated into a computer program that was capable of simulating soil-structure interaction behaviour. The soil was simulated using a hyperbolic model while the block-block and soil-block interactions were simulated using interface elements. Comparison of numerical and measured experimental results indicated that the finite element model was capable of simulating the construction behaviour of concrete-block geosynthetic-reinforced soil structures.

Pinto and Cousens (2000) carried out a study on geotextile reinforced, brick faced retaining walls built with different foundation conditions and reinforcement geometry in order to examine the effect of foundation quality. A total of five different foundations were tested in order to investigate if either a good foundation or a large and expensive wall-face footing might be necessary to ensure good performance of rigid faced walls with short reinforcement layers. The result showed that the foundation quality is indeed a very important factor in determining the behaviour of the walls.

Mittal et al (2001) studied the performance of a retaining wall of 3.5 m height and 10 m length retaining cohesionless backfill (bottom ash) reinforced with geogrid. This study had shown that there is a considerable saving in cost, space and construction time. They had also shown that the bottom ash which is a waste material can be used as the backfill material.

Garg et al (2002) studied two instrumented prototype rigid walls, retaining geogrid reinforced cohesionless earth fill in the field to establish the validity of the analytical approach developed by Garg (1988) and reported by Saran et al. (1992) for designing such walls. The backfill of the wall was subjected to uniform surcharge load intensity at its top.

2.2 Conclusions

From the above review of literature, it has been found that a good amount of work has been done on cantilever retaining wall both theoretical and experimental. However, the observed failure modes are assumed as planar. Again, no data is available on the behavior of counterfort retaining walls and retaining walls with shelves.

Also the analyses so far done are based on the planar failure surface. No analysis is done considering parabolic failure surface. In this present study the analysis of the retaining walls has been done by considering both the planar and the parabolic failure surfaces.

Fly ash is a waste material from thermal power stations. A huge amount of fly ash is wasted from different thermal power stations of India. The disposal of these materials poses a serious problem. In the present study, attempt has been made to use this waste material as a backfill material behind a retaining wall so that the sites close to thermal power stations this material could also be used. Therefore, the present experimental and analytical investigations have been taken up.

Chapter III

Experimental Setup and Testing Programme

3.1 General

The purpose of the present investigation is to study the performance of different types of retaining walls with and without reinforced backfill with different loading conditions and also to study the failure modes of retaining walls. Full scale field tests, though highly desirable, are generally expensive and difficult to perform. However, model tests can be conducted under controlled conditions with dependable values of engineering properties of backfill material. The advantage of the model study is that the pertinent parameters influencing the behaviour of retaining walls can be controlled properly as per the requirements. Also, the cost of carrying out model investigation is much less as compared to the field test. The parameters considered here for the studies are loading conditions, backfill material, reinforcing material. Properly conducted laboratory model tests considering the above parameters would provide information qualitatively on the performance of the retaining walls.

This chapter describes the detailed account of experimental set up, testing programme and test procedure.

3.2 Experimental Setup

The experimental setup consists of the following:

a) Model tank

b) Retaining walls.

c) Backfill material.

d) Reinforcing material.

e) Device for pouring backfill material.

f) Positioning of wall.

g) Loading arrangement.

h) Measurement of overturning force and lateral movement of wall.

i) Measurement of failure surface.

a) Model Tank

The model tests were conducted in a fabricated mild steel tank of size 900mmx900mmx670mm deep shown in Figure 3.1 and Plate No 3. 1. On one side wall of the tank a perspex sheet of size 800mmx350mmx2mm was placed. It was held in position by clamps both at its top and bottom. To check the entry of soil particles into the space between the tank wall and perspex sheet, quick fix was used at the outside edge of the perspex sheet all along its height. The model retaining walls were hinged at its bottom to the tank wall. It was ensured before filling of the soil that the wall rotates freely to & fro without touching the two sides of tank. The inside length of the tank behind the wall was 370 mm. The height of the backfill was kept as 0.9m. A specially fabricated handle was attached to the tank at a height of 0.3m from the bottom of the tank for attachment of overturning force measuring device. On one side of the tank a pulley is attached to initialize the motion of the counterfort retaining wall.

b) Retaining Walls

Mild steel plates of dimension 1000mm X 900mm X 8mm were used as retaining walls. These are cantilever retaining wall, counterfort retaining wall, counterfort with shelves (Shown in figure 3.2). The bottom ends of the walls were hinged with the test tank. Initially these walls were clamped at the top of the tank at their two ends and just before the period of observations, these were released from the clamp enabling the backfill to exert earth pressure on the wall. For allowing slow moving of the walls these were attached with a proving ring fixed with a handle attached with the test tank.

c) Backfill Materials

Two different soils used in the testing programme are as follows:

i) Poorly graded "Ennore Sand" grade II obtained from Chennai (India) and

ii) Well graded fly ash, collected form Panki Thermal Power Plant.

Before conducting the model tests, physical and engineering properties of each soil type were worked out.

i) Ennore sand obtained from Chennai, India was used as one of the backfill material. Selection of sand as backfill material made because its behavior is free from time effects and reproducible densities can be achieved reasonably well. The specific gravity, uniformity coefficient and co-efficient of curvature of the Ennore sand were 2.66, 1.58 and 0.96 respectively. Grain size distribution curve is shown in Figure 3.3. The sand grains are sub angular and limiting void ratios were, e_{min} = 0.577, e_{max} = 0.896 corresponding to maximum and minimum dry densities 1.69 gm/cc and 1.42 gm/cc

respectively. The placement density was 1.49gm/cc, loose packing R.D 29.04%. The angle of shearing resistance for medium dense packing was 38^0 and sand-geotextile friction angle was 29.75^0.

ii) Fly ash is a waste material from thermal Power Station. The maximum dry density and optimum moisture content of fly ash was 1.087 gm/cc and 32% respectively. It had no plasticity and had a liquid limit of 54.94%. The specific gravity of the fly ash was 2.05. Grain size distribution curve of the fly ash is shown in Figure 3.4. The placement density was 0.87gm/cc (80% of the maximum dry density). The cohesion and the angle of shearing resistance for the placement density were 2.5 kN/m^2 and 39^0 respectively. The cohesion and angle of internal friction between fly ash and geotextile was 1.5 kN/m^2 and 26^0 respectively.

d) Reinforcing Material

Non-woven geotextile was used as the reinforcing material in this study. Tensile strength and elongation of the geotextile were 63.33N and 97.8% under 160mm/min strain rate respectively. The geotextile was cut to desired sizes as per the test conditions. The length and width of the reinforcing strip used for this study were 300mm and 150mm respectively. Vertical spacings of reinforcing strips for sand backfill were 200mm and fly ash backfill were 300mm for all types of the retaining walls. Horizontal spacings of reinforcing strips were 110mm for cantilever retaining wall and 86mm for counterfort and counterfort with shelves types of retaining walls for all types of backfill materials.

e) Device for Pouring Backfill Materials

Slot hopper having 5mm slot at one edge was used for pouring the sand by rainfall technique [Patra and Pise (2001)] in the tank. Fly ash was filled with the help of a shovel [Mittal et al. (2001)]. Figure 3.5(a), 3.5(b) and Plate No 3.2 show the sand pouring device.

f) Positioning of Walls

Each of the test walls were hinged at its bottom with the test tank. The wall was held in vertical position with the help of two clamps at its two ends on the top. To set the initial reading, the proving ring was moved forward so as to just touch the wall. It is checked that wall does not touch the side walls of the tank as there should not be any friction between the two. An air gap was maintained between these two plates which was covered by a folded polyethylene sheet strip along the height of the wall so that the soil does not move out from these gaps. The polyethylene sheet was kept in position with the help of cello tape pasted on side wall of the tank and the retaining wall.

g) Loading Arrangement

The uniform surcharge loading of 1.8 kN/m^2 was applied on the backfill by the dead load through bricks (shown in Plate No.3.6) and line load of 1.6kN/m was applied on the backfill by two thin and long plates and some weights (shown in Plate No.3.7) to simulate the actual loading condition. Desired position of the line load was marked on top

surface of soil and the plates were placed there carefully. Desired line load was applied through some weights placed over the plates.

In case of counterfort retaining wall, a pulley system was used to pull the retaining wall in active state, because, counterfort retaining wall is very stable wall and it can not be moved by the soil only, to its limiting value.

h) Measurement of Overturning Force and Lateral Movement of Wall

Measurement of the overturning force had been done with the help of a horizontally held calibrated proving ring attached to the handle fixed on the wall of the tank. The proving ring used had a maximum capacity of 250kg. On each ends of the retaining wall two nos. of dial gauges were fixed on two positions along the height of the retaining wall to record the outward rotation of the wall about its base. The sensitivity of dial gauge is 0.01mm. Placement of proving ring and dial gauges is shown in Plate No 3.3.

i) Measurement of Failure Surface

Different layers of coloured soils were used to observe the failure surface through perspex glass fixed on one side of the tank. The shape and size of the failure wedge was measured through the breaks visible through the bands of coloured soil observed through the perspex plate.

3.3 Testing Programme

The detailed experimental program is shown in Table 3.1 & 3.2.

3.4 Experimental Procedure

The experimental testing procedures for all retaining walls are similar. It is described below.

3.4.1 Placement of Retaining Walls

Retaining walls were placed in the empty tank and bottom ends of the retaining walls were hinged with the tank wall. It was kept vertical with the help of the clamps fixed with the tank wall.

3.4.2 Pouring of Backfill Materials and Placement of Reinforcement

The technique of soil pouring plays an important role in the process of achieving reproducible density. After proper placement of the walls in empty tank, soil was poured in the tank on the side where perspex sheet was attached. Sand was poured continuously through the slot of the hopper keeping height of fall about 20cm for loose packing, moving horizontally by hand. This technique of sand pouring (shown in Plate No 3.4) is termed as rainfall technique and this technique was reported to achieve good reproducible densities [Patra &Pise (2001)]. Fly ash was filled with the help of a shovel [Mittal et al. (2001)], rainfall technique could not be adopted as the soil chosen was very fine particles. Before pouring the soil, it was checked that the wall was clamped at its top in the vertical position. To ensure a particular density of the fly ash in the tank, known quantity of soil

was poured in a known volume of tank. For this, the graduation marks at 15cm interval were marked on the inner side of the tank. The top surface of soil was leveled properly and the pre-determined numbers of reinforcing strips were placed as shown in Plate No. 3.5 at specified horizontal spacing. The horizontal and vertical spacings of the reinforcing strips were ensured by drawing lines with chalk on the inner surfaces of the steel walls. The reinforcing strips had been aligned perpendicular to the wall and were just touching to the inner face of it. Again the soil was filled over these reinforcing strips in the tank till the next location of strips. Different layers of coloured soil have been used to observe the failure surface through perspex glass. Thus total height of reinforced backfill was attained behind retaining wall.

3.4.3 Testing Procedure

After the filling of the backfill material, proving ring at a height of 0.3m from the bottom of the retaining wall ($1/3^{rd}$ of the height of the backfill material from the base) and four dial gauges along the height of the retaining wall were fixed with the tank wall. Then loading was applied on the backfill. After application of loading, clamps were released, so that retaining wall could move laterally. Then the handle of the proving ring was rotated so that the wall could move laterally away from the backfill to create active condition. During the movement of the wall different readings were taken from the dial gauges and corresponding reading of the proving ring was also taken. Dial gauge reading gives the lateral movement of the wall and proving ring reading gives the active overturning force. From this active force, overturning moment was calculated by multiplying the active force with the distance of application force from the base of the

retaining wall i.e. 0.3m. Also average of the lateral movement of the top of the retaining wall was taken.

3.4.5 Verification of Backfill Material Density

Density of the backfill material in the tank was checked at the end of each test by a dynamic penetrometer. Figure 3.5(c) shows the sketch of the penetrometer. It consists of 9.5mm diameter mild steel rod with a conical tip at the bottom, and is provided with an arrangement such that a 2.49kg annular weight falls freely through a height of 20cm, on a platform fixed to the rod. The number blows was recorded for full depth of penetration i.e. for 750mm. It was recorded at different locations in the tank. For sand backfill, in all the cases it gave the value of number of blows in the range of 1 to 2 for 75 cm depth of penetration indicating loose packing of the sand. For fly ash backfill, in all the cases it gave the value of number of blows in the range of 3 to 4 for 75 cm depth of penetration indicating loose packing of the fly ash. So, almost the equal number of blows in all the tests for 75cm depth of penetration indicating uniformity of density during different soil filling.

3.4.6 Repetition of Tests

Different tests are repeated thrice to check the validity of the test results and results show that the tests are congruous.

Table 3.1

Details of experiments performed on model retaining walls with sand backfill

Test No.	Type of the retaining wall	Reinforcing Material	Test Details						Surcharge	Remarks
			D_P	L/H	L (m)	S_x (m)	S_z (m)	w (m)		
1	CRW	-	3.9	0.30	0.30	0.11	0.20	0.15	0.0	UF
2	-Do-	Geotextile	3.9	0.30	0.30	0.11	0.20	0.15	0.0	RF
3	-Do-	-	3.9	0.30	0.30	0.11	0.20	0.15	1.6 kN/m	UF
4	-Do-	Geotextile	3.9	0.30	0.30	0.11	0.20	0.15	1.6 kN/m	RF
5	-Do-	-	3.9	0.30	0.30	0.11	0.20	0.15	1.8 kN/m^2	UF
6	-Do-	Geotextile	3.9	0.30	0.30	0.11	0.20	0.15	1.8 kN/m^2	RF
7	CORW	-	5.0	0.30	0.30	0.086	0.20	0.15	0.0	UF
8	-Do-	Geotextile	5.0	0.30	0.30	0.086	0.20	0.15	0.0	RF
9	-Do-	-	5.0	0.30	0.30	0.086	0.20	0.15	1.6 kN/m	UF
10	-Do-	Geotextile	5.0	0.30	0.30	0.086	0.20	0.15	1.6 kN/m	RF
11	-Do-	-	5.0	0.30	0.30	0.086	0.20	0.15	1.8 kN/m^2	UF
12	-Do-	Geotextile	5.0	0.30	0.30	0.086	0.20	0.15	1.8 kN/m^2	RF
13	CORWS	-	5.0	0.30	0.30	0.086	0.20	0.15	0.0	UF
14	-Do-	-	5.0	0.30	0.30	0.086	0.20	0.15	1.6 kN/m	UF
15	-Do-	-	5.0	0.30	0.30	0.086	0.20	0.15	1.8 kN/m^2	UF

Symbols:

CRW = Cantilever Retaining Wall

CORW = Counterfort Retaining Wall

CORWS = Counterfort Retaining Wall with Shelves

UF = Unreinforced fill

RF = Reinforced fill

Table 3.2

Details of experiments performed on model retaining walls with fly ash backfill

Test No.	Type of the retaining wall	Reinforcing Material	Test Details						Surcharge	Remarks
			D_P	L/H	L (m)	S_x (m)	S_z (m)	w (m)		
1	CRW	-	3.325	0.30	0.30	0.11	0.20	0.15	0.0	UF
2	-Do-	Geotextile	3.325	0.30	0.30	0.11	0.20	0.15	0.0	RF
3	-Do-	-	3.325	0.30	0.30	0.11	0.20	0.15	1.6 kN/m	UF
4	-Do-	Geotextile	3.325	0.30	0.30	0.11	0.20	0.15	1.6 kN/m	RF
5	-Do-	-	3.325	0.30	0.30	0.11	0.20	0.15	1.8 kN/m^2	UF
6	-Do-	Geotextile	3.325	0.30	0.30	0.11	0.20	0.15	1.8 kN/m^2	RF
7	CORW	-	4.25	0.30	0.30	0.086	0.20	0.15	0.0	UF
8	-Do-	Geotextile	4.25	0.30	0.30	0.086	0.20	0.15	0.0	RF
9	-Do-	-	4.25	0.30	0.30	0.086	0.20	0.15	1.6 kN/m	UF
10	-Do-	Geotextile	4.25	0.30	0.30	0.086	0.20	0.15	1.6 kN/m	RF
11	-Do-	-	4.25	0.30	0.30	0.086	0.20	0.15	1.8 kN/m^2	UF
12	-Do-	Geotextile	4.25	0.30	0.30	0.086	0.20	0.15	1.8 kN/m^2	RF
13	CORWS	-	4.25	0.30	0.30	0.086	0.20	0.15	0.0	UF
14	-Do-	-	4.25	0.30	0.30	0.086	0.20	0.15	1.6 kN/m	UF
15	-Do-	-	4.25	0.30	0.30	0.086	0.20	0.15	1.8 kN/m^2	UF

Total no. of experiments = 15+15 = 30.

Symbols:

CRW = Cantilever Retaining Wall

CORW = Counterfort Retaining Wall

CORWS = Counterfort Retaining Wall with Shelves

UF = Unreinforced fill, RF = Reinforced fill.

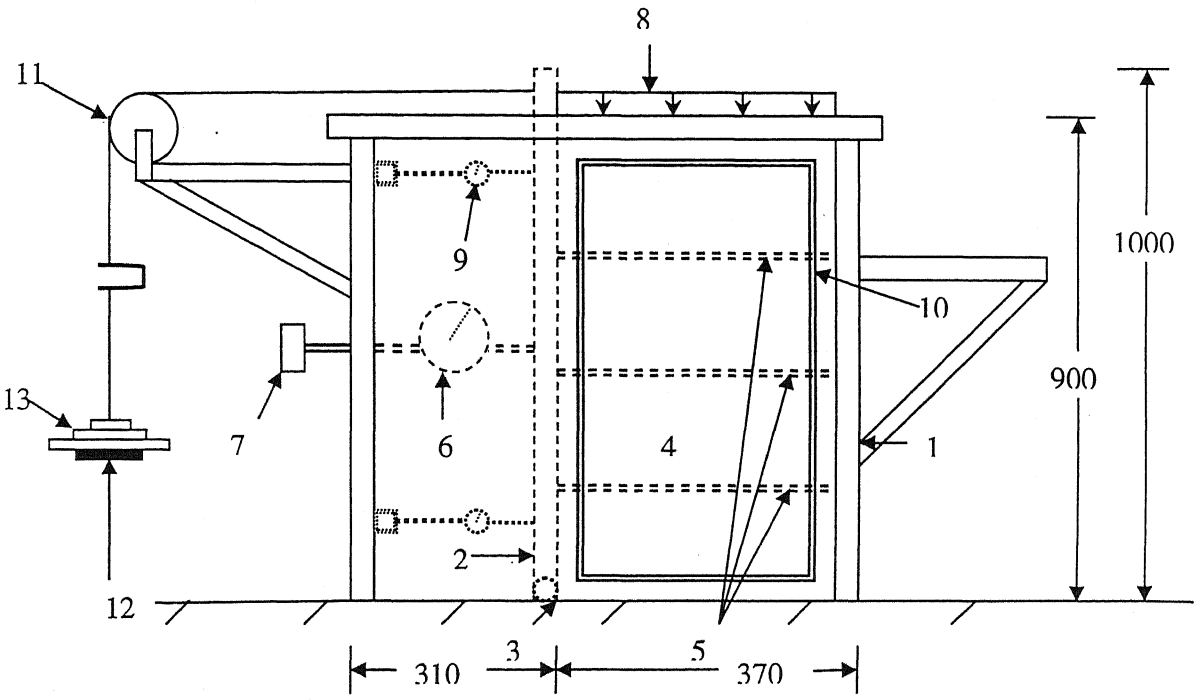

Figure 3.1: Experimental setup

1. Model Tank.
2. Cantilever Retaining Wall.
3. Hinge Support.
4. Backfill (Sand or Fly Ash)
5. Reinforcing Strips (Geotextile
6. Proving Ring.
7. Handle For Proving Ring.
8. Uniform Surcharge Application.
9. Dial Gauge.
10. Perspex Sheet.
11. Pulley for Active state.
12. Pan For Load Application.
13. Load.

All dimensions are in mm.

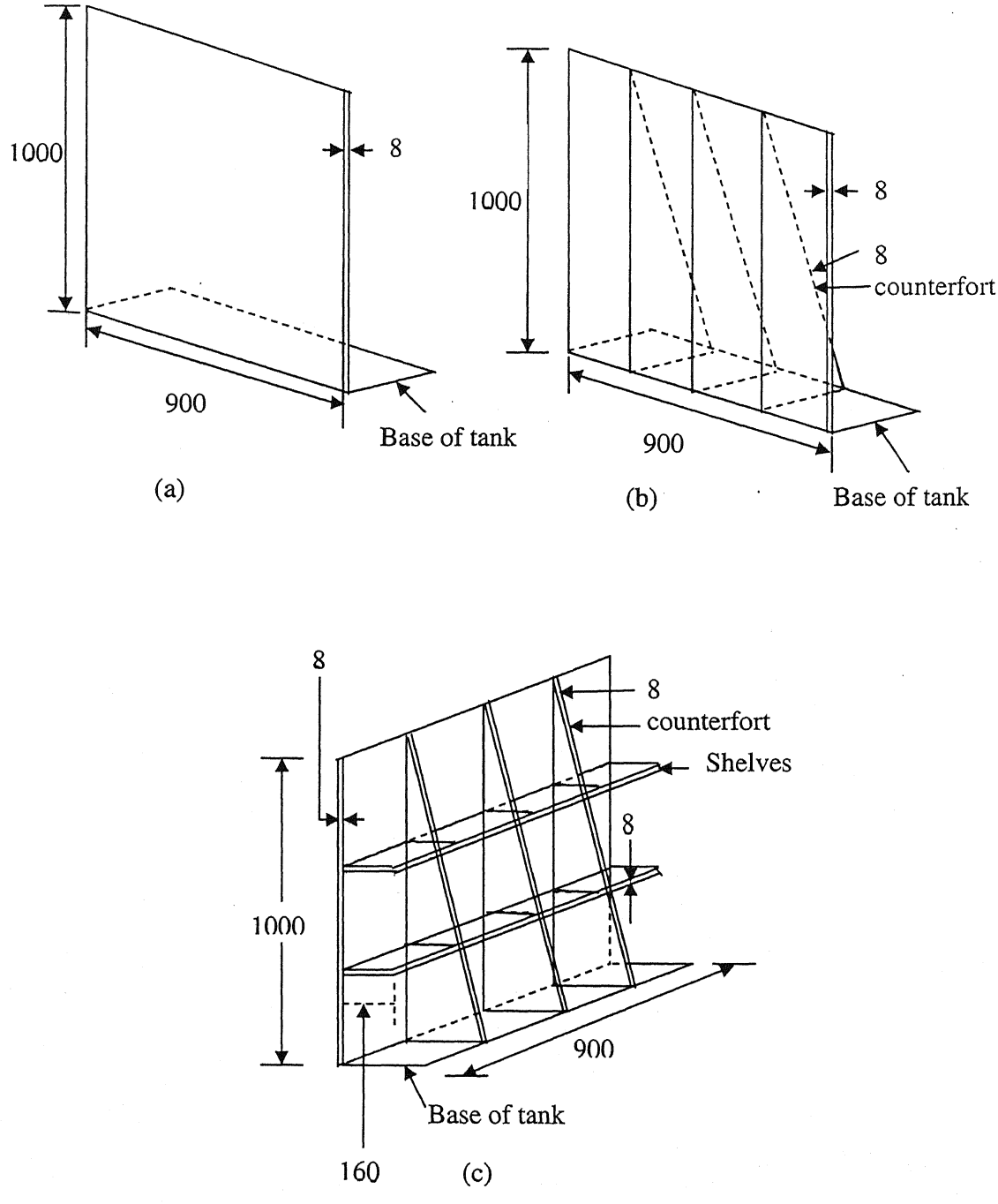

All dimensions are in mm.

Figure 3.2: Sketches of different types of retaining walls (a) Cantilever retaining wall, (b) Counterfort retaining wall and (c) Counterfort retaining wall with shelves

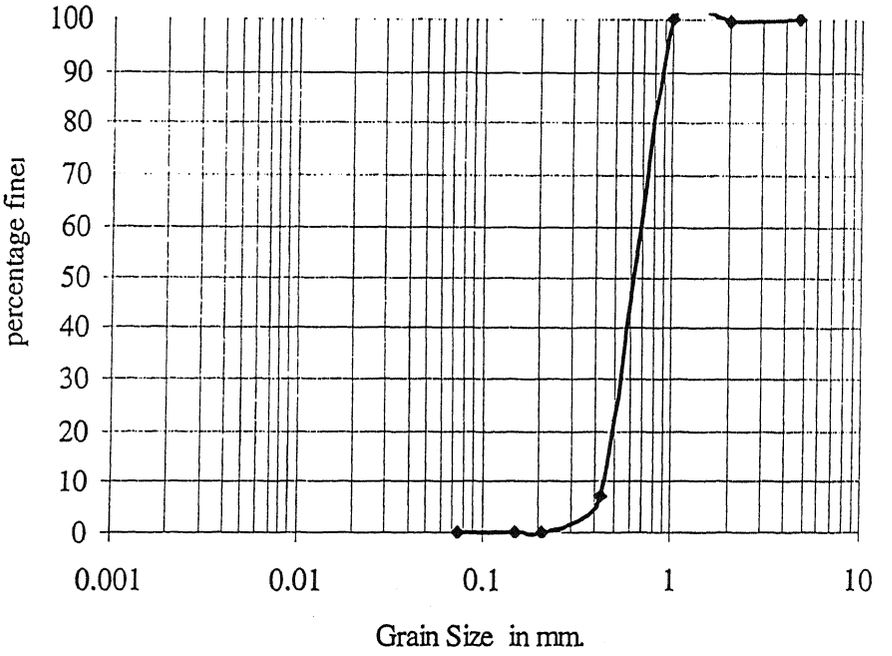

D_{60} = 0.68mm.
D_{30} = 0.53mm.
D_{10} = 0.43mm.
C_u = 1.58
C_c = 0.96

Figure 3.3: Grain size distribution curve for standard grade-II Ennore sand

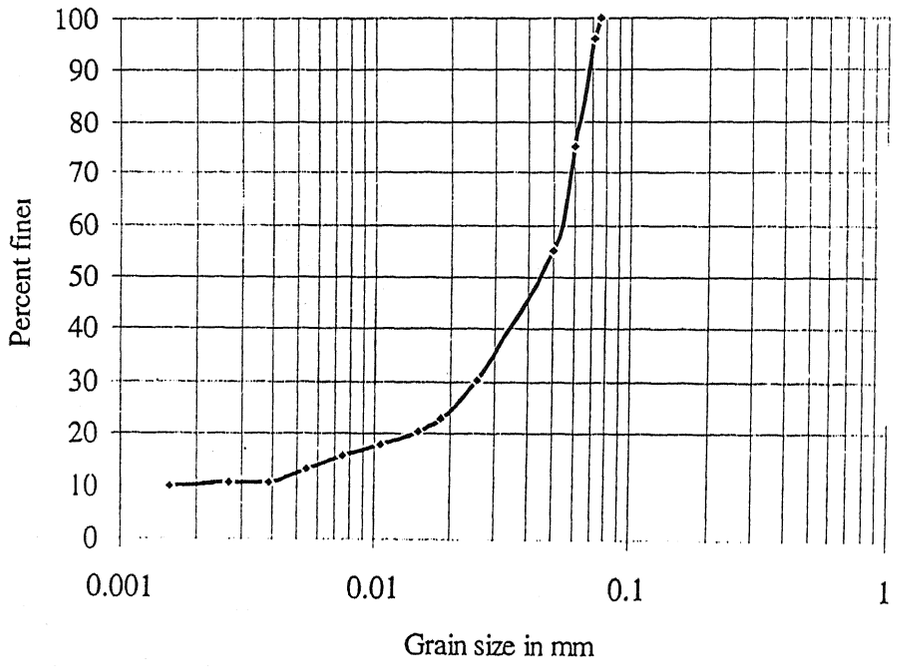

Figure 3.4: Grain size distribution curve for fly ash

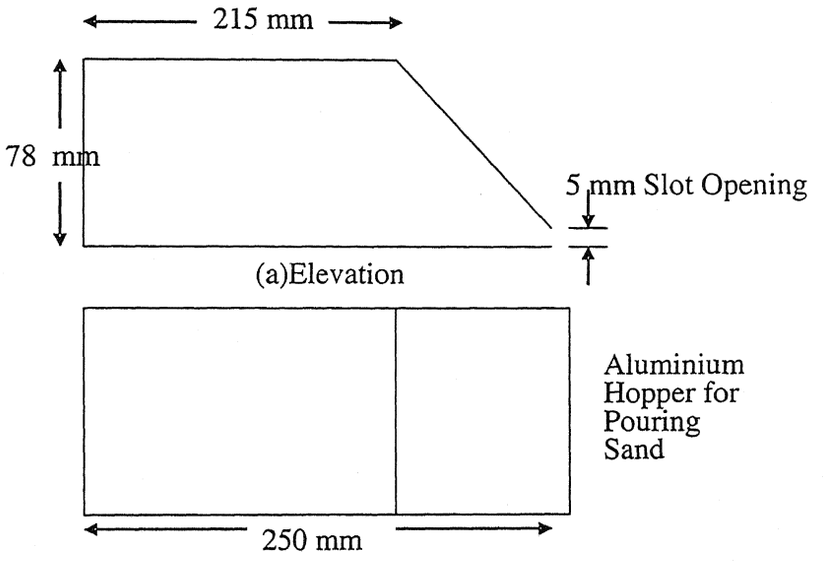

(b) Plan

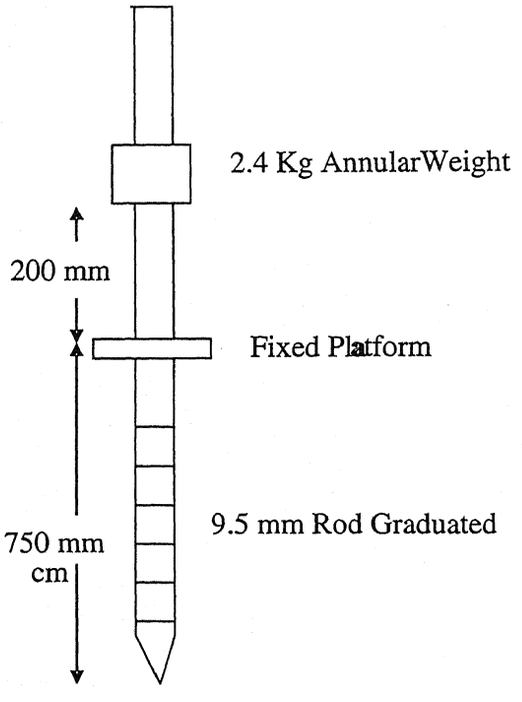

(c)

Figure 3.5 (a) The elevation (b) Plan view of hopper and (c) Penetrometer

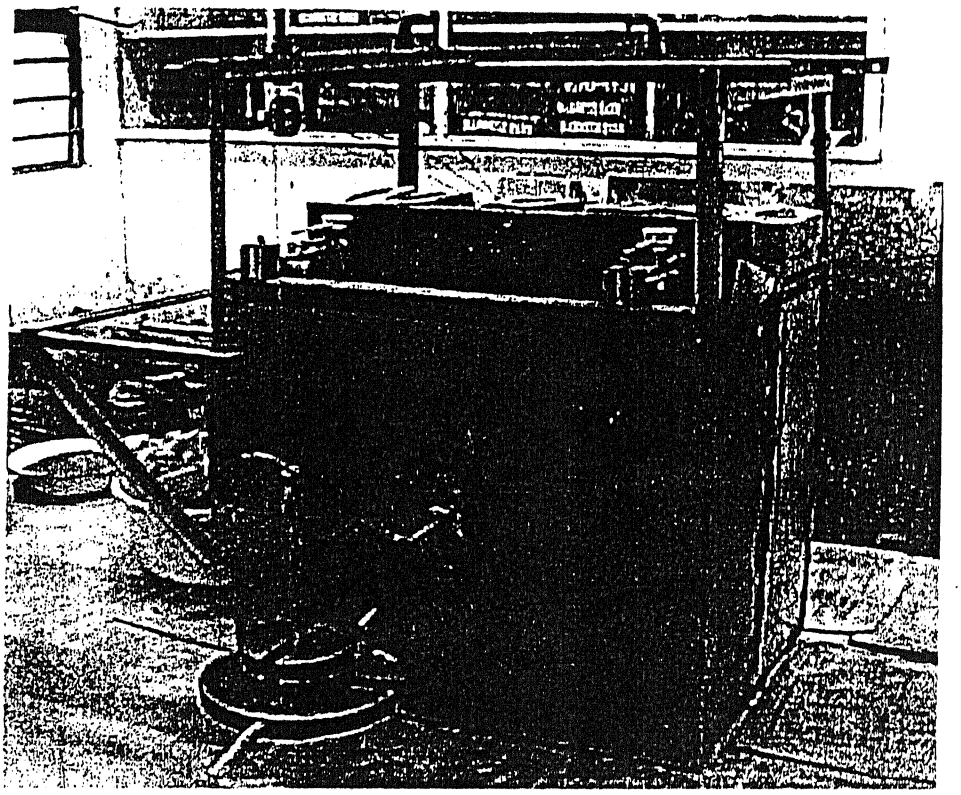

Plate No. 3.1 Complete experimental setup

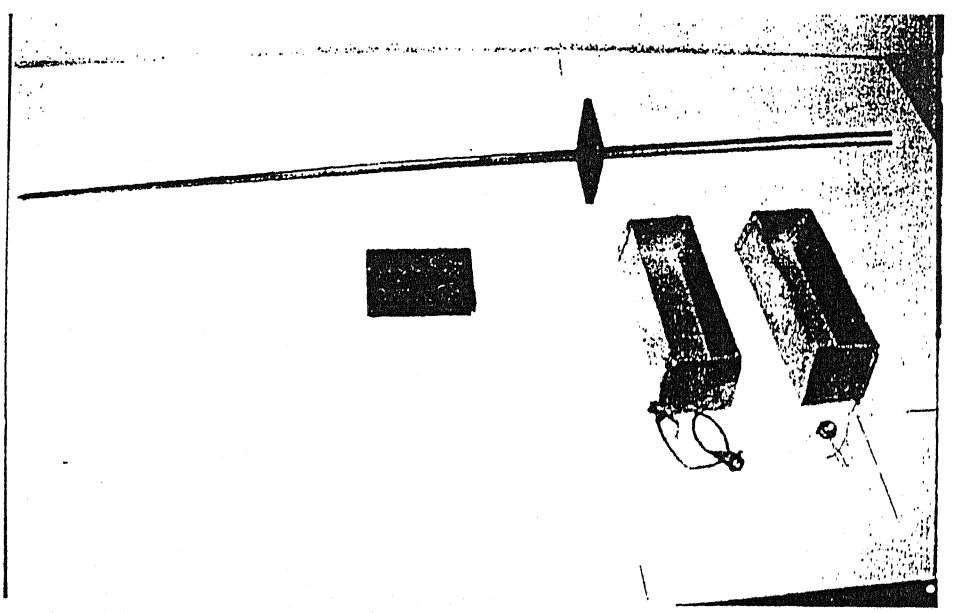

Plate No. 3.2 Hoppers and Dynamic penetrometer

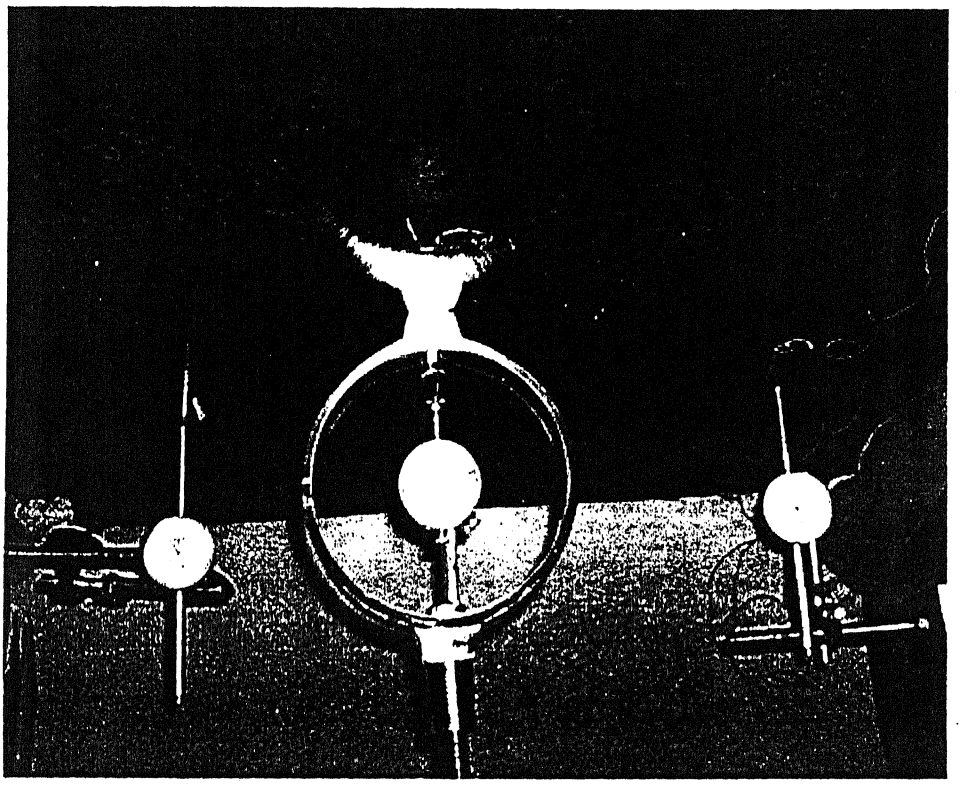

Plate No. 3.3 Placement of proving ring and dial gauges

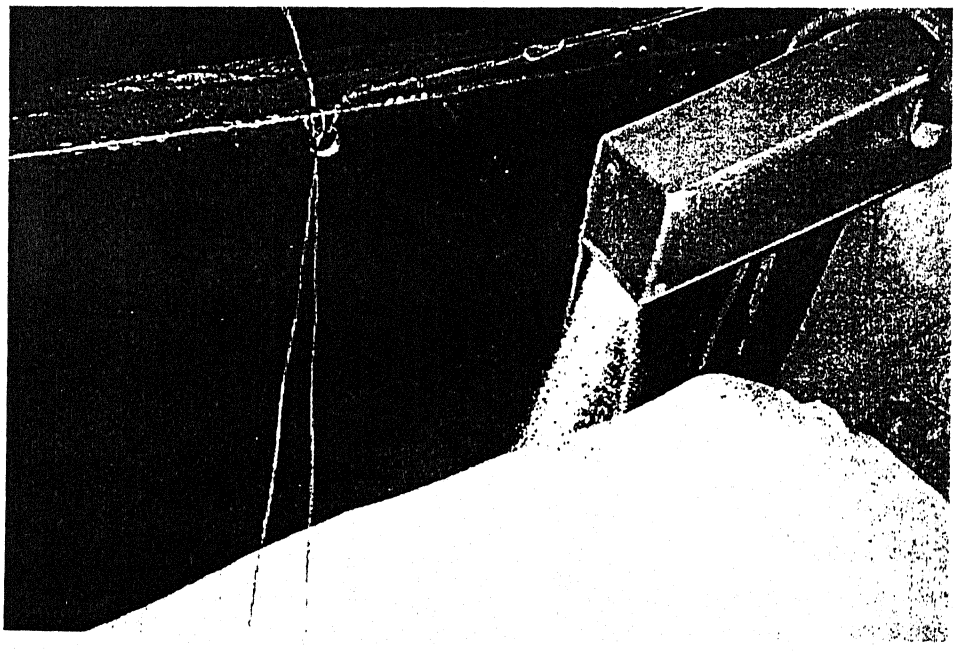

Plate No. 3.4 Sand pouring technique through hopper

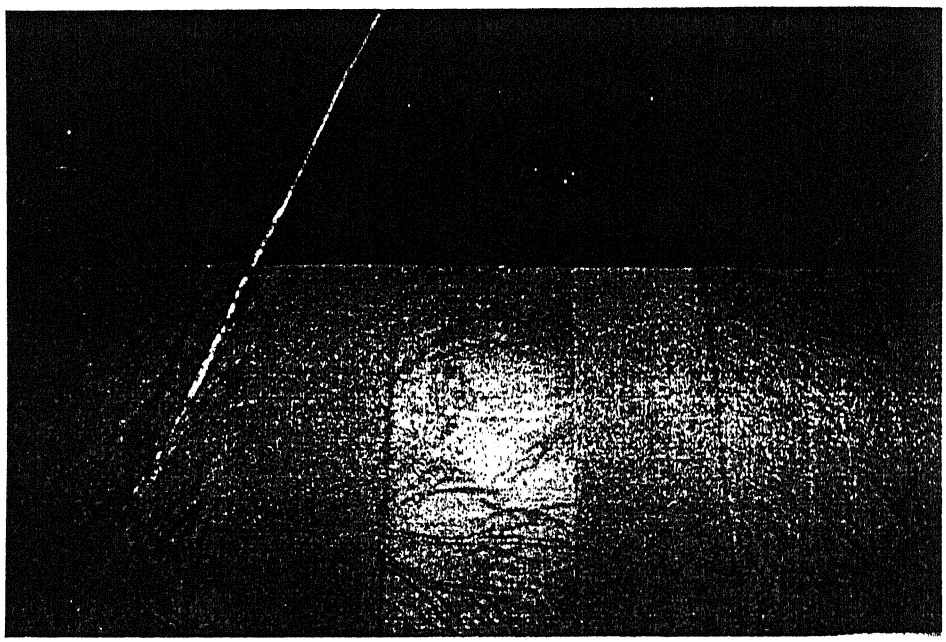

Plate No. 3.5 Laying of reinforcing strips

Plate No. 3.6 Model wall with uniform surcharge

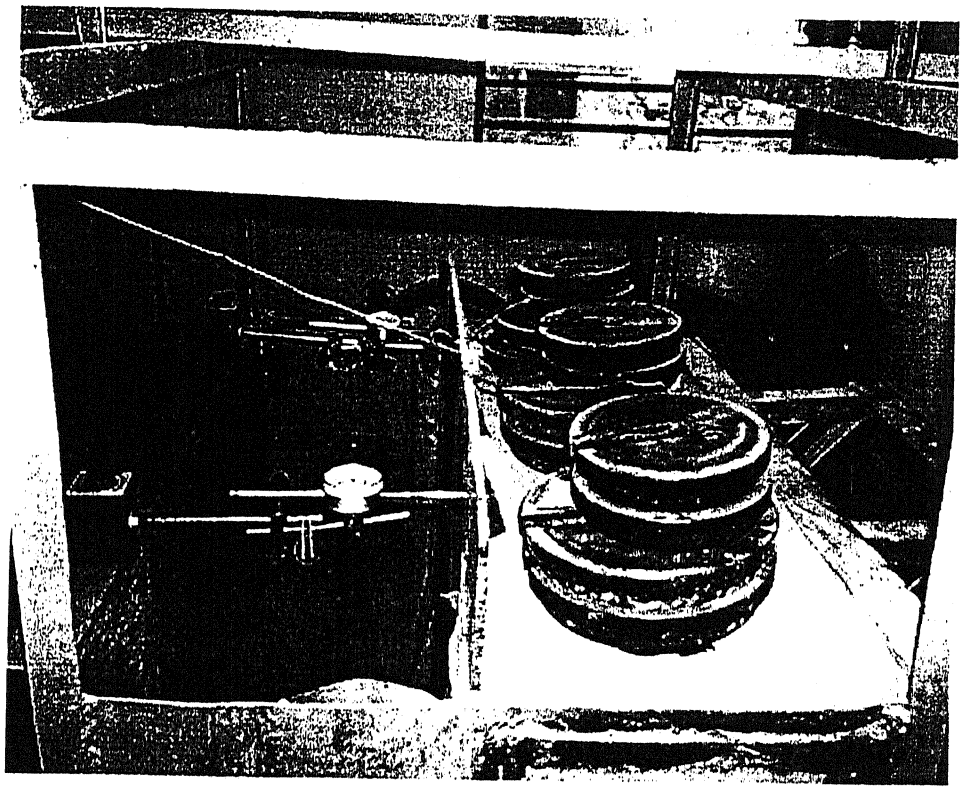

Plate No. 3.7 Model wall with line load surcharge

CHAPTER IV

Experimental Results and Discussion

4. 1 General

Model tests on three types of rigid retaining walls such as cantilever retaining wall, counterfort retaining wall and counterfort retaining wall with shelves were carried out in the laboratory. Ennore sand and fly ash were taken as the backfill material and non-woven geotextile was taken as the reinforcing material. Two types of loading were applied such as line load and uniform surcharge. Also tests had been carried out without applying any loading.

4. 2 Results and Discussion

Overturning moments (M), acting on the model retaining walls without and with reinforced backfill were plotted against the rotation of wall top expressed as percentage of height (H) of wall for active earth pressure condition. Also failure surfaces as measured on the side of the Perspex plate along the broken bands of coloured soil for model retaining walls without and with reinforcement were plotted.

4. 2. 1 Cantilever retaining wall

Experimental investigations on model cantilever retaining wall with sand and fly ash backfill were carried out. The results for different backfill material are discussed in the following sub headings:

a) Sand backfill

b) fly ash backfill

4.2.1.1 Sand backfill

Model tests were carried out by applying line load and uniform surcharge on the reinforced and unreinforced backfill. Also tests had been carried out without applying any loading. The results for different loading conditions are given in the following sub headings:

i) Without any loading

ii) With line load

iii) With uniform surcharge

4.2.1.1.1 Without any loading

Plot of overturning moment against wall rotation and plot of failure surface for retaining wall without and with reinforced backfill are shown in figures 4.1 (a) and (b). It is observed from the figure (a) that the minimum value of moment corresponding to active condition in unreinforced case has been reached at rotations 1.88 per cent of H (where H is the height of the wall) and in reinforced case it has been reached at rotations 2.60 per cent of H. The overturning moment is 41.67% less in case of the reinforced backfill than the unreinforced backfill. The failure surfaces are parabolic in nature [shown in figure 4.1(b)].

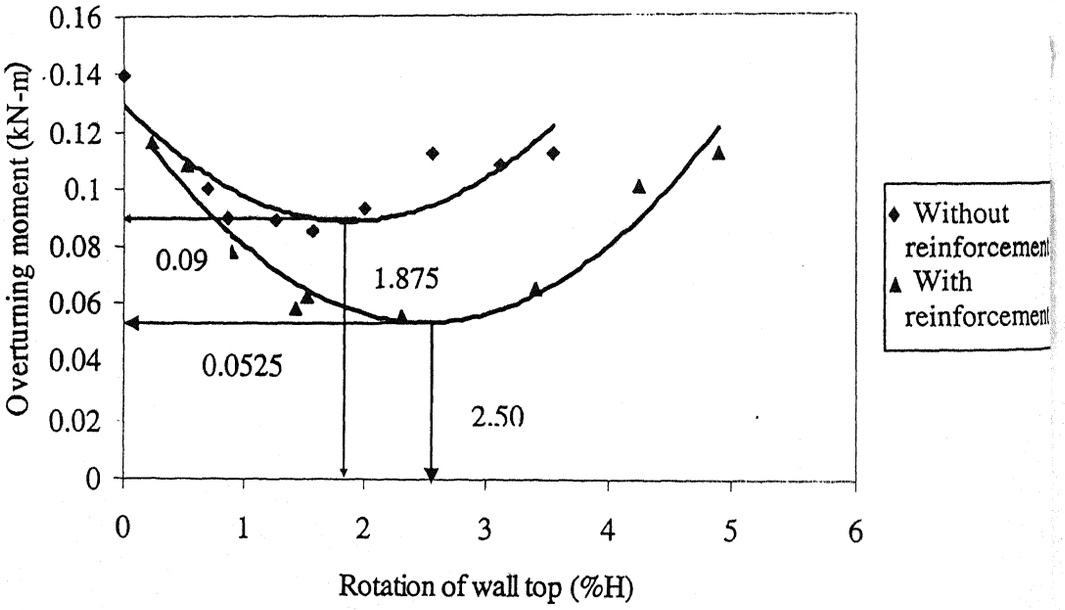

Figure 4.1(a): Observed overturning moment vs. rotation of wall top for cantilever retaining wall (without surcharge, sand backfill)

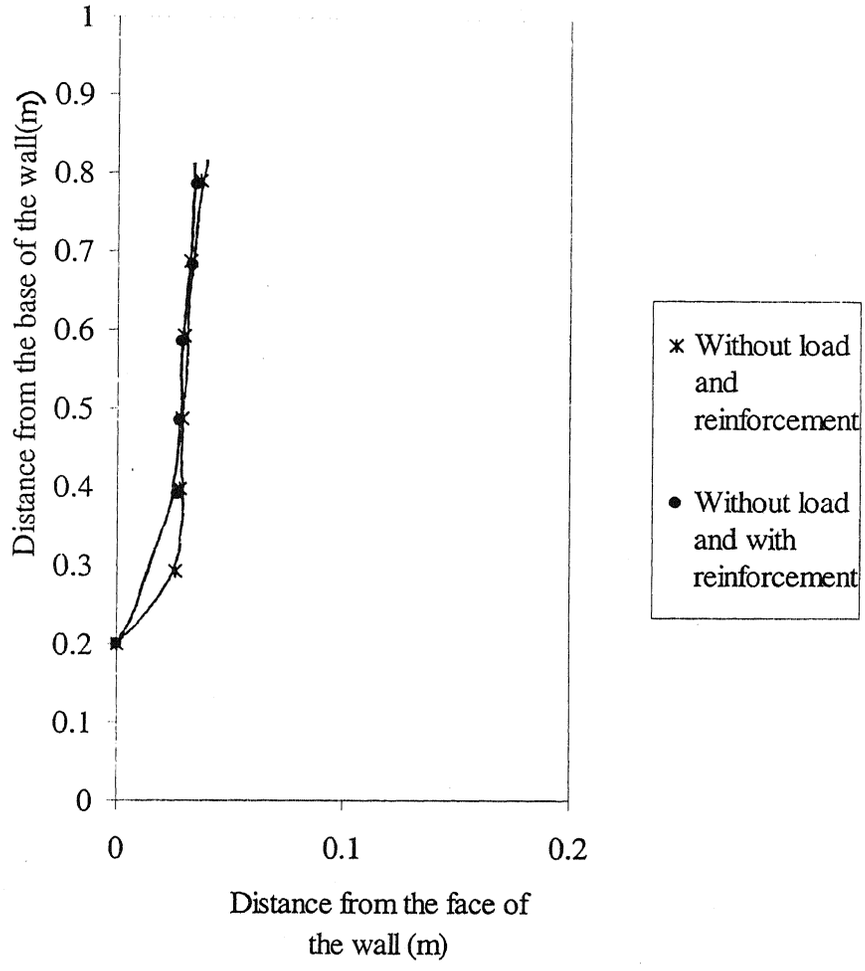

Figure 4.1(b): Observed failure surface for cantilever retaining wall (without surcharge, sand backfill)

4.2.1.1.2 With line load

Plot of overturning moment against wall rotation and plot of failure surface for retaining wall without and with reinforced backfill are shown in figures 4.2 (a) and (b). It is observed from the figure (a) that the minimum value of moment corresponding to active condition in unreinforced case has been reached at rotations 2.8 per cent of H (where H is the height of the wall) and in reinforced case it has been reached at rotations 1.88 per cent of H. The overturning moment is 37.5% less in case of the reinforced backfill than the unreinforced backfill. The failure surfaces are parabolic in nature [shown in figure 4.2(b)].

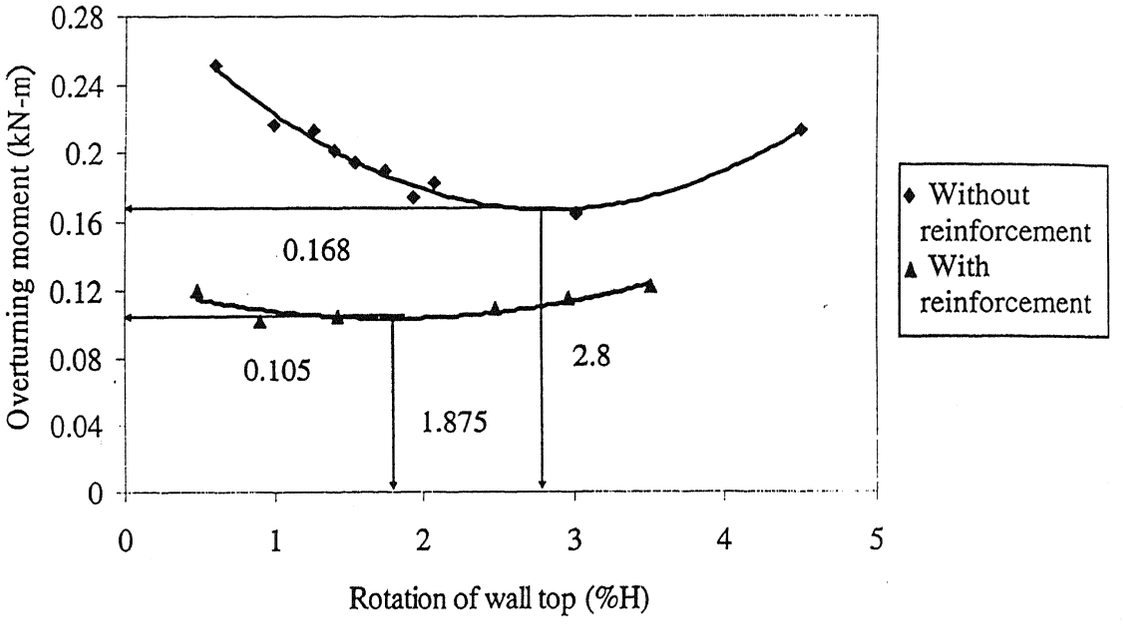

Figure 4.2(a): Observed overturning moment vs. rotation of wall top for cantilever retaining wall (line load, sand backfill)

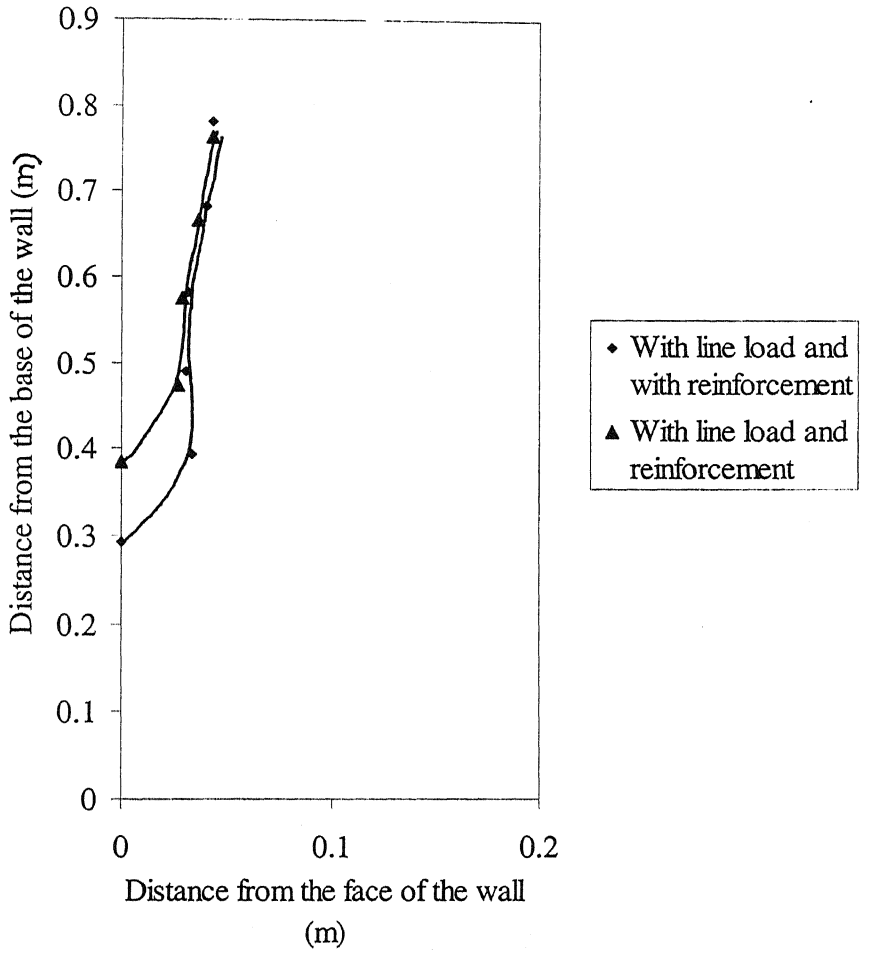

Figure 4.2(b): Observed failure surface for cantilever retaining wall (line load, sand backfill)

4.2.1.1.3 With Uniform Surcharge

Plot of overturning moment against wall rotation and plot of failure surface for retaining wall without and with reinforced backfill are shown in figures 4.3 (a) and (b). It is observed from the figure (a) that the minimum value of moment corresponding to active condition in unreinforced case has been reached at rotations 2.8 per cent of H (where H is the height of the wall) and in reinforced case it has been reached at rotations 1.8 per cent of H. The overturning moment is 25% less in case of the reinforced backfill than the unreinforced backfill. The failure surfaces are parabolic in nature [shown in figure 4.3(b)].

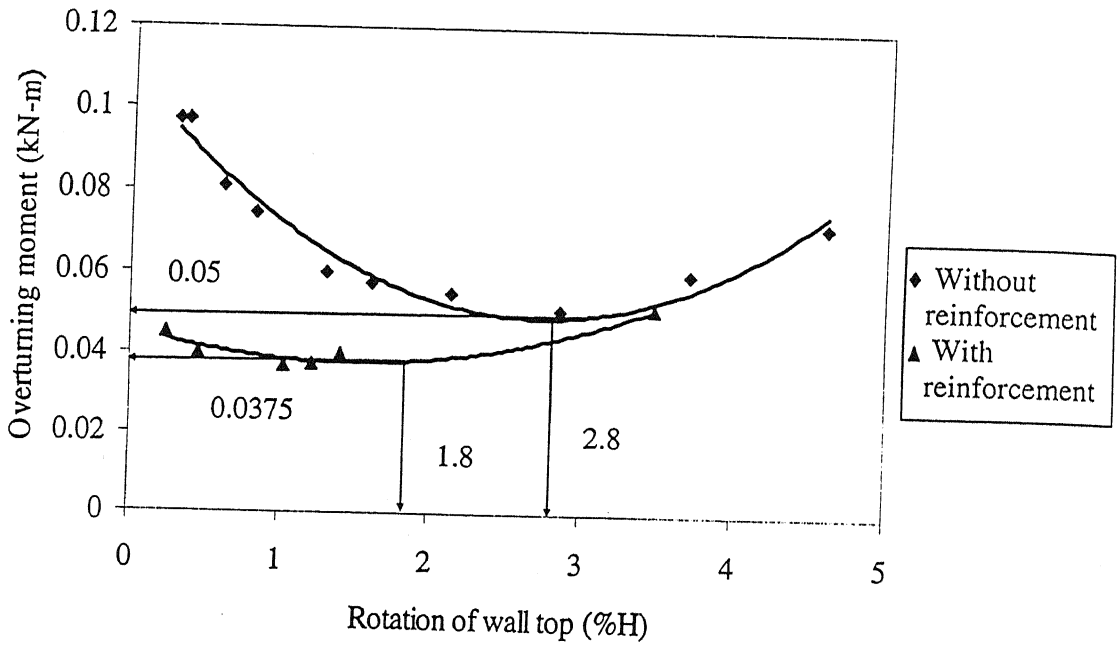

Figure 4.3(a): Observed overturning moment vs. rotation of wall top for cantilever retaining wall (uniform surcharge, sand backfill)

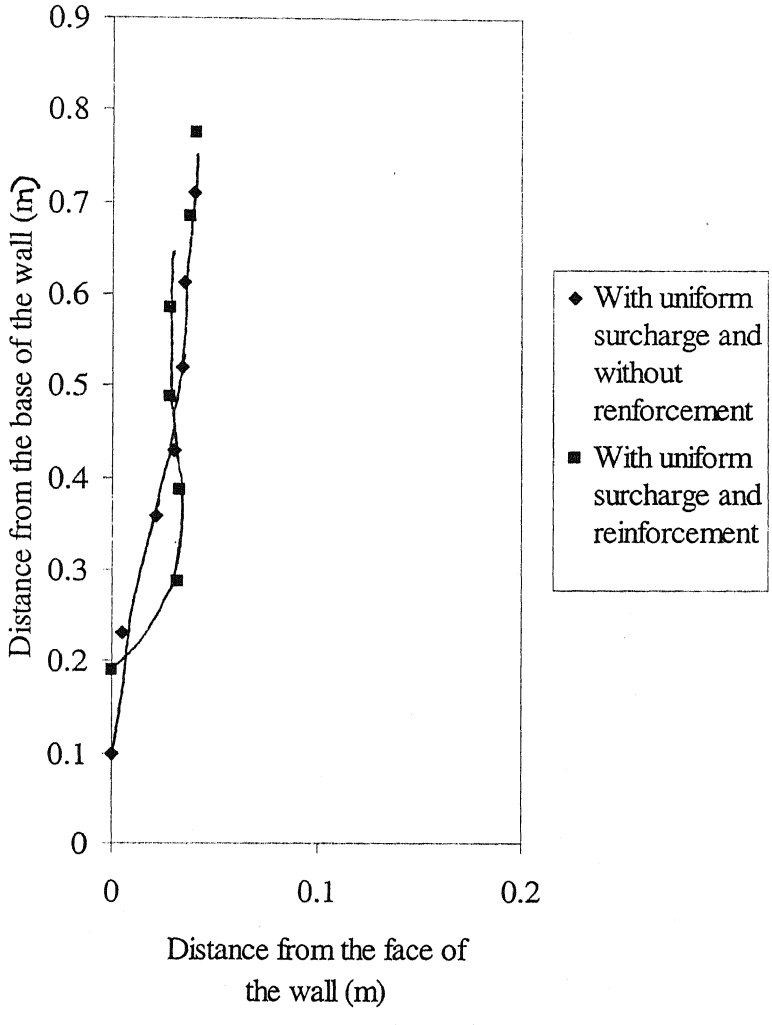

Figure 4.3(b): Observed failure surface for cantilever retaining wall (uniform surcharge, sand backfill)

It is observed from the figures that with increasing rotation, there is a gradual decrease in the overturning moment and after achieving the limiting value the moment is increased with the increase of rotation. The minimum values of moments in these tests corresponding to active condition have been reached at rotations 1.5 to 2.8 per cent of H (where H is the height of the wall). The overturning moments are about 25% to 41.67% less in case of the reinforced backfill than the unreinforced backfill. So, in case of the reinforced backfill the retaining wall is more stable than in case of the unreinforced one.

The failure surfaces are parabolic in nature. Summary of test results is shown in Table 4.1.

4.2.1.2 Fly ash backfill

Model tests were carried out by applying line load and uniform surcharge on the reinforced and unreinforced backfill. Also tests had been carried out without applying any loading. The results for different loading conditions are given in the following sub headings:

i) Without any loading

ii) With line load

iii) With uniform surcharge

4.2.1.2.1 Without any loading

Plot of overturning moment against wall rotation and plot of failure surface for retaining wall without and with reinforced backfill are shown in figures 4.4 (a) and (b). It is observed from the figure (a) that the minimum value of moment corresponding to active condition in unreinforced case has been reached at rotations 2.9 per cent of H (where H is the height of the wall) and in reinforced case it has been reached at rotations 2.6 per cent of H. The overturning moment is 79.35% less in case of the reinforced backfill than the unreinforced backfill. The failure surfaces are parabolic in nature [shown in figure 4.4(b)].

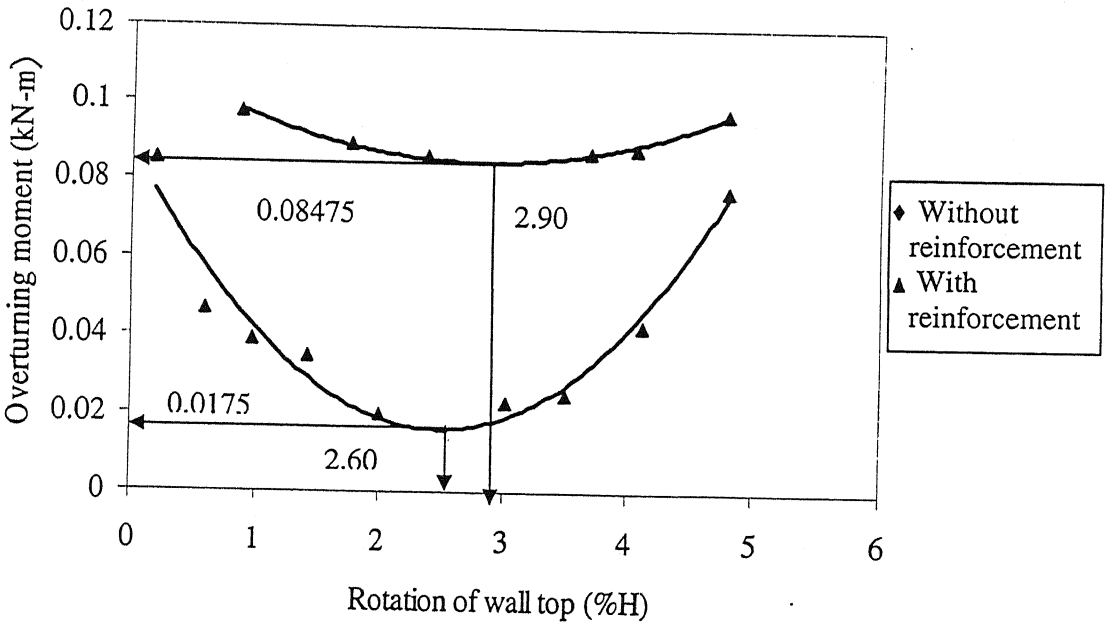

Figure 4.4(a): Observed overturning moment vs. rotation of wall top for cantilever retaining wall (without surcharge, fly ash backfill)

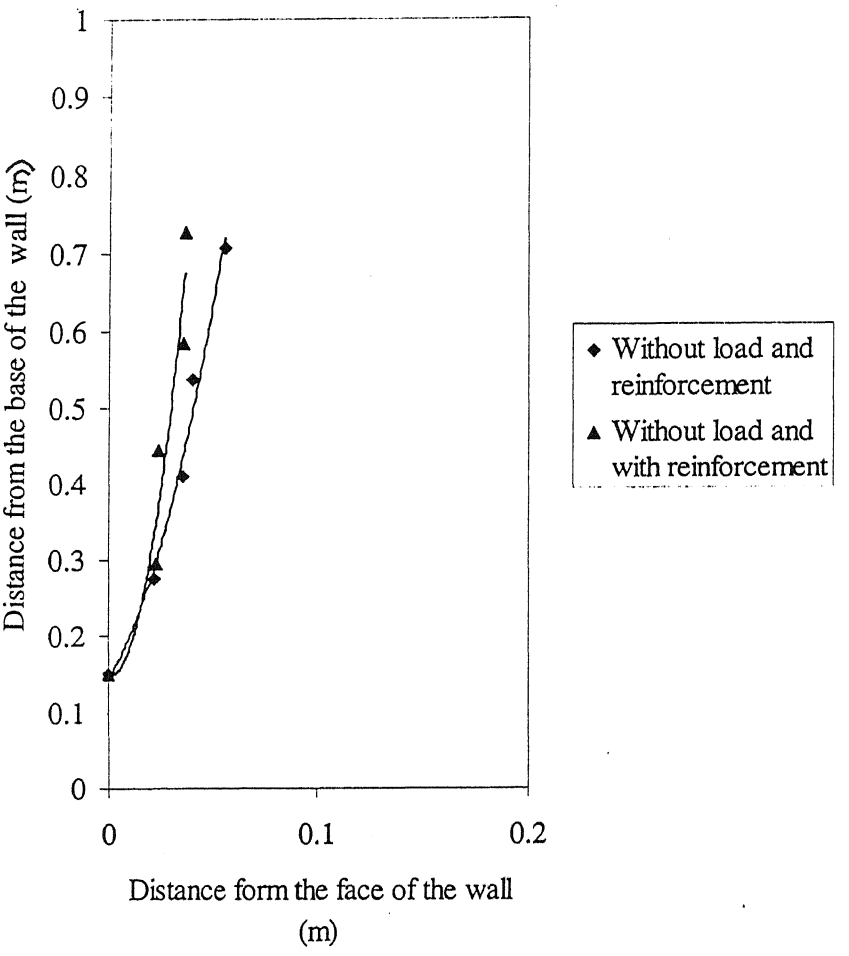

Figure 4.4(b): Observed failure surface for cantilever retaining wall (without surcharge, fly ash backfill)

4.2.1.2.2 With line load

Plot of overturning moment against wall rotation and plot of failure surface for retaining wall without and with reinforced backfill are shown in figures 4.5 (a) and (b). It is observed from the figure (a) that the minimum value of moment corresponding to active condition in unreinforced case has been reached at rotations 2.65 per cent of H (where H is the height of the wall) and in reinforced case it has been reached at rotations 2.5 per cent of H. The overturning moment is 73.68% less in case of the reinforced backfill than the unreinforced backfill. The failure surfaces are parabolic in nature [shown in figure 4.5(b)].

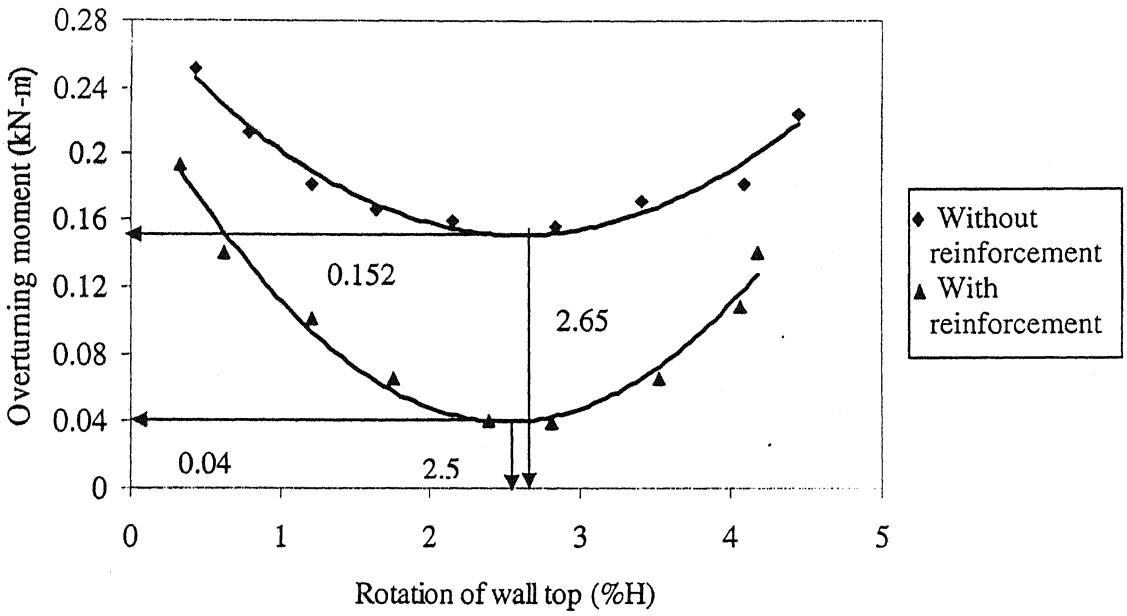

Figure 4.5(a): Observed overturning moment vs. rotation of wall top for cantilever retaining wall (line load, fly ash backfill)

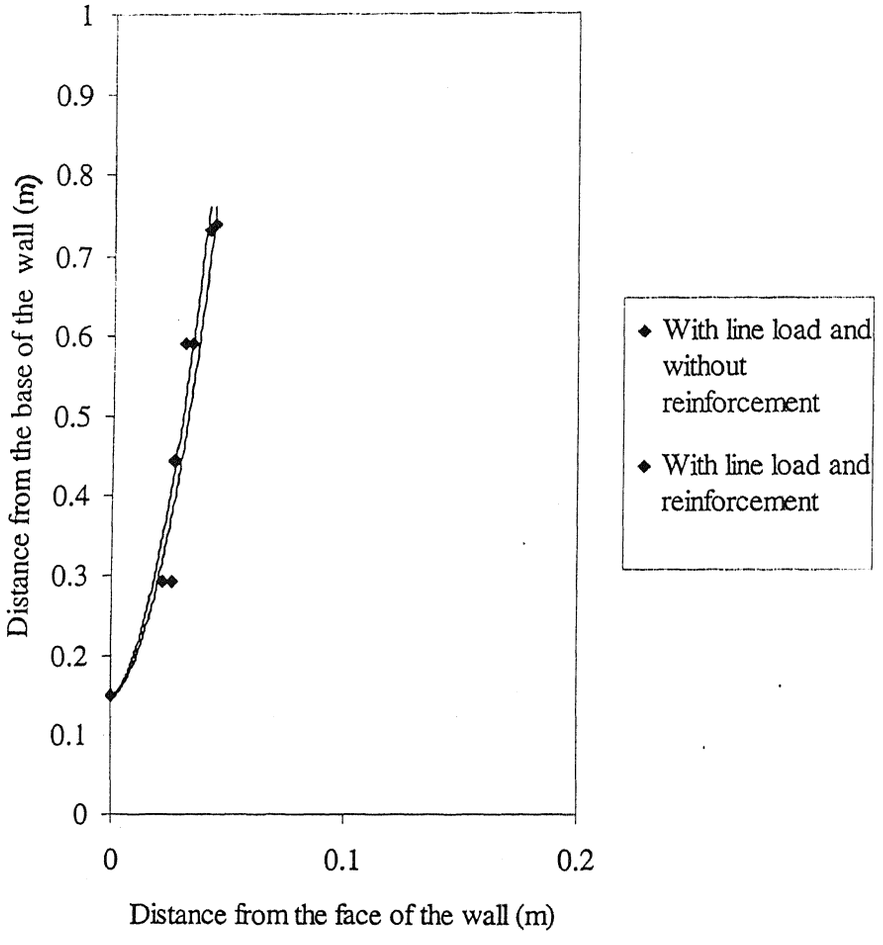

Figure 4.5(b): Observed failure surface for cantilever retaining wall (line load, fly ash backfill)

4.2.1.2.3 With Uniform Surcharge

Plot of overturning moment against wall rotation and plot of failure surface for retaining wall without and with reinforced backfill are shown in figures 4.6 (a) and (b). It is observed from the figure (a) that the minimum value of moment corresponding to active condition in unreinforced case has been reached at rotations 2.4 per cent of H (where H is the height of the wall) and in reinforced case it has been reached at rotations 2.55 per cent of H. The overturning moment is 22.73% less in case of the reinforced backfill than the unreinforced backfill. The failure surfaces are parabolic in nature [shown in figure 4.6(b)].

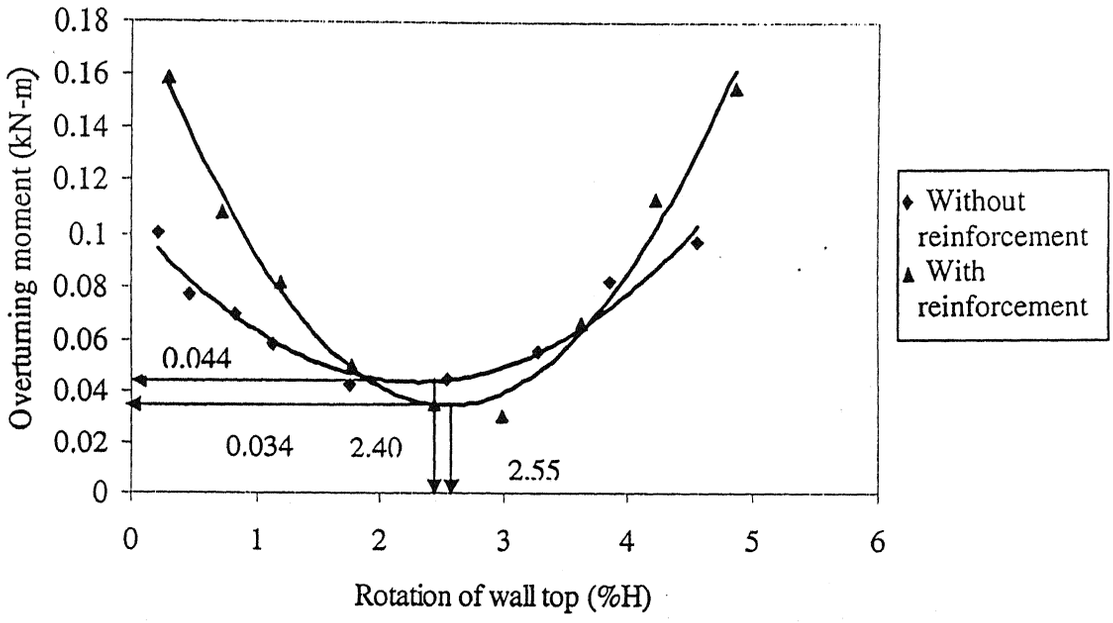

Figure 4.6(a): Observed overturning moment vs. rotation of wall top for cantilever retaining wall (uniform surcharge, fly ash backfill)

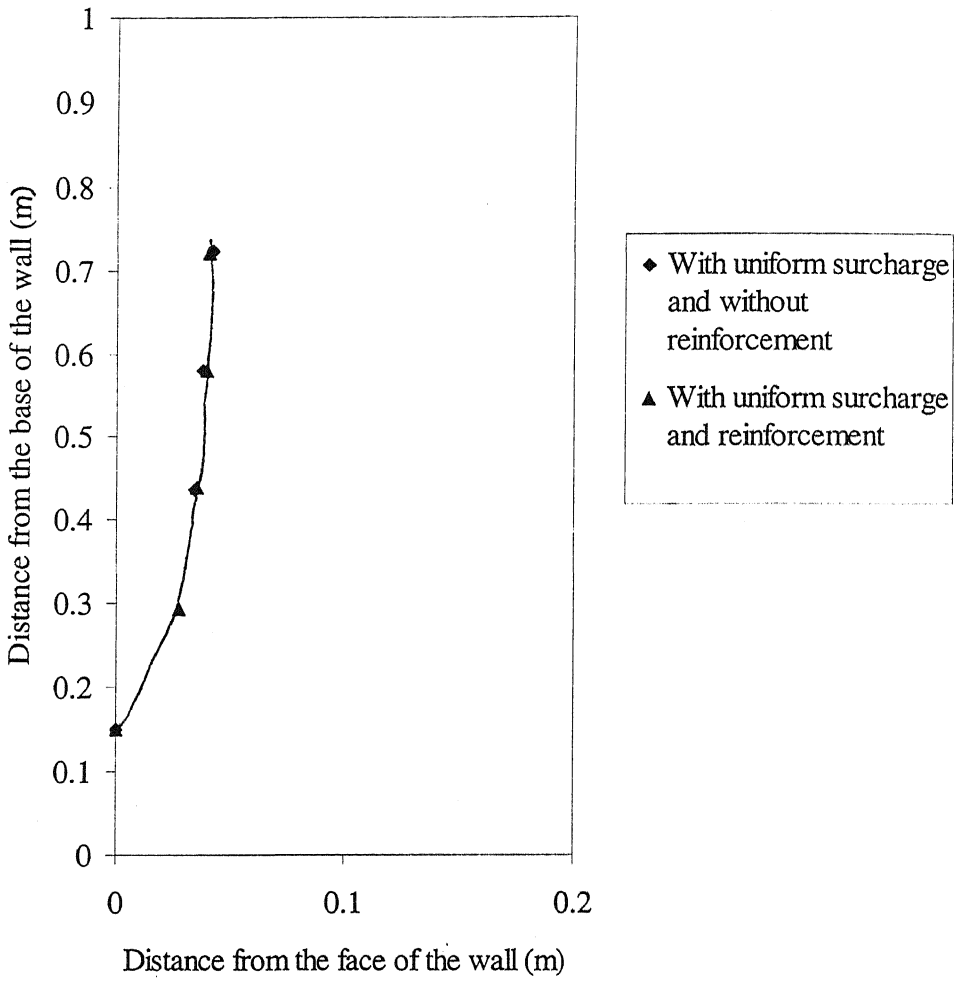

Figure 4.6(b): Observed failure surface for cantilever retaining wall (uniform surcharge, fly ash backfill)

It is observed from the figures that with increasing rotation, there is a gradual decrease in the overturning moment and after achieving the limiting value the moment is increased with the increase of rotation. The minimum values of moments in these tests corresponding to active condition have been reached at rotations 2.4 to 2.9 per cent of H (where H is the height of the wall). The overturning moments are about 22.73% to 79.35% less in case of the reinforced backfill than the unreinforced backfill. So, in case of the reinforced backfill the retaining wall is more stable than in case of the unreinforced one. The failure surfaces are parabolic in nature. Summary of test results is shown in Table 4.2.

4. 2. 2 Counterfort retaining wall

Experimental investigations on model counterfort retaining wall with sand and fly ash backfill were carried out. The results for different backfill material are discussed in the following sub headings:

a) Sand backfill

b) fly ash backfill

4.2.2.1 Sand backfill

Model tests were carried out by applying line load and uniform surcharge on the reinforced and unreinforced backfill. Also tests had been carried out without applying any loading. The results for different loading conditions are given in the following sub headings:

i) Without any loading

ii) With line load

iii) With uniform surcharge

4.2.2.1.1 Without any loading

Plot of overturning moment against wall rotation and plot of failure surface for retaining wall without and with reinforced backfill are shown in figures 4.7 (a) and (b). It is observed from the figure (a) that the minimum value of moment corresponding to active condition in unreinforced case has been reached at rotations 2.7 per cent of H (where H is the height of the wall) and in reinforced case it has been reached at rotations 1.6 per cent of H. The overturning moment is 40.87% less in case of the reinforced backfill than the unreinforced backfill. The failure surfaces are linear in nature [shown in figure 4.7(b)].

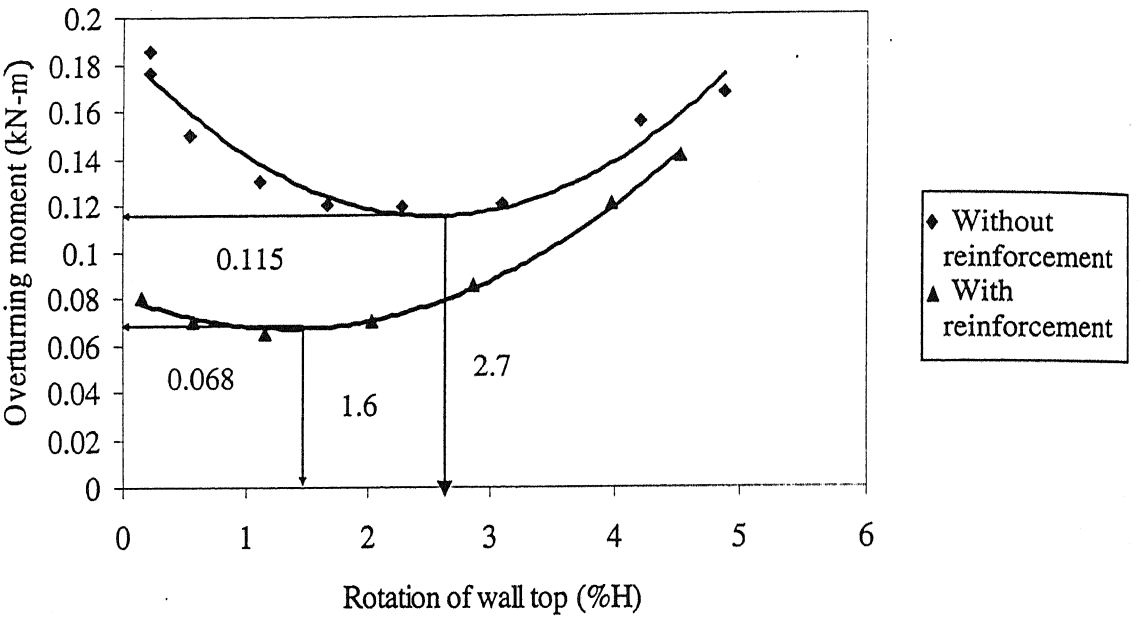

Figure 4.7(a): Observed overturning moment vs. rotation of wall top for counterfort retaining wall (without surcharge, sand backfill)

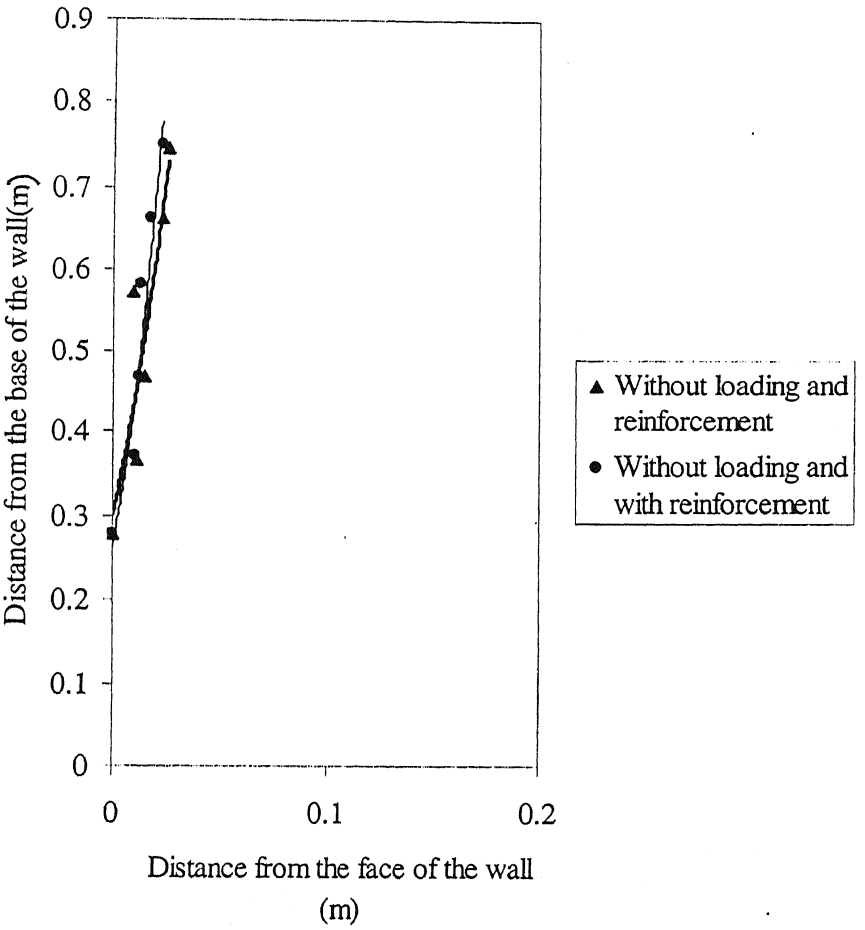

Figure 4.7(b): Observed failure surface for counterfort retaining wall (without surcharge, sand backfill)

4.2.2.1.2 With line load

Plot of overturning moment against wall rotation and plot of failure surface for retaining wall without and with reinforced backfill are shown in figures 4.8 (a) and (b). It is observed from the figure (a) that the minimum value of moment corresponding to active condition in unreinforced case has been reached at rotations 3.9 per cent of H (where H is the height of the wall) and in reinforced case it has been reached at rotations 1.85 per cent of H. The overturning moment is 71.93% less in case of the reinforced backfill than the unreinforced backfill. The failure surfaces are parabolic in nature [shown in figure 4.8(b)].

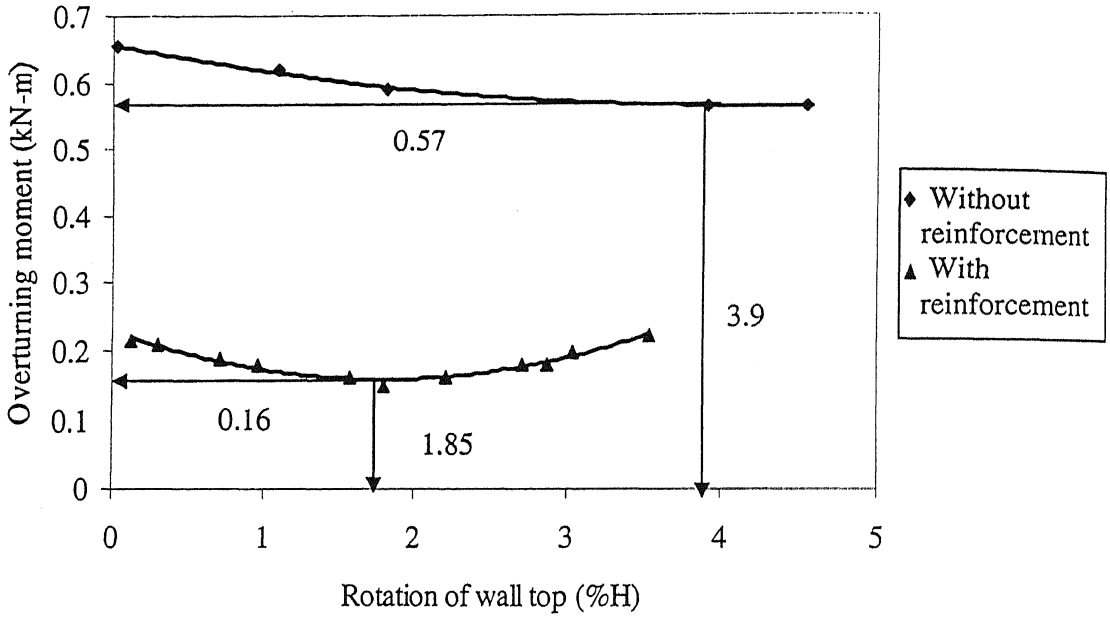

Figure 4.8(a): Observed overturning moment vs. rotation of wall top for counterfort retaining wall (line load, sand backfill)

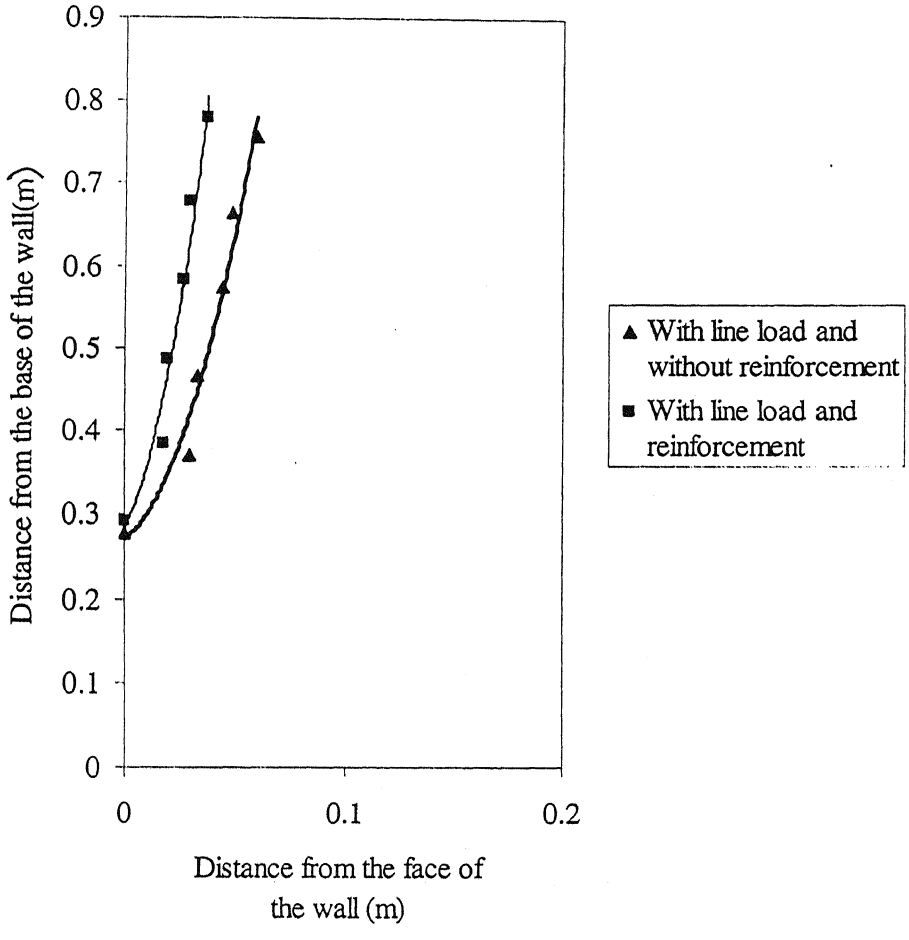

Figure 4.8(b): Observed failure surface for counterfort retaining wall (line load, sand backfill)

4.2.2.1.3 With Uniform Surcharge

Plot of overturning moment against wall rotation and plot of failure surface for retaining wall without and with reinforced backfill are shown in figures 4.9 (a) and (b). It is observed from the figure (a) that the minimum value of moment corresponding to active condition in unreinforced case has been reached at rotations 2.5 per cent of H (where H is the height of the wall) and in reinforced case it has been reached at rotations 2.93 per cent of H. The overturning moment is 75.44% less in case of the reinforced backfill than the unreinforced backfill. The failure surfaces are parabolic in nature [shown in figure 4.9(b)].

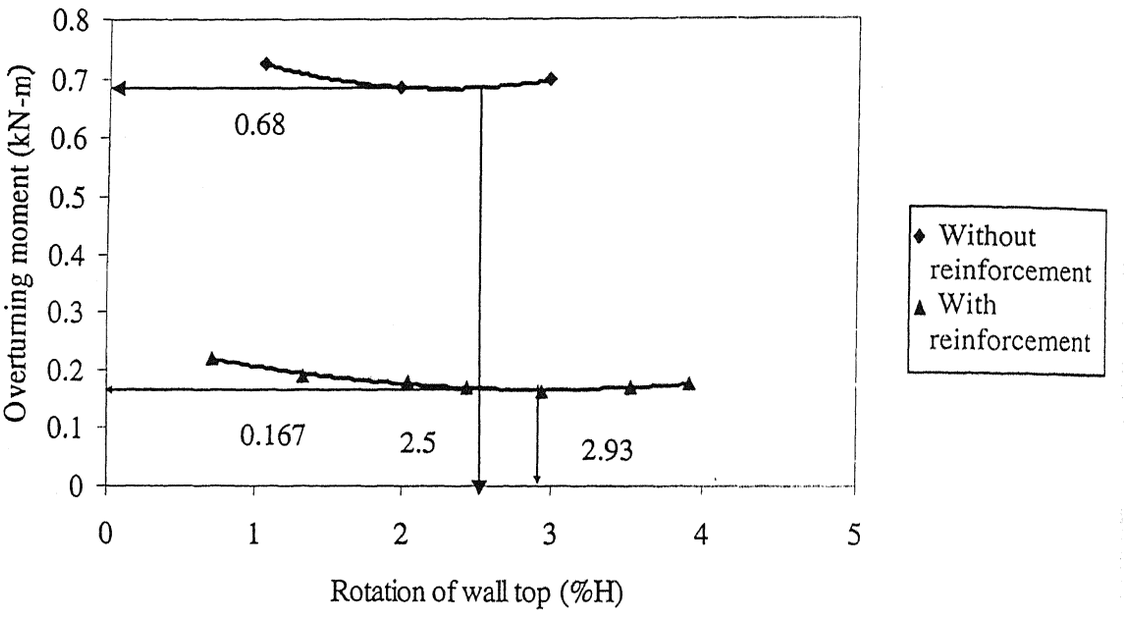

Figure 4.9(a): Observed overturning moment vs. rotation of wall top for counterfort retaining wall (uniform surcharge, sand backfill)

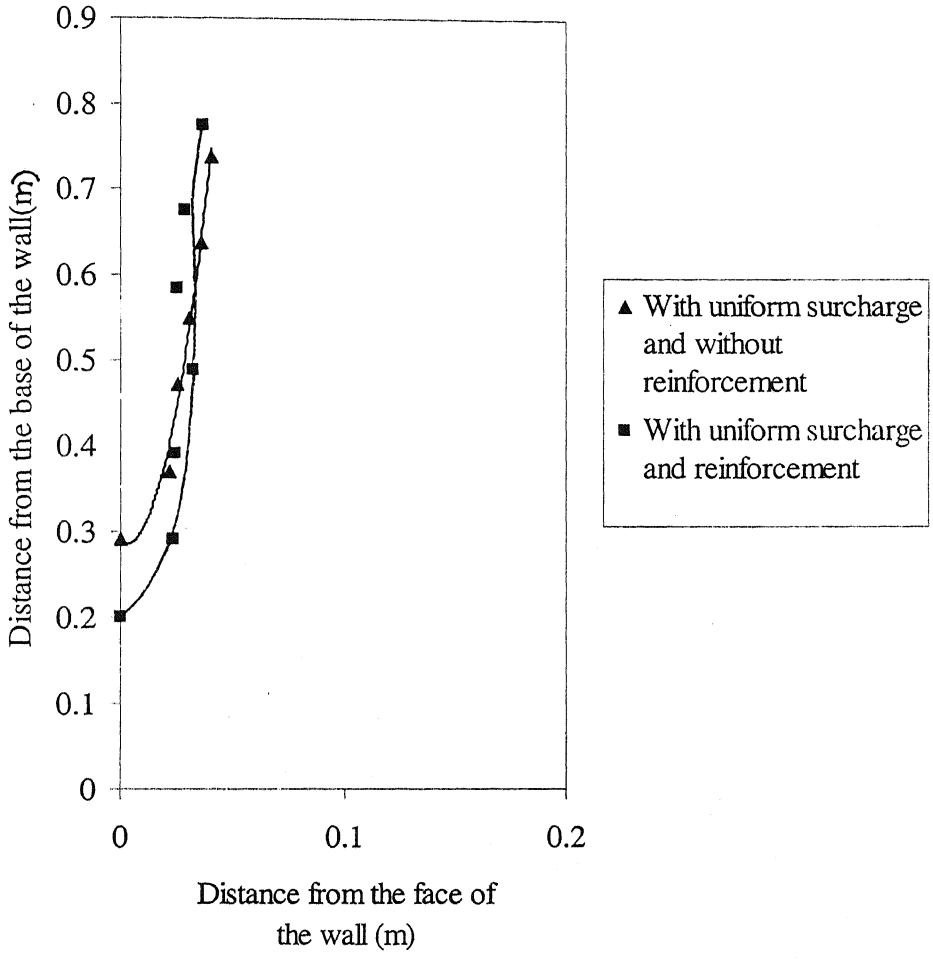

Figure 4.9(b): Observed failure surface for counterfort retaining wall (uniform surcharge, sand backfill)

It is observed from the figures that with increasing rotation, there is a gradual decrease in the overturning moment and after achieving the limiting value the moment is increased with the increase of rotation. The minimum values of moments in these tests corresponding to active condition have been reached at rotations 1.6 to 3.9 per cent of H (where H is the height of the wall). The overturning moments are about 40.87% to 75.44% less in case of the reinforced backfill than the unreinforced backfill. So, in case of the reinforced backfill the retaining wall is more stable than in case of the unreinforced one. The failure surfaces are mostly linear and parabolic in nature. Summary of test results is shown in Table 4.3.

4.2.2.2 Fly ash backfill

Model tests were carried out by applying line load and uniform surcharge on the reinforced and unreinforced backfill. Also tests had been carried out without applying any loading. The results for different loading conditions are given in the following sub headings:

i) Without any loading

ii) With line load

iii) With uniform surcharge

4.2.2.2.1 Without any loading

Plot of overturning moment against wall rotation and plot of failure surface for retaining wall without and with reinforced backfill are shown in figures 4.10 (a) and (b). It is observed from the figure (a) that the minimum value of moment corresponding to active condition in unreinforced case has been reached at rotations 1.8 per cent of H (where H is the height of the wall) and in reinforced case it has been reached at rotations 2.2 per cent of H. The overturning moment is 37.5% less in case of the reinforced backfill than the unreinforced backfill. The failure surfaces are parabolic in nature [shown in figure 4.10(b)].

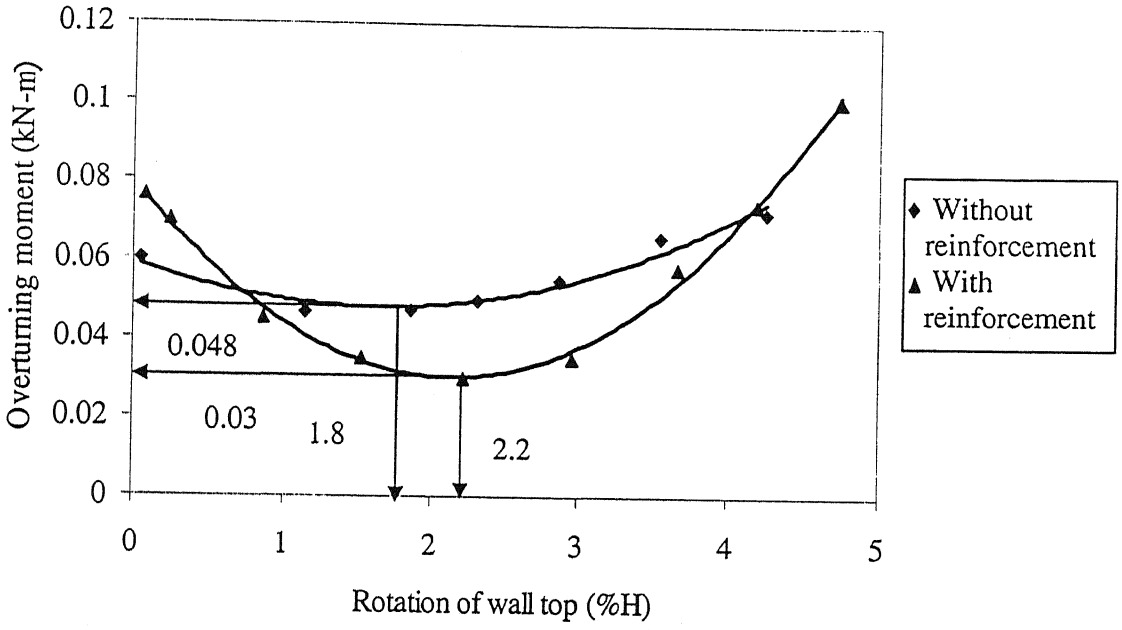

Figure 4.10(a): Observed overturning moment vs. rotation of wall top for counterfort retaining wall (without surcharge, fly ash backfill)

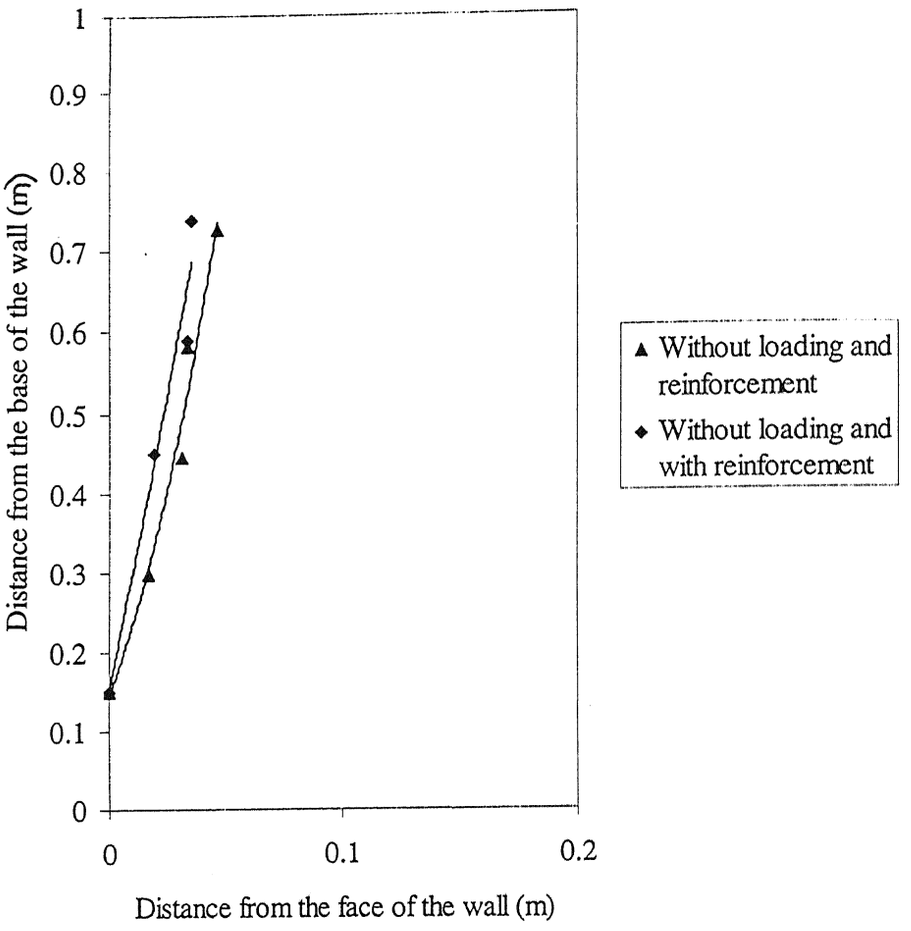

Figure 4.10(b): Observed failure surface for counterfort retaining wall (without surcharge, fly ash backfill)

4.2.2.2.2 With line load

Plot of overturning moment against wall rotation and plot of failure surface for retaining wall without and with reinforced backfill are shown in figures 4.11 (a) and (b). It is observed from the figure (a) that the minimum value of moment corresponding to active condition in unreinforced case has been reached at rotations 2.2 per cent of H (where H is the height of the wall) and in reinforced case it has been reached at rotations 2.15 per cent of H. The overturning moment is 29.73% less in case of the reinforced backfill than the unreinforced backfill. The failure surfaces are parabolic in nature [shown in figure 4.11(b)].

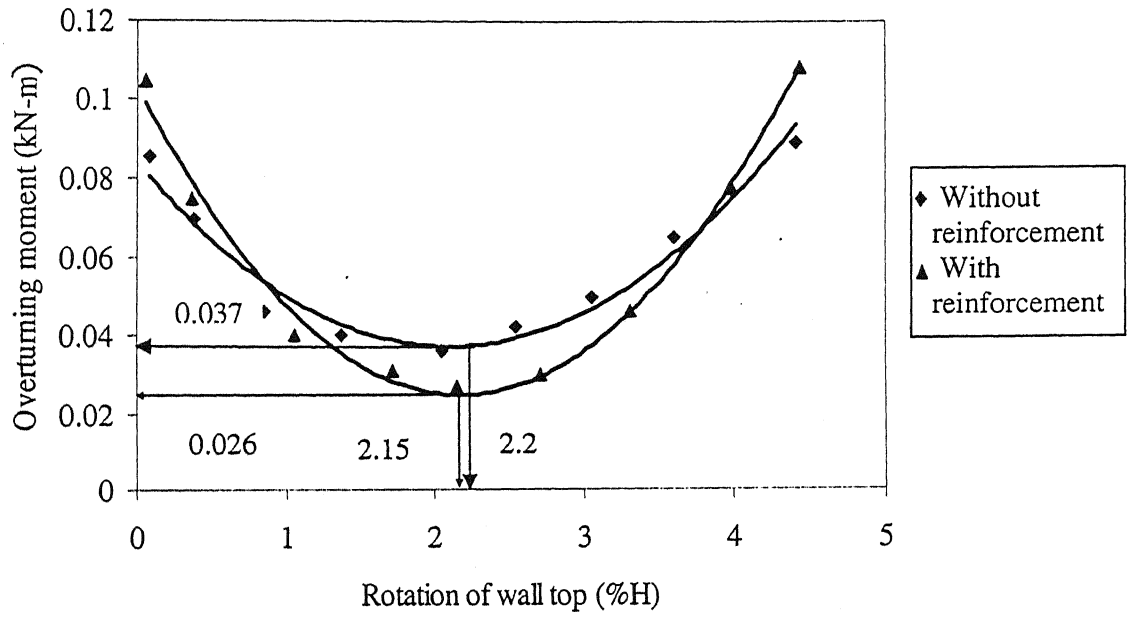

Figure 4.11(a): Observed overturning moment vs. rotation of wall top for counterfort retaining wall (line load, fly ash backfill)

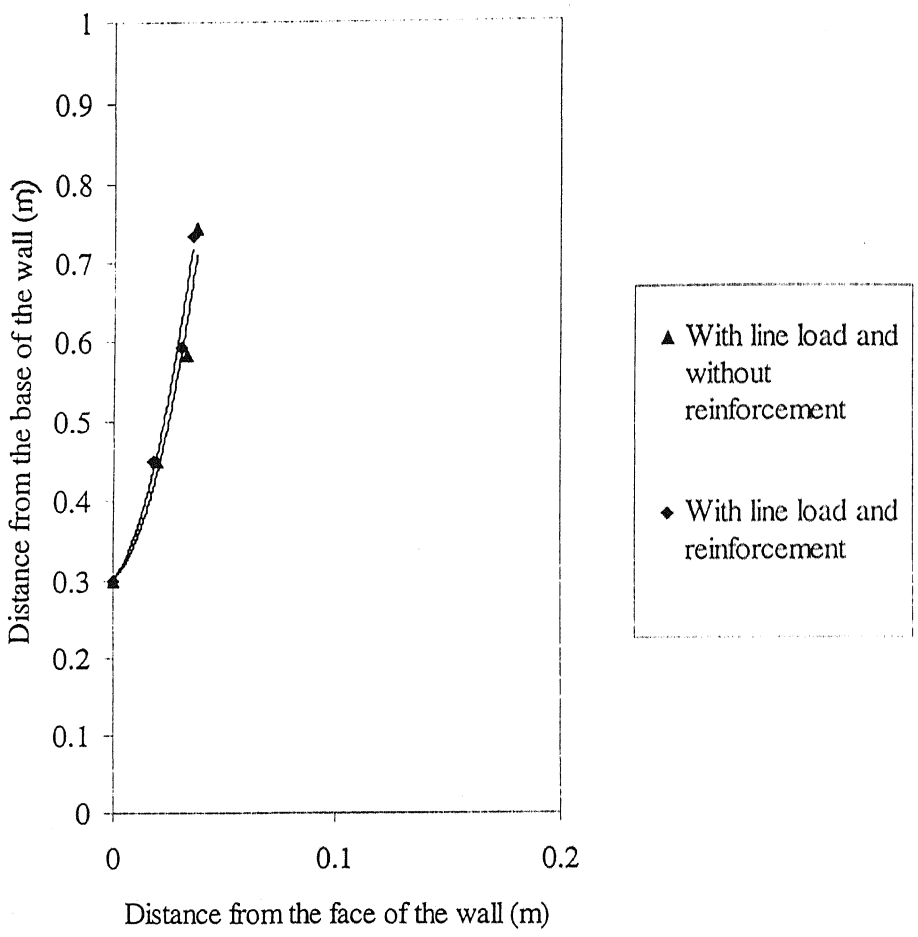

Figure 4.11(b): Observed failure surface for counterfort retaining wall (line load, fly ash backfill)

4.2.2.2.3 With Uniform Surcharge

Plot of overturning moment against wall rotation and plot of failure surface for retaining wall without and with reinforced backfill are shown in figures 4.12 (a) and (b). It is observed from the figure (a) that the minimum value of moment corresponding to active condition in unreinforced case has been reached at rotations 2.8 per cent of H (where H is the height of the wall) and in reinforced case it has been reached at rotations 2.4 per cent of H. The overturning moment is 27.08% less in case of the reinforced backfill than the unreinforced backfill. The failure surfaces are parabolic in nature [shown in figure 4.12(b)].

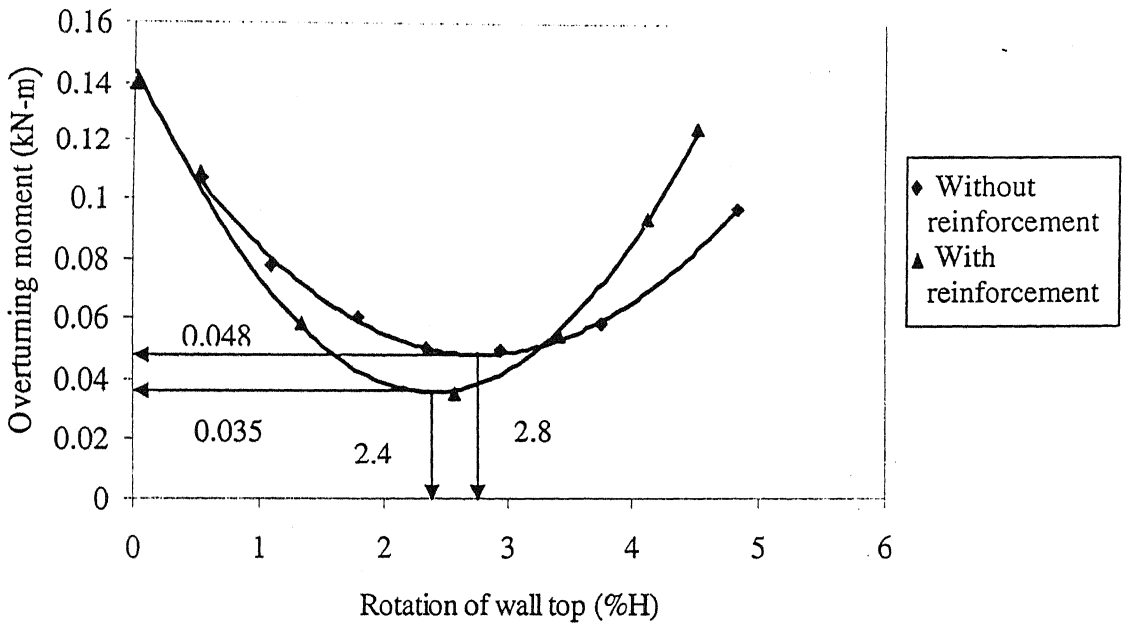

Figure 4.12(a): Observed overturning moment vs. rotation of wall top for counterfort retaining wall (uniform surcharge, fly ash backfill)

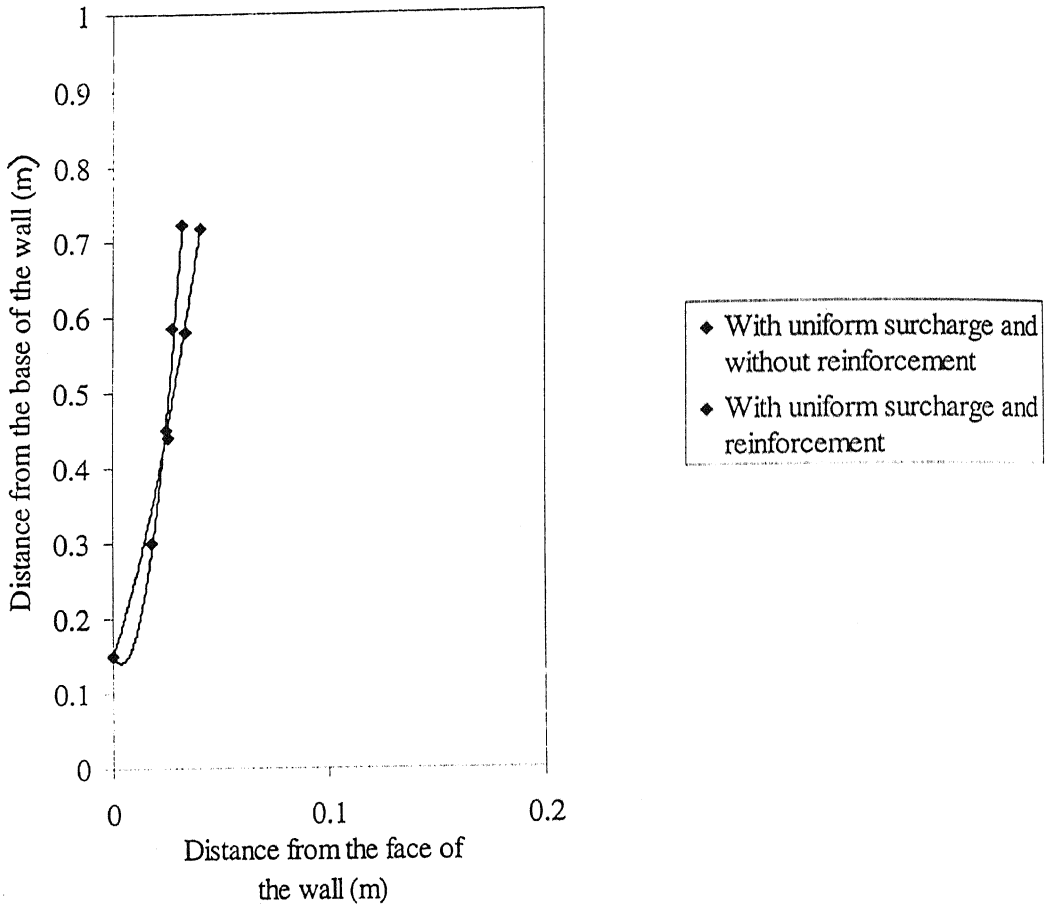

Figure 4.12(b): Observed failure surface for counterfort retaining wall (uniform surcharge, fly ash backfill)

It is observed from the figures that with increasing rotation, there is a gradual decrease in the overturning moment and after achieving the limiting value the moment is increased with the increase of rotation. The minimum values of moments in these tests corresponding to active condition have been reached at rotations 1.4 to 2.92 per cent of H (where H is the height of the wall). The overturning moments are about 27.08% to 37.5% less in case of the reinforced backfill than the unreinforced backfill. So, in case of the reinforced backfill the retaining wall is more stable than in case of the unreinforced one. The failure surfaces are parabolic in nature. Summary of test results is shown in Table 4.4.

4. 2. 3 Counterfort retaining wall with shelves

Experimental investigations on model counterfort retaining wall with shelves with sand and fly ash backfill were carried out. The results for different backfill material are discussed in the following sub headings:

a) Sand backfill

b) Fly ash backfill

4.2.3.1 Sand backfill

Model tests were carried out by applying line load and uniform surcharge on the unreinforced backfill. Also tests had been carried out without applying any loading. The results for different loading conditions are given in the following sub headings:

i) Without any loading

ii) With line load

iii) With uniform surcharge

4.2.3.1.1 Without any loading

Plot of overturning moment against wall rotation and plot of failure surface for retaining wall without reinforced backfill are shown in figures 4.13 (a) and (b). It is observed from the figure 4.13 (a) that the minimum value of moment corresponding to active condition has been reached at rotations 1.75 per cent of H (where H is the height of the wall). It can be observed from the figure 4.13 (b) that there are breakages in the failure surface corresponding to the position of the shelves (Jumikis, 1964) along the height of the retaining wall. There are three parallel failure surfaces at 0.33m, 0.67m and 1.0m from the top of the retaining wall. The failure surfaces are linear in nature.

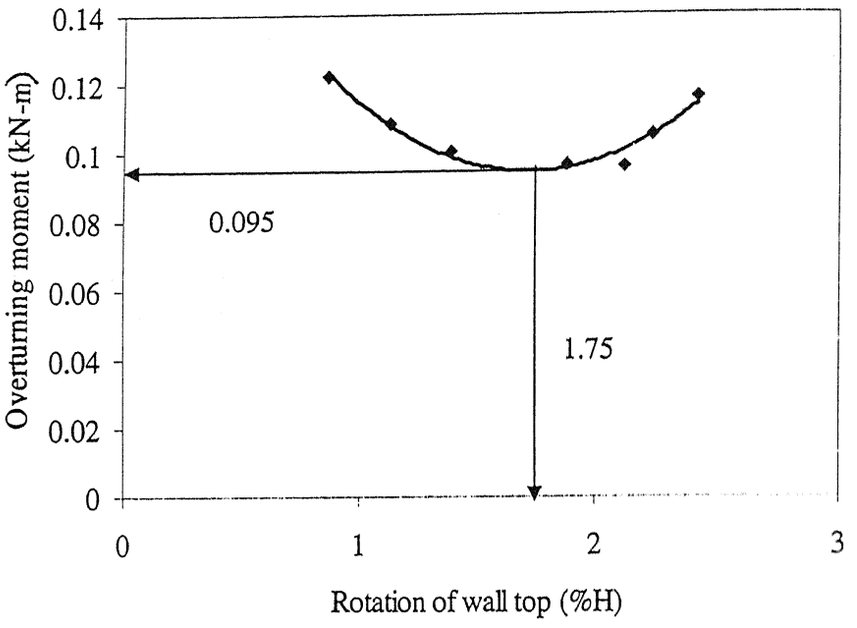

Figure 4.13(a): Observed overturning moment vs. rotation of wall top for counterfort retaining wall with shelves (without surcharge, unreinforced sand backfill)

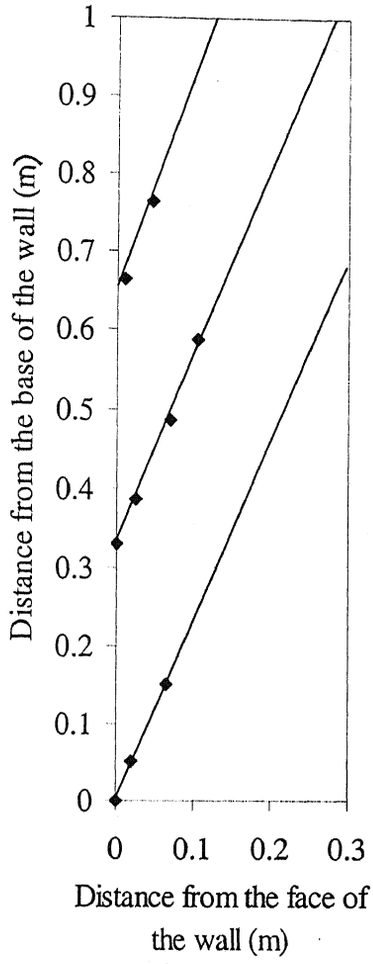

Figure 4.13(b): Observed failure surface for counterfort retaining wall with shelves (without surcharge, unreinforced sand backfill)

4.2.3.1.2 With line load

Plot of overturning moment against wall rotation and plot of failure surface for retaining wall without reinforced backfill are shown in figures 4.14 (a) and (b). It is observed from the figure 4.14 (a) that the minimum value of moment corresponding to active condition has been reached at rotations 2.8 per cent of H (where H is the height of the wall). It can be observed from the figure 4.14 (b) that there are breakages in the failure surface corresponding to the position of the shelves (Jumikis, 1964) along the height of the retaining wall. There are three parallel failure surfaces at 0.33m, 0.67m and 1.0m from the top of the retaining wall. The failure surfaces are linear in nature.

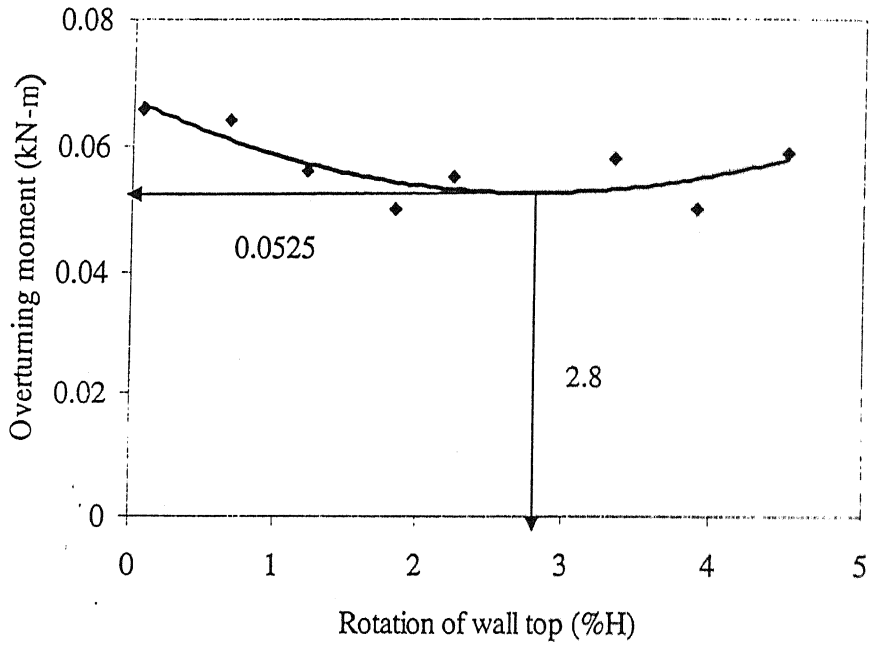

Figure 4.14(a): Observed overturning moment vs. rotation of wall top for counterfort retaining wall with shelves (line load, unreinforced sand backfill)

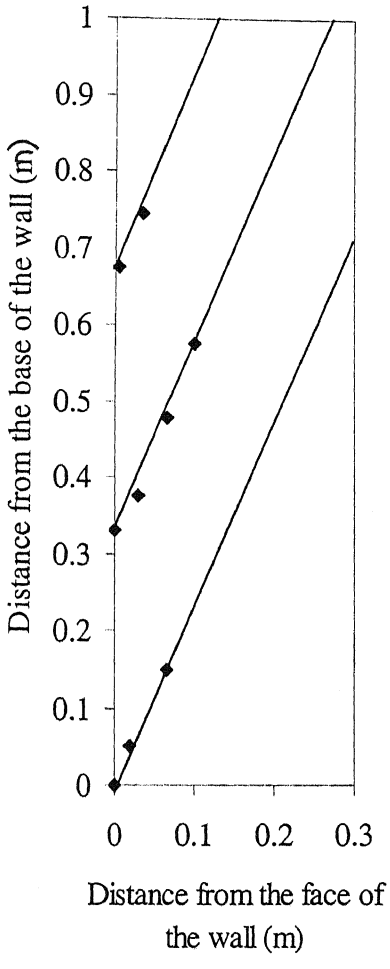

Figure 4.14(b): Observed failure surface for counterfort retaining wall with shelves (line load, unreinforced sand backfill)

4.2.3.1.3 With Uniform Surcharge

Plot of overturning moment against wall rotation and plot of failure surface for retaining wall without reinforced backfill are shown in figures 4.15 (a) and (b). It is observed from the figure 4.15 (a) that the minimum value of moment corresponding to active condition has been reached at rotations 2.7 per cent of H (where H is the height of the wall). It can be observed from the figure 4.15 (b) that there are breakages in the failure surfaces corresponding to the position of the shelves (Jumikis, 1964) along the height of the retaining wall. There are three parallel failure surfaces at 0.33m, 0.67m and 1.0m from the top of the retaining wall. The failure surfaces are linear in nature.

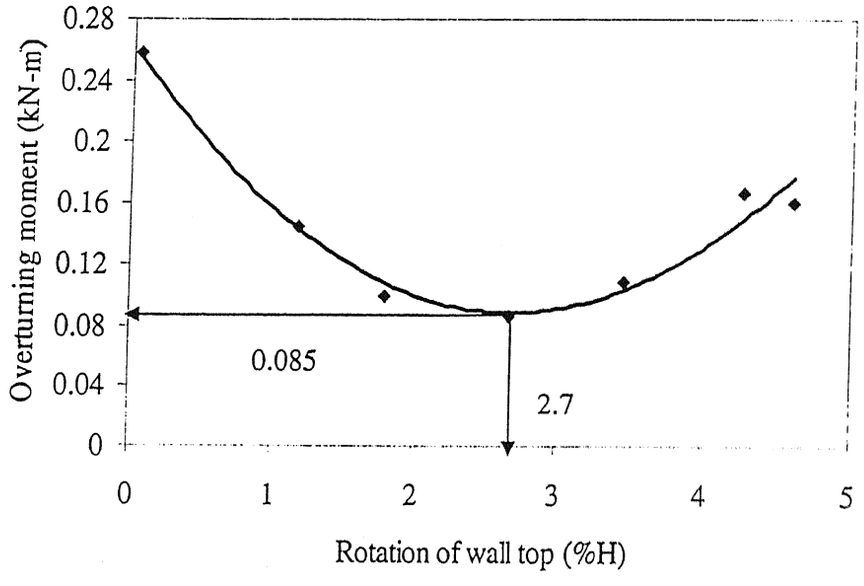

Figure 4.15(a): Observed overturning moment vs. rotation of wall top for counterfort retaining wall with shelves (uniform surcharge, unreinforced sand backfill)

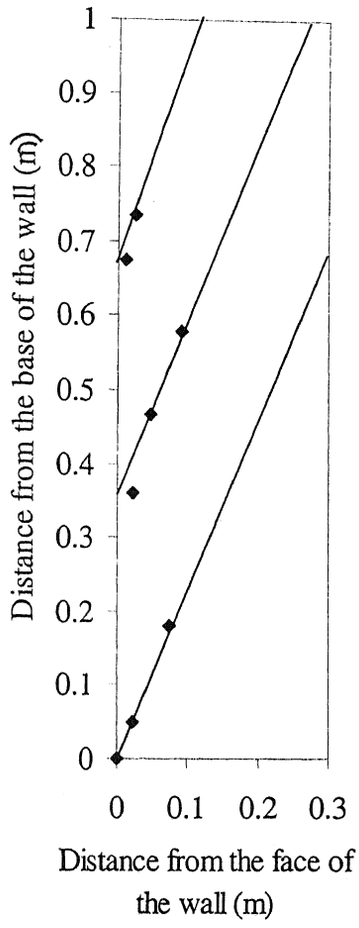

Figure 4.15(b): Observed failure surface for counterfort retaining wall with shelves (uniform surcharge, unreinforced sand backfill)

It is observed from the figures that with increasing rotation, there is a gradual decrease in the overturning moment and after achieving the limiting value the moment is increased with the increase of rotation. The minimum values of moments in these tests corresponding to active condition have been reached at rotations 1.75 to 2.8 per cent of H (where H is the height of the wall). It is also observed from the figures of the rupture surfaces that there are breakages in the failure surfaces corresponding to the position of the shelves (Jumikis, 1964) along the height of the retaining wall. There are three parallel failure surfaces at 0.33m, 0.67m and 1.0m from the top of the retaining wall. The failure surfaces are linear in nature. Summary of test results is shown in Table 4.5.

4.2.3.2 Fly ash backfill

Model tests were carried out by applying line load and uniform surcharge on the unreinforced backfill. Also tests had been carried out without applying any loading. The results for different loading conditions are given in the following sub headings:

i) Without any loading

ii) With line load

iii) With uniform surcharge

4.2.3.2.1 Without any loading

Plot of overturning moment against wall rotation and plot of failure surface for retaining wall without reinforced backfill are shown in figures 4.16 (a) and (b). It is observed from the figure 4.16 (a) that the minimum value of moment corresponding to active condition has been reached at rotations 1.65 per cent of H (where H is the height of the wall). It can be observed from the figure 4.16 (b) that there are breakages in the failure surfaces corresponding to the position of the shelves (Jumikis, 1964) along the height of the retaining wall. There are three parallel failure surfaces at 0.33m, 0.67m and 1.0m from the top of the retaining wall. The failure surfaces are linear in nature.

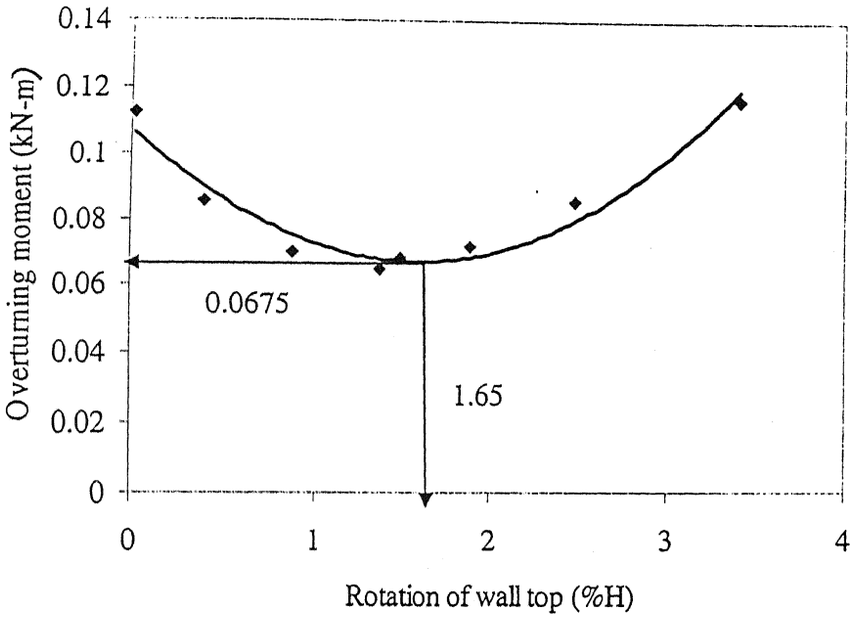

Figure 4.16(a): Observed overturning moment vs. rotation of wall top for counterfort retaining wall with shelves (without surcharge, unreinforced fly ash backfill)

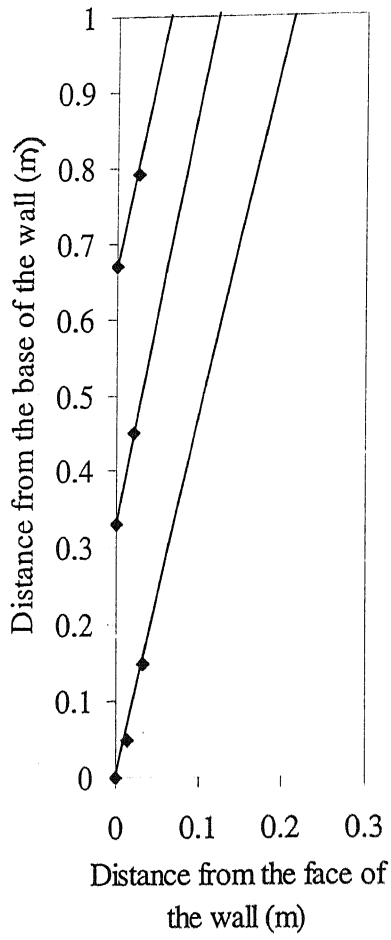

Figure 4.16(b): Observed failure surface for counterfort retaining wall with shelves (without surcharge, unreinforced fly ash backfill)

4.2.3.2.2 With line load

Plot of overturning moment against wall rotation and plot of failure surface for retaining wall without reinforced backfill are shown in figure 4.17 (a) and (b). It is observed from the figure 4.17 (a) that the minimum value of moment corresponding to active condition has been reached at rotations 2.4 per cent of H (where H is the height of the wall). It can be observed from the figure 4.17 (b) that there are breakages in the failure surfaces corresponding to the position of the shelves (Jumikis, 1964) along the height of the retaining wall. There are three parallel failure surfaces at 0.33m, 0.67m and 1.0m from the top of the retaining wall. The failure surfaces are linear in nature.

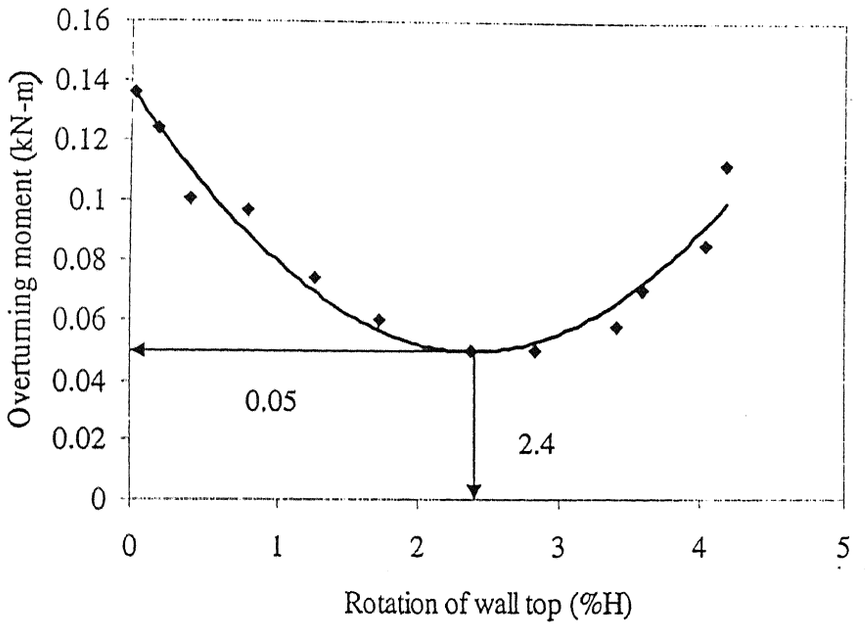

Figure 4.17(a): Observed overturning moment vs. rotation of wall top for counterfort retaining wall with shelves (line load, unreinforced fly ash backfill)

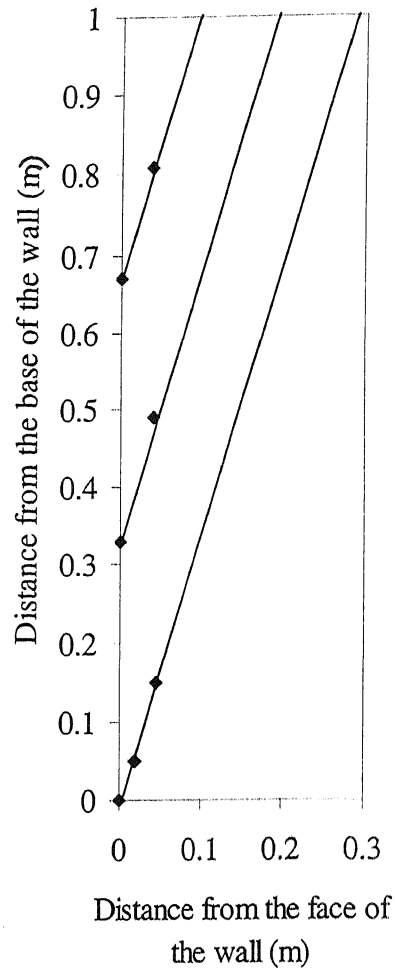

Figure 4.17(b): Observed failure surface for counterfort retaining wall with shelves (line load, unreinforced fly ash backfill)

4.2.3.2.3 With Uniform Surcharge

Plot of overturning moment against wall rotation and plot of failure surface for retaining wall without reinforced backfill are shown in figures 4.18 (a) and (b). It is observed from the figure 4.18 (a) that the minimum value of moment corresponding to active condition has been reached at rotations 2.2 per cent of H (where H is the height of the wall). It can be observed from the figure 4.18 (b) that there are breakages in the failure surfaces corresponding to the position of the shelves (Jumikis, 1964) along the height of the retaining wall. There are three parallel failure surfaces at 0.33m, 0.67m and 1.0m from the top of the retaining wall. The failure surfaces are linear in nature.

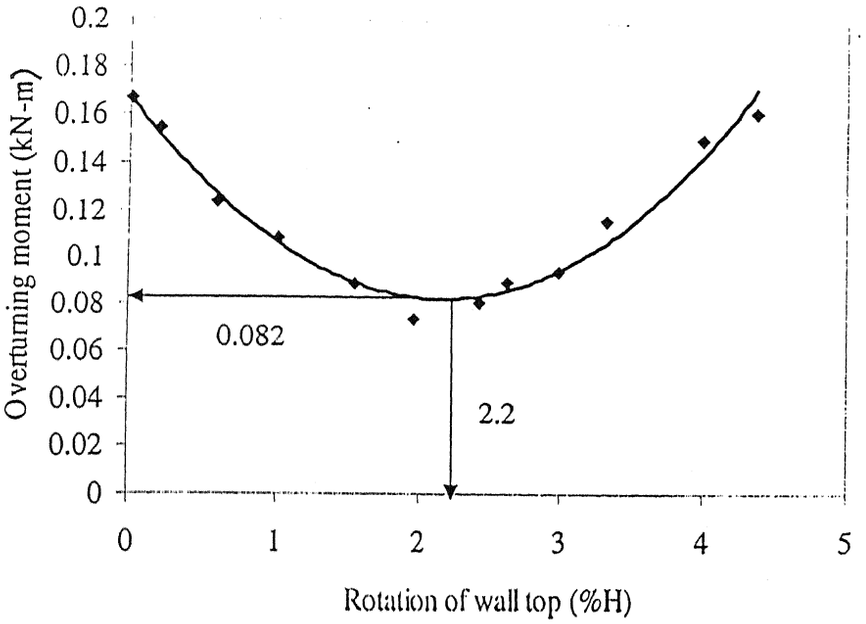

Figure 4.18(a): Observed overturning moment vs. rotation of wall top for counterfort retaining wall with shelves (uniform surcharge, unreinforced fly ash backfill)

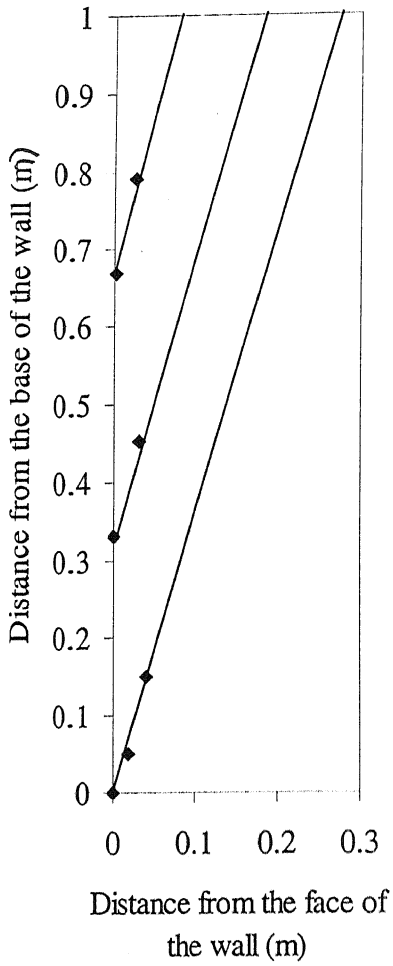

Figure 4.18(b): Observed failure surface for counterfort retaining wall with shelves (uniform surcharge, unreinforced fly ash backfill)

It is observed from the figures that with increasing rotation, there is a gradual decrease in the overturning moment and after achieving the limiting value the moment is increased with the increase of rotation. The minimum values of moments in these tests corresponding to active condition have been reached at rotations 1.65 to 2.4 per cent of H (where H is the height of the wall). It is observed from the figures of the rupture surfaces that there are breakages in the failure surfaces corresponding to the position of the shelves (Jumikis, 1964) along the height of the retaining wall. There are three parallel failure surfaces at 0.33m, 0.67m and 1.0m from the top of the retaining wall. The failure surfaces are linear in nature. Summary of test results is shown in Table 4.6.

4.3 Comparison of Results between Fly Ash and Sand Backfill

The overturning moments of fly ash backfill are compared with sand backfill for different types of retaining wall. It is observed that the overturning moments for fly ash backfill are less than the sand backfill. So, retaining walls with fly ash backfill are more stable than the sand one.

4.3.1 Cantilever retaining wall

In case of cantilever retaining wall the overturning moments of fly ash backfill are about 5 to 66% less than the sand backfill. The comparison is shown in Table 4.7.

4.3.2 Counterfort retaining wall

In case of counterfort retaining wall the overturning moments of fly ash backfill are about 55 to 93% less than the sand backfill. The comparison is shown in Table 4.8.

4.3.3 Counterfort retaining wall with Shelves

In case of counterfort retaining wall with shelves the overturning moments of fly ash backfill are about 3 to 28% less than the sand backfill. The comparison is shown in Table 4.9.

Table: 4.1 Summary of test results for cantilever retaining wall for sand backfill

Test No.	Test Type	Overturning moment (kN-m)	Rotation of wall(%H)	Wedge angle	Percent variation in moment
1	Without loading and without reinforcement	0.09	1.88%	5	
2	Without loading and with reinforcement	0.0525	2.60%	5	41.67
3	With line load and without reinforcement	0.168	2.80%	6	
4	With line load and reinforcement	0.105	1.88%	5.5	37.5
5	With uniform surcharge and without reinforcement	0.05	2.80%	5.5	
6	With uniform surcharge and reinforcement	0.0375	1.50%	5.5	25

Table: 4.2 Summary of test results for cantilever retaining wall for fly ash backfill

Test No.	Test Type	Overturning moment (kN-m)	Rotation of wall(%H)	Wedge angle	Percent variation in moment
1	Without loading and without reinforcement	0.08475	1.88%	8	
2	Without loading and with reinforcement	0.0175	2.60%	7	79.35
3	With line load and without reinforcement	0.152	2.80%	6.5	
4	With line load and reinforcement	0.04	1.88%	6	73.68
5	With uniform surcharge and without reinforcement	0.044	2.80%	8.5	
6	With uniform surcharge and reinforcement	0.034	1.50%	8.5	22.73

Table: 4.3 Summary of test results for counterfort retaining wall for sand backfill

Test No.	Test Type	Overturning moment (kN-m)	Rotation of wall(%H)	Wedge angle	Percent variation in moment
1	Without loading and without reinforcement	0.115	2.70%	4.5	
2	Without loading and with reinforcement	0.068	1.60%	4	40.87
3	With line load and without reinforcement	0.57	3.90%	8	
4	With line load and reinforcement	0.16	1.85%	5	71.93
5	With uniform surcharge and without reinforcement	0.68	2.50%	5.5	
6	With uniform surcharge and reinforcement	0.167	2.93%	5	75.44

Table: 4.4 Summary of test results for counterfort retaining wall for fly ash backfill

Test No.	Test Type	Overturning moment (kN-m)	Rotation of wall(%H)	Wedge angle	Percent variation in moment
1	Without loading and without reinforcement	0.048	2.70%	6.5	
2	Without loading and with reinforcement	0.03	1.60%	4	37.5
3	With line load and without reinforcement	0.037	3.90%	7.5	
4	With line load and reinforcement	0.026	1.85%	7	29.73
5	With uniform surcharge and without reinforcement	0.048	2.50%	5.5	
6	With uniform surcharge and reinforcement	0.035	2.93%	5	27.08

Table: 4.5 Summary of test results for counterfort retaining wall with shelves for sand backfill

Test No.	Test Type	Overturning moment (kN-m)	Rotation of wall(%H)	Wedge angle
1	Without loading and without reinforcement	0.095	1.75%	23.5
2	With line load and without reinforcement	0.0525	2.80%	23.5
3	With uniform surcharge and without reinforcement	0.085	2.70%	23

Table: 4.6 Summary of test results for counterfort retaining wall with shelves for fly ash backfill

Test No.	Test Type	Overturning moment (kN-m)	Rotation of wall(%H)	Wedge angle
1	Without loading and without reinforcement	0.0675	1.65%	14
2	With line load and without reinforcement	0.05	2.40%	17
3	With uniform surcharge and without reinforcement	0.082	2.20%	16.5

Table 4.7 Comparison of experimental overturning moments between sand and fly ash backfill for cantilever retaining wall

Experiment No.	Test Type	Overturning Moments (kN-m)		% Variation
		Sand Backfill	Fly ash Backfill	
1	Without loading and without reinforcement	0.09	0.08475	5.83
2	Without loading and with reinforcement	0.0525	0.0175	66.67
3	With line load and without reinforcement	0.168	0.152	9.52
4	With line load and reinforcement	0.105	0.04	61.90
5	With uniform surcharge and without reinforcement	0.05	0.044	12.00
6	With uniform surcharge and reinforcement	0.0375	0.034	9.33

Table 4.8 Comparison of experimental overturning moments between sand and fly ash backfill for counterfort retaining wall

Experiment No.	Test Type	Overturning Moments (kN-m)		% Variation
		Sand Backfill	Fly ash Backfill	
1	Without loading and without reinforcement	0.115	0.048	58.26
2	Without loading and with reinforcement	0.068	0.03	55.88
3	With line load and without reinforcement	0.57	0.037	93.51
4	With line load and reinforcement	0.16	0.026	83.75
5	With uniform surcharge and without reinforcement	0.68	0.048	92.94
6	With uniform surcharge and reinforcement	0.167	0.035	79.04

Table 4.9 Comparison of experimental overturning moments between sand and fly ash backfill for counterfort retaining wall with shelves

Experiment No.	Test Type	Overturning Moments (kN-m)		% Variation
		Sand Backfill	Fly ash Backfill	
1	Without loading and without reinforcement	0.095	0.0675	28.95
2	With line load and without reinforcement	0.0525	0.05	4.76
3	With uniform surcharge and without reinforcement	0.085	0.082	3.53

CHAPTER V

Analysis

5.1 General

The lateral earth pressure acting on a retaining wall supporting reinforced earth backfill has been determined by considering the stability of the failure wedge. Two types of analysis have been done by considering parabolic and planar failure surface.

5.2 Parabolic failure surface

Analytical Methods based on observed parabolic failure surfaces, have been developed to predict the lateral earth pressure on the retaining wall with vertical back face having horizontal unreinforced and reinforced frictional cohesive backfill subjected to line load and uniformly distributed surcharge load by considering equilibrium of the failure wedge. Retaining wall without any surcharge is also considered in the analysis.

5.2.1 Assumptions

Following are the assumptions used in the analysis:

a) The soil behind the retaining wall is considered to be dry isotropic and cohesive frictional material.

b) Rupture plane is assumed to be parabolic passing through the heel of the wall.

c) The wall yields to the extent that the rupture of the backfill soil takes place and a soil wedge is torn off from the rest the soil mass.

d) Resultant earth pressure acts at an angle δ to the normal of the wall where δ is the angle of wall friction.

e) The failure plane divides the length of reinforcing strip in two zones, one that lies within failure wedge and another outside. Only the part of strip which experiences movement of soil relative to itself is assumed to be contributing frictional resistance.

5.2.2 Analysis of a cantilever retaining wall

Analysis is developed by considering different conditions. There may be six cases of analysis.

a) Retaining wall without loading and without reinforced backfill.

b) Retaining wall with line load and without reinforced backfill.

c) Retaining wall with uniform surcharge and without reinforced backfill.

d) Retaining wall without loading and with reinforced backfill.

e) Retaining wall with line load and reinforced backfill.

f) Retaining wall with uniform surcharge and reinforced backfill.

5.2.2.1 Retaining wall without loading and without reinforced backfill

Consider a retaining wall of height H with vertical back, retaining a horizontal cohesive-frictional backfill of dry density γ, internal friction angle ϕ and cohesion c_s. There is no surcharge on the unreinforced backfill (shown in figure 5.1).

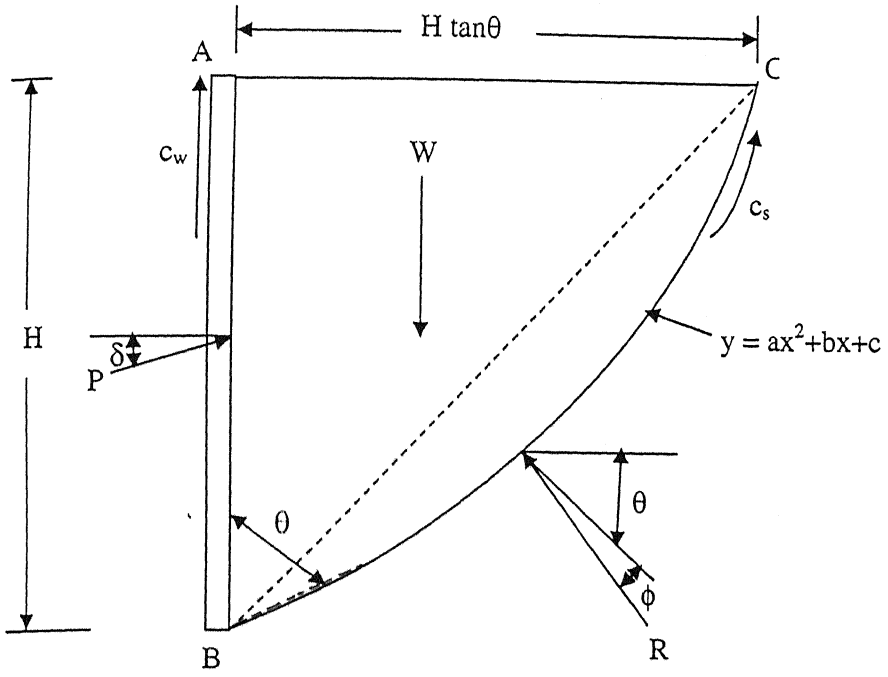

Figure 5.1: Forces acting on cantilever retaining wall (without loading, unreinforced backfill)

Following forces act on the wedge ABC:

c_w = Adhesion for wall-soil interface.

c_s = Cohesion between soil particles.

R = Reaction acting at an angle of ϕ with the normal to BC

P = Total earth pressure acting at an angle δ with the normal to AB.

W = Weight of wedge ABC.

It is known that, equation of the parabola: $y = ax^2+bx+c$

Where a, b and c are constants.

Area of the wedge = $\int_0^{H\tan\theta} (ax^2 + bx + c)dx$

$$= H\tan\theta\left[\frac{aH^2\tan^2\theta}{3} + \frac{bH\tan\theta}{2} + c\right]$$

Weight of the failure wedge = W = $\gamma.H\tan\theta\left[\frac{aH^2\tan^2\theta}{3}+\frac{bH\tan\theta}{2}+c\right]$

(i) Balancing all the forces acting on the wedge in the horizontal direction:

$\sum H = 0.$

$P\cos\delta = R\cos(\theta+\phi) - c_s.H.\tan\theta$

or, $R = \frac{P\cos\delta + c_s H\tan\theta}{\cos(\theta+\phi)}$ (5.1)

(ii) Balancing all the forces acting on the wedge in the vertical direction:

$\sum V = 0.$

$W = c_w H + c_s H + P\sin\delta + R\sin(\theta+\phi)$ (5.2)

Substituting the value of R from equation (5.1) in equation (5.2) and solving it, we get,

$P = \frac{W\cos(\theta+\phi)}{\sin(\theta+\phi+\delta)} - \frac{c_w H\cos(\theta+\phi)+c_s H\cos\phi\sec\theta}{\sin(\theta+\phi+\delta)}$ (5.3)

5.2.2.2 Retaining wall with line load and without reinforced backfill

Consider a retaining wall of height H with vertical back, retaining a horizontal cohesive-frictional backfill of dry density γ, internal friction angle ϕ and cohesion c_s. The unreinforced backfill supports line load of intensity of Q per unit length of wall acting at a distance of X from back face of wall (shown in figure 5.2).

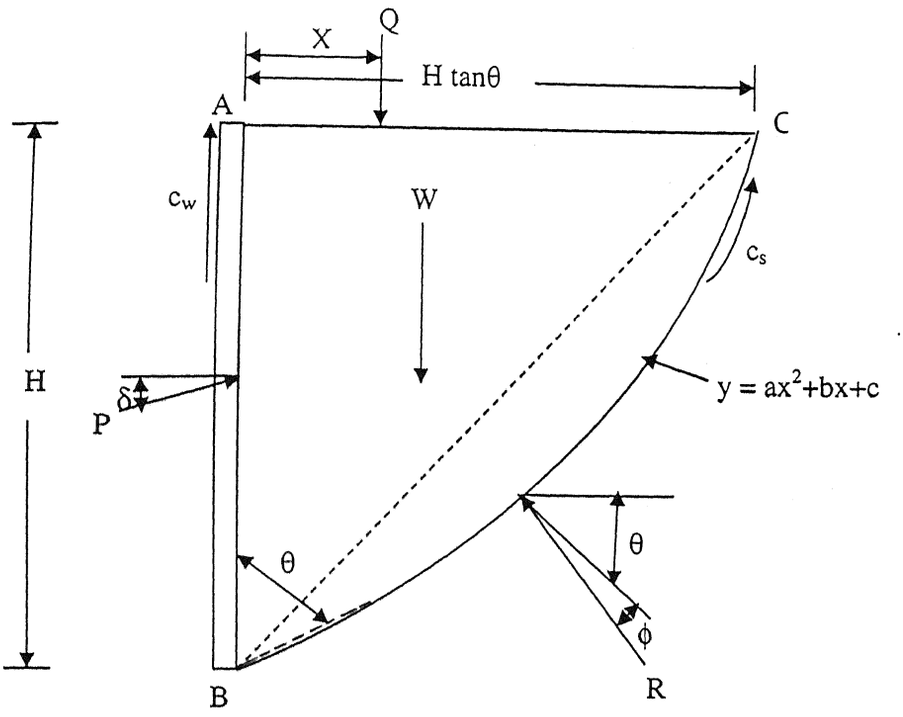

Figure 5.2: Forces acting on cantilever retaining wall (line load, unreinforced backfill)

Following forces act on the wedge ABC:

Q = Line load per unit length of wall.

All other forces acting are same as shown in figure 5.1.

Weight of the failure wedge = $W=\gamma.H\tan\theta\left[\frac{aH^2\tan^2\theta}{3}+\frac{bH\tan\theta}{2}+c\right]$

(i) Balancing all the forces acting on the wedge in the horizontal direction:

$\sum H = 0.$

$P\cos\delta = R\cos(\theta+\phi)-c_s.H.\tan\theta$

or, $R=\frac{P\cos\delta+c_sH\tan\theta}{\cos(\theta+\phi)}$ (5.4)

(ii) Balancing all the forces acting on the wedge in the vertical direction:

$\sum V = 0.$

(a) If $H \tan 6 < X$ then,

$$W = c_w H + c_s H + P \sin \delta + R \sin(6 + \phi) \quad (5.5a)$$

(b) If $H \tan 6 \geq X$ then,

$$W + Q = c_w H + c_s H + P \sin \delta + R \sin(6 + \phi) \quad (5.5b)$$

Substituting the value of R from equation (5.4) in equation (5.5a) and (5.5b) and solving it, we get,

$$\text{(a) } P = \frac{W \cos(\theta + \phi)}{\sin(\theta + \phi + \delta)} - \frac{c_w H \cos(6 + \phi) + c_s H \cos\phi \sec 6}{\sin(\theta + \phi + \delta)} \quad (5.6a)$$

$$\text{(b) } P = \frac{(W + Q).\cos(\theta + \phi)}{\sin(\theta + \phi + \delta)} - \frac{c_w H \cos(6 + \phi) + c_s H \cos\phi \sec 6}{\sin(\theta + \phi + \delta)} \quad (5.6b)$$

5.2.2.3 Retaining wall with uniform surcharge and without reinforced backfill

Consider a retaining wall of height H with vertical back, retaining a horizontal cohesive-frictional backfill of dry density γ, internal friction angle ϕ and cohesion c_s. The unreinforced backfill supports uniformly distributed surcharge load of intensity q per square unit length of wall (shown in figure 5.3).

Following forces act on the wedge ABC:

q = Uniformly distributed surcharge load per square unit length of wall.

All other forces acting are same as shown in figure 5.1.

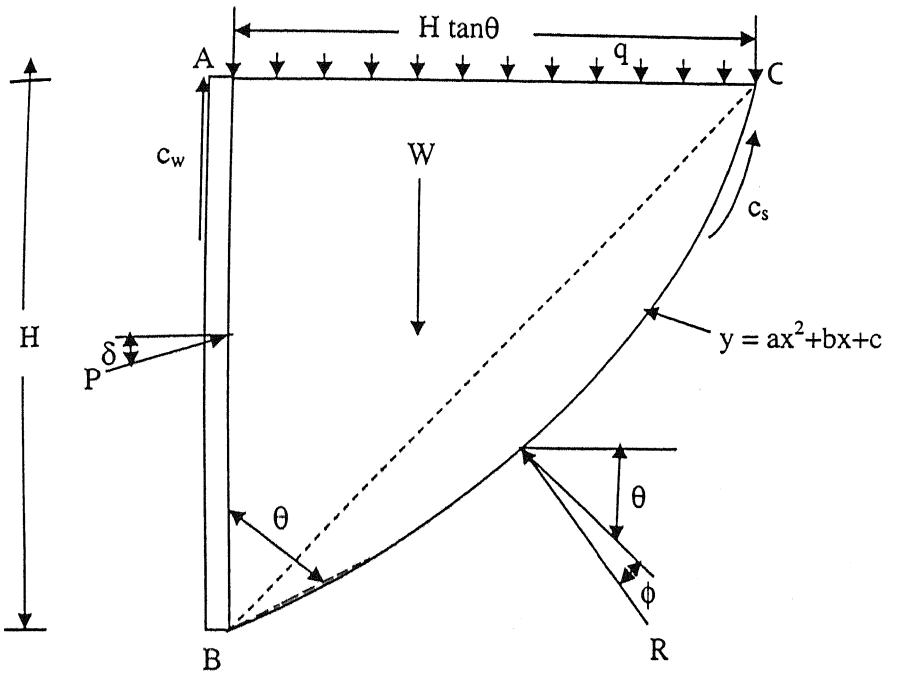

Figure 5.3: Forces acting on cantilever retaining wall (uniform surcharge, unreinforced backfill)

Weight of the failure wedge = W = $\gamma.H\tan\theta\left[\frac{aH^2\tan^2\theta}{3}+\frac{bH\tan\theta}{2}+c\right]$

(i) Balancing all the forces acting on the wedge in the horizontal direction:

$\sum H = 0.$

$P\cos\delta = R\cos(\theta+\phi)-c_s.H.\tan\theta$

or, $R=\frac{P\cos\delta+c_sH\tan\theta}{\cos(\theta+\phi)}$ (5.7)

(ii) Balancing all the forces acting on the wedge in the vertical direction:

$\sum V = 0.$

$W+qH\tan\theta = c_wH+c_sH+P\sin\delta+R\sin(\theta+\phi)$ (5.8)

Substituting the value of R from equation (5.7) in equation (5.8) and solving it, we get,

$$P = \frac{(W + qH\tan\theta).\cos(\theta+\phi)}{\sin(\theta+\phi+\delta)} - \frac{c_w H\cos(\theta+\phi) + c_s H\cos\phi\sec\theta}{\sin(\theta+\phi+\delta)} \qquad (5.9)$$

5.2.2.4 Retaining wall without loading and with reinforced backfill

Consider a retaining wall of height H with vertical back, retaining a horizontal cohesive-frictional backfill of dry density γ, internal friction angle ϕ and cohesion c_s. There is no surcharge on the reinforced backfill (shown in figure 5.4).

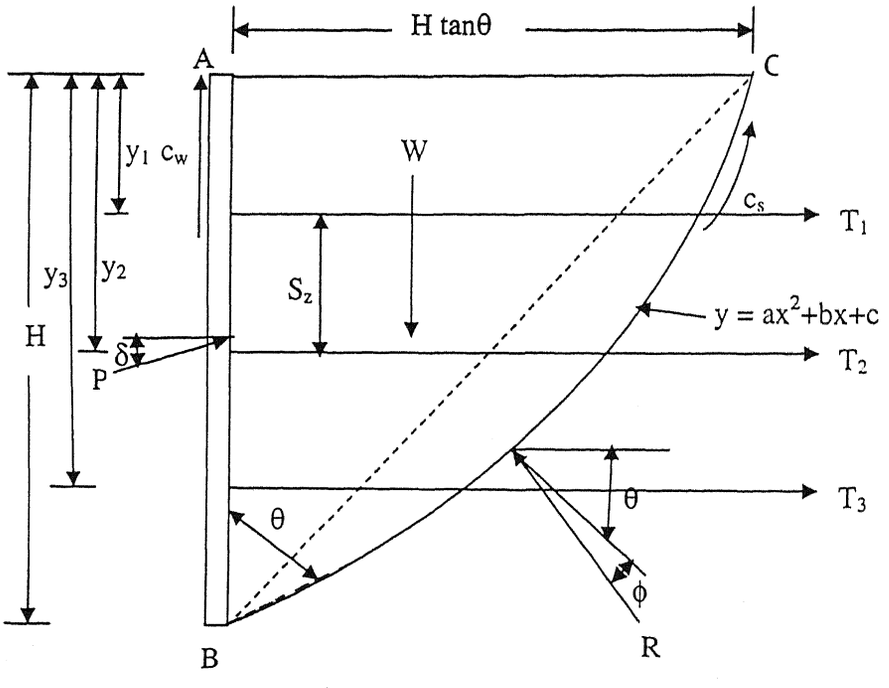

Figure 5.4: Forces acting on cantilever retaining wall (without loading, reinforced backfill)

Following forces act on the wedge ABC:

T_1, T_2 and T_3 are the tensile force in the reinforcing strip assumed transmitted uniformly to soil layer of thickness S_z encompassing the strip.

$$T_1 = 2[\gamma.y_1 + q]w.l_{e_1}.f^*$$
$$T_2 = 2[\gamma.y_2 + q]w.l_{e_2}.f^*$$

$T_3 = 2[\gamma.y_3 + q]w.l_{e_3}.f^*$

Where, y_1, y_2 and y_3 are the distances of the reinforcing strip from the top of the retaining wall.

w and l_{e_1}, l_{e_2} and l_{e_3} are the width and effective length of the different reinforcing strips respectively.

f^* = apparent co-efficient of friction between soil and reinforcement = $\tan\delta$.

q will be applicable when there will be any uniformly distributed surcharge load on the reinforced backfill.

S_z = vertical spacing between reinforcing strips.

Now, $T = T_1+T_2+T_3$.

Where, T is the total tensile force in the reinforcing strip.

All other forces acting are same as shown in figure 5.1.

Weight of the failure wedge = $W = \gamma.H\tan\theta\left[\frac{aH^2\tan^2\theta}{3}+\frac{bH\tan\theta}{2}+c\right]$

(i) Balancing all the forces acting on the wedge in the horizontal direction:

$\sum H = 0.$

$P\cos\delta = R\cos(\theta+\phi) - c_s.H.\tan\theta - T$

or, $R = \frac{P\cos\delta + c_s H\tan\theta + T}{\cos(\theta+\phi)}$ (5.10)

(ii) Balancing all the forces acting on the wedge in the vertical direction:

$\sum V = 0.$

$W = c_w H + c_s H + P\sin\delta + R\sin(\theta+\phi)$ (5.11)

Substituting the value of R from equation (5.10) in equation (5.11) and solving it, we get,

$P = \frac{W\cos(\theta+\phi)}{\sin(\theta+\phi+\delta)} - \frac{c_w H\cos(\theta+\phi) + c_s H\cos\phi\sec\theta + T\sin(\theta+\phi)}{\sin(\theta+\phi+\delta)}$ (5.12)

5.2.2.5 Retaining wall with line load and reinforced backfill

Consider a retaining wall of height H with vertical back, retaining a horizontal cohesive-frictional backfill of dry density γ, internal friction angle ϕ and cohesion c_s. The reinforced backfill supports line load of intensity of Q per unit length of wall acting at a distance of X from back face of wall (shown in figure 5.5).

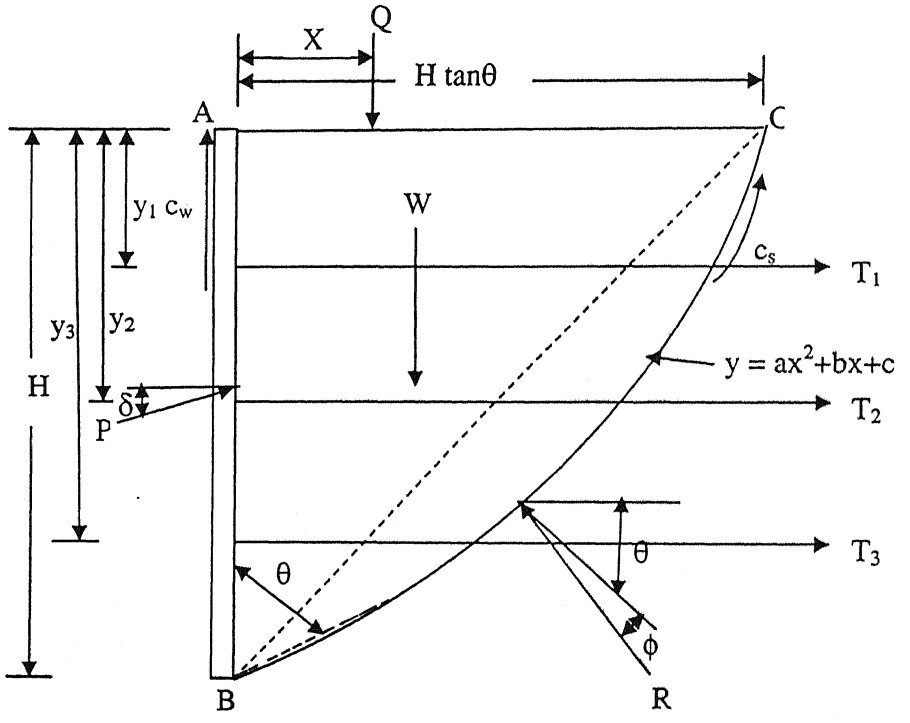

Figure 5.5: Forces acting on cantilever retaining wall (line load, reinforced backfill)

Following forces act on the wedge ABC:

Q = Line load per unit length of wall.

All other forces acting are same as shown in figure 5.4.

Balancing all the forces acting on the wedge, as solved in the previous cases,

(a) If $H \tan\delta < X$ then,

$$P = \frac{W\cos(\theta+\phi)}{\sin(\theta+\phi+\delta)} - \frac{c_w H\cos(\theta+\phi)+c_s H\cos\phi\sec\theta+T\sin(\theta+\phi)}{\sin(\theta+\phi+\delta)} \qquad (5.13a)$$

(b) If $H\tan\theta \geq X$ then,

$$P = \frac{(W+Q).\cos(\theta+\phi)}{\sin(\theta+\phi+\delta)} - \frac{c_w H\cos(\theta+\phi)+c_s H\cos\phi\sec\theta+T\sin(\theta+\phi)}{\sin(\theta+\phi+\delta)} \qquad (5.13b)$$

5.2.2.6 Retaining wall with uniform surcharge and reinforced backfill

Consider a retaining wall of height H with vertical back, retaining a horizontal cohesive-frictional backfill of dry density γ, internal friction angle ϕ and cohesion c_s. The reinforced backfill supports uniformly distributed surcharge load of intensity q per square unit length of wall (shown in figure 5.6).

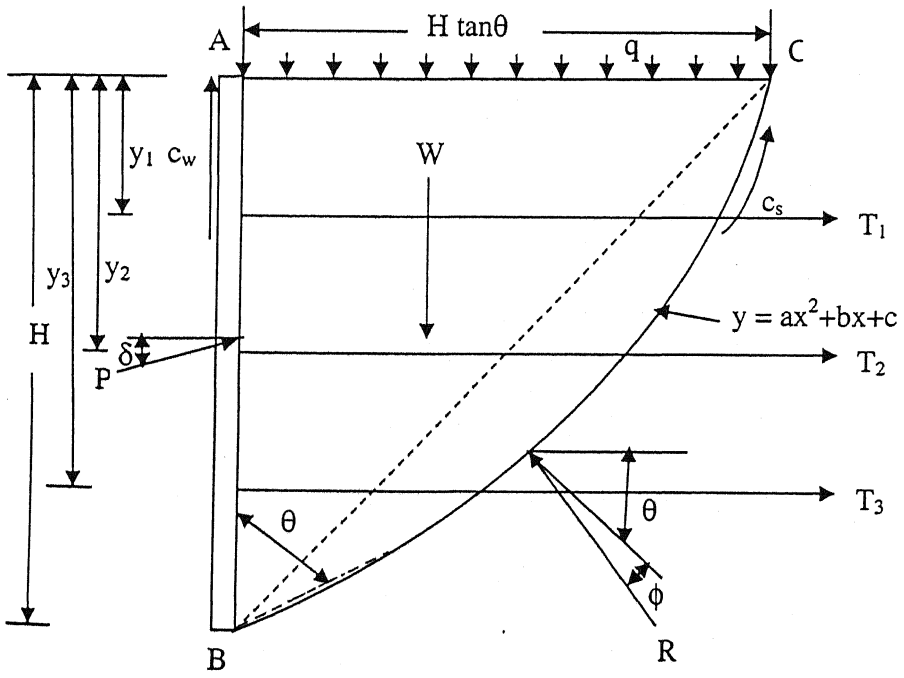

Figure 5.6: Forces acting on cantilever retaining wall (uniform surcharge, reinforced backfill)

Following forces act on the wedge ABC:

q = Uniformly distributed surcharge load per square unit length of wall.

All other forces acting are same as shown in figure 5.4.

Balancing all the forces acting on the wedge, as solved in the previous cases,

$$P = \frac{(W + qH\tan\theta).\cos(\theta+\phi)}{\sin(\theta+\phi+\delta)} - \frac{c_w H\cos(\delta+\phi) + c_s H\cos\phi\sec\delta + T\sin(\delta+\phi)}{\sin(\theta+\phi+\delta)} \qquad (5.14)$$

5.2.3 Analysis of a counterfort retaining wall

Analysis is developed by considering different conditions. There may be six cases of analysis.

a) Retaining wall without loading and without reinforced backfill.

b) Retaining wall with line load and without reinforced backfill.

c) Retaining wall with uniform surcharge and without reinforced backfill.

d) Retaining wall without loading and with reinforced backfill.

e) Retaining wall with line load and reinforced backfill.

f) Retaining wall with uniform surcharge and reinforced backfill.

5.2.3.1 Retaining wall without loading and without reinforced backfill

Consider a retaining wall of height H with vertical back and counterfort made of mild steel making an angle θ_1 with the wall, retaining a horizontal cohesive-frictional backfill of dry density γ, internal friction angle ϕ and cohesion c_s. The density of the steel is γ_c. There is no surcharge on the unreinforced backfill (shown in figure 5.7).

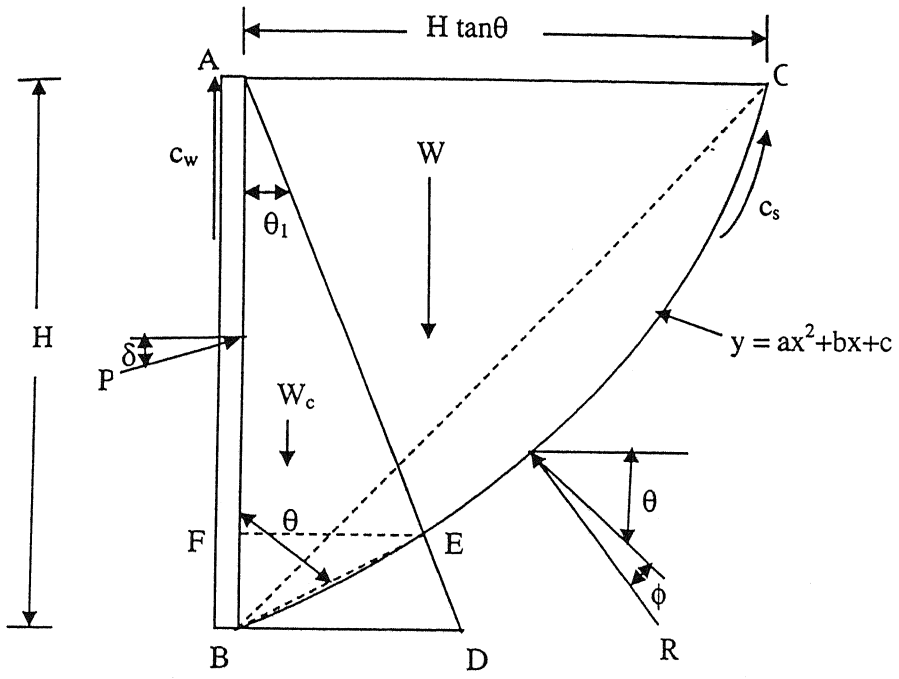

Figure 5.7: Forces acting on counterfort retaining wall (without loading, unreinforced backfill)

Following forces act on the wedge ABC:

W_c = Weight of the ABE portion of the counterfort.

All other forces acting are same as shown in figure 5.1.

It is known that, equation of the parabola: $y = ax^2+bx+c$ (5.15)

Where a, b and c are constants.

Now, equation of the line AD is:

$$y = -\frac{x}{\tan\theta_1} + H = -mx + H \qquad (5.16)$$

So, we can get the intersection point E of the equations 5.15 and 5.16 by solving these two equations.

So, FE = x_E = x co-ordinate of E = $\dfrac{-b-m+\sqrt{(b+m)^2-4a(c-H)}}{2a}$

$W_c = \gamma_c . \frac{1}{2} . x_E . H$, by taking BE portion as linear.

Balancing all the forces acting on the wedge, as solved in the previous cases,

$$P = \frac{(W+W_c).\cos(\delta+\phi)}{\sin(\theta+\phi+\delta)} - \frac{c_w H\cos(\delta+\phi)+c_s H\cos\phi\sec\delta}{\sin(\theta+\phi+\delta)} \qquad (5.17)$$

5.2.3.2 Retaining wall with line load and without reinforced backfill

Consider a retaining wall of height H with vertical back and counterfort made of mild steel making an angle θ_1 with the wall, retaining a horizontal cohesive-frictional backfill of dry density γ, internal friction angle ϕ and cohesion c_s. The density of the steel is γ_c. The unreinforced backfill supports line load of intensity of Q per unit length of wall acting at a distance of X from back face of wall (shown in figure 5.8).

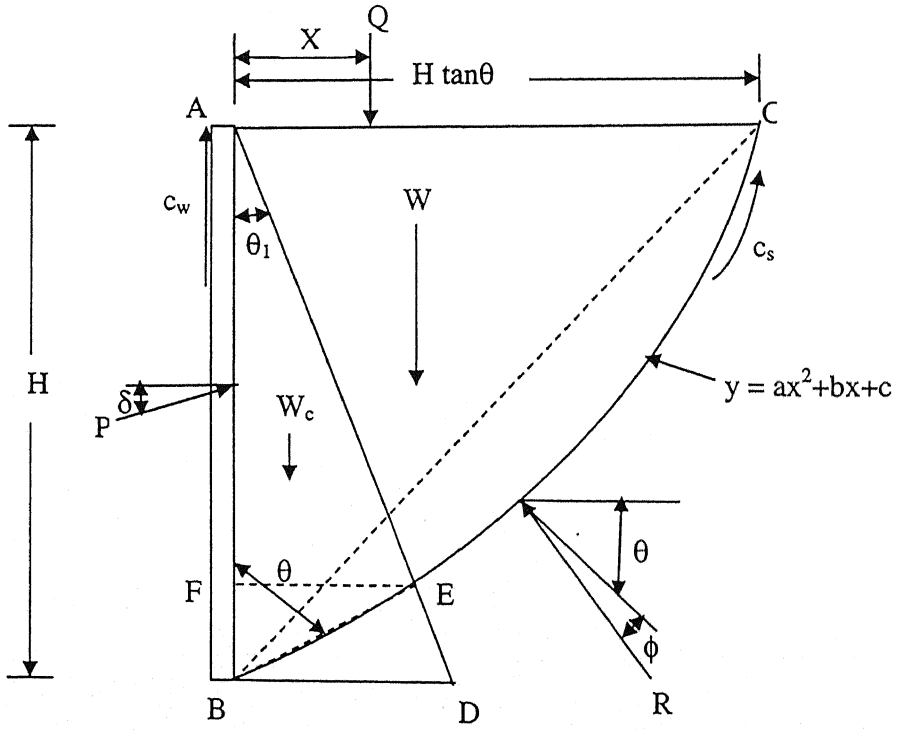

Figure 5.8: Forces acting on counterfort retaining wall (line load, unreinforced backfill)

Following forces act on the wedge ABC:

W_c = Weight of the ABE portion of the counterfort.

All other forces acting are same as shown in figure 5.2.

Balancing all the forces acting on the wedge, as solved in the previous cases,

(a) If $H \tan\delta < X$ then,

$$P = \frac{(W + W_c).\cos(\delta + \phi)}{\sin(\theta + \phi + \delta)} - \frac{c_w H \cos(\delta + \phi) + c_s H \cos\phi \sec\delta}{\sin(\theta + \phi + \delta)} \qquad (5.18a)$$

(b) If $H \tan\delta \geq X$ then,

$$P = \frac{(W + Q + W_c).\cos(\delta + \phi)}{\sin(\theta + \phi + \delta)} - \frac{c_w H \cos(\delta + \phi) + c_s H \cos\phi \sec\delta}{\sin(\theta + \phi + \delta)} \qquad (5.18b)$$

5.2.3.3 Retaining wall with uniform surcharge and without reinforced backfill

Consider a retaining wall of height H with vertical back and counterfort made of mild steel making an angle θ_1 with the wall, retaining a horizontal cohesive-frictional backfill of dry density γ, internal friction angle ϕ and cohesion c_s. The density of the steel is γ_c. The unreinforced backfill supports uniformly distributed surcharge load of intensity q per square unit length of wall (shown in figure 5.9).

Following forces act on the wedge ABC:

W_c = Weight of the ABE portion of the counterfort.

All other forces acting are same as shown in figure 5.3.

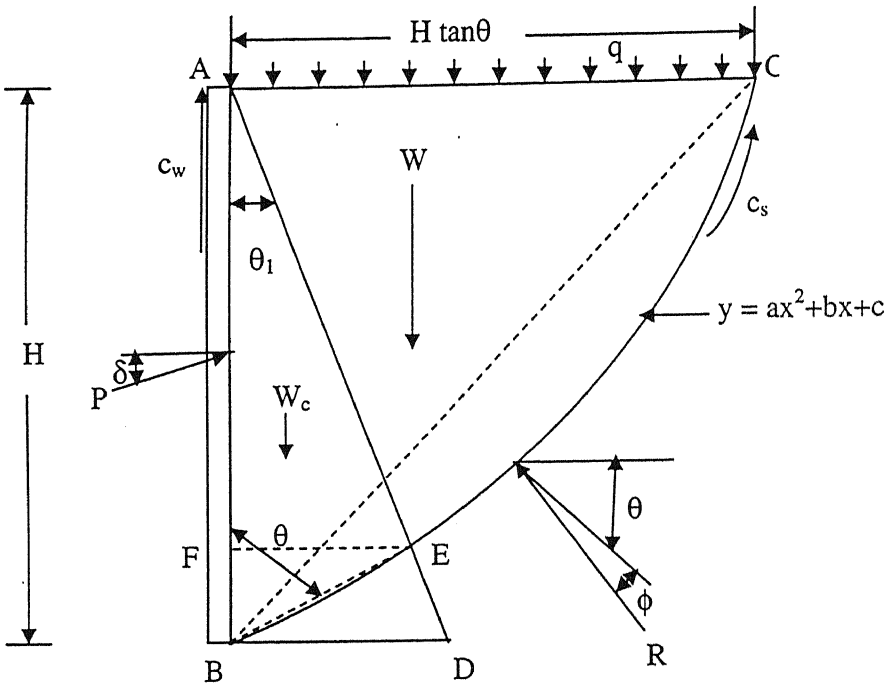

Figure 5.9: Forces acting on counterfort retaining wall (uniform surcharge, unreinforced backfill)

Balancing all the forces acting on the wedge, as solved in the previous cases,

$$P = \frac{(W + qH\tan\theta + W_c).\cos(\theta+\phi)}{\sin(\theta+\phi+\delta)} - \frac{c_w H\cos(\theta+\phi) + c_s H\cos\phi\sec\theta}{\sin(\theta+\phi+\delta)} \qquad (5.19)$$

5.2.3.4 Retaining wall without loading and with reinforced backfill

Consider a retaining wall of height H with vertical back and counterfort made of mild steel making an angle θ_1 with the wall, retaining a horizontal cohesive-frictional backfill of dry density γ, internal friction angle ϕ and cohesion c_s. The density of the steel is γ_c. There is no surcharge on the reinforced backfill (shown in figure 5.10).

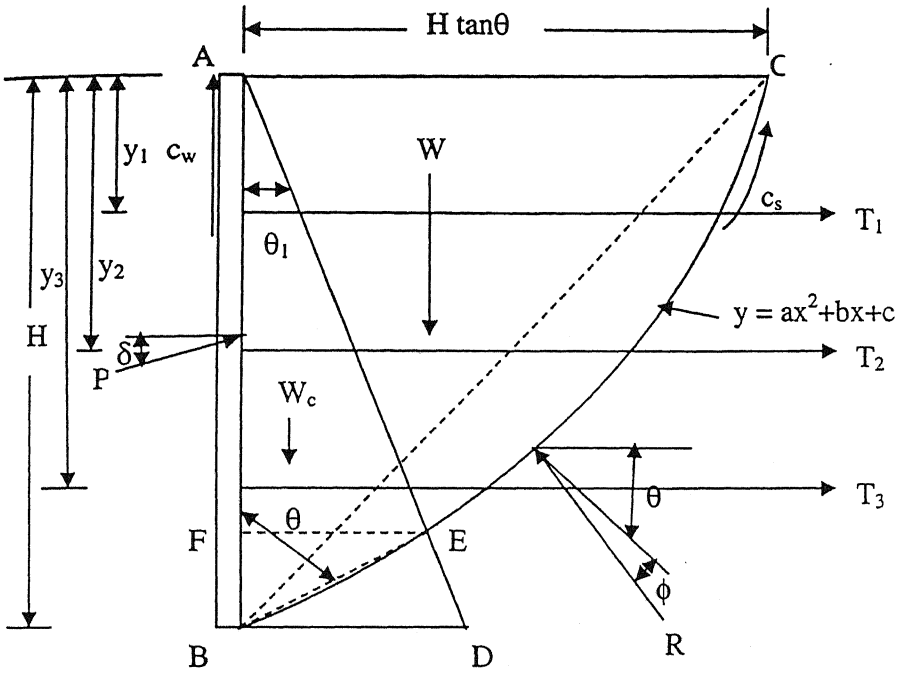

Figure 5.10: Forces acting on counterfort retaining wall (without loading, reinforced backfill)

Following forces act on the wedge ABC:

W_c = Weight of the ABE portion of the counterfort.

All other forces acting are same as shown in figure 5.4.

Balancing all the forces acting on the wedge, as solved in the previous cases,

$$P = \frac{(W+W_c).\cos(\theta+\phi)}{\sin(\theta+\phi+\delta)} - \frac{c_w H\cos(\theta+\phi)+c_s H\cos\phi\sec\theta+T\sin(\theta+\phi)}{\sin(\theta+\phi+\delta)} \quad (5.20)$$

5.2.3.5 Retaining wall with line load and reinforced backfill

Consider a retaining wall of height H with vertical back and counterfort made of mild steel making an angle θ_1 with the wall, retaining a horizontal cohesive-frictional backfill of dry density γ, internal friction angle ϕ and cohesion c_s. The density of the steel is γ_c. The reinforced

backfill supports line load of intensity of Q per unit length of wall acting at a distance of X from back face of wall (shown in figure 5.11).

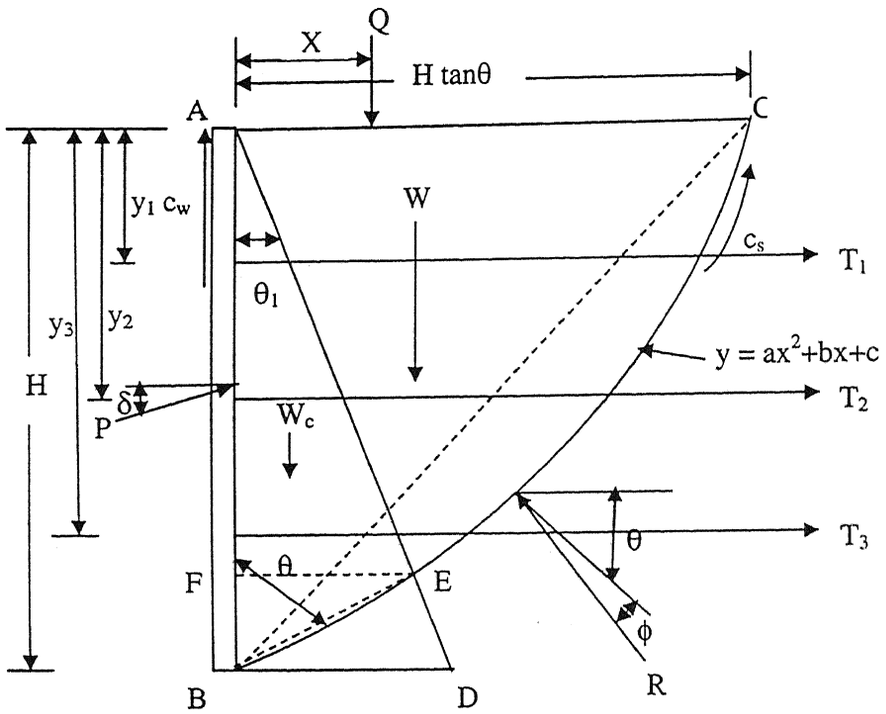

Figure 5.11: Forces acting on counterfort retaining wall (line load, reinforced backfill)

Following forces act on the wedge ABC:

W_c = Weight of the ABE portion of the counterfort.

All other forces acting are same as shown in figure 5.5.

Balancing all the forces acting on the wedge, as solved in the previous cases,

(a) If $H \tan\theta < X$ then,

$$P = \frac{(W + W_c).\cos(\theta + \phi)}{\sin(\theta + \phi + \delta)} - \frac{c_w H \cos(\theta + \phi) + c_s H \cos\phi \sec\theta + T \sin(\theta + \phi)}{\sin(\theta + \phi + \delta)} \qquad (5.21a)$$

(b) If $H \tan\theta \geq X$ then,

$$P = \frac{(W + Q + W_c).\cos(\theta + \phi)}{\sin(\theta + \phi + \delta)} - \frac{c_w H \cos(\theta + \phi) + c_s H \cos\phi \sec\theta + T \sin(\theta + \phi)}{\sin(\theta + \phi + \delta)} \qquad (5.21b)$$

5.2.3.6 Retaining wall with uniform surcharge and reinforced backfill

Consider a retaining wall of height H with vertical back and counterfort made of mild steel making an angle θ_1 with the wall, retaining a horizontal cohesive-frictional backfill of dry density γ, internal friction angle ϕ and cohesion c_s. The density of the steel is γ_c. The reinforced backfill supports uniformly distributed surcharge load of intensity q per square unit length of wall (shown in figure 5.12).

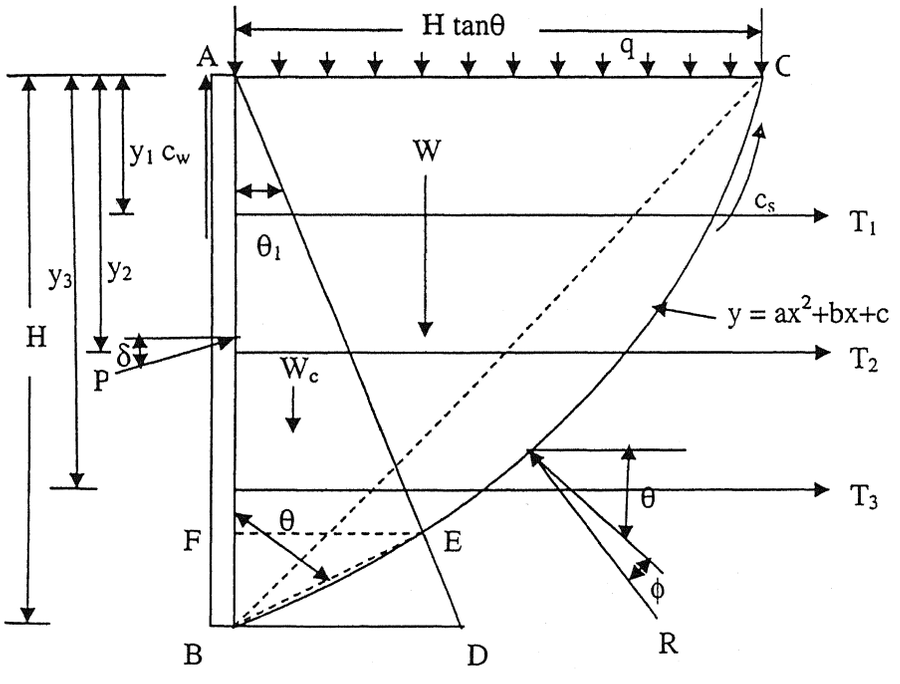

Figure 5.12: Forces acting on counterfort retaining wall (uniform surcharge, reinforced backfill)

Following forces act on the wedge ABC:

W_c = Weight of the ABE portion of the counterfort.

All other forces acting are same as shown in figure 5.6.

Balancing all the forces acting on the wedge, as solved in the previous cases,

$$P = \frac{(W + qH\tan\theta + W_c).\cos(\theta + \phi)}{\sin(\theta + \phi + \delta)} - \frac{c_w H\cos(\theta + \phi) + c_s H\cos\phi\sec\theta + T\sin(\theta + \phi)}{\sin(\theta + \phi + \delta)} \quad (5.22)$$

5.3 Planar failure surface

Analytical Methods based on planar failure surfaces, have been developed to predict the lateral earth pressure and overturning moment on the retaining wall with vertical back face having horizontal reinforced frictional cohesive backfill subjected to uniformly distributed surcharge load by considering stability of the failure wedge. The analyses generally involve certain assumptions to arrive at simple solutions. Since soil is highly variable in nature, it needs to have some assumptions about its behavior and composition to develop analytical solutions.

5.3.1 Assumptions

The following assumptions were made in order to proceed with the analysis of a rigid wall retaining reinforced fill:

a) The backfill is homogeneous and isotropic.

b) The coefficient of friction between the soil and the reinforcement is independent of the overburden pressure and the dimensions of the reinforcement.

c) The failure surface is a plane passing through the heel of the retaining wall.

d) The frictional resistance offered by each reinforcing strip to the lateral movement of the wedge is uniformly distributed over a fill height equal to the vertical spacing of the reinforcement encompassing that fill layer.

e) The failure plane divides the length of reinforcing strip in two zones, one that lies within failure wedge and another outside. Only the part of strip which experiences movement of soil relative to itself is assumed to be contributing frictional resistance.

f) The retaining wall undergoes an outward movement or rotation about the base which is sufficient to cause mobilization of frictional resistance in the soil as well as reinforcing strips.

g) No water pressures develop within the reinforced backfill.

5.3.2 Analysis of a cantilever retaining wall

This analysis is for a retaining wall of height H with a vertical back face, retaining a horizontal cohesive-frictional fill of dry density γ and an angle of internal friction ϕ supporting uniformly distributed surcharge load of intensity q (shown in figure 5.13a). It is reinforced with unattached horizontally laid strips of length L and width w at vertical spacing S_z and horizontal spacing S_x. A failure plane BC making an angle θ with the vertical passes through the heel of the retaining wall. The frictional resistance to the lateral movement of the wedge ABC contributed by a reinforcing strip is computed from its effective length (l_e). Effective length is the portion of the strip that experiences movement of soil relative to itself. Reinforcing strip located completely within the moving wedge will not contribute any frictional resistance to the movement of the wedge.

An element PQRS (shown in figure 5.13a) of the failure wedge of thickness dy, located at a distance y from the top of the wedge, is in equilibrium under the following intensities of forces:

σ_y = pressure intensity acting on PQ in the downward vertical direction.

$(\sigma_y + d\sigma_y)$ = pressure intensity acting on RS in the upward vertical direction.

R' = reaction intensity on SQ acting at an angle ϕ to the normal to SQ.

p = pressure intensity on PR acting at an angle δ with the normal to PR.

W = weight of slice PQSR acting downwards.

T = Tensile force in the strip assumed transmitted uniformly to soil layer of thickness S_z encompassing the strip.

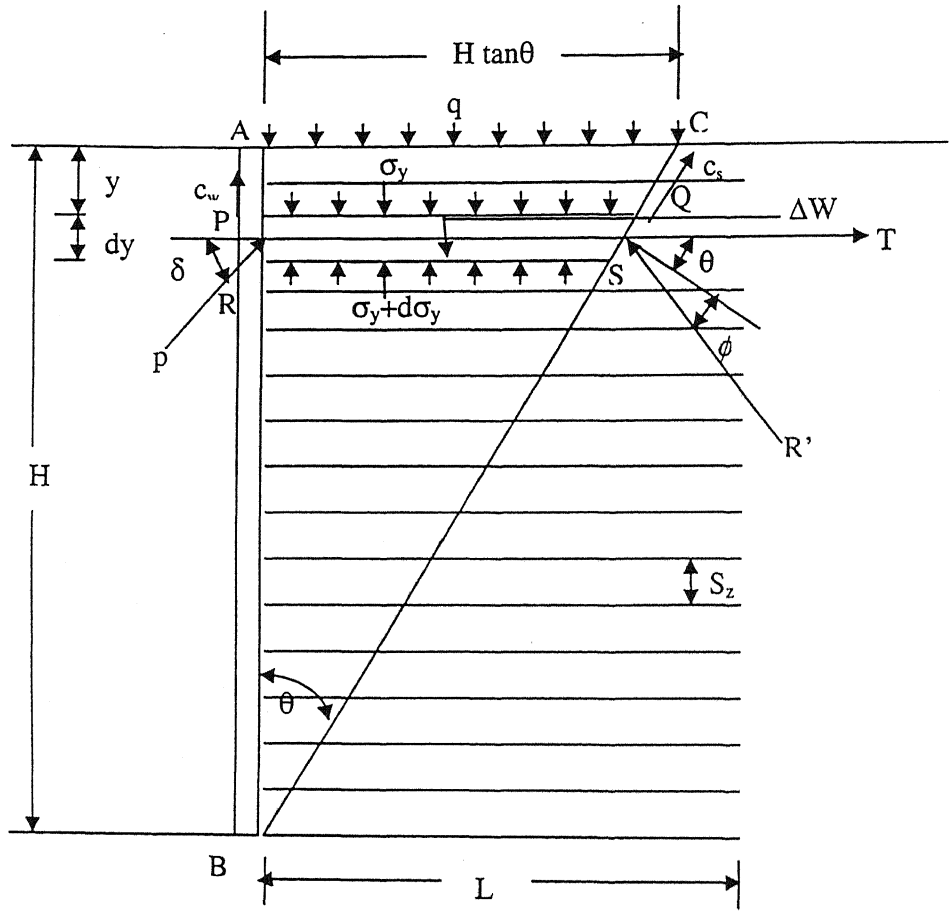

Figure 5.13(a): Wall details with reinforcement (cantilever retaining wall)

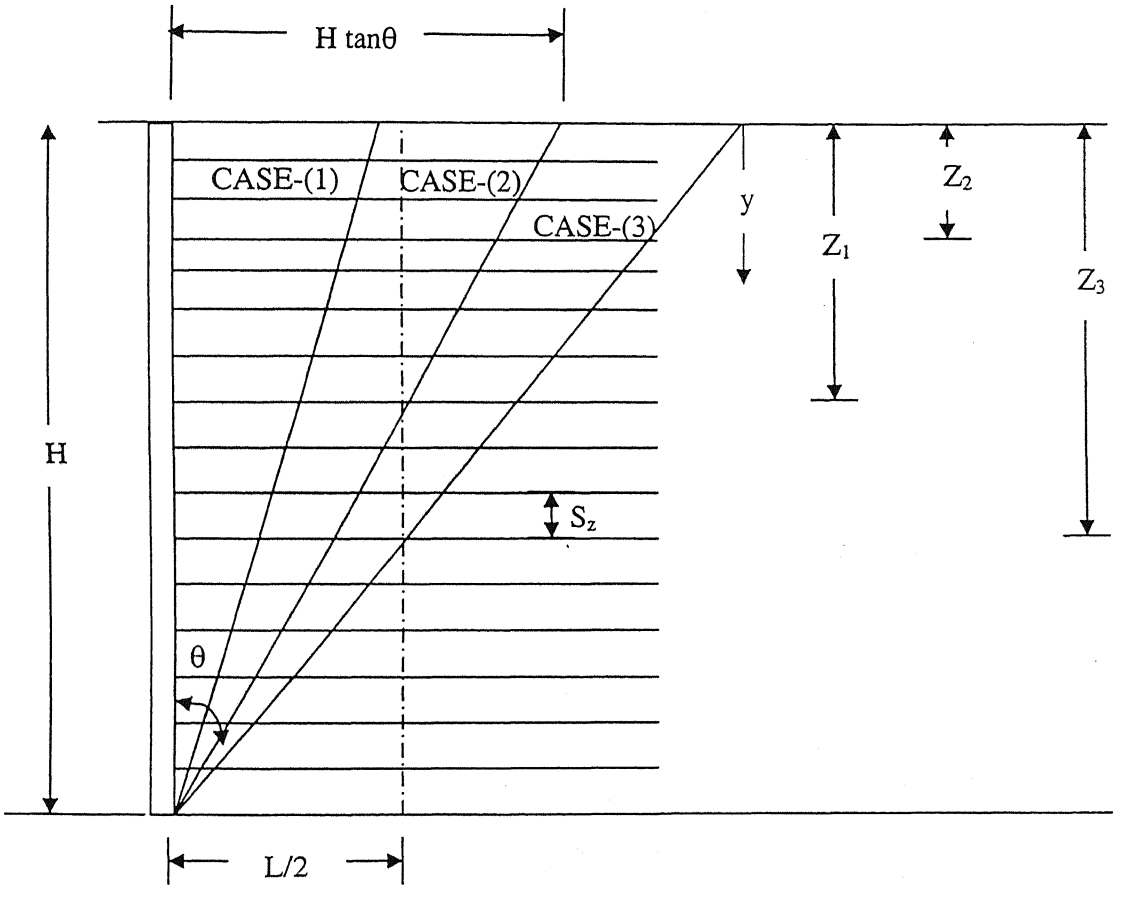

Figure 5.13(b): Schematic representation of three cases of analysis (cantilever retaining wall)

$$t = \frac{T}{S_z} = \frac{2.w.f * l_e.\sigma_v}{S_x.S_z}$$

c_s = cohesion of the soil.

c_w = adhesion between the soil and wall acting per unit length.

θ = angle of the rupture surface with vertical.

(i) Considering static equilibrium of element under the action of all forces in the horizontal direction, i.e,

$$\sum H = 0.$$

$$p\cos\delta.PR - R'\cos(\theta + \phi).QS + c_s.\sin\theta.QS + t.dy = 0.$$

Where, $PQ = (H - y)\tan\theta$, $RS = (H - y - dy)\tan\theta$, $QS = \frac{dy}{\cos\theta}$, PR = dy.

$$\text{Thus, } R' = \frac{p.\cos\phi.\cos\theta}{\cos(\theta + \phi)} + c_s.\frac{\sin\theta}{\cos(\theta + \phi)} + \frac{t.\cos\theta}{\cos(\theta + \phi)} \qquad (5.23)$$

(ii) Weight of element PQRS is,

$$\Delta W = \gamma.(H - y).\tan\theta.dy$$

Considering static equilibrium of element under action of all forces in the vertical direction, i.e,

$$\sum V = 0.$$

$$p\sin\delta.PR + R'\sin(\theta + \phi).QS + (\sigma_y + d\sigma_y).RS - \Delta W - \sigma_y.PQ + c_w.PR + c_s\cos\theta.QS = 0$$

Substituting the value of PR, QS, RS, PQ and ΔW in the above equation and on further simplification [after substituting the value of R' from equation (5.23)] we get,

$$\frac{d\sigma_y}{dy} = \gamma + \frac{\sigma_y}{(H-y)} - \frac{p\cos\phi}{(H-y)\sin\theta}\{\sin\delta + \cos\delta.\tan(\theta+\phi)\} - \frac{c_s}{(H-y)}\{\frac{\cos\theta}{\sin\theta} + \tan(\theta+\phi)\}$$

$$-\frac{c_w}{(H-y)}.\frac{\cos\theta}{\sin\theta} - \frac{t.\tan(\theta+\phi).\cos\theta}{\sin\theta.(H-y)}.$$ or

$$\frac{d\sigma_y}{dy} = \frac{\sigma_y}{H-y} + \gamma - \frac{p}{H-y}V_3 - \frac{c_s}{H-y}V_4 - \frac{c_w}{H-y}V_5 - \frac{t}{H-y}V_6 \qquad (5.24)$$

Where, $V_1 = \tan\delta$

$$V_2 = \frac{\cos\theta}{\cos(\theta+\phi)}$$

$$V_3 = \left\{\frac{\sin\delta}{V_1} + \frac{V_2}{V_1}.\frac{\sin(\theta+\phi).\cos\delta}{\cos\theta}\right\}$$

$$V_4 = \left\{\frac{1}{V_1} + \frac{V_2}{V_1}\tan\theta.\frac{\sin(\theta+\phi)}{\cos\theta}\right\}$$

$$V_5 = \frac{1}{V_1}$$

$$V_6 = \left\{\frac{V_2}{V_1}\frac{\sin(\theta+\phi)}{\cos\theta}\right\}$$

(iii) Taking moments of all the forces about the mid point (D) of element PQRS between Q and S, i.e.

$$c_w.dy(H-y).A - \frac{\gamma A^2}{2}(H-y)^2dy - \sigma_y(H-y)A\left\{\frac{(H-y)A}{2} - \frac{\sin\theta.dyB}{2}\right\} + p.\sin\delta.(H-y).A.dy$$

$$+(\sigma_y + d\sigma_y).A.(H-y-dy)\left\{\frac{(H-y-dy)A}{2} + \frac{\sin\theta.dy.B}{2}\right\} = 0.$$

where, $A = \frac{\sin\delta}{\cos\delta}$ and $B = \frac{1}{\cos\delta.}$

On simplification and neglecting small quantities of higher order, the above equation reduces to –

$$\frac{d\sigma_y}{dy} = \gamma - \frac{2p\sin\delta}{(H-y).V_1} - \frac{2c_w}{V_1(H-y)} \qquad (5.25)$$

Equating equations (5.24) and (5.25) we get, after simplification,

$$p = \frac{\sigma_y}{V_7} - c_s \cdot \frac{V_4}{V_7} - c_w \cdot \frac{1}{V_7}\left\{V_5 - \frac{2}{V_1}\right\} - t.\frac{V_6}{V_7} \tag{5.26}$$

Where, $V_7 = \left\{V_3 - \frac{2.\sin\delta}{V_1}\right\}$

or, $p = \sigma_y(S_1) - c_s(S_2) - c_w(S_3) - t(S_4)$

Where, $S_1 = \frac{1}{V_7}$

$S_2 = \frac{V_4}{V_7}$

$S_3 = \frac{\left(V_5 - \frac{2}{V_1}\right)}{V_7}$

$S_4 = \frac{V_6}{V_7}$

On differentiating equation (5.26) w.r.t. y, we get,

$$\frac{dp}{dy} = \frac{d\sigma_y}{dy}(S_1) - \frac{dt}{dy}(S_4) \tag{5.27}$$

Substituting the value of $\frac{d\sigma_y}{dy}$ from equation (5.25) into equation (5.27),

$$\frac{dp}{dy} = -\frac{p}{(H-y)}C_1 + \gamma.C_2 + \frac{c_w}{(H-y)}C_3 - \frac{dt}{dy}C_4 \tag{5.28}$$

Where, $C_1 = \frac{2S_1\sin\delta}{V_1}$

$C_2 = S_1$

$C_3 = -\frac{2S_1}{V_1}$

$C_4 = S_4$

Tension, T at limiting equilibrium can be taken as given below:

$$T = 2\left\{\gamma\left(y + \frac{dy}{2}\right) + q\right\}.w.l_e.f^* + 2.C_r.w.l_e \qquad (5.29)$$

Where, l_e = effective length of reinforcing strip.

w = width of reinforcing strip.

C_r = co-efficient of adhesion with reinforcement.

$f^* = \tan\delta$ = apparent co-efficient of friction between soil and reinforcement

from equation (5.29),

$$t = \frac{2wf^* l_e\left[\gamma\left(y + \frac{dy}{2}\right) + q\right] + 2C_r w l_e}{S_x.S_z} \qquad (5.30)$$

where, S_x and S_z are horizontal and vertical spacings of reinforcing strips respectively.

The values of l_e will vary from strip to strip and will depend on wedge angle θ and length L of the strip. There may be three cases of analysis [as shown in the figure 5.13(b)].

CASE 1 $H\tan\theta \le L/2$

$$l_e = \left(H - y - \frac{dy}{2}\right)\tan\theta \text{ for all reinforcing elements} \qquad (5.31)$$

CASE 2 $L./2 \le H\tan\theta \le L$

$$l_e = L - (H - y - \frac{dy}{2})\tan\theta, \quad \text{for } y \le Z_1 \qquad (5.32)$$

$$l_e = (H - y - \frac{dy}{2})\tan\theta, \quad \text{for } y > Z_1 \qquad (5.33)$$

CASE 3 $H\tan\theta \ge L$

$$l_e = 0, \quad \text{for } y \le Z_2 \qquad (5.34)$$

$$l_e = L - (H - y - \frac{dy}{2})\tan\theta, \quad \text{for } Z_2 \le y \le Z_3 \qquad (5.35)$$

$$l_e = (H - y - \frac{dy}{2}) \tan\theta, \qquad \text{for} \quad y > Z_3 \tag{5.36}$$

Z_1, Z_2 and Z_3 are shown in fig (5.13b).

PRESSURE INTENSITY ON WALL

CASE 1 $H \tan 6 \leq L/2$

$$l_e = \left(H - y - \frac{dy}{2} \right) \tan\theta$$

$$= (H - y) \tan 6, \text{ neglecting dy/2 being small.}$$

$$t = \frac{2wf^* \left[\gamma \left(y + \frac{dy}{2} \right) + q \right] .(H - y) \tan\theta + 2C_r w.(H - y) \tan\theta}{S_x . S_z} \tag{5.37}$$

$$\frac{dt}{dy} = 2D_P \gamma \tan\theta \left[\left(1 - \frac{2y}{H} \right) - \frac{q}{\gamma H} \right] - 2D_C \tan\theta . \gamma \tag{5.38}$$

Where, $D_P = \frac{wf^* H}{S_x S_z}$ and $D_C = \frac{C_r w H}{\gamma H . S_x S_z}$

Here,

D_P = non-dimensional spacing coefficient

D_C = non-dimensional coefficient for adhesion with reinforcement.

Substituting the values of dt/dy from equation (5.38) to (5.28), we get,

$$\frac{dp}{dy} = -\frac{p}{(H - y)} C_1 + \gamma . C_2 + \frac{c_w}{(H - y)} C_3 - C_4 \left[2D_P . \gamma . \tan\theta \left\{ \left(1 - \frac{2y}{H} \right) - \frac{q}{\gamma H} \right\} - 2D_C . \tan\theta . \gamma \right] \tag{5.28a}$$

Integral function of the above equation is $(H - y)^{-C_1}$

Therefore,

$$\frac{p}{(H-y)^{C_1}} = -\frac{C_2.\gamma.(H-y)^{1-C_1}}{1-C_1} + \frac{c_w.C_3(H-y)^{-C_1}}{C_1} - 2C_4 D_P.\gamma.\tan\theta.$$

$$\left[\frac{2(H-y)^{2-C_1}}{H(1-C_1)(2-C_1)} - \left\{1 - \frac{2y}{H} - \frac{q}{\gamma H}\right\}\frac{(H-y)^{(1-C_1)}}{1-C_1}\right] - 2.D_C.C_4\tan\theta.\gamma\frac{(H-y)^{1-C_1}}{1-C_1} + I \qquad (5.39)$$

Where, I = Constant of integration.

Applying boundary condition that at y = 0, $\sigma_y = q$ in equation (5.26), we get,

$$\frac{p}{H^{C_1}} = \frac{q\sin\theta}{\cos\theta.D_1.H^{C_1}} - \frac{c_s.\cos\phi}{D_1.\cos(\theta+\phi)\cos\theta.H^{C_1}} + \frac{c_w.\sin\delta}{H^{C_1}.\cos\theta.D_1}.\frac{1}{A} - \frac{t.\tan(\theta+\phi)}{D_1.H^{C_1}} \qquad (5.26a)$$

Now, $t = t_q + t_{ca}$ $\qquad (t_\gamma = 0)$

Here, $t_q = \dfrac{2wf^*q(H-y)\tan\theta}{S_xS_z}$

$$t_{ca} = \frac{2C_r(H-y)\tan\theta.w}{S_xS_z}$$

$$t_{q_0} = 2.D_P.q\tan\delta$$

$$t_{ca_0} = 2D_C.\tan\theta.\gamma.H$$

Equation (5.26a) can be written as,

$$\frac{p}{H^{C_1}} = \frac{q\sin\theta}{H^{C_1}\cos\theta.D_1} + \frac{c_w\sin\theta}{H^{C_1}.\cos\theta.D_1}.U_1 - \frac{c_s.\cos\phi}{D_1.\cos(\theta+\phi).\cos\theta.H^{C_1}}$$

$$-\frac{2.D_P.q.\tan\theta.\tan(\theta+\phi)}{D_1.H^{C_1}} - \frac{2.D_C.\tan\theta.\gamma.H\tan(\theta+\phi)}{D_1.H^{C_1}} \qquad (5.26b)$$

Where, $U_1 = \dfrac{1}{A}$ and $D_1 = \sin(\delta+\phi-\delta)$

Equating equations (5.39) and (5.26b) for y=0, we get the value of I. Substituting this value of I in equation (5.39), we get on simplification,

$$p_1 = \frac{C_2\gamma H}{1-C_1}\left\{(1-y/H)^{C_1} - (1-y/H)\right\} + 2.C_4.D_P.\gamma.H\tan\theta.$$

$$\left\{\frac{2(1-y/H)^{C_1}}{(1-C_1)(2-C_1)} - \frac{\left(1-\frac{q}{\gamma H}\right)(1-y/H)^{C_1}}{1-C_1} - \frac{2(1-y/H)^2}{(1-C_1)(2-C_1)} + \frac{\left(1-2y-\frac{q}{\gamma H}\right)(1-y/H)}{1-C_1}\right\}$$

$$-c_s.(1-y/H)^{C_1}.\frac{\cos\phi}{D_1.\cos\theta.\cos(\theta+\phi)} + c_w.\left[\frac{C_3}{C_1} + (1-y/H)^{C_1}\left\{\frac{\sin\theta.U_1}{\cos\theta.D_1} - \frac{C_3}{C_1}\right\}\right]$$

$$-2.D_C.\tan\theta.\gamma.H\left[\frac{C_4(1-y/H)}{1-C_1} - (1-y/H)^{C_1}\left\{\frac{C_4}{1-C_1} - \frac{\tan(\theta+\phi)}{D_1}\right\}\right]$$

$$+\frac{q\sin\delta}{\cos\theta.D_1}[1-2.D_P.\tan(\theta+\phi)](1-y/H)^{C_1} \qquad (5.40)$$

CASE II A $L./2 \le H\tan\delta \le L$

$$l_e = L-(H-y-\frac{dy}{2})\tan\theta, \quad \text{for } y \le Z_1$$

$$t = \frac{2wf*\left[\gamma\left(y+\frac{dy}{2}\right)+q\right].\{L-(H-y-\frac{dy}{2})\tan\theta\} + 2C_r w.\{L-(H-y-\frac{dy}{2})\tan\theta\}}{S_x.S_z} \qquad (5.41)$$

$$\text{Therefore, } \frac{dt}{dy} = \gamma.T_1\left[\frac{L}{HT_3} - 1 + \frac{2y}{H} + \frac{q}{\gamma.H}\right] + \gamma.T_2 \qquad (5.42)$$

Where, $T_1 = 2.\tan\delta.D_P$

$$T_2 = 2.\tan\delta.D_C$$

$$T_3 = \tan\delta \qquad (5.43)$$

Equation (5.28) may be written as below,

$$\frac{dp_{2a}}{dy} = -\frac{p}{(H-y)}C_1 + \gamma.C_2 + \frac{c_w}{(H-y)}C_3 - \frac{dt}{dy}C_4$$

Substituting the value of $\frac{dt}{dy}$ from equation (5.42) in above equation,

$$\frac{dp_{2a}}{dy}+\frac{p}{(H-y)}C_1=\gamma.C_2+\frac{c_w}{(H-y)}C_3-C_4.\gamma.T_1\left\{\frac{L}{HT_3}-1+\frac{2y}{H}+\frac{q}{\gamma H}\right\}-C_4\gamma T_2 \qquad (5.44)$$

Solution of equation (5.44) is,

$$\frac{p_{2a}}{(H-y)^{C_1}}=-\frac{C_2.\gamma(H-y)^{1-C_1}}{1-C_1}+\frac{c_w.C_3(H-y)^{-C_1}}{C_1}+C_4.\gamma.\frac{L}{H}.\frac{T_1}{T_3}.\frac{(H-y)^{1-C_1}}{1-C_1}-C_4.\gamma.T_1\frac{(H-y)^{1-C_1}}{(1-C_1)}$$

$$-C_4.\gamma.T_1\frac{2}{H}\left\{-\frac{y(H-y)^{1-C_1}}{1-C_1}-\frac{(H-y)^{2-C_1}}{(1-C_1)(2-C_1)}\right\}+C_4.\gamma.T_1.\frac{q}{\gamma.H}.\frac{(H-y)^{1-C_1}}{(1-C_1)}+C_4.\gamma.T_2\frac{(H-y)^{1-C_1}}{(1-C_1)}+I \qquad (5.45)$$

Equating the above equation with (5.26b) at boundary condition that at y = 0, $\sigma_y = q$, we get

on simplification,

$$p_{2a}=\{(1-y/H)-(1-y/H)^{C_1}\}\left\{\frac{C_4.\gamma.L}{1-C_1}.\frac{T_1}{T_3}-\frac{C_4\gamma T_1H}{1-C_1}+\frac{C_4.T_1q}{1-C_1}+\frac{C_4T_2\gamma H}{1-C_1}-\frac{\gamma.C_2H}{1-C_1}\right\}$$

$$+\left\{1-\left(1-\frac{y}{H}\right)^{C_1}\right\}\frac{c_w.C_3}{C_1}+\frac{2.C_4\gamma HT_1}{(1-C_1)(2-C_1)}\{(1-y/H)^2-(1-y/H)^{C_1}\}+\frac{2C_4\gamma T_1y(1-y/H)}{(1-C_1)}$$

$$+\frac{q\sin\theta(1-y/H)^{C_1}}{\cos\theta.D_1}-\frac{c_s.\cos\phi(1-y/H)^{C_1}}{D_1\cos(\theta+\phi)\cos\theta}+\frac{c_w\sin\theta}{\cos\theta.D_1}.\frac{1}{A}.(1-y/H)^{C_1}$$

$$-\{2.D_P.q\tan\theta+2.D_C.\gamma.H\tan\theta\}\frac{\tan(\theta+\phi)(1-y/H)^{C_1}(L/H-1)}{D_1} \qquad (5.46)$$

CASE II (B)

For $y > Z_1$, the effective length will be (H-y) tanθ and pressure intensity p_{2b} can be obtained by integrating equation (5.28a) over the domain $y = Z_1$ to H for the boundary condition that at $y = Z_1$, $p_{2b} = (p_2)_{y=Z_1}$, where p_{2b} represents the pressure intensity at any depth $Z_1 < y < H$.

Equation (5.39) at $y = Z_1$ shall be

$$p_{2b} = -\frac{C_2.\gamma(H-Z_1)}{1-C_1} + \frac{c_w.C_3}{C_1} - 2.C_4.D_P.\gamma.\tan\theta\left\{\frac{2(H-Z_1)^2}{H(1-C_1)(2-C_1)} - \left(1-\frac{2Z_1}{H}-\frac{q}{\gamma H}\right)\frac{(H-Z_1)}{1-C_1}\right\}$$

$$-2.D_C.C_4.\tan\theta.\gamma.\frac{(H-Z_1)}{1-C_1} + I.(H-Z_1)^{C_1} \qquad (5.39a)$$

To evaluate I, apply boundary conditions same as before and equate it to equation (5.46). After substituting the value of I in equation (5.39), the pressure intensity p_{2b} is given by following equation,

$$p_{2b} = \frac{(1-y/H)}{1-C_1}\left\{-C_2.\gamma.H + C_4\gamma HT_1\left(1-\frac{2y}{H}-\frac{q}{\gamma H}\right) - T_2C_4\gamma H\right\}$$

$$-\frac{2C_4\gamma HT_1}{(1-C_1)(2-C_1)}\left\{(1-y/H)^2 - (1-Z_1/H)^{2-C_1}.(1-y/H)^{C_1}\right\} + \frac{c_wC_3}{C_1}\left\{1-\frac{(1-y/H)^{C_1}}{(1-Z_1/H)^{C_1}}\right\}$$

$$+\frac{C_2\gamma.H(1-Z_1/H)^{1-C_1}(1-y/H)^{C_1}}{1-C_1} - C_4.\gamma.H.T_1\left(1-\frac{2Z_1}{H}-\frac{q}{\gamma H}\right)\frac{(1-Z_1/H)^{1-C_1}(1-y/H)^{C_1}}{1-C_1}$$

$$+\frac{T_2C_4\gamma.H(1-Z_1/H)^{1-C_1}(1-y/H)^{C_1}}{1-C_1} + \left\{(1-Z_1/H)^{1-C_1}-1\right\}$$

$$\left\{-\frac{\gamma.C_2.H}{1-C_1} + \frac{C_4\gamma.L}{1-C_1}.\frac{T_1}{T_3} - \frac{C_4\gamma HT_1}{1-C_1} + \frac{C_4T_1q}{1-C_1} + \frac{C_4T_2\gamma.H}{1-C_1}\right\}.(1-y/H)^{C_1}$$

$$+\left\{\frac{1}{(1-Z_1/H)^{C_1}}-1\right\}(1-y/H)^{C_1}.\left\{\frac{c_w.C_3}{C_1}\right\} + \frac{2C_4\gamma HT_1(1-y/H)^{C_1}}{(1-C_1)(2-C_1)}.\left\{(1-Z_1/H)^{2-C_1}-1\right\}$$

$$+\frac{2C_4.\gamma.Z_1T_1(1-Z_1/H)^{1-C_1}.(1-y/H)^{C_1}}{1-C_1} + \frac{(1-y/H)^{C_1}}{\cos\theta.D_1}\left\{q\sin\theta - \frac{c_1\cos\phi}{\cos(\theta+\phi)}\right\}$$

$$+\frac{(1-y/H)^{C_1}}{\cos\theta.D_1}.c_w.\sin\theta.\frac{1}{A} - \frac{\{qT_1+\gamma.HT_2\}\tan(\theta+\phi)(1-y/H)^{C_1}(L/H-1)}{D_1} \qquad (5.47)$$

CASE III A

$H \tan 6 \geq L$

For the domain y =0 to y = Z_2, the failure surface is not cut by any reinforcing element and passes through soil alone. Therefore, no part of strip will experience movement of soil relative to itself and the value of it will be equal to zero. The differential equation (5.28) will thus become,

$$\frac{dp}{dy} = -\frac{p}{(H-y)}C_1 + \gamma.C_2 + \frac{c_w}{(H-y)}C_3 \qquad (5.48)$$

Solution of the above equation will also be done for the boundary condition that at y = 0, $\sigma_y = q$.

From equation (5.48), we can get,

$$\frac{dp}{dy} + C_1.\frac{p}{(H-y)} = \gamma.C_2 + \frac{c_w.C_3}{(H-y)}$$

$$\text{or, } \frac{p}{(H-y)^{C_1}} = -\frac{\gamma.C_2(H-y)^{1-C_1}}{1-C_1} + \frac{c_w.C_3(H-y)^{-C_1}}{C_1} + I \qquad (5.48a)$$

$$\text{or, } p = -\frac{\gamma.C_2(H-y)}{1-C_1} + \frac{c_w.C_3}{C_1} + I.(H-y)^{C_1} \qquad (5.48b)$$

Substituting the value of I by equating equation (5.48a) with equation (5.26) for $\sigma_y = q$ and t = 0, in equation (5.48b), we get on simplification,

$$\text{Or, } p_{3a} = \frac{\gamma.C_2.H}{1-C_1}\left\{(1-y/H)^{C_1} - (1-y/H)\right\} + \left[\left\{1-(1-y/H)^{C_1}\right\}\left\{\frac{c_w.C_3}{C_1}\right\}\right]$$

$$-(1-y/H)^{C_1}\left\{\frac{c_s.\cos\phi}{D_1.\cos(\theta+\phi)\cos\theta} - \frac{q\sin\theta}{\cos\theta.D_1} - \frac{c_w\sin\theta}{D_1\cos\theta}.\frac{1}{A}\right\} \qquad (5.49)$$

CASE III B

For the region y = Z_2 to Z_3, the equation for pressure intensity p_{3b} can be evaluated by solving equation (5.45) with the boundary condition that at y = Z_2, $p_{3b} = (p_3)_{y=Z_2}$.

$$\text{Thus, } \frac{p}{(H-y)^{C_1}} = -\frac{y.C_2(H-y)^{1-C_1}}{(1-C_1)} + \frac{c_w.C_3(H-y)^{-C_1}}{C_1} + \frac{C_4.\gamma.H(H-y)^{1-C_1}}{H(1-C_1)}.\frac{T_1}{T_3}$$

$$-\frac{C_4\gamma.T_1(H-y)^{1-C_1}}{(1-C_1)} + \frac{2.C_4.\gamma.T_1y(H-y)^{1-C_1}}{H(1-C_1)} + \frac{2.C_4\gamma.T_1(H-y)^{2-C_1}}{H(1-C_1)(2-C_1)}$$

$$+\frac{C_4\gamma.T_1q(H-y)^{1-C_1}}{\gamma.H(1-C_1)} + \frac{C_4\gamma.T_2(H-y)^{1-C_1}}{(1-C_1)} + I \qquad (5.45a)$$

Equation (2.49) may be equated with equation (5.45a) at y = Z_2 for the determination of I. The pressure intensity after substituting the value of I in equation (5.45a) is determined as:

$$p_{3b} = \frac{(1-y/H)}{1-C_1}\left\{-\gamma.C_2H - C_4.\gamma.T_1H + 2.C_4\gamma.T_1y + C_4.q.T_1 + C_4.\gamma.T_2H + C_4.\gamma.H\frac{T_1}{T_3}\right\}$$

$$+\frac{C_3c_w}{C_1} + \frac{2.C_4.\gamma.T_1H(1-y/H)^2}{(1-C_1)(2-C_1)} + \frac{(1-Z_2/H)^{1-C_1}.(1-y/H)^{C_1}}{1-C_1}.\left\{C_2.\gamma.H - C_4.\gamma.H.\frac{T_1}{T_3}\right.$$

$$\left.+C_4.\gamma.T_1H - 2.C_4.\gamma.T_1Z_2 - C_4T_1q - C_4.\gamma.HT_2\right\} + \frac{(1-y/H)^{C_1}}{(1-Z_2/H)^{C_1}}\left[\frac{\gamma.C_2}{1-C_1}\left\{(1-Z_2/H)^{C_1} - (1-Z_2/H)\right\}\right.$$

$$\left.-\frac{C_3.c_w}{C_1}\right] + \frac{(1-y/H)^{C_1}}{(1-Z_2/H)^{C_1}}\left[\left\{1-(1-Z_2/H)^{C_1}\right\}\frac{C_3.c_w}{C_1}\right] - \frac{2.C_4.\gamma.HT_1(1-Z_2/H)^{2-C_1}.(1-y/H)^{C_1}}{(1-C_1)(2-C_1)}$$

$$-(1-y/H)^{C_1}\left\{\frac{c_s.\cos\phi}{D_1.\cos(\theta+\phi)\cos\theta} - \frac{q.\sin\theta}{\cos\theta.D_1} - \frac{T_3c_w\sin\theta}{D_1.\cos\theta}\right\} \qquad (5.50)$$

CASE III C

For the domain y = Z_3 to h, the pressure intensity can be computed by solving equation (28a) for boundary condition that at y = Z_3, $p_{3c} = (p_{3b})_{y=Z_3}$ equation (28a) may also be written as:

$$\frac{dp}{dy} = -\frac{p}{(H-y)}C_1 + \gamma.C_2 + \frac{c_w}{(H-y)}C_3 - C_4.\gamma.T_1\left\{1-\frac{2y}{H}-\frac{q}{\gamma.H}\right\} + C_4.T_2.\gamma$$

$$\text{or, } \frac{p_{3C}}{(H-y)^{C_1}} = -\frac{\gamma.C_2(H-y)^{1-C_1}}{1-C_1} + \frac{c_w.C_3(H-y)^{-C_1}}{C_1} + \frac{C_4.\gamma.T_1(H-y)^{1-C_1}}{1-C_1}$$

$$+\frac{2.C_4\gamma.T_1}{H}\left\{-\frac{y(H-y)^{1-C_1}}{1-C_1}-\frac{(H-y)^{2-C_1}}{(1-C_1)(2-C_1)}\right\}-\frac{C_4.\gamma.T_1.q(H-y)^{1-C_1}}{\gamma.H(1-C_1)}-\frac{C_4T_2.\gamma.(H-y)^{1-C_1}}{1-C_1}+I' \quad (5.51a)$$

he above equation (5.51a) can be equated with equation (5.50) at y = Z_3 to determine the value of I. After substituting the value of I in equation (5.51a), the pressure intensity p_{3C} may be determined by following equation:

$$p_{3C} = \frac{(1-y/H)^{C_1}}{1-C_1}\left\{-C_4.\gamma.HT_1(1-Z_3/H)^{1-C_1}+\gamma.C_2H(1-Z_3/H)^{1-C_1}+\frac{2C_4\gamma.HT_1Z_3(1-Z_3/H)^{1-C_1}}{H}\right.$$

$$\left.+C_4.T_1.q.(1-Z_3/H)^{1-C_1}+\frac{2C_4.\gamma.HT_1(1-Z_3/H)^{2-C_1}}{(2-C_1)}+C_4.T_2.\gamma.H.(1-Z_3/H)^{1-C_1}+\frac{2C_4.\gamma.H.(1-Z_3/H)^2T_1}{(2-C_1)(1-Z_3/H)^{C_1}}\right\}$$

$$+\frac{c_w.C_3}{C_1}+\frac{(1-y/H)}{1-C_1}\{-\gamma.C_2.H+C_4\gamma.HT_1-C_4T_1q-C_4T_2\gamma.H\}+2C_4\gamma.T_1(1-y/H)\left\{-\frac{y}{1-C_1}\right.$$

$$\left.-\frac{H(1-y/H)}{(1-C_1)(2-C_1)}\right\}+\frac{(1-Z_3/H)^{1-C_1}.(1-y/H)^{C_1}}{(1-C_1)}.\{-\gamma.C_2H-C_4.\gamma.T_1H+2C_4.\gamma.T_1y+C_4qT_1+C_4.\gamma.HT_2$$

$$+C_4.\gamma.H\}+I_1+I_2+I_3-(1-y/H)^{C_1}\left\{\frac{c_s.\cos\phi}{D_1.\cos(\theta+\phi)\cos\theta}-\frac{q.\sin\theta}{\cos\theta.D_1}\right\}+(1-y/H)^{C_1}\left\{\frac{c_w.\sin\theta}{\cos\theta.D_1A}\right\} \quad (5.52)$$

Where,

$$I_1 = \frac{(1-Z_2/H)^{1-C_1}.(1-y/H)^{C_1}}{1-C_1}\left\{C_2.\gamma.H - C_4.\gamma.\frac{T_1}{T_3} + C_4.\gamma.HT_1 - 2C_4\gamma.T_1Z_2 - C_4T_1q - C_4.\gamma.HT_2\right\}$$

$$I_2 = \frac{(1-y/H)^{C_1}}{(1-Z_2/H)^{C_1}}\left[\frac{\gamma.C_2}{1-C_1}\left\{(1-Z_2/H)^{C_1} - (1-Z_2/H)^{1}\right\} - \frac{c_wC_3}{C_1}\right] + \left\{1-(1-Z_2/H)^{C_1}\right\}\frac{c_wC_3}{C_1}$$

$$I_3 = \frac{2.C_4\gamma.HT_1(1-Z_2/H)^{2-C_1}.(1-y/H)^{C_1}}{(1-C_1)(2-C_1)} \qquad (5.52a)$$

5.3.3 Analysis of a counterfort retaining wall

This analysis is for a Counterfort retaining wall of height H and counterfort made of mild steel making an angle θ_1 with the wall and a vertical back face, retaining a horizontal cohesive-frictional fill of dry density γ and an angle of internal friction ϕ supporting uniformly distributed surcharge load of intensity q (shown in figure 5.14a). The density of the steel is γ_c. The wall is reinforced with unattached horizontally laid strips of length L and width w at vertical spacing S_z and horizontal spacing S_x. A failure plane BC making an angle θ with the vertical passes through the heel of the retaining wall. The frictional resistance to the lateral movement of the wedge ABC contributed by a reinforcing strip is computed from its effective length (l_e). Effective length is the portion of the strip that experiences movement of soil relative to itself. Reinforcing strip located completely within the moving wedge will not contribute any frictional resistance to the movement of the wedge.

An element PQRS (shown in figure 5.14a) of the failure wedge of thickness dy, located at a distance y from the top of the wedge, is in equilibrium under the following intensities of forces:

σ_y = pressure intensity acting on PQ in the downward vertical direction.

$(\sigma_y + d\sigma_y)$ = pressure intensity acting on RS in the upward vertical direction.

R' = reaction intensity on SQ acting at an angle ϕ to the normal to SQ.

p = pressure intensity on PR acting at an angle δ with the normal to PR.

W = weight of slice PQSR acting downwards.

T = Tensile force in the strip assumed transmitted uniformly to soil layer of thickness S_z encompassing the strip.

$$t = \frac{T}{S_z} = \frac{2.w.f * l_e.\sigma_v}{S_x.S_z}$$

c_s = cohesion of the soil.

c_w = adhesion between the soil and wall acting per unit length.

θ = angle of the rupture surface with vertical.

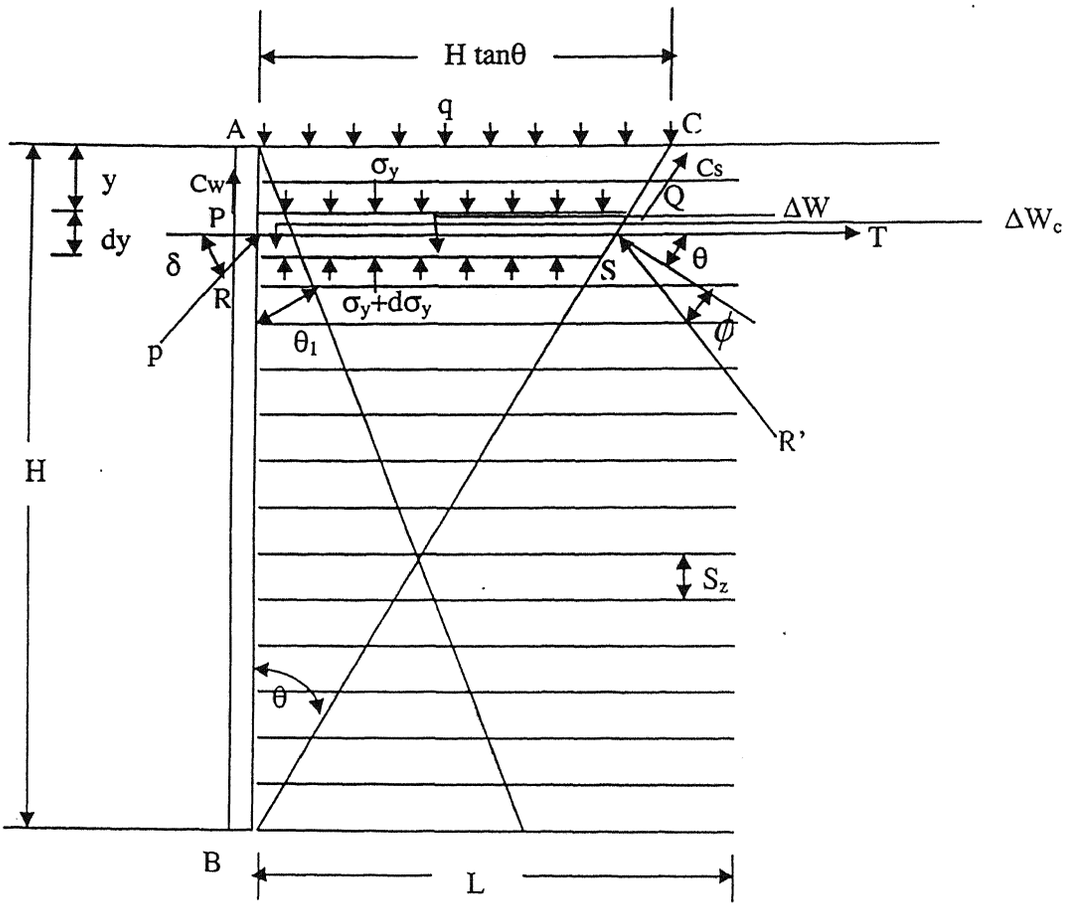

Figure 5.14(a): Wall details with reinforcement (counterfort retaining wall)

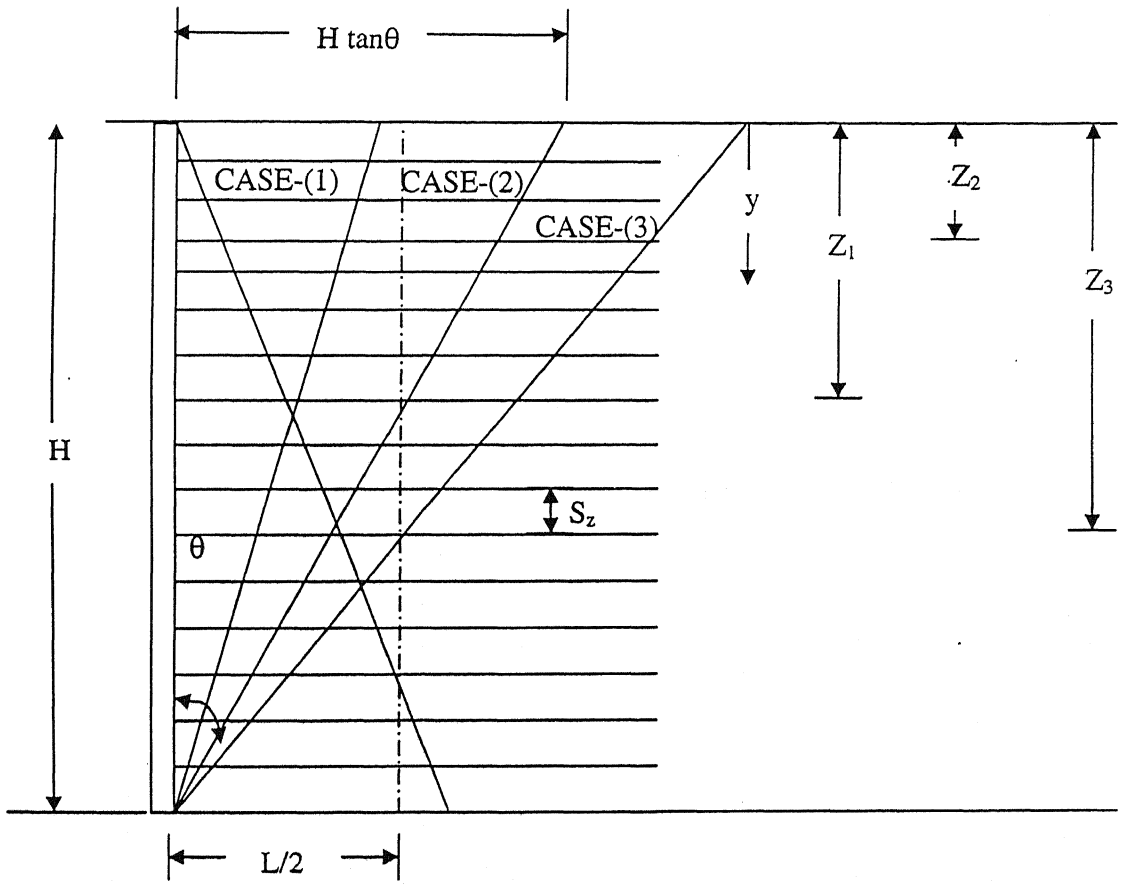

Figure 5.14(b): Schematic representation of three cases of analysis (counterfort retaining wall)

(i) Considering static equilibrium of element under the action of all forces in the horizontal direction, i.e,

$\sum H = 0.$

$p\cos\delta.PR - R'\cos(\theta+\phi).QS + c_s.\sin\theta.QS + t.dy = 0.$

Where, $PQ = (H-y)\tan\theta$, $RS = (H-y-dy)\tan\theta$, $QS = \frac{dy}{\cos\theta}$, PR = dy.

Thus, $R' = \frac{p.\cos\delta.\cos\theta}{\cos(\theta+\phi)} + c_s.\frac{\sin\theta}{\cos(\theta+\phi)} + \frac{t.\cos\theta}{\cos(\theta+\phi)}$ (5.53)

(ii) Weight of element PQRS is,

$\Delta W = \gamma.(H-y).\tan\theta.dy$

Weight of counterfort within the element = $\Delta W_C = \gamma_C.y.\tan\theta_1.dy$

Considering static equilibrium of element under action of all forces in the vertical direction, i.e,

$\sum V = 0.$

$p\sin\delta.PR + R'\sin(\theta+\phi).QS + (\sigma_y + d\sigma_y).RS - \Delta W - \Delta W_C - \sigma_y.PQ + c_w.PR + c_s\cos\theta.QS = 0$

Substituting the value of PR, QS, RS, PQ, ΔW and ΔW_C in the above equation and on further simplification [after substituting the value of R' from equation (5.53)] we get,

$$\frac{d\sigma_y}{dy} = \gamma + \gamma_C.\frac{y.\tan\theta_1}{(H-y)\tan\theta} + \frac{\sigma_y}{(H-y)} - \frac{p\cos\theta}{(H-y)\sin\theta}\{\sin\delta + \cos\delta.\tan(\theta+\phi)\} - \frac{c_s}{(H-y)}.$$
$$\{\frac{\cos\theta}{\sin\theta} + \tan(\theta+\phi)\} - \frac{c_w}{(H-y)}.\frac{\cos\theta}{\sin\theta} - \frac{t.\tan(\theta+\phi).\cos\theta}{\sin\theta.(H-y)}.$$

let, $\frac{\tan\theta_1}{\tan\theta} = k.$

Therefore,

$$\frac{d\sigma_y}{dy} = \frac{\sigma_y}{H-y} + \gamma + \gamma_C\frac{yk}{H-y} - \frac{p}{H-y}V_3 - \frac{c_s}{H-y}V_4 - \frac{c_w}{H-y}V_5 - \frac{t}{H-y}V_6 \quad (5.54)$$

Where, $V_1 = \tan 6$

$$V_2 = \frac{\cos\theta}{\cos(\theta+\phi)}$$

$$V_3 = \left\{\frac{\sin\delta}{V_1} + \frac{V_2}{V_1}.\frac{\sin(\theta+\phi).\cos\delta}{\cos\theta}\right\}$$

$$V_4 = \left\{\frac{1}{V_1} + \frac{V_2}{V_1}\tan\theta.\frac{\sin(\theta+\phi)}{\cos\theta}\right\}$$

$$V_5 = \frac{1}{V_1}$$

$$V_6 = \left\{\frac{V_2}{V_1}\frac{\sin(\theta+\phi)}{\cos\theta}\right\}$$

(iii) Taking moments of all the forces about the mid point (D) of element PQRS between Q and S, i.e.

$$c_w.dy(H-y).A - \frac{\gamma A^2}{2}(H-y)^2dy - \frac{\gamma_C A_1^2 y^2}{2}dy - \sigma_y(H-y)A\left\{\frac{(H-y)A}{2} - \frac{\sin\theta.dy.B}{2}\right\} + p.\sin\delta.(H-y).A.dy$$

$$+(\sigma_y+d\sigma_y).A.(H-y-dy)\left\{\frac{(H-y-dy)A}{2} + \frac{\sin\theta.dy.B}{2}\right\} = 0.$$

Where, $A = \frac{\sin 6}{\cos 6}$, $B = \frac{1}{\cos 6}$ and $A_1 = \tan 6_1$.

On simplification and neglecting small quantities of higher order, the above equation reduces to –

$$\frac{d\sigma_y}{dy} = \gamma + \gamma_C \frac{k^2y^2}{(H-y)^2} - \frac{2p\sin\delta}{(H-y).V_1} - \frac{2c_w}{V_1(H-y)} \qquad (5.55)$$

Equating equations (5.54) and (5.55) we get,

$$\frac{\sigma_y}{(H-y)} - \frac{p}{(H-y)}\left\{V_3 - \frac{2\sin\delta}{V_1}\right\} - \frac{c_s}{(H-y)}V_4 - \frac{c_w}{(H-y)}\left\{V_5 - \frac{2}{V_1}\right\} - \frac{t}{(H-y)}V_6$$

$$-\frac{\gamma_C.yk}{(H-y)}\left[\frac{yk}{(H-y)} - 1\right] = 0.$$

$$\text{or, } p = \frac{\sigma_y}{V_7} - c_s.\frac{V_4}{V_7} - c_w.\frac{1}{V_7}\left\{V_5 - \frac{2}{V_1}\right\} - t.\frac{V_6}{V_7} - \gamma_C.\frac{ky}{V_7}\left[\frac{yk}{(H-y)} - 1\right] \tag{5.56}$$

$$\text{Where, } V_7 = \left\{V_3 - \frac{2.\sin\delta}{V_1}\right\}$$

$$\text{or, } p = \sigma_y(S_1) - c_s(S_2) - c_w(S_3) - t(S_4) - \gamma_C.y\left(\frac{yk^2}{H-y} - k\right)(S_1)$$

Where,

$$S_1 = \frac{1}{V_7}$$

$$S_2 = \frac{V_4}{V_7}$$

$$S_3 = \frac{\left(V_5 - \frac{2}{V_1}\right)}{V_7}$$

$$S_4 = \frac{V_6}{V_7}$$

On differentiating equation (5.56) w.r.t. y, we get,

$$\frac{dp}{dy} = \frac{d\sigma_y}{dy}(S_1) - \frac{dt}{dy}(S_4) - \gamma_C\left(\frac{yk^2(2H-y)}{(H-y)^2} - k\right)(S_1) \tag{5.57}$$

Substituting the value of $\frac{d\sigma_y}{dy}$ from equation (5.55) into equation (5.57),

$$\frac{dp}{dy} = S_1\left\{\gamma + \gamma_C\frac{k^2y^2}{(H-y)^2} - \frac{2p\sin\delta}{V_1(H-y)} - \frac{2c_w}{V_1(H-y)}\right\} - \frac{dt}{dy}S_4 - \gamma_C\left[\frac{yk^2(2H-y)}{(H-y)^2} - k\right].S_1$$

$$\text{or, } \frac{dp}{dy} = -\frac{p}{(H-y)}C_1 + \gamma.C_2 + \frac{c_w}{(H-y)}C_3 - \frac{dt}{dy}C_4 + \gamma_C.C_5 + \gamma_C.\frac{y^2}{(H-y)^2}.C_6 - \gamma_C\frac{Hy}{(H-y)^2}.C_6 \tag{5.58}$$

Where, $C_1 = \frac{2S_1 \sin\delta}{V_1}$

$C_2 = S_1$

$C_3 = -\frac{2S_1}{V_1}$

$C_4 = S_4$

$C_5 = S_1 k$

$C_6 = 2k^2 S_1$

Tension, T at limiting equilibrium can be taken as given below:

$$T = 2\left\{\gamma\left(y + \frac{dy}{2}\right) + q\right\}.w.l_e.f^* + 2.C_r.w.l_e \qquad (5.59)$$

Where, l_e = effective length of reinforcing strip.

w = width of reinforcing strip.

C_r = co-efficient of adhesion with reinforcement.

f* = apparent co-efficient of friction between soil and reinforcement

From equation (5.59),

$$t = \frac{2wf^* l_e\left[\gamma\left(y + \frac{dy}{2}\right) + q\right] + 2C_r w l_e}{S_x.S_z} \qquad (5.60)$$

Where, S_x and S_z are horizontal and vertical spacings of reinforcing strips respectively.

The values of l_e will vary from strip to strip and will depend on wedge angle θ and length L of the strip. There may be three cases of analysis [as shown in the figure 5.14(b)].

CASE 1 $H\tan 6 \le L/2$

$$l_e = \left(H - y - \frac{dy}{2}\right)\tan\theta \text{ for all reinforcing elements} \qquad (5.61)$$

CASE 2 $L./2 \le H\tan 6 \le L$

$$l_e = L - (H - y - \frac{dy}{2})\tan\theta, \quad \text{for } y \le Z_1 \qquad (5.62)$$

$$l_e = (H - y - \frac{dy}{2})\tan\theta, \qquad \text{for } y > Z_1 \tag{5.63}$$

CASE 3 $H\tan\theta \geq L$

$$l_e = 0, \qquad \text{for } y \leq Z_2 \tag{5.64}$$

$$l_e = L - (H - y - \frac{dy}{2})\tan\theta, \quad \text{for } Z_2 \leq y \leq Z_3 \tag{5.65}$$

$$l_e = (H - y - \frac{dy}{2})\tan\theta, \qquad \text{for } y > Z_3 \tag{5.66}$$

Z_1, Z_2 and Z_3 are shown in fig (5.14b).

PRESSURE INTENSITY ON WALL

CASE 1 $H\tan\theta \leq L/2$

$$l_e = \left(H - y - \frac{dy}{2}\right)\tan\theta$$

$= (H - y)\tan\theta$, neglecting dy/2 being small.

$$t = \frac{2wf^*\left[\gamma\left(y + \frac{dy}{2}\right) + q\right].(H - y)\tan\theta + 2C_r w.(H - y)\tan\theta}{S_x.S_z} \tag{5.67}$$

$$\frac{dt}{dy} = 2D_P\gamma\tan\theta\left[\left(1 - \frac{2y}{H}\right) - \frac{q}{\gamma H}\right] - 2D_C\tan\theta.\gamma \tag{5.68}$$

Where, $D_P = \frac{wf^*H}{S_x S_z}$ and $D_C = \frac{C_r wH}{\gamma H.S_x S_z}$

Here,

D_P = non-dimensional spacing coefficient

D_C = non-dimensional coefficient for adhesion with reinforcement.

Substituting the values of dt/dy from eqn. (5.68) to (5.58), we get,

$$\frac{dp}{dy} = -\frac{p}{(H-y)}C_1 + \gamma.C_2 + \frac{c_w}{(H-y)}C_3 - C_4\left[2D_P.\gamma.\tan\theta\left\{\left(1-\frac{2y}{H}\right)-\frac{q}{\gamma H}\right\}-2D_C.\tan\theta.\gamma\right]$$

$$+\gamma_C.C_5 + \gamma_C.\frac{y^2}{(H-y)^2}.C_6 - \gamma_C.\frac{Hy}{(H-y)^2}.C_6 \qquad (5.68a)$$

Integral function of the above equation is $(H-y)^{-C_1}$

Therefore,

$$\int\frac{dp}{dy}(H-y)^{-C_1}dy + C_1\int\frac{p}{H-y}(H-y)^{-C_1}dy = \gamma.C_2\int(H-y)^{-C_1}dy + \frac{c_w.C_3}{H-y}\int(H-y)^{-C_1}dy$$

$$-2C_4.D_P.\gamma\tan\theta\int\left\{(H-y)^{-C_1}\left(1-\frac{2y}{H}-\frac{q}{\gamma H}\right)\right\}dy + 2D_C.C_4.\tan\theta.\gamma\int(H-y)^{-C_1}dy + \gamma_C C_5\int(H-y)^{-C_1}dy$$

$$+\gamma_C C_6\int y^2(H-y)^{-2-C_1}dy - \gamma_C HC_6\int y.(H-y)^{-2-C_1}dy \qquad (5.69)$$

or, $$\frac{p}{(H-y)^{C_1}} = -\frac{C_2.\gamma.(H-y)^{1-C_1}}{1-C_1} + \frac{c_w.C_3(H-y)^{-C_1}}{C_1} - 2C_4D_P.\gamma.\tan\theta.$$

$$\left[\frac{2(H-y)^{2-C_1}}{H(1-C_1)(2-C_1)} - \left\{1-\frac{2y}{H}-\frac{q}{\gamma.H}\right\}\frac{(H-y)^{1-C_1}}{1-C_1}\right] - 2.D_C.C_4\tan\theta.\gamma\frac{(H-y)^{1-C_1}}{1-C_1}$$

$$-\frac{\gamma_C.C_5(H-y)^{1-C_1}}{1-C_1} + \gamma_C.C_6\left[\frac{y^2(H-y)^{-(1+C_1)}}{1+C_1} - \frac{2y(H-y)^{-C_1}}{(1+C_1).C_1} - \frac{2(H-y)^{1-C_1}}{C_1(1+C_1)(1-C_1)}\right]$$

$$-\gamma_C.HC_6\left[\frac{y.(H-y)^{-(1+C_1)}}{1+C_1} - \frac{(H-y)^{-C_1}}{(1+C_1).C_1}\right] + I \qquad (5.70)$$

Where, I = Constant of integration.

Applying boundary condition that at y = 0, $\sigma_y = q$ in equation (5.56), we get,

$$\frac{p}{H^{C_1}} = \frac{q\sin\theta}{\cos\theta.D_1.H^{C_1}} - \frac{c_s.\cos\phi}{D_1.\cos(\theta+\phi)\cos\theta.H^{C_1}} + \frac{c_w.\sin 6}{H^{C_1}.\cos\theta.D_1}.\frac{1}{A} - \frac{t.\tan(\theta+\phi)}{D_1.H^{C_1}} \qquad (5.56a)$$

Now, $t = t_q + t_{ca}$ $\qquad (t_\gamma = 0)$

Here, $$t_q = \frac{2wf^*q(H-y)\tan\theta}{S_xS_z}$$

$$t_{ca} = \frac{2C_r(H-y)\tan\theta.w}{S_x S_z}$$

$$t_{q_0} = 2.D_P.q\tan\delta$$

$$t_{ca_0} = 2D_C.\tan\theta.\gamma.H$$

Equation (5.56a) can be written as,

$$\frac{p}{H^{C_1}} = \frac{q\sin\theta}{H^{C_1}\cos\theta.D_1} + \frac{c_w\sin\theta}{H^{C_1}.\cos\theta.D_1}.U_1 - \frac{c_s.\cos\phi}{D_1.\cos(\theta+\phi).\cos\theta.H^{C_1}}$$

$$-\frac{2.D_P.q.\tan\theta.\tan(\theta+\phi)}{D_1.H^{C_1}} - \frac{2.D_C.\tan\theta.\gamma.H\tan(\theta+\phi)}{D_1.H^{C_1}} \qquad (5.56b)$$

Where, $U_1 = \frac{1}{A}$ and $D_1 = \sin(\delta+\phi-\delta)$

Equating equations (5.70) and (5.56b) for y=0, we get the value of I. Substituting this value of I in equation (5.70), we get on simplification,

$$p_1 = \frac{C_2\gamma.H}{1-C_1}\left\{(1-y/H)^{C_1} - (1-y/H)\right\} + 2.C_4.D_P.\gamma.H\tan\theta.$$

$$\left\{\frac{2(1-y/H)^{C_1}}{(1-C_1)(2-C_1)} - \frac{\left(1-\frac{q}{\gamma H}\right)(1-y/H)^{C_1}}{1-C_1} - \frac{2(1-y/H)^2}{(1-C_1)(2-C_1)} + \frac{\left(1-2y-\frac{q}{\gamma H}\right)(1-y/H)}{1-C_1}\right\}$$

$$-c_s.(1-y/H)^{C_1}.\frac{\cos\phi}{D_1.\cos\theta.\cos(\theta+\phi)} + c_w.\left[\frac{C_3}{C_1} + (1-y/H)^{C_1}\left\{\frac{\sin\theta.U_1}{\cos\theta.D_1} - \frac{C_3}{C_1}\right\}\right]$$

$$-2.D_C.\tan\theta.\gamma.H\left[\frac{C_4(1-y/H)}{1-C_1} - (1-y/H)^{C_1}\left\{\frac{C_4}{1-C_1} - \frac{\tan(\theta+\phi)}{D_1}\right\}\right]$$

$$+\frac{q\sin 6}{\cos\theta.D_1}[1-2.D_p.\tan(\theta+\phi)](1-y/H)^{C_1}+\frac{\gamma_C.C_5}{(1-C_1)}\left[-(H-y)+H(1-y/H)^{C_1}\right]$$

$$+\gamma_C.C_6\left[\frac{y^2}{(H-y)(1+C_1)}-\frac{2y}{C_1(1+C_1)}-\frac{2}{C_1(1+C_1)(1-C_1)}\{(H-y)-H(1-y/H)^{C_1}\}\right]$$

$$-\gamma_C.H.C_6\left[\frac{y}{(H-y)(1+C_1)}-\frac{1}{C_1(1+C_1)}\{1-(1-y/H)^{C_1}\}\right] \qquad (5.71)$$

CASE II A $L./2 \le H\tan 6 \le L$

$$l_e = L-(H-y-\frac{dy}{2})\tan\theta, \quad \text{for } y \le Z_1$$

$$t=\frac{2wf*\left[\gamma\left(y+\frac{dy}{2}\right)+q\right].\{L-(H-y-\frac{dy}{2})\tan\theta\}+2C_r w.\{L-(H-y-\frac{dy}{2})\tan\theta\}}{S_x.S_z} \qquad (5.72)$$

$$\frac{dt}{dy}=2.\gamma.D_p.\tan\theta\left\{\frac{L}{H\tan\theta}-1+\frac{2y}{H}+\frac{q}{\gamma.H}\right\}+2D_C.\gamma\tan\theta$$

$$\text{or, } \frac{dt}{dy}=\gamma.T_1\left[\frac{L}{HT_3}-1+\frac{2y}{H}+\frac{q}{\gamma.H}\right]+\gamma.T_2 \qquad (5.73)$$

Where, $T_1 = 2.\tan 6.D_P$

$$T_2 = 2.\tan 6.D_C$$

$$T_3 = \tan 6 \qquad (5.74)$$

Equation (5.58) may be written as below,

$$\frac{dp_{2a}}{dy}=-\frac{p}{(H-y)}C_1+\gamma.C_2+\frac{c_w}{(H-y)}C_3-\frac{dt}{dy}C_4+\gamma_C.C_5+\gamma_C.\frac{y^2}{(H-y)^2}.C_6-\gamma_C.\frac{Hy}{(H-y)^2}.C_6\,\mathrm{S}$$

ubstituting the value of $\frac{dt}{dy}$ from equation (5.73) in above equation,

$$\frac{dp_{2a}}{dy}+\frac{p}{(H-y)}C_1=\gamma.C_2+\frac{c_w}{(H-y)}C_3-C_4.\gamma.T_1\left\{\frac{L}{HT_3}-1+\frac{2y}{H}+\frac{q}{\gamma H}\right\}-C_4\gamma T_2$$

$$+\gamma_C.C_5+\gamma_C.\frac{y^2}{(H-y)^2}.C_6-\gamma_C.\frac{Hy}{(H-y)^2}.C_6 \qquad (5.75)$$

Solution of equation (5.75) is,

$$\frac{p_{2a}}{(H-y)^{C_1}}=-\frac{C_2.\gamma(H-y)^{1-C_1}}{1-C_1}+\frac{c_w.C_3(H-y)^{-C_1}}{C_1}+C_4.\gamma.\frac{L}{H}.\frac{T_1}{T_3}.\frac{(H-y)^{1-C_1}}{1-C_1}-C_4.\gamma.T_1\frac{(H-y)^{1-C_1}}{(1-C_1)}$$
$$-C_4.\gamma.T_1\frac{2}{H}\left\{-\frac{y(H-y)^{1-C_1}}{1-C_1}-\frac{(H-y)^{2-C_1}}{(1-C_1)(2-C_1)}\right\}+C_4.\gamma.T_1.\frac{q}{\gamma.H}.\frac{(H-y)^{1-C_1}}{(1-C_1)}+C_4.\gamma.T_2\frac{(H-y)^{1-C_1}}{(1-C_1)}$$
$$-\frac{\gamma_C.C_5(H-y)^{1-C_1}}{1-C_1}+\gamma_C.C_6\left[\frac{y^2(H-y)^{-(1+C_1)}}{1+C_1}-\frac{2y(H-y)^{-C_1}}{(1+C_1).C_1}-\frac{2(H-y)^{1-C_1}}{C_1(1+C_1)(1-C_1)}\right]$$
$$-\gamma_C.HC_6\left[\frac{y.(H-y)^{-(1+C_1)}}{1+C_1}-\frac{(H-y)^{-C_1}}{(1+C_1).C_1}\right]+I \qquad (5.76)$$

Equating the above equation with (5.56b) at boundary condition that at y = 0, $\sigma_y = q$, we get on simplification,

$$p_{2a}=\{(1-y/H)-(1-y/H)^{C_1}\}\left\{\frac{C_4.\gamma.L}{1-C_1}.\frac{T_1}{T_3}-\frac{C_4\gamma T_1H}{1-C_1}+\frac{C_4.T_1q}{1-C_1}+\frac{C_4T_2\gamma H}{1-C_1}-\frac{\gamma.C_2H}{1-C_1}\right\}$$

$$+\left\{1-\left(1-\frac{y}{H}\right)^{C_1}\right\}\frac{c_w.C_3}{C_1}+\frac{2.C_4\gamma HT_1}{(1-C_1)(2-C_1)}\{(1-y/H)^2-(1-y/H)^{C_1}\}+\frac{2C_4\gamma T_1y(1-y/H)}{(1-C_1)}$$

$$+\frac{q\sin\theta(1-y/H)^{C_1}}{\cos\theta.D_1}-\frac{c_s.\cos\phi(1-y/H)^{C_1}}{D_1\cos(\theta+\phi)\cos\theta}+\frac{c_w\sin\theta}{\cos\theta.D_1}.\frac{1}{A}.(1-y/H)^{C_1}$$

$$-\{2.D_P.q\tan\theta+2.D_C.\gamma.H\tan\theta\}\frac{\tan(\theta+\phi)(1-y/H)^{C_1}(L/H-1)}{D_1}+\frac{\gamma_C.C_5}{(1-C_1)}\left[-(H-y)+H(1-y/H)^{C_1}\right]$$

$$+\gamma_C.C_6\left[\frac{y^2}{(H-y)(1+C_1)}-\frac{2y}{C_1(1+C_1)}-\frac{2}{C_1(1+C_1)(1-C_1)}\{(H-y)-H(1-y/H)^{C_1}\}\right]$$

$$-\gamma_C.H.C_6\left[\frac{y}{(H-y)(1+C_1)}-\frac{1}{C_1(1+C_1)}\left\{1-(1-y/H)^{C_1}\right\}\right] \qquad (5.77)$$

CASE II (B)

For $y > Z_1$, the effective length will be (H-y)tanθ and pressure intensity p_{2b} can be obtained by integrating equation (5.58a) over the domain $y = Z_1$ to H for the boundary condition that at $y = Z_1$, $p_{2b} = (p_2)_{y=Z_1}$, where p_{2b} represents the pressure intensity at any depth $Z_1 < y < H$.

Equation (5.70) at $y = Z_1$ shall be

$$p_{2b} = -\frac{C_2.\gamma(H-Z_1)}{1-C_1}+\frac{c_w.C_3}{C_1}-2.C_4.D_P.\gamma.\tan\theta\left\{\frac{2(H-Z_1)^2}{H(1-C_1)(2-C_1)}-\left(1-\frac{2Z_1}{H}-\frac{q}{\gamma H}\right)\frac{(H-Z_1)}{1-C_1}\right\}$$

$$-2.D_C.C_4.\tan\theta.\gamma.\frac{(H-Z_1)}{1-C_1}-\frac{\gamma_C.C_5(H-Z_1)}{1-C_1}+\gamma_C.C_6\left[\frac{Z_1^{\,2}}{(H-Z_1)(1+C_1)}-\frac{2Z_1}{(1+C_1).C_1}-\frac{2(H-Z_1)}{C_1(1+C_1)(1-C_1)}\right]$$

$$-\gamma_C.HC_6\left[\frac{Z_1}{(H-Z_1)(1+C_1)}-\frac{1}{(1+C_1).C_1}\right]+I.(H-Z_1)^{C_1} \qquad (5.70a)$$

To evaluate I, apply boundary conditions same as before and equate it to equation (5.77). After substituting the value of I in equation (5.70), the pressure intensity p_{2b} is given by following equation,

$$p_{2b}=\frac{(1-y/H)}{1-C_1}\left\{-C_2.\gamma.H+C_4\gamma HT_1\left(1-\frac{2y}{H}-\frac{q}{\gamma H}\right)-T_2C_4\gamma H\right\}$$

$$-\frac{2C_4\gamma HT_1}{(1-C_1)(2-C_1)}\left\{(1-y/H)^2-(1-Z_1/H)^{2-C_1}.(1-y/H)^{C_1}\right\}+\frac{c_wC_3}{C_1}\left\{1-\frac{(1-y/H)^{C_1}}{(1-Z_1/H)^{C_1}}\right\}$$

$$+\frac{C_2\gamma.H(1-Z_1/H)^{1-C_1}(1-y/H)^{C_1}}{1-C_1}-C_4.\gamma.H.T_1\left(1-\frac{2Z_1}{H}-\frac{q}{\gamma H}\right)\frac{(1-Z_1/H)^{1-C_1}(1-y/H)^{C_1}}{1-C_1}$$

$$+\frac{T_2C_4\gamma.H(1-Z_1/H)^{1-C_1}(1-y/H)^{C_1}}{1-C_1}+\left\{(1-Z_1/H)^{1-C_1}-1\right\}$$

$$\left\{-\frac{\gamma.C_2.H}{1-C_1}+\frac{C_4\gamma.L}{1-C_1}.\frac{T_1}{T_3}-\frac{C_4\gamma.HT_1}{1-C_1}+\frac{C_4T_1q}{1-C_1}+\frac{C_4T_2\gamma.H}{1-C_1}\right\}.(1-y/H)^{C_1}$$

$$+\left\{\frac{1}{(1-Z_1/H)^{C_1}}-1\right\}(1-y/H)^{C_1}.\left\{\frac{c_w.C_3}{C_1}\right\}+\frac{2C_4\gamma.HT_1(1-y/H)^{C_1}}{(1-C_1)(2-C_1)}.\left\{(1-Z_1/H)^{2-C_1}-1\right\}$$

$$+\frac{2C_4.\gamma.Z_1T_1(1-Z_1/H)^{1-C_1}.(1-y/H)^{C_1}}{1-C_1}+\frac{(1-y/H)^{C_1}}{\cos\theta.D_1}\left\{q\sin\theta-\frac{c_s\cos\phi}{\cos(\theta+\phi)}\right\}$$

$$+\frac{(1-y/H)^{C_1}}{\cos\theta.D_1}.c_w.\sin\theta.\frac{1}{A}-\frac{\{qT_1+\gamma.HT_2\}\tan(\theta+\phi)(1-y/H)^{C_1}(L/H-1)}{D_1}$$

$$+\frac{\gamma_C.C_5}{(1-C_1)}\left[-(H-y)+H(1-y/H)^{C_1}\right]$$

$$+\gamma_C.C_6\left[\frac{y^2}{(H-y)(1+C_1)}-\frac{2y}{C_1(1+C_1)}-\frac{2}{C_1(1+C_1)(1-C_1)}\left\{(H-y)-H(1-y/H)^{C_1}\right\}\right]$$

$$-\gamma_C.H.C_6\left[\frac{y}{(H-y)(1+C_1)}-\frac{1}{C_1(1+C_1)}\left\{1-(1-y/H)^{C_1}\right\}\right] \qquad (5.78)$$

CASE III A

$H \tan 6 \geq L$

For the domain y =0 to y = Z_2, the failure surface is not cut by any reinforcing element and passes through soil alone. Therefore, no part of strip will experience movement of soil relative to itself and the value of it will be equal to zero. The differential equation (5.58) will thus become,

$$\frac{dp}{dy} = -\frac{p}{(H-y)}C_1 + \gamma.C_2 + \frac{c_w}{(H-y)}C_3 + \gamma_C.C_5 + \gamma_C.\frac{y^2}{(H-y)^2}.C_6 - \gamma_C.\frac{Hy}{(H-y)^2}.C_6 \qquad (5.79)$$

Solution of the above equation will also be done for the boundary condition that at y = 0, $\sigma_y = q$.

From equation (5.79), we can get,

$$\frac{dp}{dy} + C_1.\frac{p}{(H-y)} = \gamma.C_2 + \frac{c_w.C_3}{(H-y)} + \gamma_C.C_5 + \gamma_C.\frac{y^2}{(H-y)^2}.C_6 - \gamma_C.\frac{Hy}{(H-y)^2}.C_6$$

$$\frac{p}{(H-y)^{C_1}} = -\frac{\gamma.C_2(H-y)^{1-C_1}}{1-C_1} + \frac{c_w.C_3(H-y)^{-C_1}}{C_1} - \frac{\gamma_C.C_5(H-y)^{1-C_1}}{1-C_1}$$
$$+\gamma_C.C_6\left[\frac{y^2(H-y)^{-(1+C_1)}}{1+C_1} - \frac{2y(H-y)^{-C_1}}{(1+C_1).C_1} - \frac{2(H-y)^{1-C_1}}{C_1(1+C_1)(1-C_1)}\right] - \gamma_C.HC_6\left[\frac{y.(H-y)^{-(1+C_1)}}{1+C_1} - \frac{(H-y)^{-C_1}}{(1+C_1).C_1}\right] + I \qquad (5.79a)$$

$$p = -\frac{\gamma.C_2(H-y)}{1-C_1} + \frac{c_w.C_3}{C_1} - \frac{\gamma_C.C_5(H-y)}{1-C_1} + \gamma_C.C_6\left[\frac{y^2}{(H-y)(1+C_1)} - \frac{2y}{(1+C_1).C_1} - \frac{2(H-y)}{C_1(1+C_1)(1-C_1)}\right]$$
$$-\gamma_C.HC_6\left[\frac{y}{(H-y)(1+C_1)} - \frac{1}{(1+C_1).C_1}\right] + I.(H-y)^{C_1} \qquad (5.79b)$$

Substituting the value of I by equating equation (5.79a) with equation (5.56) for $\sigma_y = q$ and t = 0, in equation (5.79b), we get after simplification,

$$p_{3a} = \frac{\gamma.C_2.H}{1-C_1}\left\{(1-y/H)^{C_1} - (1-y/H)\right\} + \left[\left\{1-(1-y/H)^{C_1}\right\}\left\{\frac{c_w.C_3}{C_1}\right\}\right]$$

$$-(1-y/H)^{C_1}\left\{\frac{c_s.\cos\phi}{D_1.\cos(\theta+\phi)\cos\theta} - \frac{q\sin\theta}{\cos\theta.D_1} - \frac{c_w\sin\theta}{D_1\cos\theta}.\frac{1}{A}\right\} + \frac{\gamma_C.C_5}{(1-C_1)}\left[-(H-y)+H(1-y/H)^{C_1}\right]$$

$$+\gamma_C.C_6\left[\frac{y^2}{(H-y)(1+C_1)} - \frac{2y}{C_1(1+C_1)} - \frac{2}{C_1(1+C_1)(1-C_1)}\left\{(H-y)-H(1-y/H)^{C_1}\right\}\right]$$

$$-\gamma_C.H.C_6\left[\frac{y}{(H-y)(1+C_1)} - \frac{1}{C_1(1+C_1)}\left\{1-(1-y/H)^{C_1}\right\}\right] \qquad (5.80)$$

CASE III B

For the region y = Z_2 to Z_3, the equation for pressure intensity p_{3b} can be evaluated by solving equation (5.76) with the boundary condition that at y = Z_2, $p_{3b} = (p_3)_{y=Z_2}$.

Thus,

$$\frac{p}{(H-y)^{C_1}} = \gamma.C_2\int(H-y)^{-C_1}dy + \frac{c_w.C_3}{(H-y)}\int(H-y)^{-C_1}dy - C_4.\gamma\frac{L}{H}.\frac{T_1}{T_3}\int(H-y)^{-C_1}dy$$

$$+C_4.\gamma T_1\int(H-y)^{-C_1}dy - 2.C_4\gamma\frac{T_1}{H}\left\{\int y(H-y)^{-C_1}dy\right\} - C_4.\gamma.T_1.\frac{q}{\gamma H}\int(H-y)^{-C_1}dy - \int C_4.\gamma.T_2(H-y)^{-C_1}dy$$

$$+\gamma_C C_5\int(H-y)^{-C_1}dy + \gamma_C C_6\int y^2(H-y)^{-2-C_1}dy - \gamma_C HC_6\int y.(H-y)^{-2-C_1}dy \qquad (5.76a)$$

or, $$\frac{p}{(H-y)^{C_1}} = -\frac{y.C_2(H-y)^{1-C_1}}{(1-C_1)} + \frac{c_wC_3(H-y)^{-C_1}}{C_1} + \frac{C_4.\gamma.H(H-y)^{1-C_1}}{H(1-C_1)}.\frac{T_1}{T_3}$$

$$-\frac{C_4\gamma.T_1(H-y)^{1-C_1}}{(1-C_1)}+\frac{2.C_4.\gamma.T_1y(H-y)^{1-C_1}}{H(1-C_1)}+\frac{2.C_4\gamma.T_1(H-y)^{2-C_1}}{H(1-C_1)(2-C_1)}$$

$$+\frac{C_4\gamma.T_1q(H-y)^{1-C_1}}{\gamma.H(1-C_1)}+\frac{C_4\gamma.T_2(H-y)^{1-C_1}}{(1-C_1)}$$

$$-\frac{\gamma_C.C_5(H-y)^{1-C_1}}{1-C_1}+\gamma_C.C_6\left[\frac{y^2(H-y)^{-(1+C_1)}}{1+C_1}-\frac{2y(H-y)^{-C_1}}{(1+C_1).C_1}-\frac{2(H-y)^{1-C_1}}{C_1(1+C_1)(1-C_1)}\right]$$

$$-\gamma_C.HC_6\left[\frac{y.(H-y)^{-(1+C_1)}}{1+C_1}-\frac{(H-y)^{-C_1}}{(1+C_1).C_1}\right]+I \qquad (5.76b)$$

Equation (5.80) may be equated with equation (5.76b) at y = Z_2 for the determination of I. The pressure intensity after substituting the value of I in equation (5.76b) is determined as:

$$p_{3b}=\frac{(1-y/H)}{1-C_1}\left\{-\gamma.C_2H-C_4.\gamma.T_1H+2.C_4\gamma.T_1y+C_4.q.T_1+C_4.\gamma.T_2H+C_4.\gamma.H\frac{T_1}{T_3}\right\}$$

$$+\frac{C_3c_w}{C_1}+\frac{2.C_4.\gamma.T_1H(1-y/H)^2}{(1-C_1)(2-C_1)}+\frac{(1-Z_2/H)^{1-C_1}.(1-y/H)^{C_1}}{1-C_1}.\left\{C_2.\gamma.H-C_4.\gamma.H.\frac{T_1}{T_3}\right.$$

$$\left.+C_4.\gamma.T_1H-2.C_4.\gamma.T_1Z_2-C_4T_1q-C_4.\gamma.HT_2\right\}+\frac{(1-y/H)^{C_1}}{(1-Z_2/H)^{C_1}}\left[\frac{\gamma.C_2}{1-C_1}\left\{(1-Z_2/H)^{C_1}-(1-Z_2/H)\right\}\right.$$

$$\left.-\frac{C_3.c_w}{C_1}\right]+\frac{(1-y/H)^{C_1}}{(1-Z_2/H)^{C_1}}\left[\left\{1-(1-Z_2/H)^{C_1}\right\}\frac{C_3.c_w}{C_1}\right]-\frac{2.C_4.\gamma.HT_1(1-Z_2/H)^{2-C_1}.(1-y/H)^{C_1}}{(1-C_1)(2-C_1)}$$

$$-(1-y/H)^{C_1}\left\{\frac{c_s.\cos\phi}{D_1.\cos(\theta+\phi)\cos\theta}-\frac{q.\sin\theta}{\cos\theta.D_1}-\frac{T_3c_w\sin\theta}{D_1.\cos\theta}\right\}+\frac{\gamma_C.C_5}{(1-C_1)}\left[-(H-y)+H(1-y/H)^{C_1}\right]$$

$$+\gamma_C.C_6\left[\frac{y^2}{(H-y)(1+C_1)}-\frac{2y}{C_1(1+C_1)}-\frac{2}{C_1(1+C_1)(1-C_1)}\left\{(H-y)-H(1-y/H)^{C_1}\right\}\right]$$

$$-\gamma_C.H.C_6\left[\frac{y}{(H-y)(1+C_1)}-\frac{1}{C_1(1+C_1)}\left\{1-(1-y/H)^{C_1}\right\}\right] \qquad (5.81)$$

CASE III C

For the domain y = Z_3 to h, the pressure intensity can be computed by solving equation (5.58a) for boundary condition that at y = Z_3, $p_{3c} = (p_{3b})_{y=Z_3}$ equation (5.58a) may also be written as:

$$\frac{dp}{dy} = -\frac{p}{(H-y)}C_1 + \gamma.C_2 + \frac{c_w}{(H-y)}C_3 - C_4.\gamma.T_1\left\{1 - \frac{2y}{H} - \frac{q}{\gamma.H}\right\} + C_4.T_2.\gamma + \gamma_C.C_5$$
$$+ \gamma_C.\frac{y^2}{(H-y)^2}.C_6 - \gamma_C.\frac{Hy}{(H-y)^2}.C_6$$

$$\text{or, } \frac{p_{3C}}{(H-y)^{C_1}} = \int \gamma.C_2(H-y)^{-C_1}dy + \frac{c_w.C_3}{(H-y)}\int (H-y)^{-C_1}dy - C_4.\gamma.T_1\int (H-y)^{-C_1}dy$$

$$+ C_4.\gamma.T_1\int \frac{2y}{H}(H-y)^{-C_1}dy + C_4.\gamma.T_1.\frac{q}{\gamma.H}\int (H-y)^{-C_1}dy + C_4.T_2.\gamma\int (H-y)^{-C_1}dy$$

$$+ \gamma_C C_5\int (H-y)^{-C_1}dy + \gamma_C C_6\int y^2(H-y)^{-2-C_1}dy - \gamma_C HC_6\int y.(H-y)^{-2-C_1}dy$$

$$\text{or, } \frac{p_{3C}}{(H-y)^{C_1}} = -\frac{\gamma.C_2(H-y)^{1-C_1}}{1-C_1} + \frac{c_w.C_3(H-y)^{-C_1}}{C_1} + \frac{C_4.\gamma.T_1(H-y)^{1-C_1}}{1-C_1}$$

$$+ \frac{2.C_4\gamma.T_1}{H}\left\{-\frac{y(H-y)^{1-C_1}}{1-C_1} - \frac{(H-y)^{2-C_1}}{(1-C_1)(2-C_1)}\right\} - \frac{C_4\gamma.T_1.q(H-y)^{1-C_1}}{\gamma.H(1-C_1)} - \frac{C_4T_2.\gamma(H-y)^{1-C_1}}{1-C_1}$$
$$- \frac{\gamma_C.C_5(H-y)^{1-C_1}}{1-C_1} + \gamma_C.C_6\left[\frac{y^2(H-y)^{-(1+C_1)}}{1+C_1} - \frac{2y(H-y)^{-C_1}}{(1+C_1).C_1} - \frac{2(H-y)^{1-C_1}}{C_1(1+C_1)(1-C_1)}\right]$$
$$- \gamma_C.HC_6\left[\frac{y.(H-y)^{-(1+C_1)}}{1+C_1} - \frac{(H-y)^{-C_1}}{(1+C_1).C_1}\right] + I \qquad (5.82a)$$

The above equation (5.82a) can be equated with equation (5.81) at y = Z_3 to determine the value of I. After substituting the value of I in equation (5.82a), the pressure intensity p_{3C} may be determined by following equation:

$$p_{3C}=\frac{(1-y/H)^{C_1}}{1-C_1}\left\{-C_4.\gamma.HT_1(1-Z_3/H)^{1-C_1}+\gamma.C_2H(1-Z_3/H)^{1-C_1}+\frac{2C_4\gamma.HT_1Z_3(1-Z_3/H)^{1-C_1}}{H}\right.$$

$$\left.+C_4.T_1.q.(1-Z_3/H)^{1-C_1}+\frac{2C_4.\gamma.HT_1(1-Z_3/H)^{2-C_1}}{(2-C_1)}+C_4.T_2.\gamma.H(1-Z_3/H)^{1-C_1}+\frac{2C_4.\gamma.H(1-Z_3/H)^2T_1}{(2-C_1)(1-Z_3/H)^{C_1}}\right\}$$

$$+\frac{c_w.C_3}{C_1}+\frac{(1-y/H)}{1-C_1}\{-\gamma.C_2.H+C_4\gamma.HT_1-C_4T_1q-C_4T_2\gamma.H\}+2C_4\gamma.T_1(1-y/H)\left\{-\frac{y}{1-C_1}\right.$$

$$\left.-\frac{H(1-y/H)}{(1-C_1)(2-C_1)}\right\}+\frac{(1-Z_3/H)^{1-C_1}.(1-y/H)^{C_1}}{(1-C_1)}.\{-\gamma.C_2H-C_4\gamma.T_1H+2C_4.\gamma.T_1y+C_4qT_1+C_4.\gamma.HT_2$$

$$+C_4.\gamma.H\}+I_1+I_2+I_3-(1-y/H)^{C_1}\left\{\frac{c_s.\cos\phi}{D_1.\cos(\theta+\phi).\cos\theta}-\frac{q.\sin\theta}{\cos\theta.D_1}\right\}+(1-y/H)^{C_1}\left\{\frac{c_w.\sin\theta}{D_1.\cos\theta.A}\right\}$$

$$+\frac{\gamma_C.C_5}{(1-C_1)}\left[-(H-y)+H(1-y/H)^{C_1}\right]$$

$$+\gamma_C.C_6\left[\frac{y^2}{(H-y)(1+C_1)}-\frac{2y}{C_1(1+C_1)}-\frac{2}{C_1(1+C_1)(1-C_1)}\left\{(H-y)-H(1-y/H)^{C_1}\right\}\right]$$

$$-\gamma_C.H.C_6\left[\frac{y}{(H-y)(1+C_1)}-\frac{1}{C_1(1+C_1)}\left\{1-(1-y/H)^{C_1}\right\}\right] \qquad (5.83)$$

Where,

$$I_1=\frac{(1-Z_2/H)^{1-C_1}.(1-y/H)^{C_1}}{1-C_1}\left\{C_2.\gamma.H-C_4.\gamma.\frac{T_1}{T_3}+C_4.\gamma.HT_1-2C_4.\gamma.T_1Z_2-C_4T_1q-C_4.\gamma.HT_2\right\}$$

$$I_2=\frac{(1-y/H)^{C_1}}{(1-Z_2/H)^{C_1}}\left[\frac{\gamma.C_2}{1-C_1}\left\{(1-Z_2/H)^{C_1}-(1-Z_2/H)^1\right\}-\frac{c_wC_3}{C_1}\right]+\left\{1-(1-Z_2/H)^{C_1}\right\}\frac{c_wC_3}{C_1}$$

$$I_3=\frac{2.C_4\gamma.HT_1(1-Z_2/H)^{2-C_1}.(1-y/H)^{C_1}}{(1-C_1)(2-C_1)} \qquad (5.83a)$$

5.3.4 Method of computations

The pressure distribution along the height of wall for few typical cases, obtained by using equations 5.40, 5.46, 5.47, 5.49, 5.50 and 5.52 (for cantilever retaining wall) and 5.71, 5.77, 5.78, 5.80, 5.81 and 5.83 (for counterfort retaining wall) are shown in the figures 5.15(a), (b) and 5.16 (a), (b).

It is evident that the pressure intensities become negative in some portion of the wall. The value of total pressure is obtained by numerical integration neglecting the negative pressure. The designed section of wall needs to be checked for its stability against sliding and overturning. The former factor needs the value of resultant lateral earth pressure which is obtained by maximizing the lateral earth pressure with respect to wedge angle θ. Similarly the moments of the positive pressure intensities were taken about the heel of the wall and the same is maximized with respect to wedge angle θ. The maximized values of resultant earth pressure and moment are denoted by P and M respectively and are presented in the charts in non-dimensional form as $\left(P/1/2\gamma.H^2\right)$ and $\left(M/1/6\gamma.H^3\right)$ respectively.

5.3.5 Parametric study

A range of design parameters, e.g. D_P, angle of internal friction ϕ, L/H ratio, C/γH, q/γH etc., likely to be used in practice has been considered and is given in Table 5.1. Values of non-dimensional resultant pressure $\left(P/1/2\gamma.H^2\right)$ for some typical cases are presented in Figures 5.17 to 5.24 (for cantilever retaining wall) and Figures 5.25 to 5.32 (for counterfort retaining wall) and values of non-dimensional moments $\left(M/1/6\gamma.H^3\right)$ are given in Figures

5.33 to 5.40 (for cantilever retaining wall) and Figures 5.41 to 5.48 (for counterfort retaining wall).

5.3.6 Validation of Analytical Results

Analytical results are compared with the work reported by Saran et al (1992) on cantilever retaining wall considering uniformly distributed surcharge load on the reinforced cohesionless backfill. The figure 5.49 shows that the present analysis is in good agreement with the analysis by Saran et al (1992).

5.4 Analysis of a counterfort retaining wall with shelves

Counterfort retaining wall with shelves with vertical back face having unreinforced backfill are analyzed by considering observed planar failure surfaces. It is analyzed by using the analytical method given by Jumikis (1964). According to Jumikis, if the counterforted wall is provided with relief shelves, then the stability analysis is performed as shown in the figure 5.50. The lateral earth pressure E_1 for the upper part of the wall is determined as usual (and without the relief platform). The earth pressure, E_2, is less than usual, and so is E_3. The uniformly distributed loads for proportioning the relief platforms are $q_1 = \gamma.H_1$ and $q_2 = \gamma.H_2$.

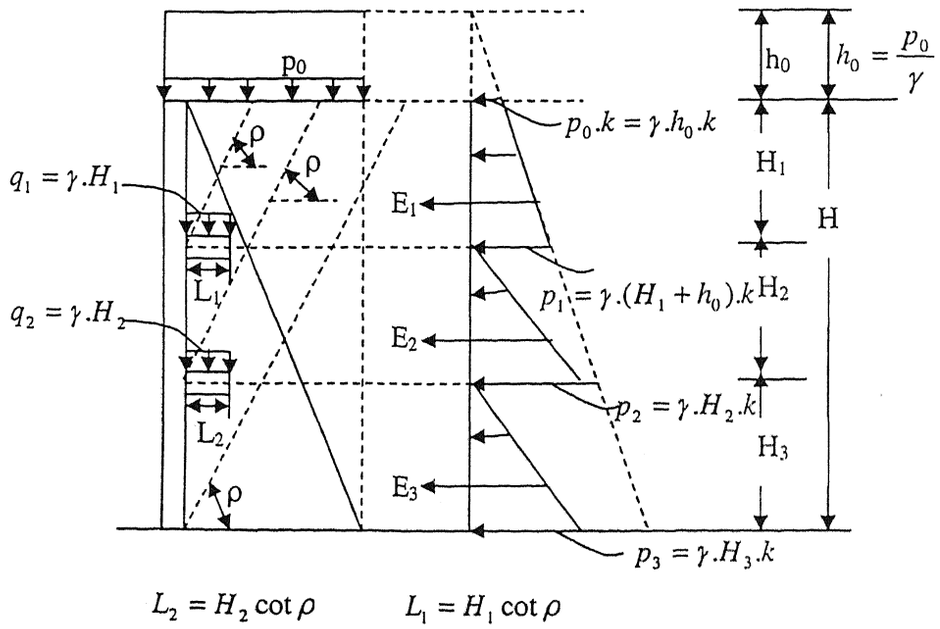

Figure 5.50: Counterforted wall with relief shelves

Here,

p_0 = uniformly distributed surcharge load on the backfill.

ρ = angle of failure surface with the horizontal.

q_1 and q_2 = uniformly distributed load on the relief shelves.

L_1 and L_2 = widths of the two relief shelves.

γ = unit weight of backfill material.

k = coefficient of active earth pressure $= \frac{(1-\sin\phi)}{(1+\sin\phi)}$.

ϕ = angle of internal friction of backfill material.

H = height of the retaining wall.

E_1, E_2 and E_3 are the earth pressures fro the H_1, H_2 and H_3 height of the retaining wall.

Table 5.1
Parameters considered for parametric study

Parameter	Range	Interval
ϕ	20°-35°	5°
δ	2 /3 for all cases	-
θ	$45^0-\phi/2$	-
D_P	0.25-1.0	0.25
L/H	0.0-1.0	0.2
$c/\gamma H$	0.0-0.10	0.05
$q/\gamma H$	0.0-0.50	0.25

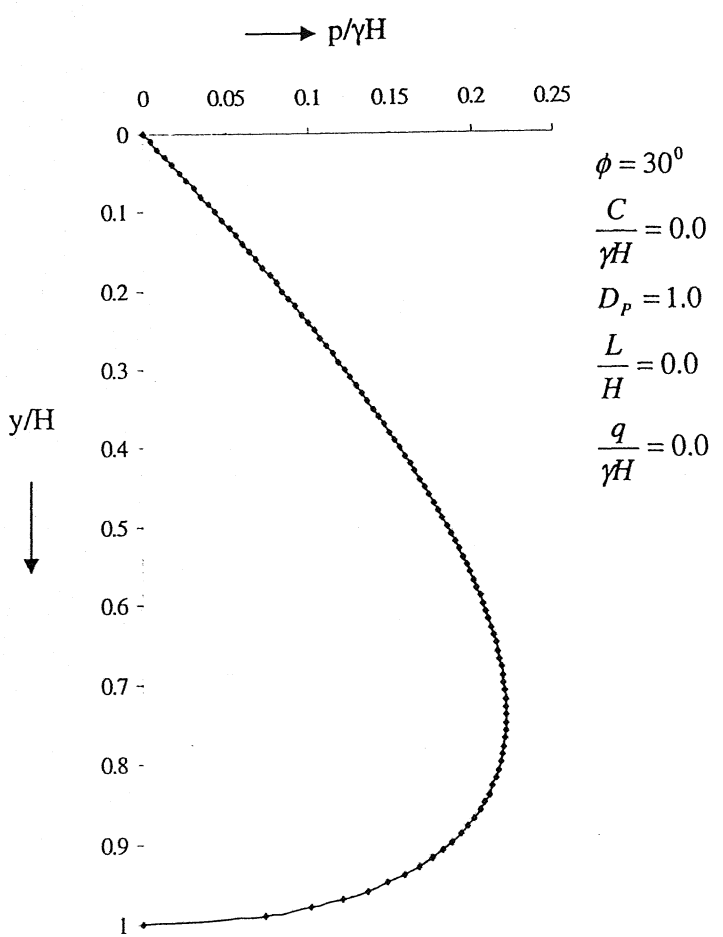

Figure 5.15a: Pressure Distribution

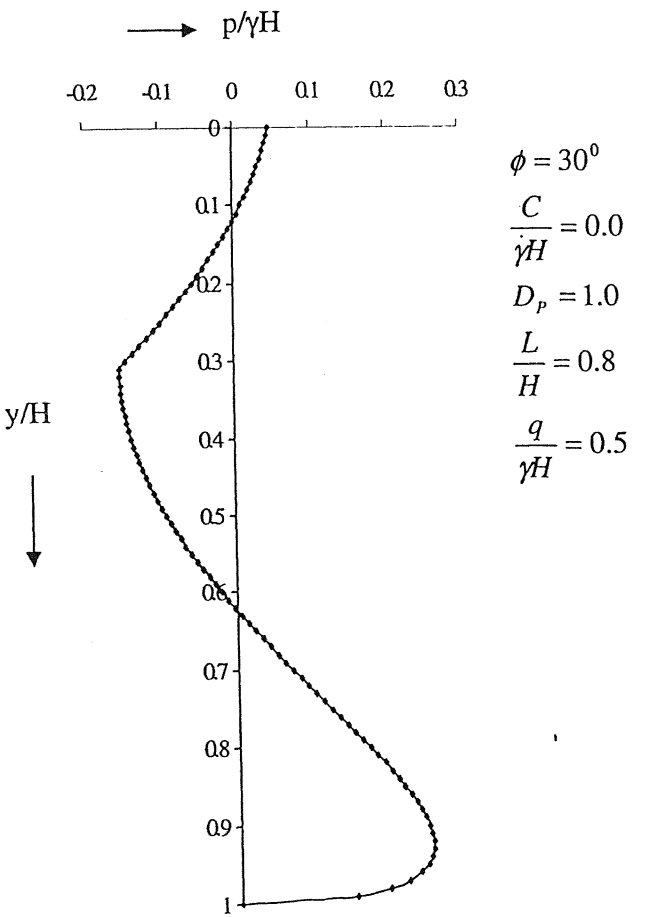

Figure 5.15b: Pressure Distribution

Figure 5.15: Pressure distribution diagram (cantilever retaining wall)

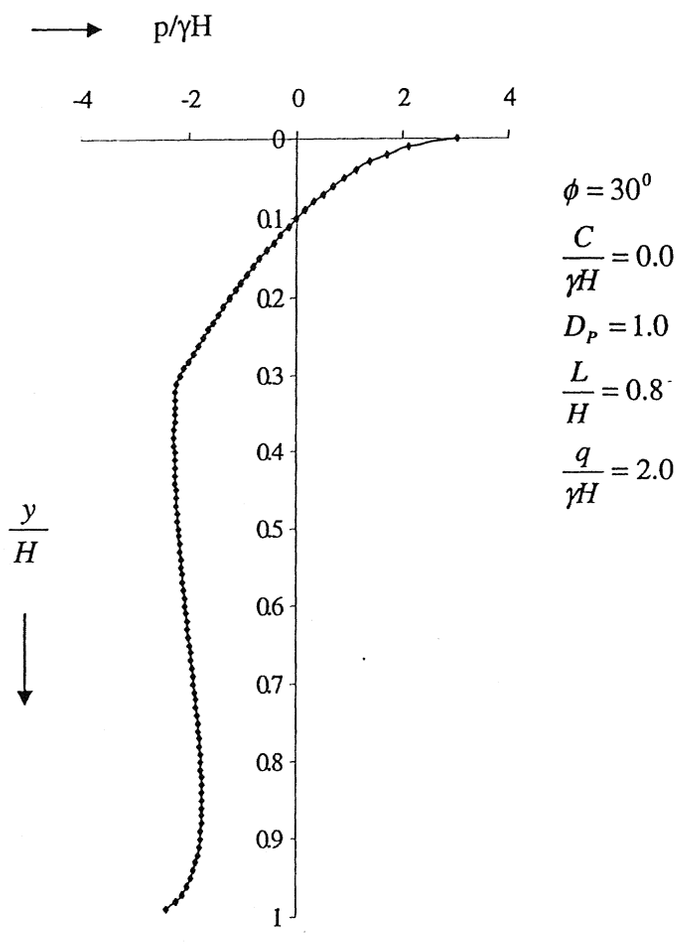

Figure 5.16a: Pressure Distribution

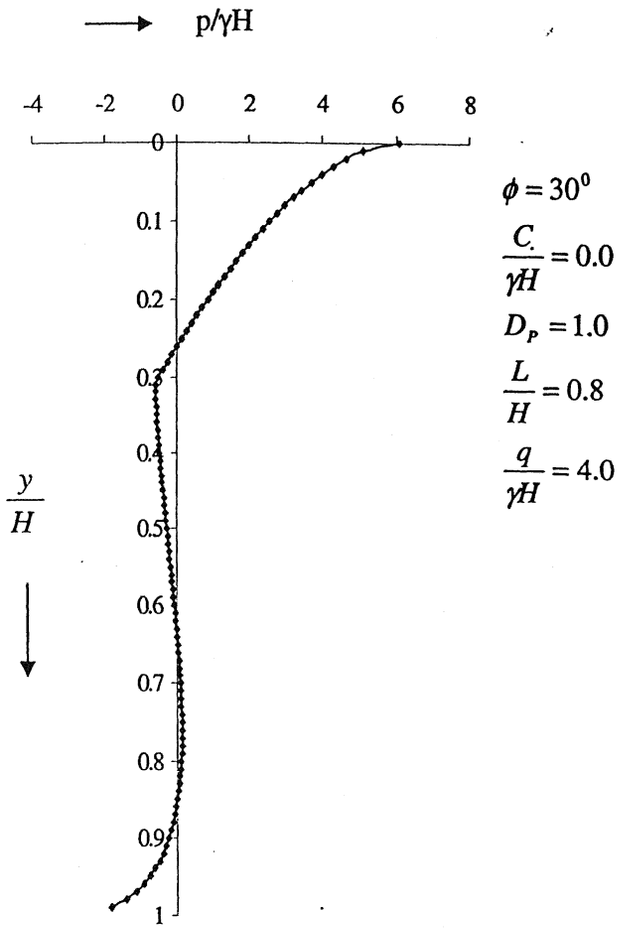

Figure 5.16b: Pressure Distribution

Figure 5.16: Pressure distribution diagram (counterfort retaining wall)

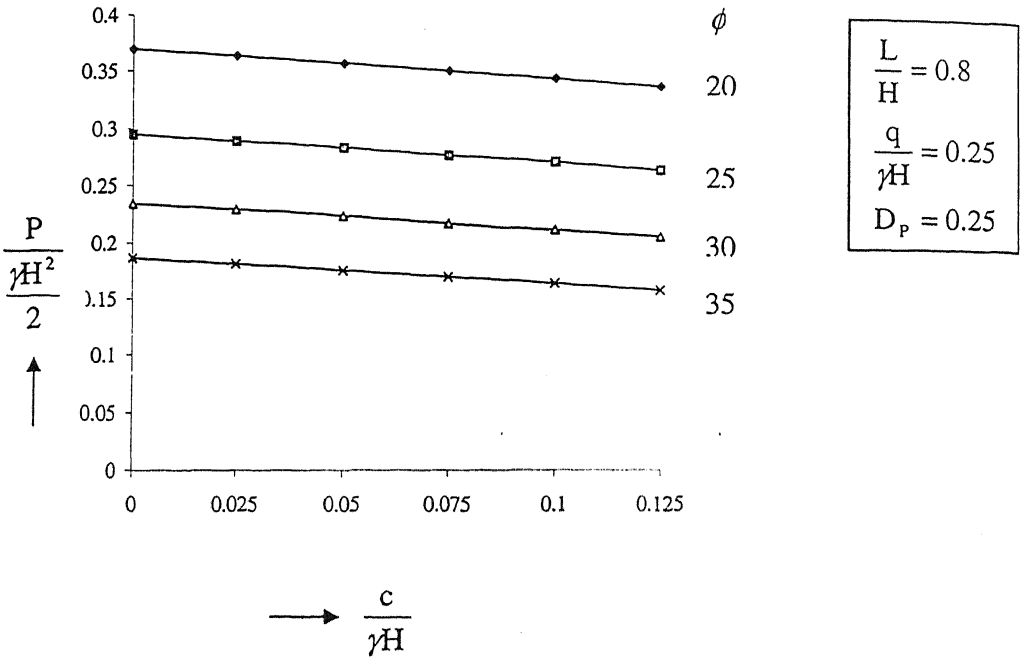

Figure 5.17: Resultant earth pressure versus $\frac{c}{\gamma H}$ (cantilever retaining wall)

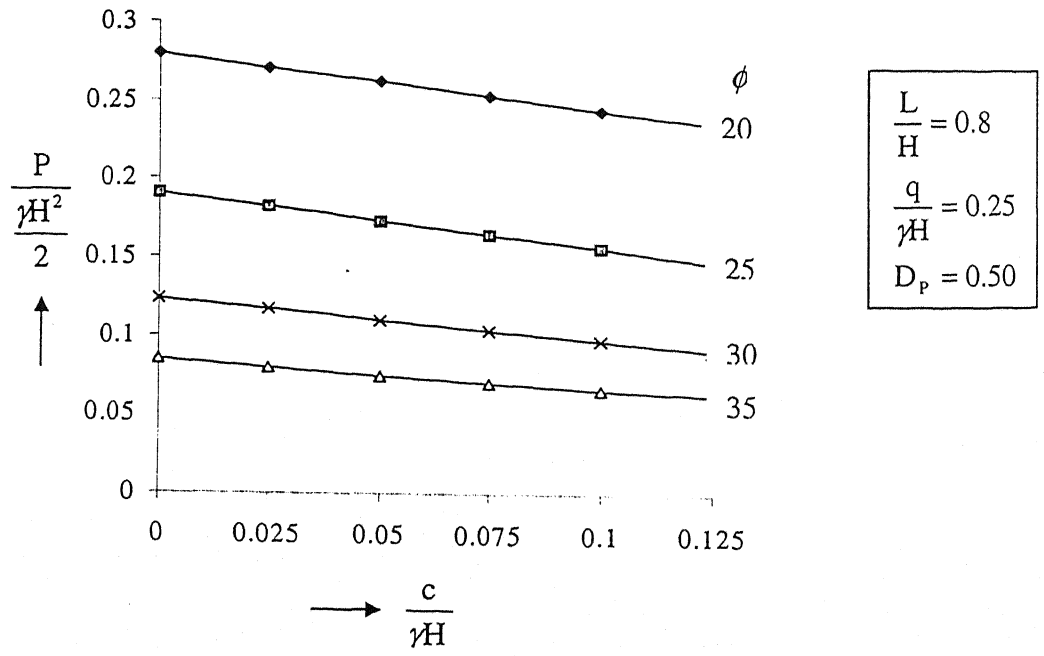

Figure 5.18: Resultant earth pressure versus $\frac{c}{\gamma H}$ (cantilever retaining wall)

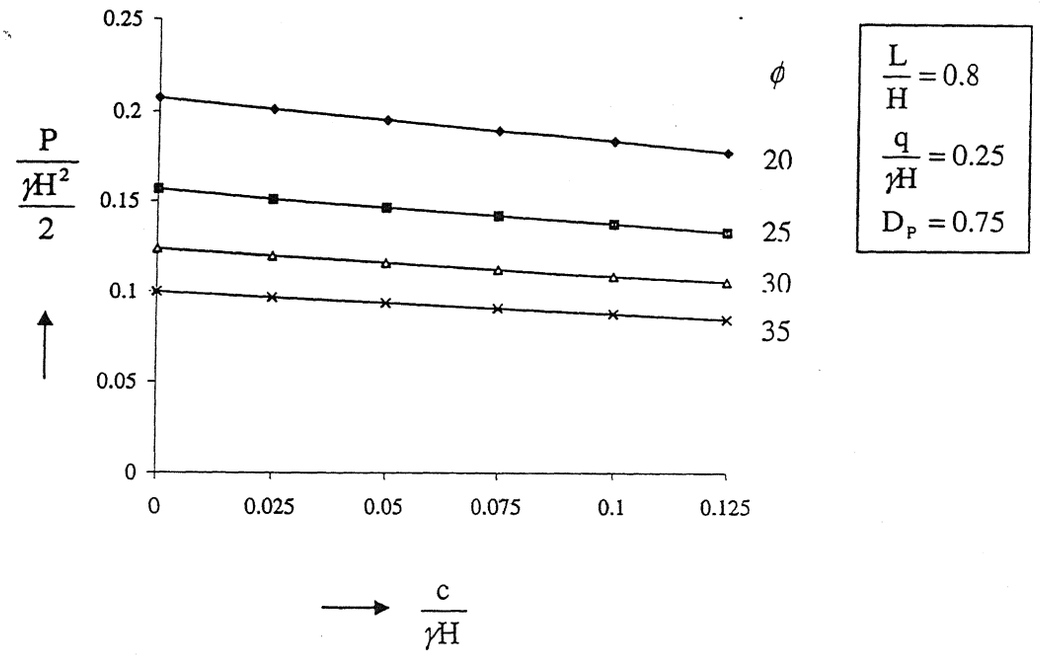

Figure 5.19: Resultant earth pressure versus $\frac{c}{\gamma H}$ (cantilever retaining wall)

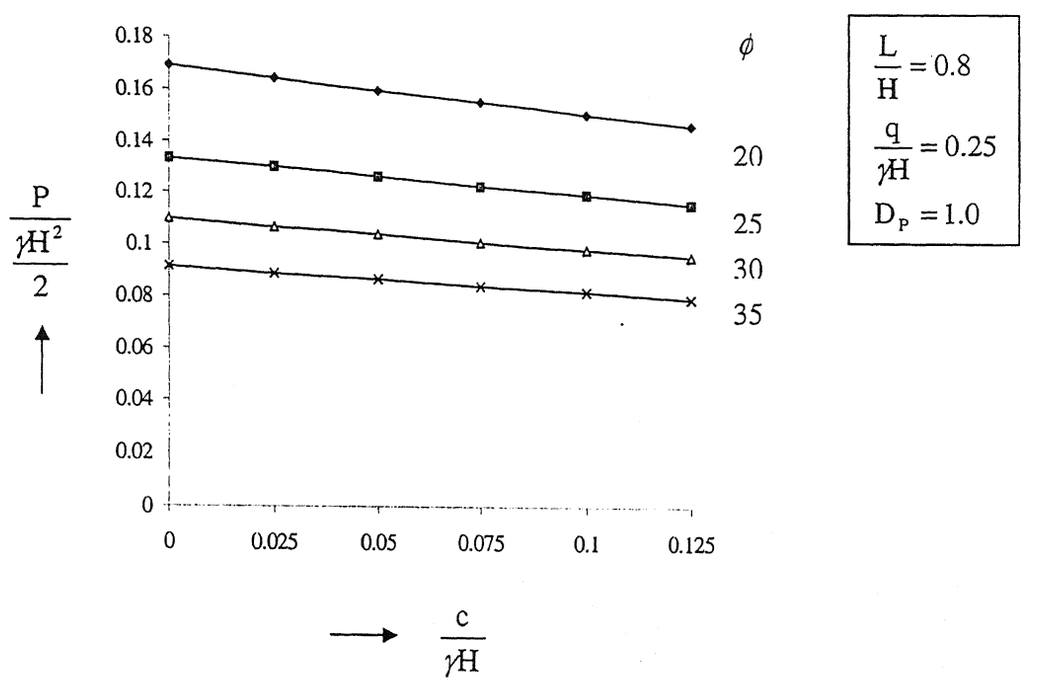

Figure 5.20: Resultant earth pressure versus $\frac{c}{\gamma H}$ (cantilever retaining wall)

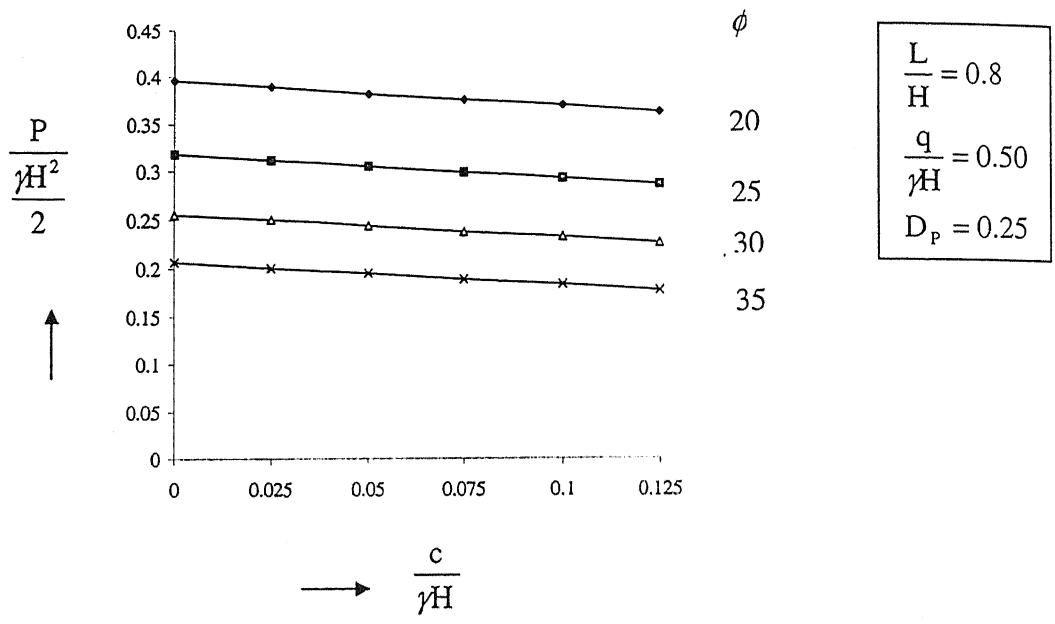

Figure 5.21: Resultant earth pressure versus $\frac{c}{\gamma H}$ (cantilever retaining wall)

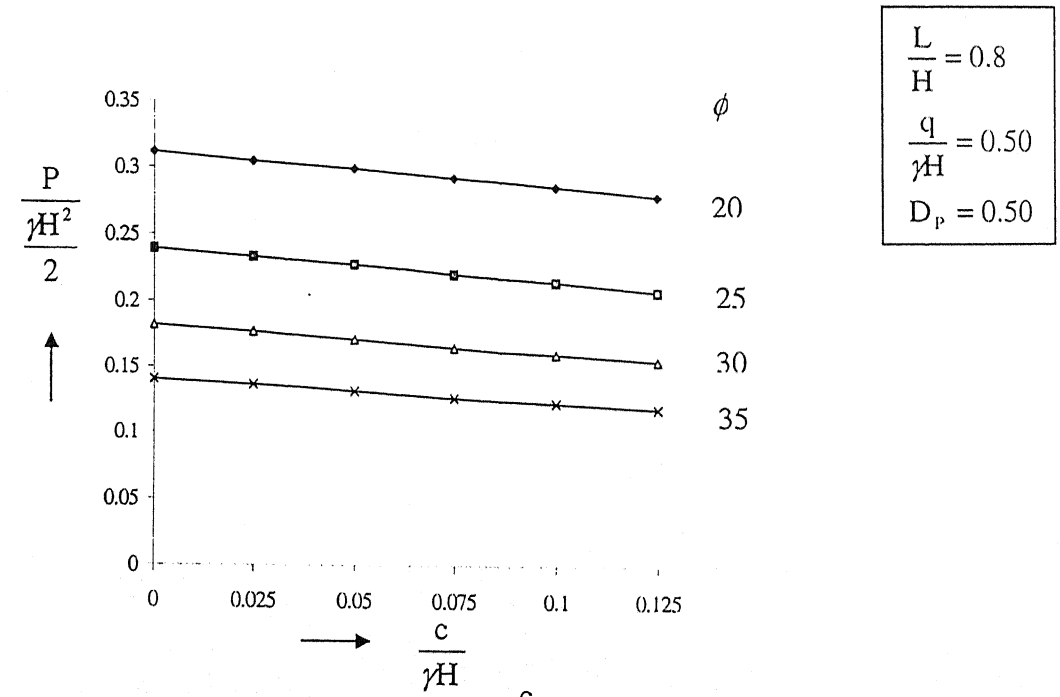

Figure 5.22: Resultant earth pressure versus $\frac{c}{\gamma H}$ (cantilever retaining wall)

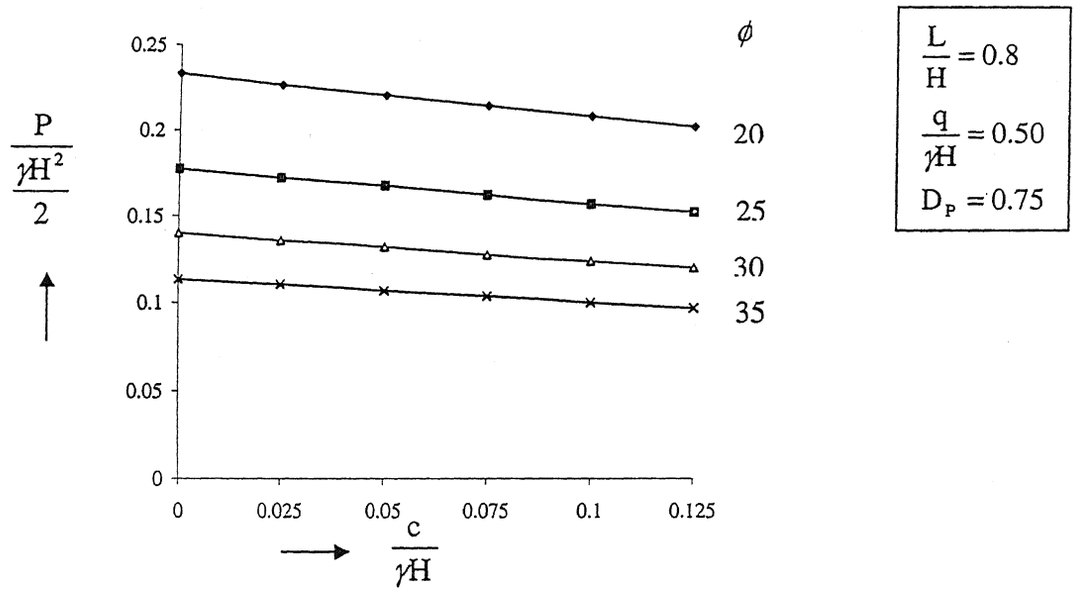

Figure 5.23: Resultant earth pressure versus $\frac{c}{\gamma H}$ (cantilever retaining wall)

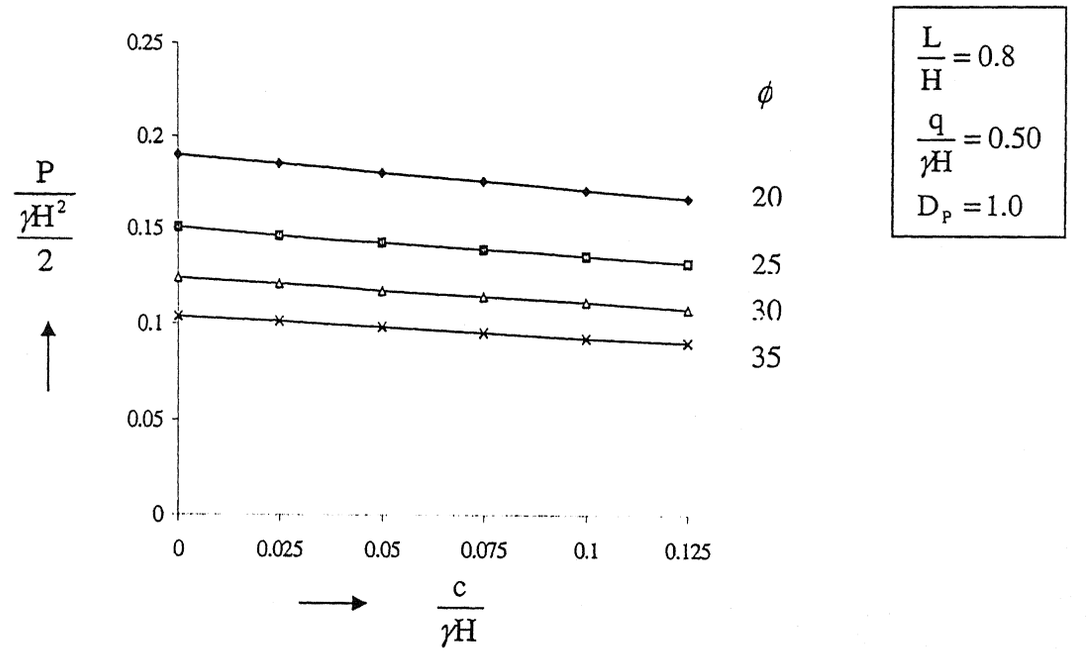

Figure 5.24: Resultant earth pressure versus $\frac{c}{\gamma H}$ for (cantilever retaining wall)

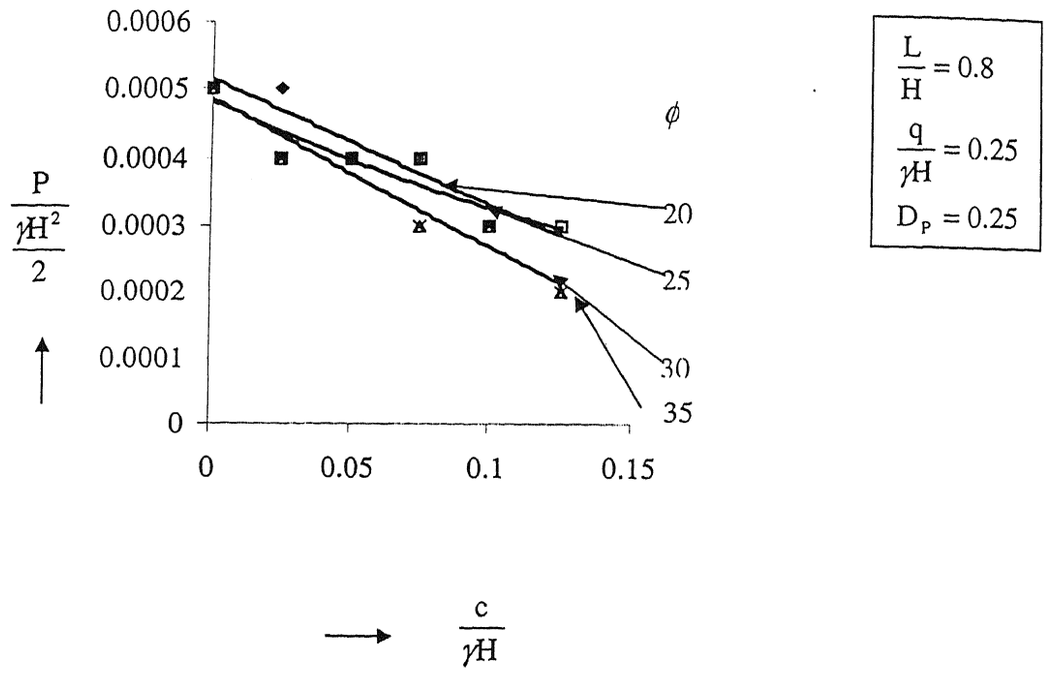

Figure 5.25: Resultant earth pressure versus $\frac{c}{\gamma H}$ (Counterfort Retaining wall)

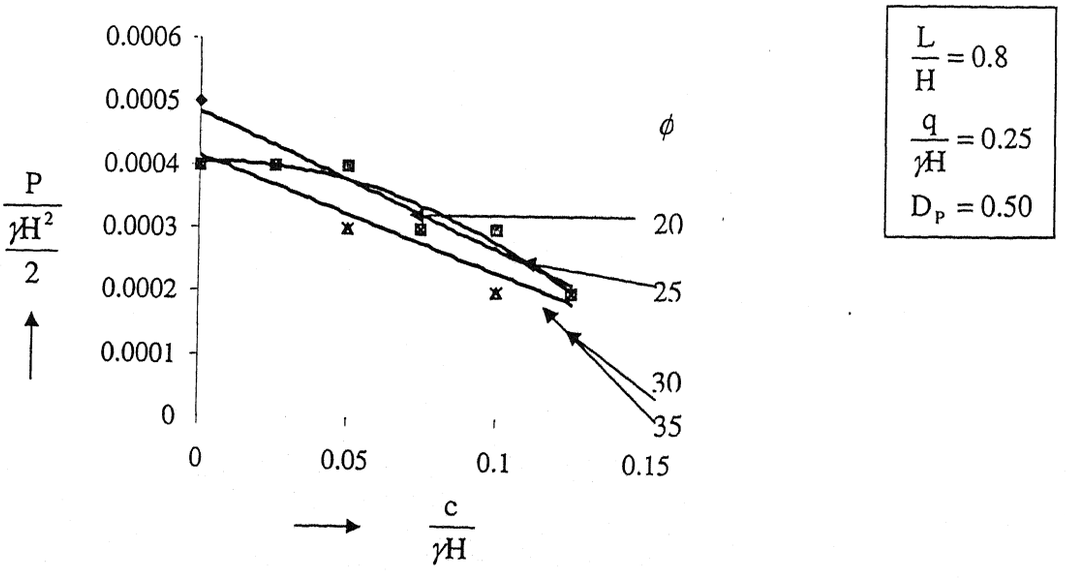

Figure 5.26: Resultant earth pressure versus $\frac{c}{\gamma H}$ (Counterfort Retaining wall)

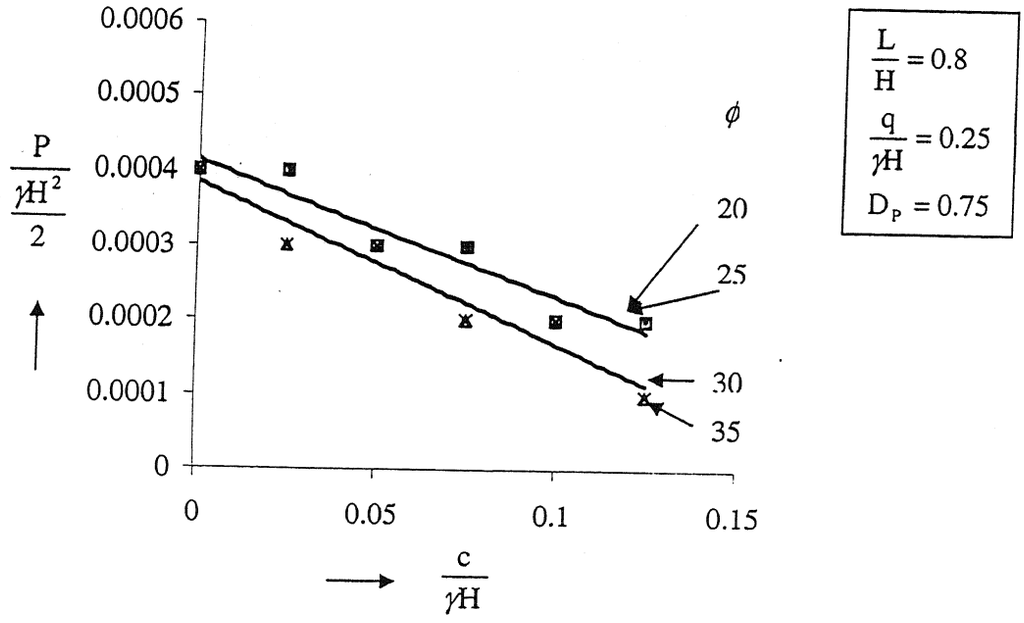

Figure 5.27: Resultant earth pressure versus $\frac{c}{\gamma H}$ (Counterfort Retaining wall)

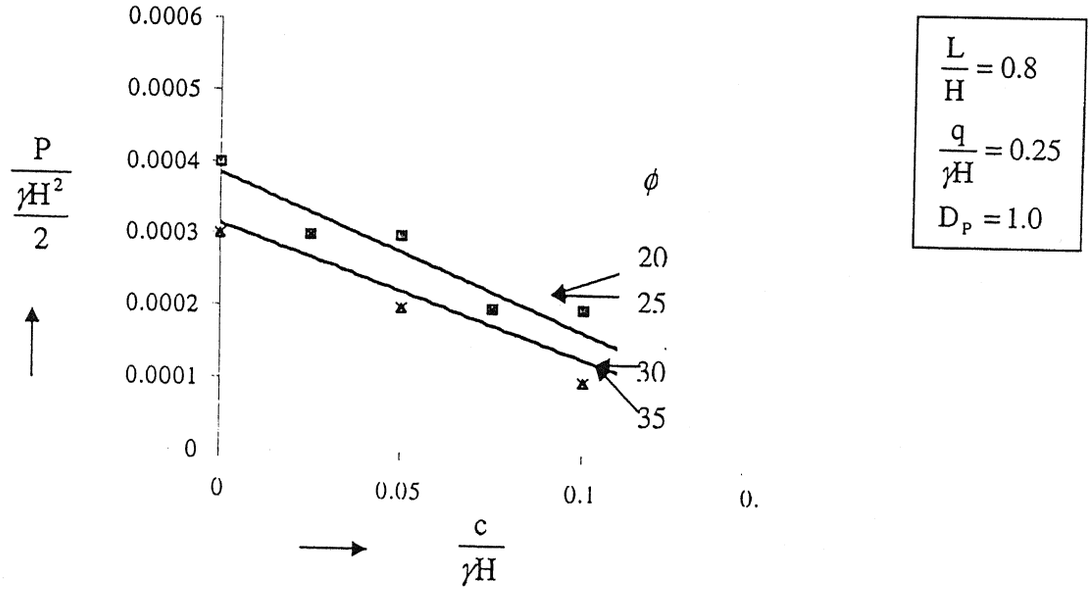

Figure 5.28: Resultant earth pressure versus $\frac{c}{\gamma H}$ (Counterfort Retaining wall)

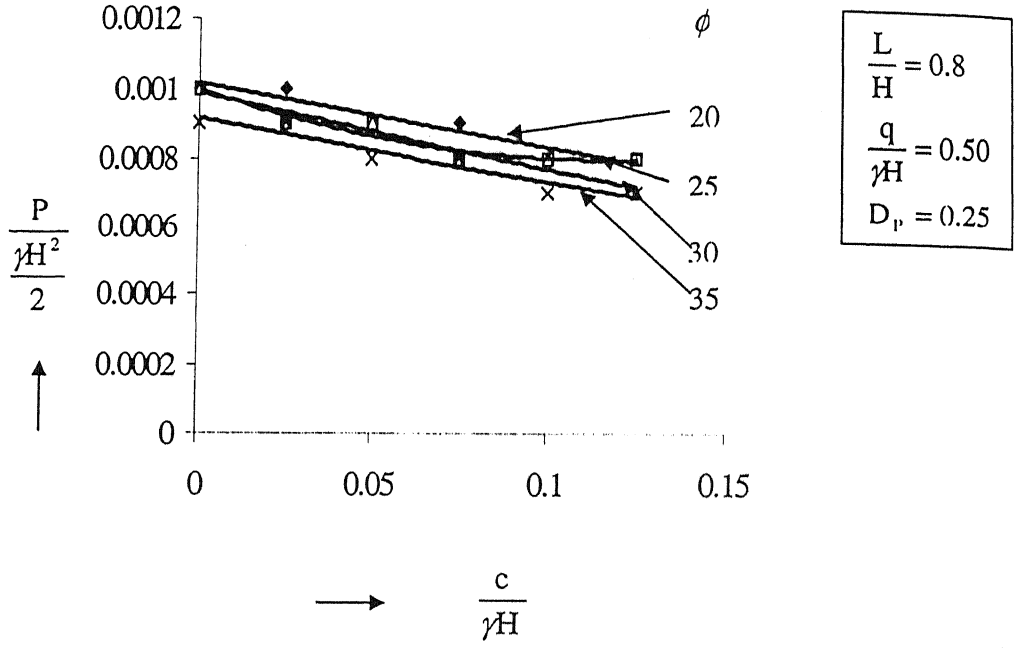

Figure 5.29: Resultant earth pressure versus $\frac{c}{\gamma H}$ (Counterfort Retaining wall)

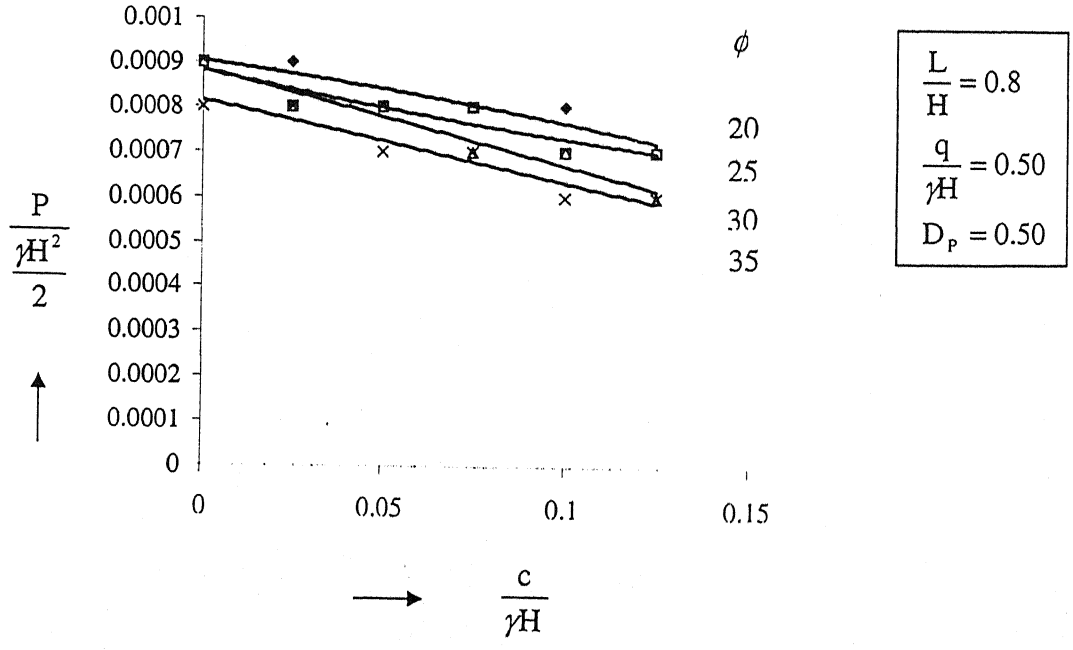

Figure 5.30: Resultant earth pressure versus $\frac{c}{\gamma H}$ (Counterfort Retaining wall)

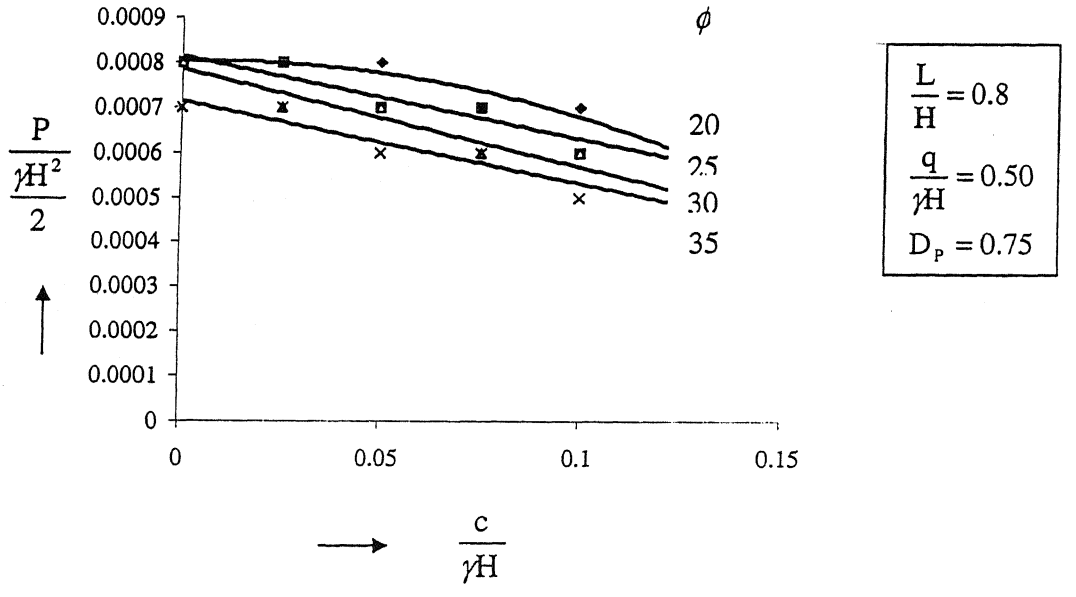

Figure 5.31: Resultant earth pressure versus $\frac{c}{\gamma H}$ (Counterfort Retaining wall)

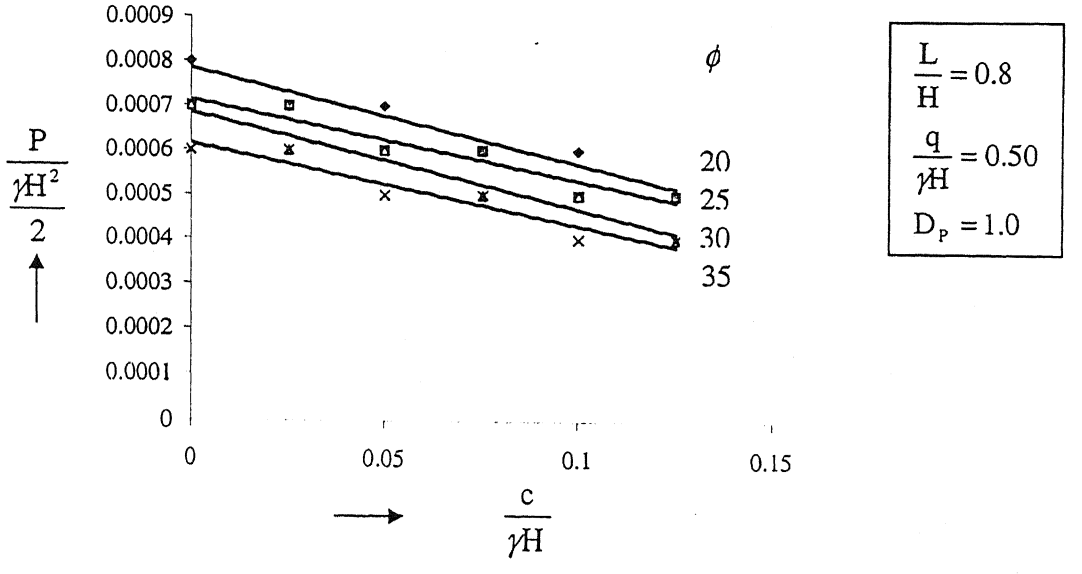

Figure 5.32: Resultant earth pressure versus $\frac{c}{\gamma H}$ (Counterfort Retaining wall)

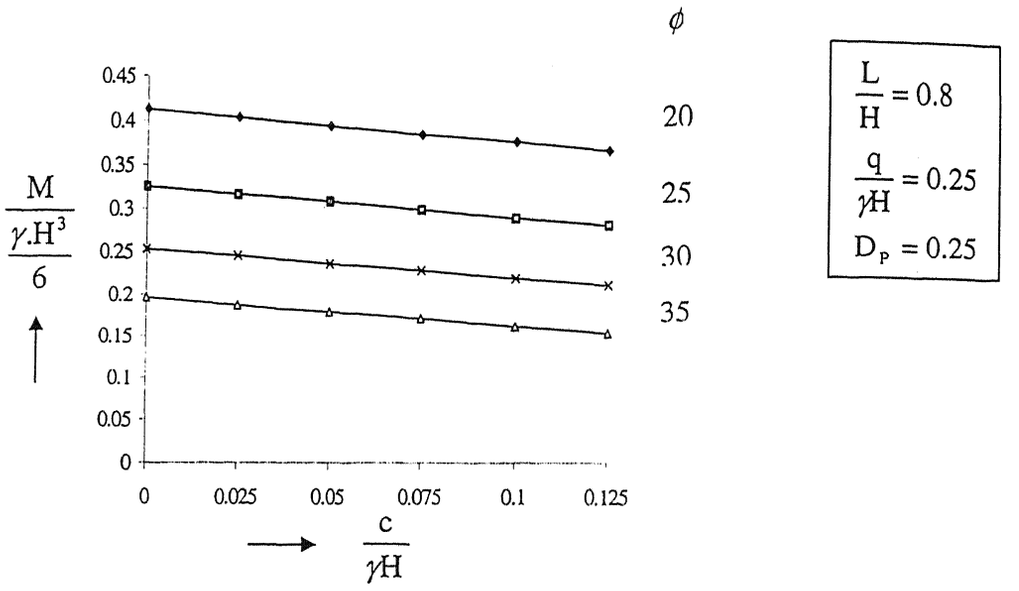

Figure 5.33: Resultant moment versus $\frac{c}{\gamma H}$ (Cantilever Retaining wall)

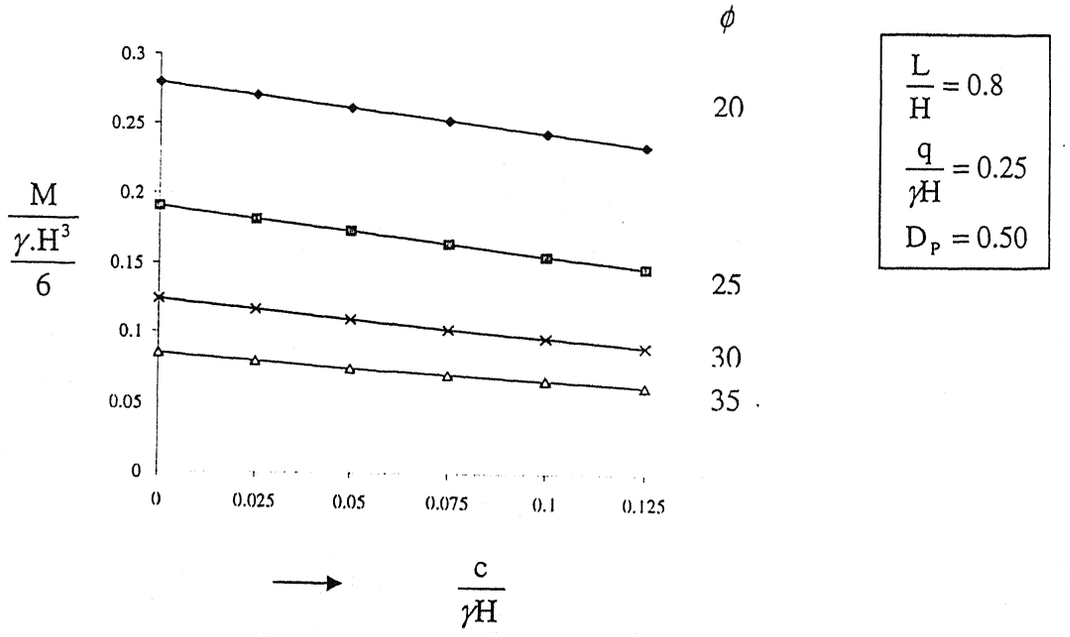

Figure 5.34: Resultant moment versus $\frac{c}{\gamma H}$ (Cantilever Retaining wall)

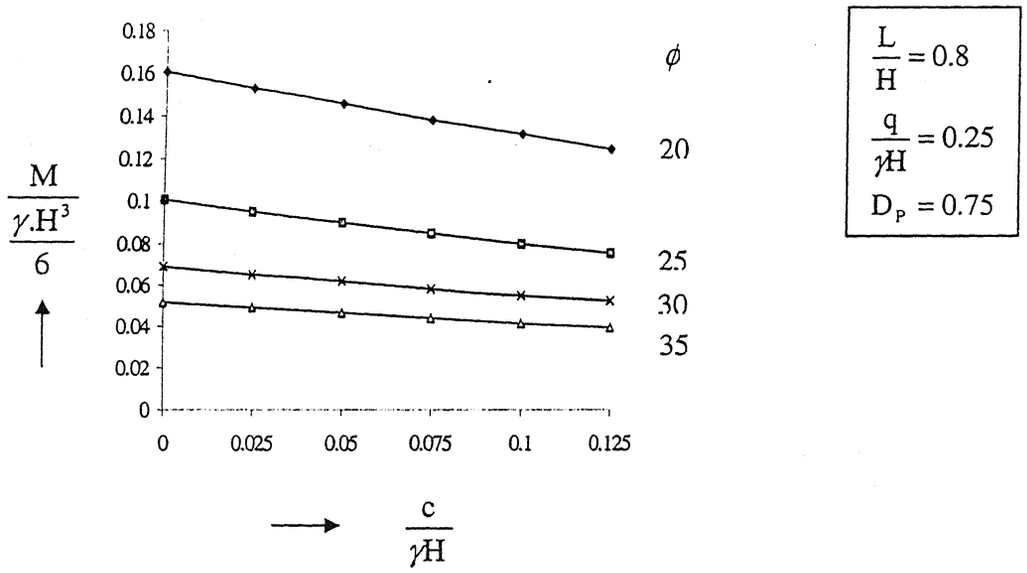

Figure 5.35: Resultant moment versus $\frac{c}{\gamma H}$ (Cantilever Retaining wall)

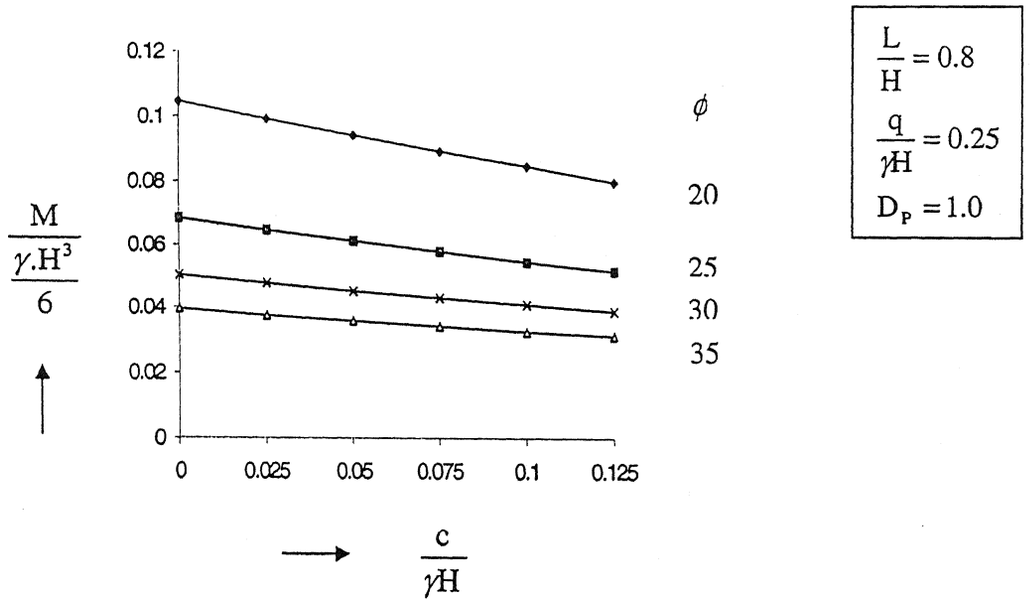

Figure 5.36: Resultant moment versus $\frac{c}{\gamma H}$ (Cantilever Retaining wall)

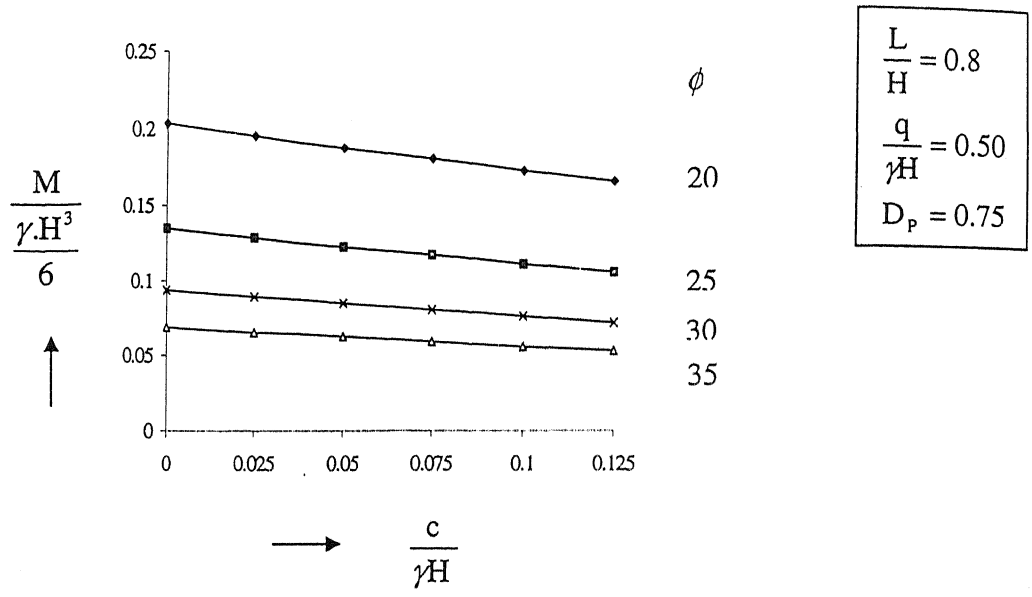

Figure 5.39: Resultant moment versus $\frac{c}{\gamma H}$ (Cantilever Retaining wall)

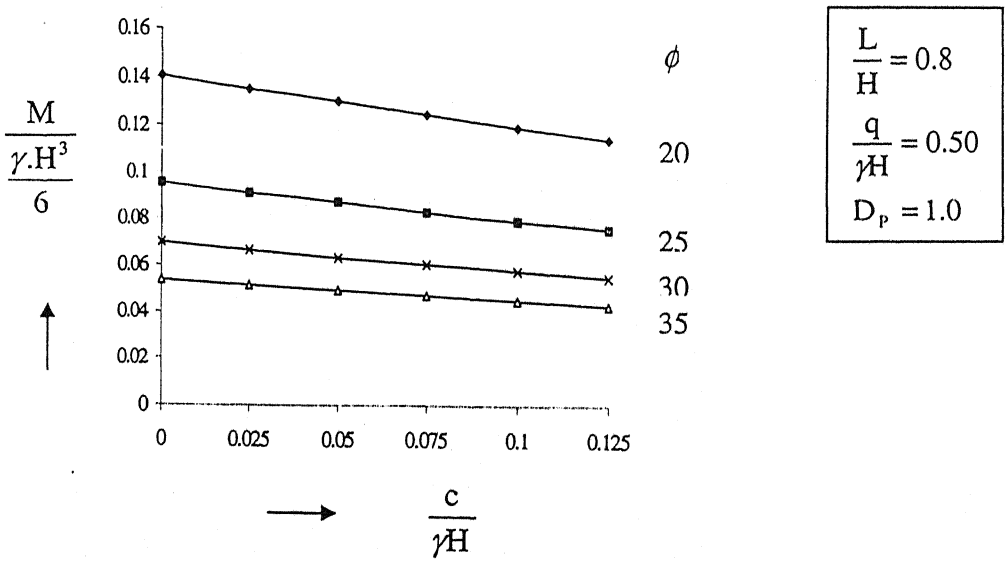

Figure 5.40: Resultant moment versus $\frac{c}{\gamma H}$ (Cantilever Retaining wall)

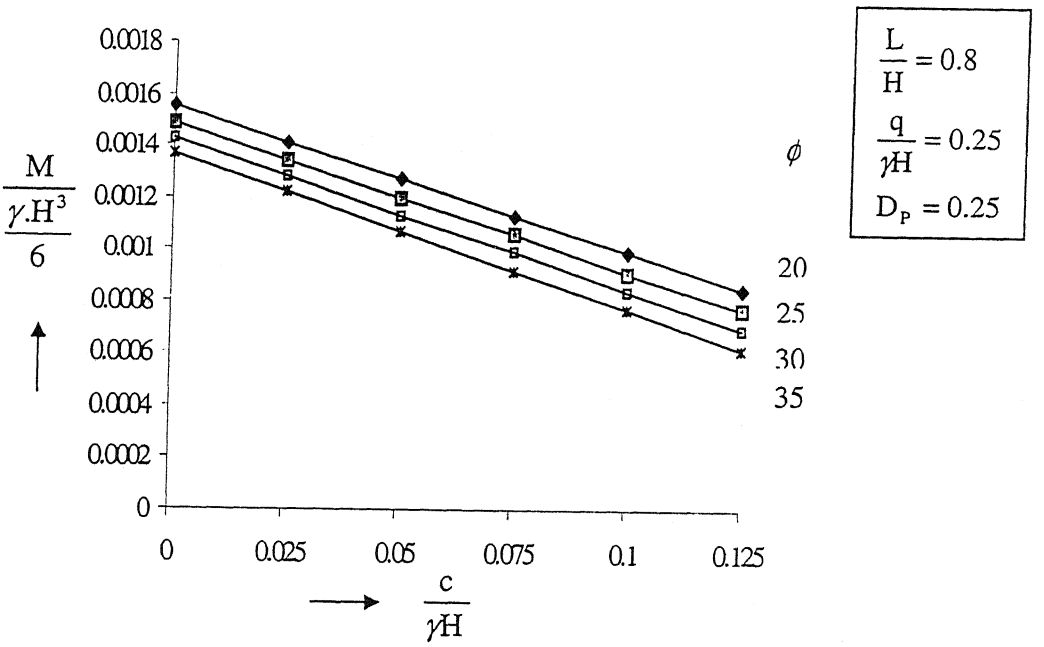

Figure 5.41: Resultant moment versus $\frac{c}{\gamma H}$ (Counterfort Retaining wall)

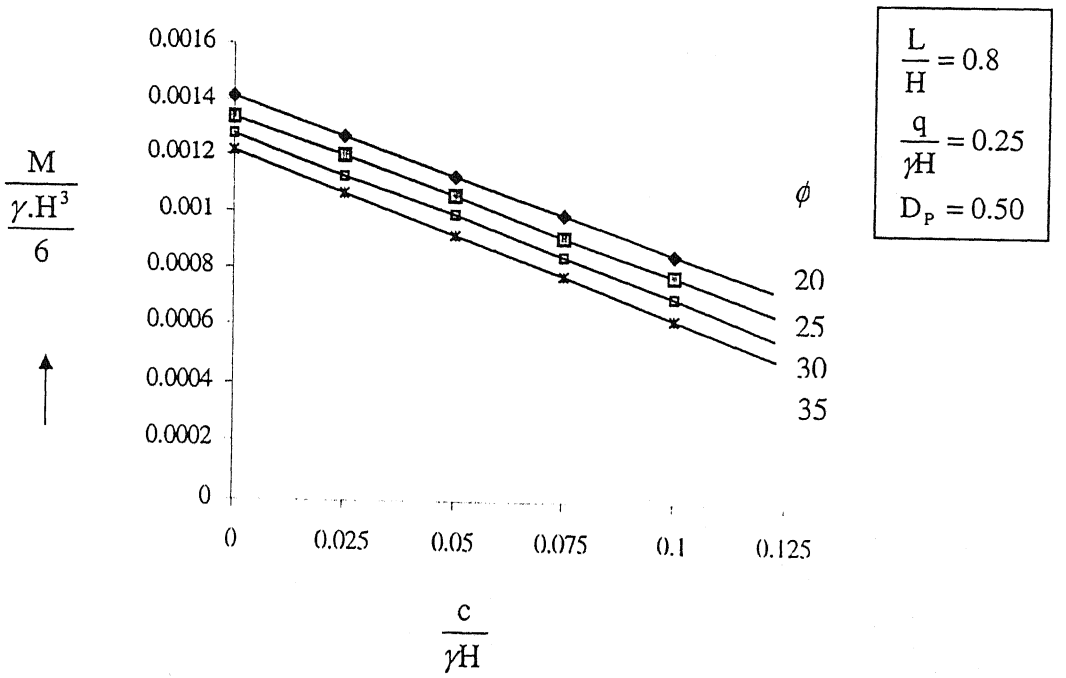

Figure 5.42: Resultant moment versus $\frac{c}{\gamma H}$ (Counterfort Retaining wall)

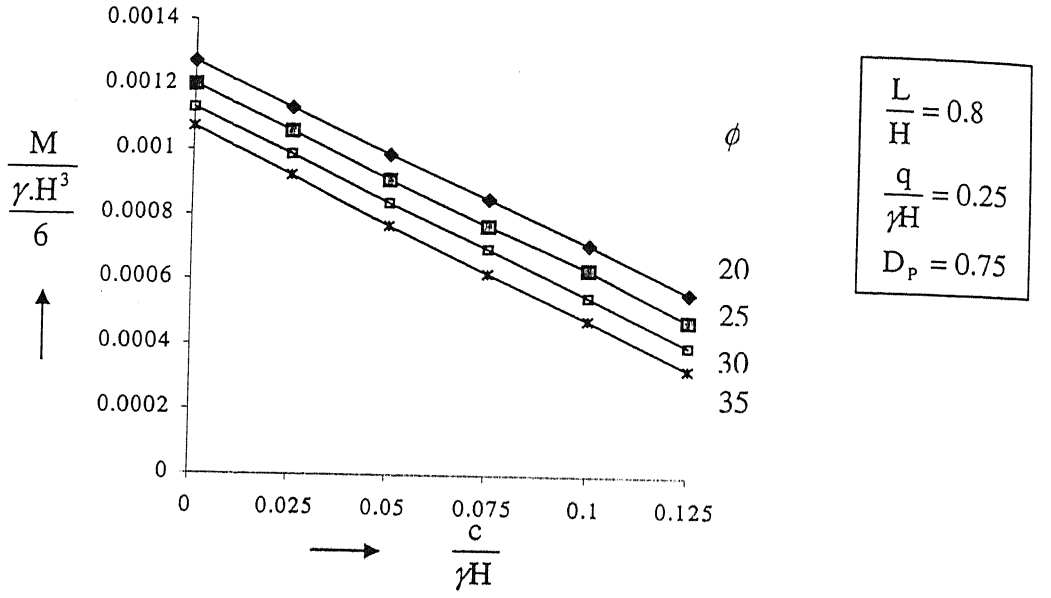

Figure 5.43: Resultant moment versus $\frac{c}{\gamma H}$ (Counterfort Retaining wall)

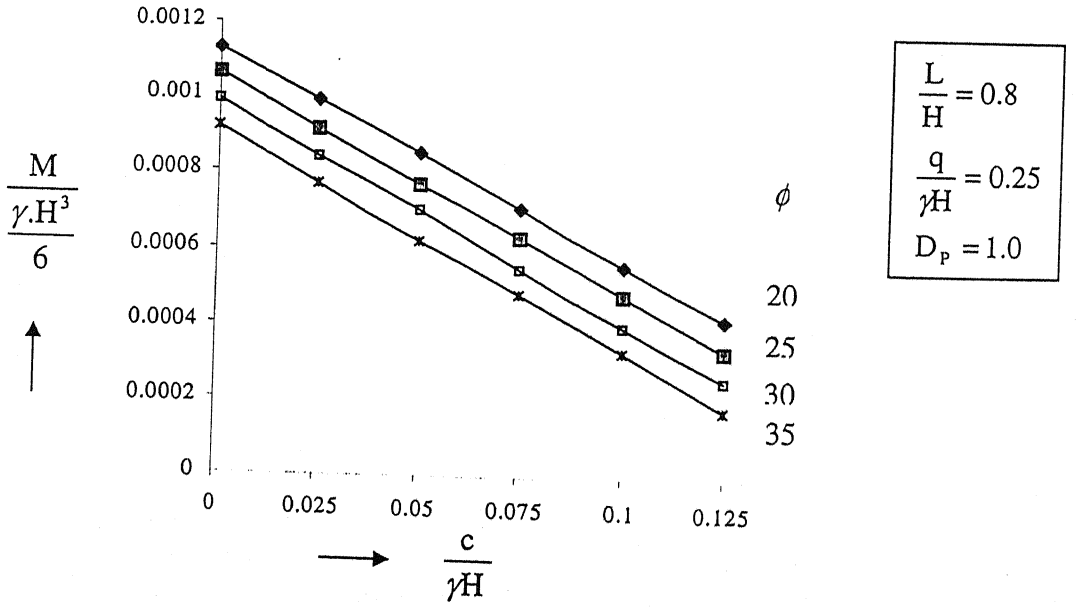

Figure 5.44: Resultant moment versus $\frac{c}{\gamma H}$ (Counterfort Retaining wall)

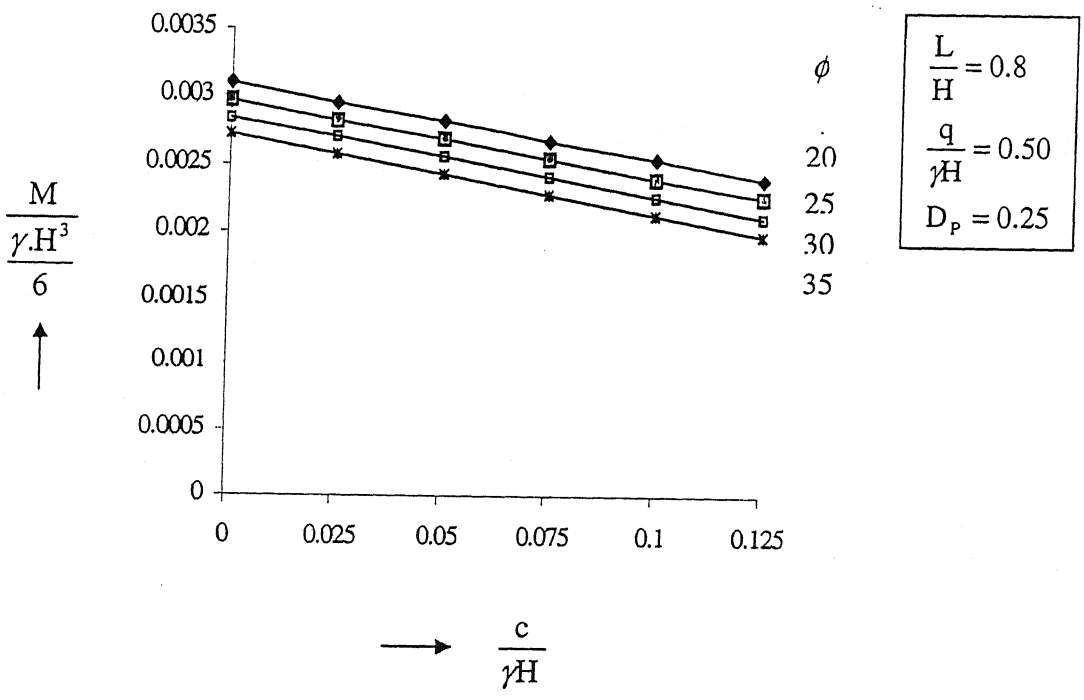

Figure 5.45: Resultant moment versus $\frac{c}{\gamma H}$ (Counterfort Retaining wall)

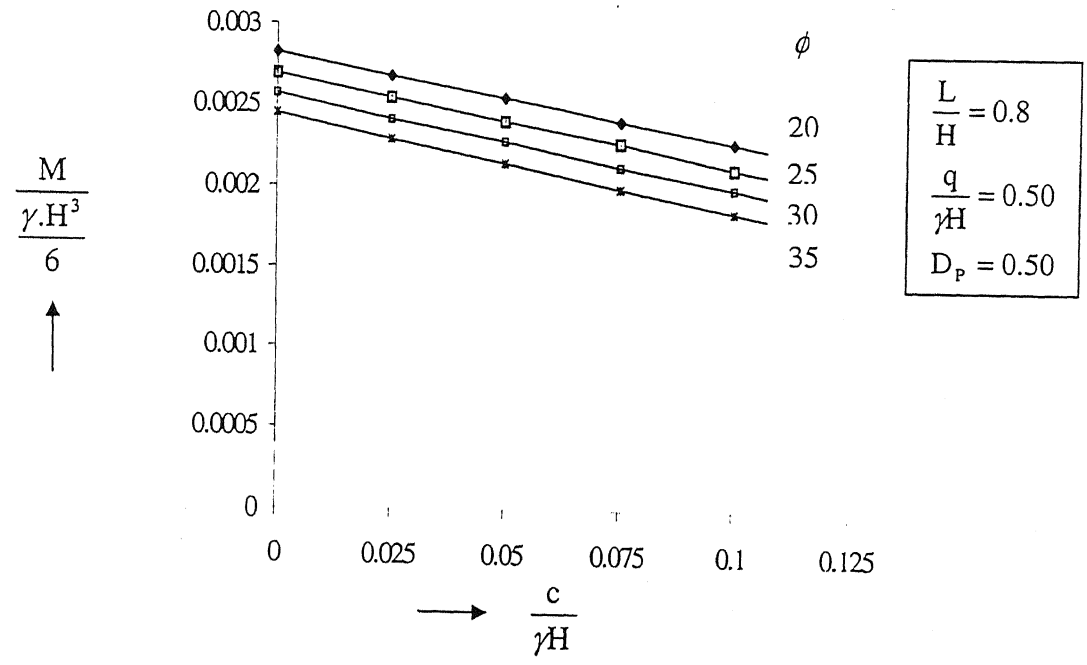

Figure 5.46: Resultant moment versus $\frac{c}{\gamma H}$ (Counterfort Retaining wall)

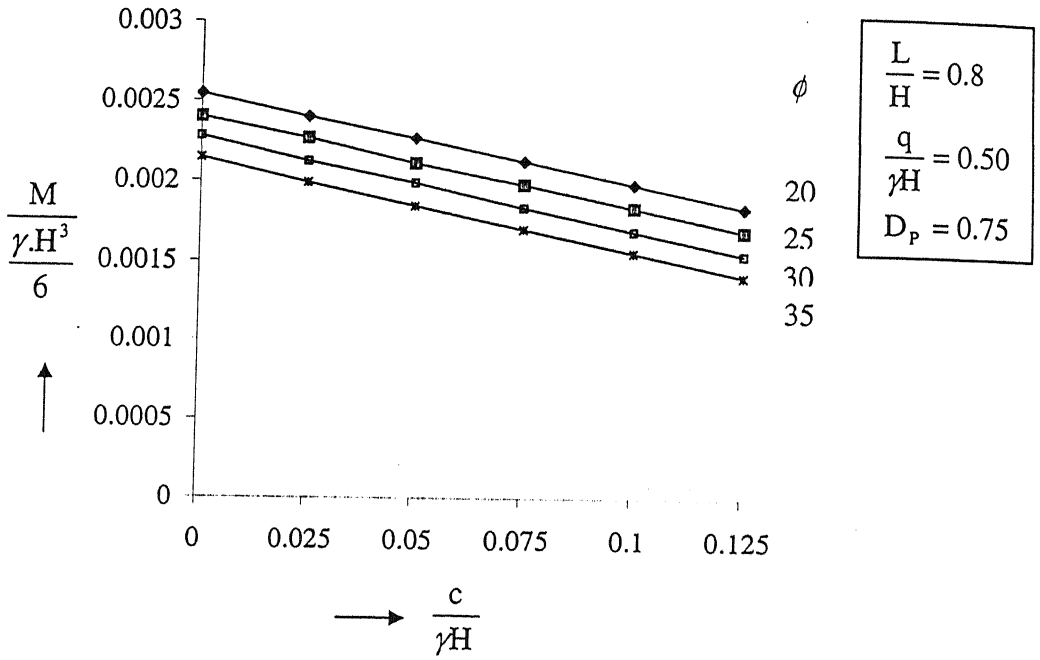

Figure 5.47: Resultant moment versus $\frac{c}{\gamma H}$ (Counterfort Retaining wall)

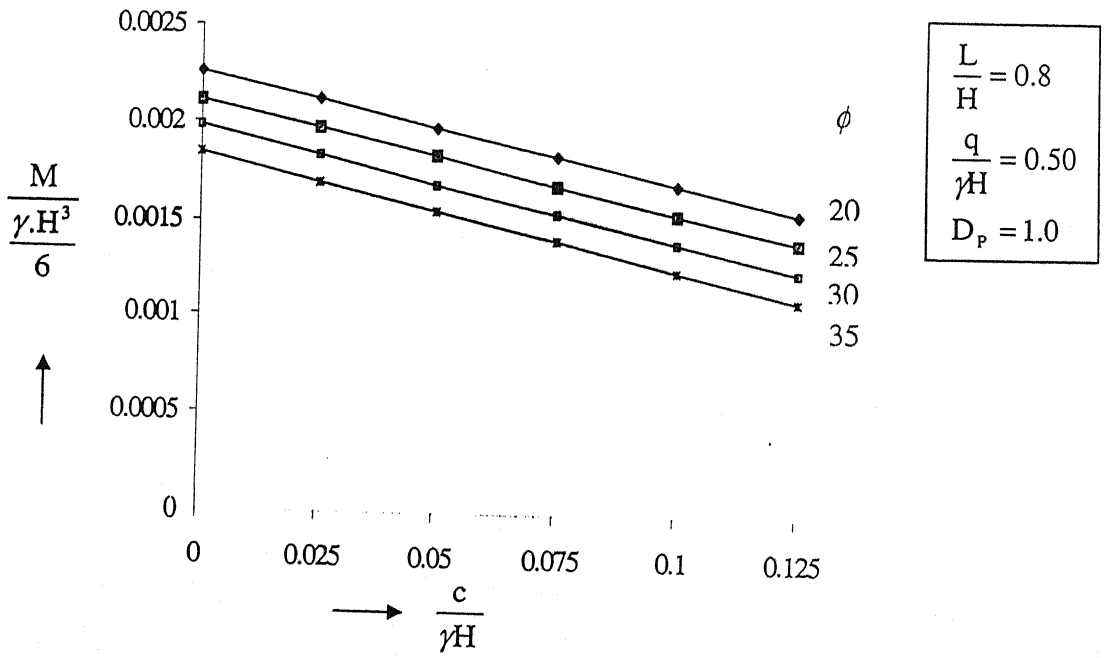

Figure 5.48: Resultant moment versus $\frac{c}{\gamma H}$ (Counterfort Retaining wall)

Analysis

$$K_\gamma = \frac{P_\gamma}{\frac{1}{2}\gamma.H^2}, \phi = 30^0$$

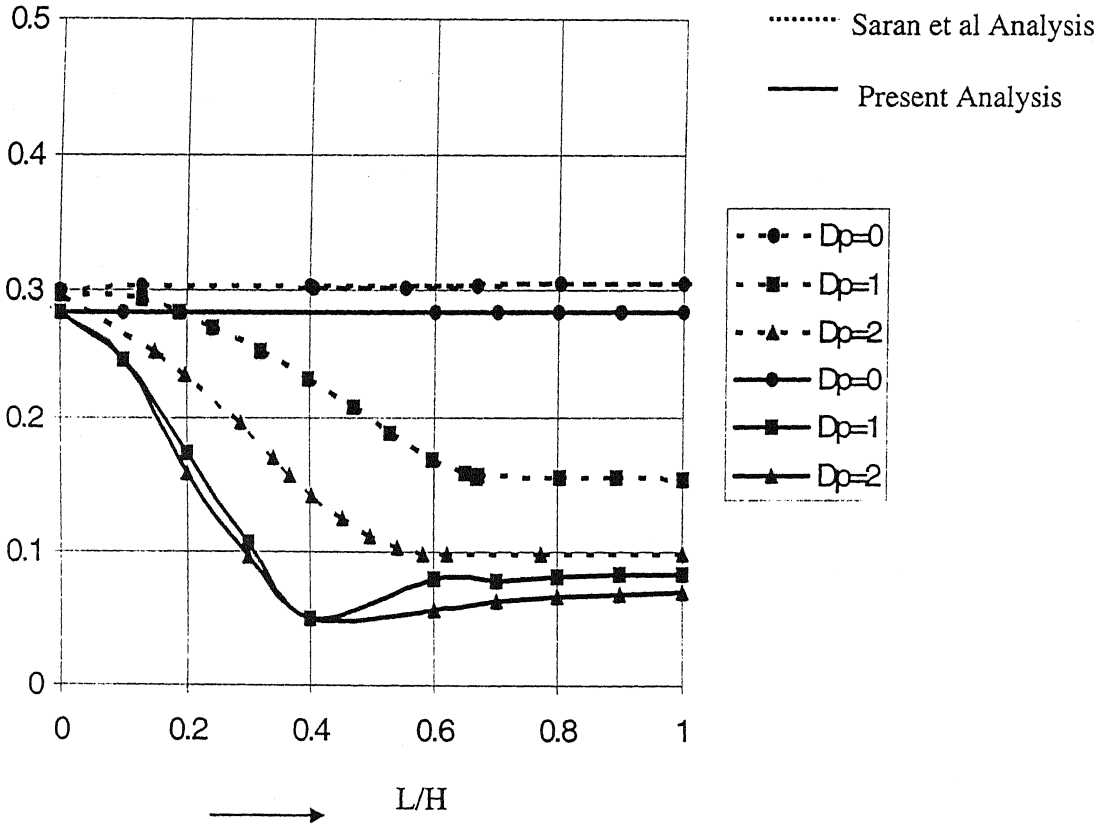

Figure 5.49: Comparison of present analysis with Saran et al (1992) analysis

CHAPTER VI

Comparison of Theoretical & Experimental Results

6.1 General

Comparisons of results are done for different case of retaining walls. Experimental results are compared with the analytical results for all the three cases of retaining walls. Also, Analytical results for counterfort retaining wall with shelves are compared with the values for counterfort retaining wall without shelves.

6.2. Comparison of experimental results with analytical results

Experimental results are compared with the analytical results for all cantilever retaining walls, counterfort retaining walls and counterfort retaining wall with shelves. The sliding friction developed between soil and the two sides of test tank are added with the experimental overturning moments. The magnitudes of moments of frictional forces, acting on the two sides of tank (adjoining model wall) are calculated theoretically with the following equations.

$$M_F = M_{fq} + M_{F\gamma} \qquad (6.1)$$

where, M_F = Moment of side frictional force about base,

M_{fq} = Moment of side frictional force about base, due to surcharge.

$$M_{fq} = \frac{1}{6}\left[K_0\gamma.H^3 \tan\theta(\tan\delta_s + \tan\delta_p)\right]$$

and

$M_{F\gamma}$ = Moment of side frictional force about base, due to backfill.

$$M_{F\gamma} = \frac{1}{12}\left[K_0\gamma.H^4 \tan\theta(\tan\delta_s + \tan\delta_p)\right]$$

Where,

k_0 = Coefficient of earth pressure at rest = $(1-\sin\phi)$.

δ_S = angle of wall friction between soil and mild steel side of tank $(=2\phi/3)$.

δ_P = angle of wall friction between soil and perspex sheet forming side wall of tank $(=\phi/3)$.

The moment of side frictional forces on both side walls was computed using equation (6.1) for observed wedge angle. This moment was added to measured experimental moment.

6.2.1 Cantilever retaining wall

Experimental results are compared with the two types of analytical results such as parabolic failure surface and planar failure surface.

6.2.1.1 Parabolic failure surface

Experimental resultant earth pressures are compared with the analytical values for sand and fly ash backfill. In the analytical method, the resultant earth pressures are calculated for sand and fly ash backfill from equations 5.3, 5.6a, 5.6b, 5.9, 5.12, 5.13a, 5.13b and 5.14 (given in chapter V).

For calculating resultant earth pressures for sand backfill, the different parameters used are given below:

i) $\phi = 38^0$, ii) $\delta = 29.75^0$, iii) $\gamma = 14.62$ kN/m^2 iv) H = 0.9m, v) $c_w = 0$, vi) $c_s = 0$,

vii) w = 0.15m, viii) $y_1 = 0.2$m, ix) $y_2 = 0.4$m, x) $y_3 = 0.6$m, xi) Q = 1.6kN/m,

xii) 1.8kN/m^2.

For calculating resultant earth pressures for fly ash backfill, the different parameters used are given below:

i) $\phi = 39^0$, ii) $\delta = 26^0$, iii) $\gamma = 8.55$ kN/m^2 iv) H = 0.9m, v) $c_w = 1$kN/m^2, vi) $c_s = 1$kN/m^2,

vii) w = 0.15m, viii) y_1 = 0.15m, ix) y_2 = 0.45m, x) y_3 = 0.75m, xi) Q = 1.6kN/m, xii) 1.8kN/m^2.

The values of θ, a, b, c, l_{e_1}, l_{e_2} and l_{e_3} are measured from the observed failure surfaces for different experimental studies.

Measured values of the resultant earth pressures are plotted against the predicted values in the figures 6.1 and 6.2 for sand and fly ash backfill respectively. The ideal line having an equation of $p_{measured} = p_{predicted}$ is also plotted. The predicted values are about 41% and 44% more than the observed values for sand and fly ash backfill respectively.

6.2.1.2 Planar failure surface

Measured values of the overturning moments are plotted against the predicted values in the figures 6.3 and 6.4 for sand and fly ash backfill respectively. The observed value of the overturning moment is satisfactorily predicted by the theory. The predictions are very close to the line having an equation of $p_{measured} = p_{predicted}$.

6.2.2 Counterfort retaining wall

Experimental results are compared with the two types of analytical results such as parabolic failure surface and planar failure surface.

6.2.2.1 Parabolic failure surface

Experimental resultant earth pressures are compared with the analytical values for sand and fly ash backfill. In the analytical method resultant earth pressures for counterfort retaining wall are calculated for sand and fly ash backfill from equations 5.17, 5.18a, 5.18b, 5.19, 5.20, 5.21a, 5.21b and 5.22.

For calculating resultant earth pressures for sand backfill, the different parameters used are given below:

i) $\phi = 38^0$, ii) $\delta = 29.75^0$, iii) γ =14.62 kN/m^3 iv) H = 0.9m, v) c_w = 0, vi) c_s = 0,

vii) w = 0.15m, viii) y_1 = 0.2m, ix) y_2 = 0.4m, x) y_3 = 0.6m, xi) Q = 1.6kN/m,

xii) 1.8kN/m^2, xiii) θ_1 =19.29^0 and xiv) γ_c = 77kN/m^3.

For calculating resultant earth pressures for fly ash backfill, the different parameters used are given below:

i) ϕ =39^0, ii) δ = 26^0, iii) γ =8.55 kN/m^3 iv) H = 0.9m, v) c_w = 1kN/m^2, vi) c_s = 1kN/m^2,

vii) w = 0.15m, viii) y_1 = 0.15m, ix) y_2 = 0.45m, x) y_3 = 0.75m, xi) Q = 1.6kN/m,

xii) 1.8kN/m^2, xiii) θ_1 =19.29^0 and xiv) γ_c = 77kN/m^3.

The values of θ, a, b, c, l_{e_1}, l_{e_2} and l_{e_3} are measured from the observed failure surfaces for different experimental studies.

Measured values of the resultant earth pressures are plotted against the predicted values in the figures 6.5 and 6.6 for sand and fly ash backfill respectively. The ideal line having an equation of $p_{measured} = p_{predicted}$ is also plotted. The predicted values are about -36 to 24% and 28% more than the observed values for sand and fly ash backfill respectively.

6.2.2.2 Planar failure surface

Measured values of the overturning moments are plotted against the predicted values in the figures 6.7 and 6.8 for sand and fly ash backfill respectively. The ideal line having an equation of $p_{measured} = p_{predicted}$ is also plotted. The predicted values are about 30% more than the observed values for sand backfill. In case of fly ash backfill the observed value of the overturning moment is satisfactorily predicted by the theory.

6.2.3 Counterfort retaining wall with shelves

Experimental resultant earth pressures are compared with the analytical values for sand and fly ash backfill considering observed planar failure surface.

For the analysis, the required parameters as referred to section 5.4 taken are as follows:

i)H = 0.9m, ii)H_1 = 0.23m, iii)H_2 = 0.33m, iv)H_3 = 0.34m.

For calculating resultant earth pressures for sand backfill, the different parameters used are given below:

i) $\phi = 38^0$, ii) $\gamma = 14.62$ kN/m^2 iii) Q = line load intensity = 1.6kN/m, iv) uniformly distributed surcharge load intensity = $p_0 = 1.8$kN/m^2.

For calculating resultant earth pressures for fly ash backfill, the different parameters used are given below:

i) $\phi = 39^0$, ii) $\gamma = 8.55$ kN/m^2 iii) Q = line load intensity = 1.6kN/m, iv) uniformly distributed surcharge load intensity = $p_0 = 1.8$kN/m^2.

Measured values of the resultant earth pressures are plotted against the predicted values in the figures 6.9 and 6.10 for sand and fly ash backfill respectively. The observed value of the resultant earth pressure is satisfactorily predicted by the theory. The predictions are very close to the line having an equation of $p_{measured} = p_{predicted}$.

6.3 Comparison of analytical results

The value of resultant earth pressures for counterfort retaining wall with shelves are compared with the value of resultant earth pressures for counterfort retaining wall without shelves. From Table 6.1 and 6.2 it is observed that the resultant earth pressure is reduced about 40 to 65 % in case of counterfort retaining wall with shelves than the counterfort retaining wall without shelves for both the backfill material.

Table 6.1

Comparison of resultant earth pressures between counterfort retaining wall with shelves and counterfort retaining wall with shelves for sand backfill

Sl. No.	Type of analysis	Resultant earth pressure(kN/m)		% Variation
		With shelves	Without shelves	
1	Without loading and without reinforcement	0.486	1.42	65.8
2	With line load and without reinforcement	1.03	1.96	47.6
3	With uniform surcharge and without reinforcement	0.5853	1.7544	66.6

Table 6.2

Comparison of resultant earth pressures between counterfort retaining wall with shelves and counterfort retaining wall with shelves for fly ash backfill

Sl. No.	Type of analysis	Resultant earth pressure(kN/m)		% Variation
		With shelves	Without shelves	
1	Without loading and without reinforcement	0.273	0.79	66.2
2	With line load and without reinforcement	0.81	1.33	39.1
3	With uniform surcharge and without reinforcement	0.37	1.21	69.4

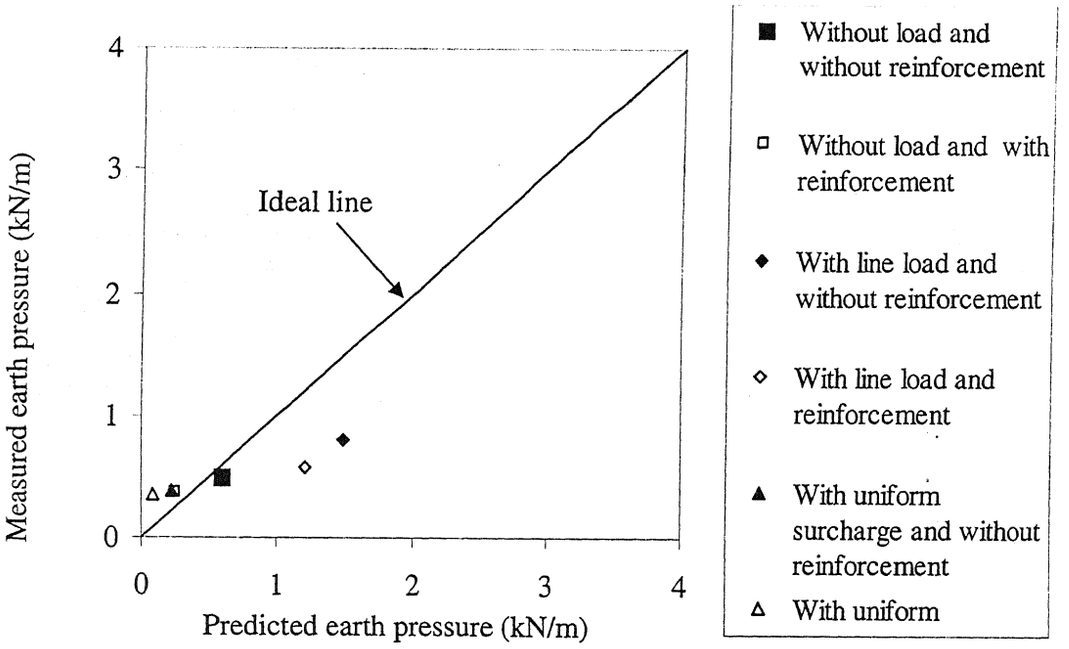

Figure 6.1: Comparison of measured and predicted values of earth pressures (cantilever retaining wall, sand backfill)

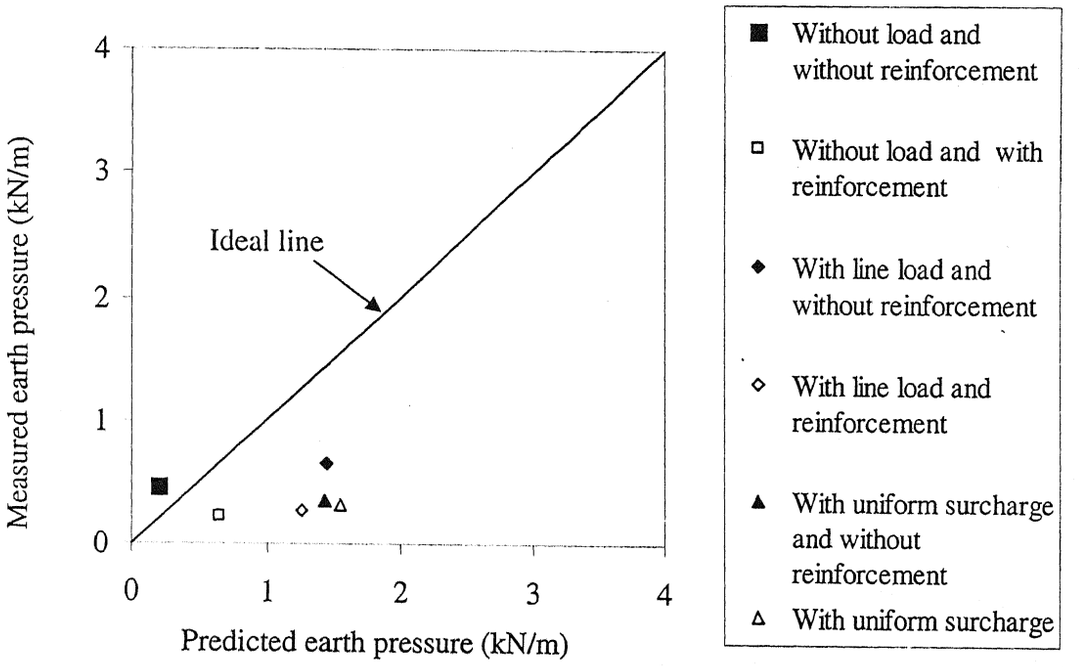

Figure 6.2: Comparison of measured and predicted values of earth pressures (cantilever retaining wall, fly ash backfill)

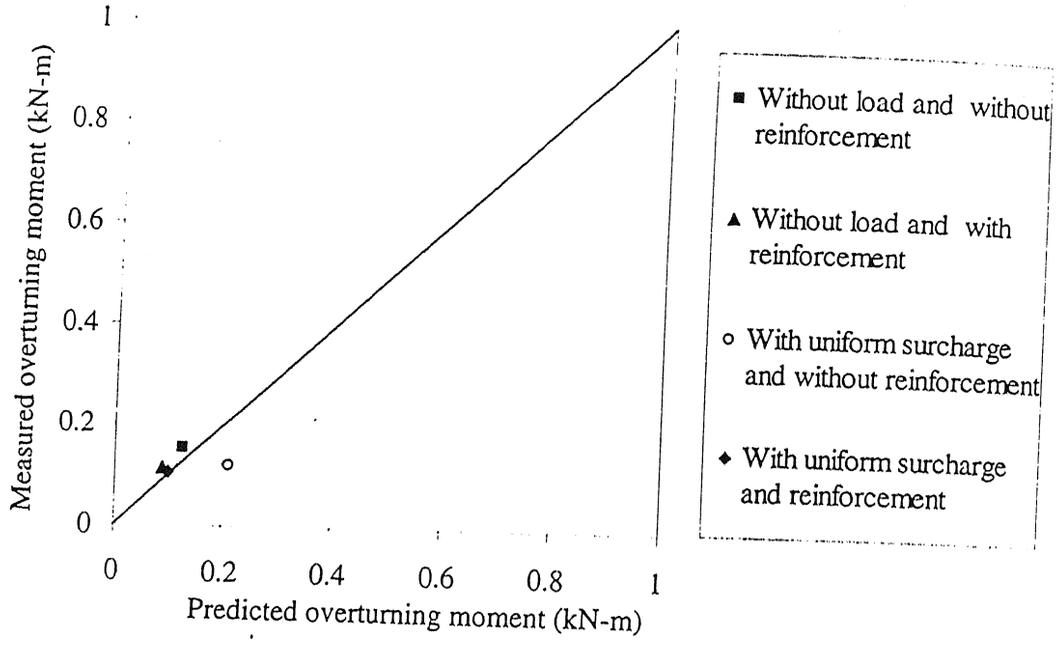

Figure 6.3: Comparison of measured and predicted values of overturning moments (cantilever retaining wall, sand backfill)

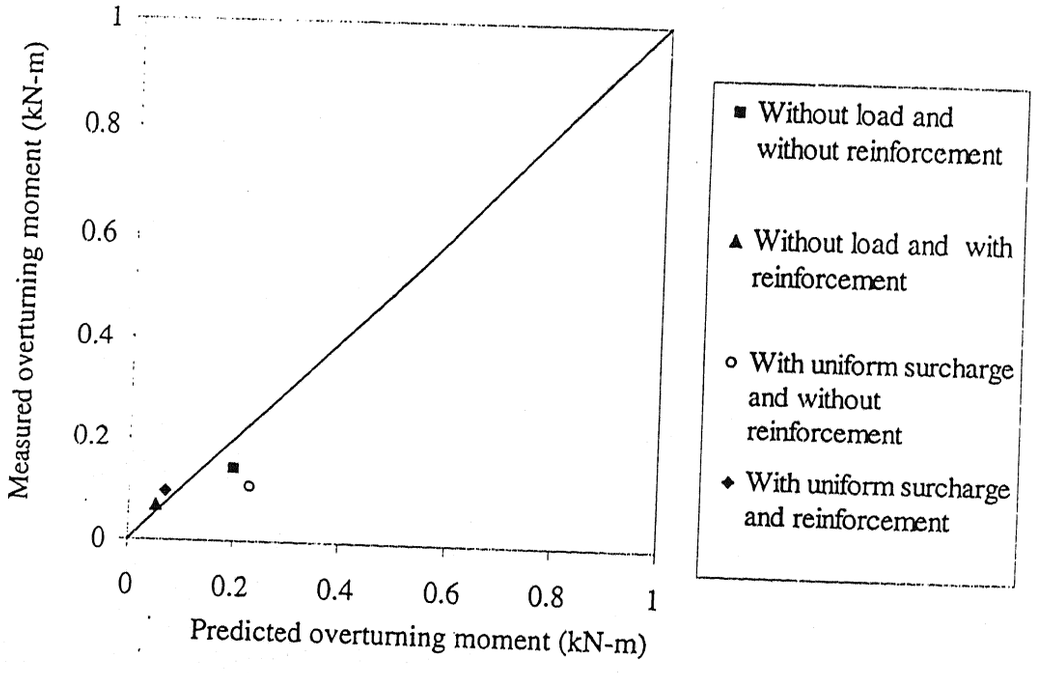

Figure 6.4: Comparison of measured and predicted values of overturning moments (cantilever retaining wall, fly ash backfill)

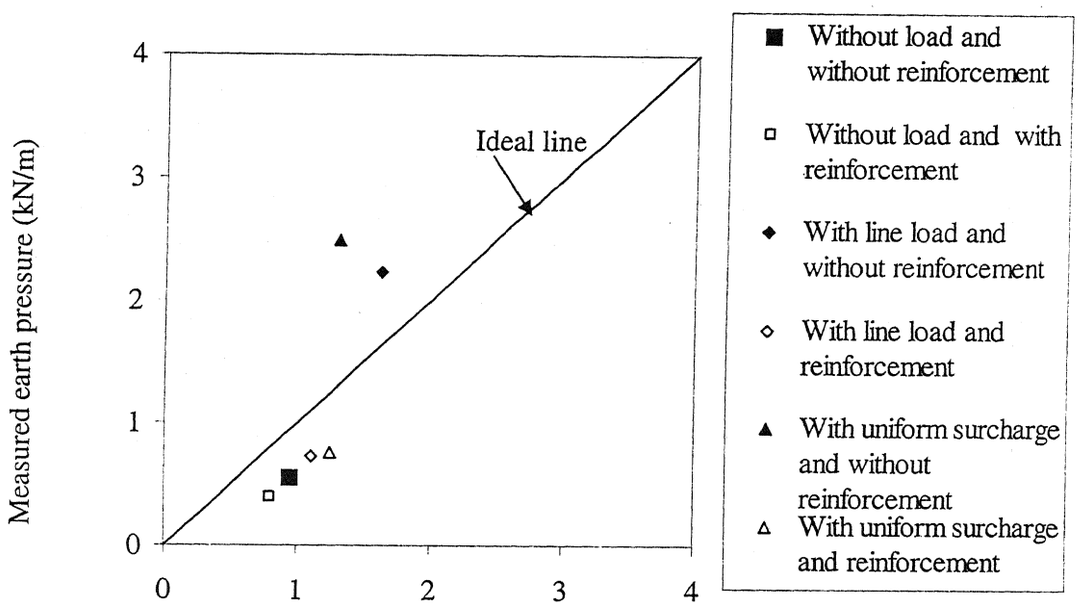

Figure 6.5: Comparison of measured and predicted values of earth pressures (counterfort retaining wall, sand backfill)

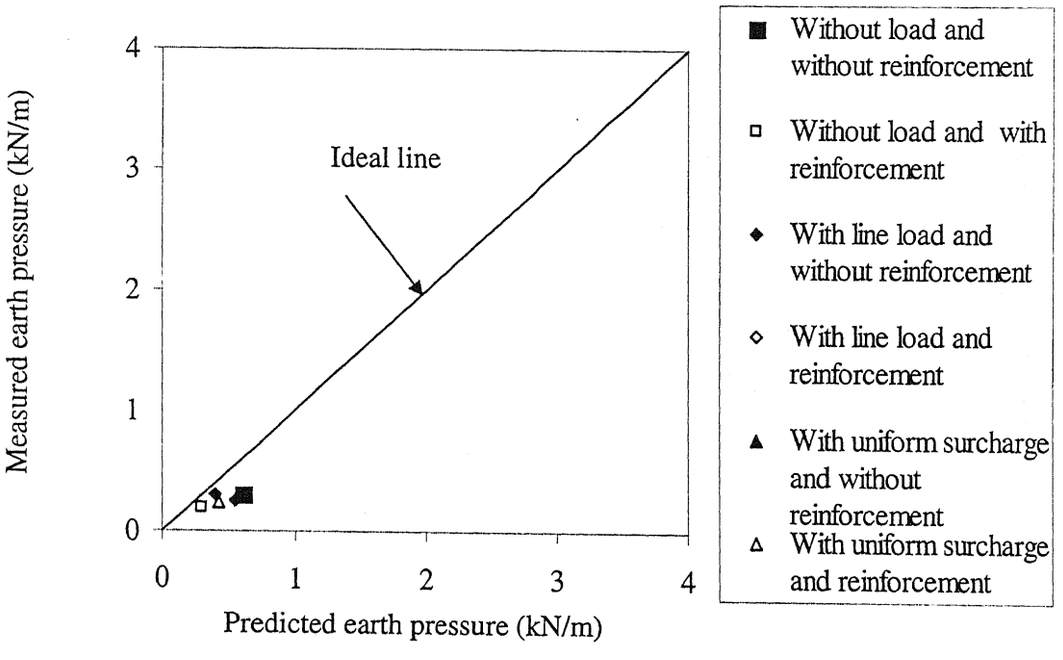

Figure 6.6: Comparison of measured and predicted values of earth pressures (counterfort retaining wall, fly ash backfill)

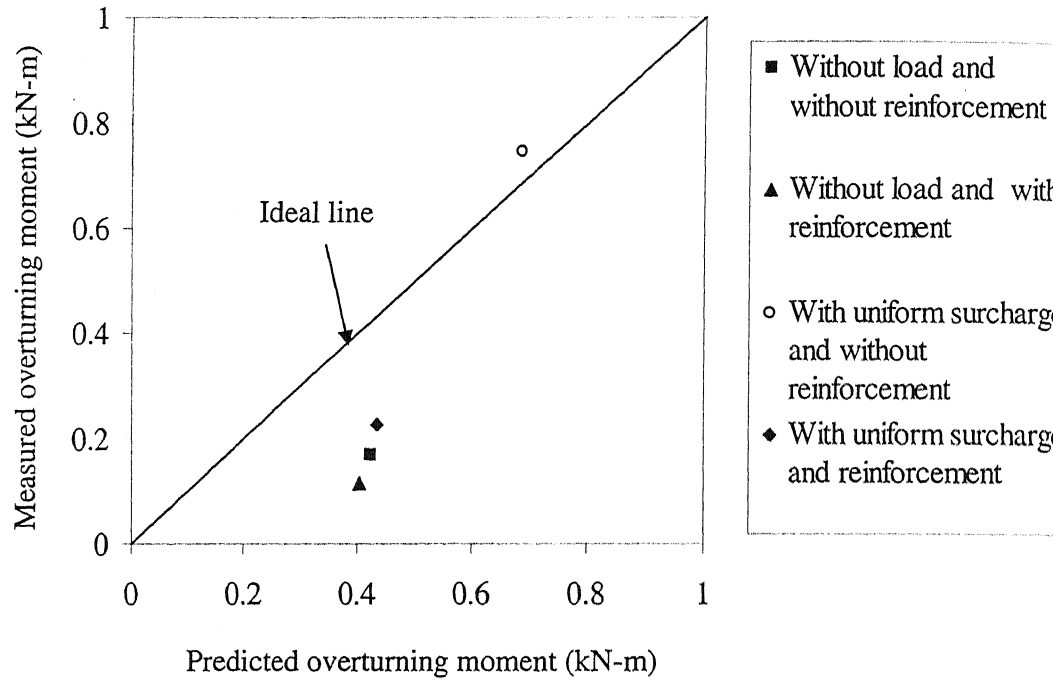

Figure 6.7: Comparison of measured and predicted values of overturning mome
(counterfort retaining wall, sand backfill)

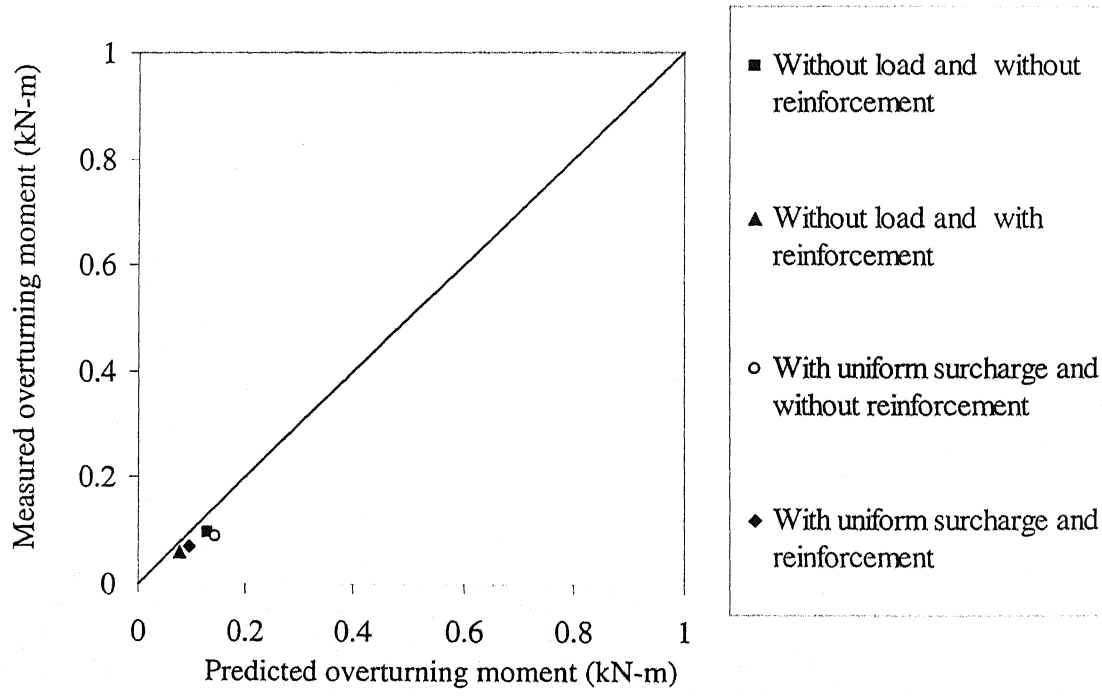

Figure 6.8: Comparison of measured and predicted values of overturning moments
(counterfort retaining wall, fly ash backfill)

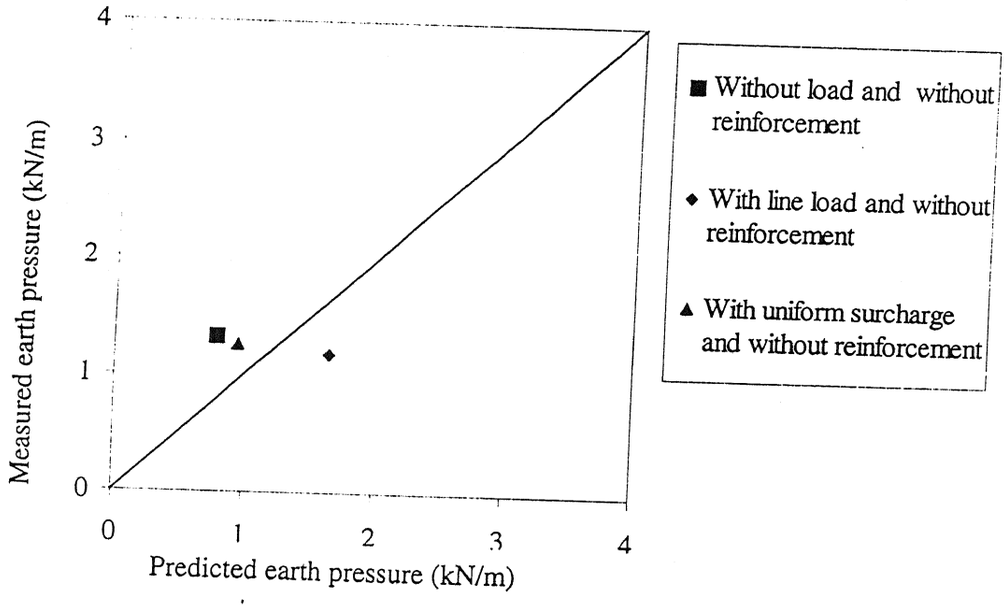

Figure 6.9: Comparison of measured and predicted values of earth pressures (counterfort retaining wall with shelves, sand backfill)

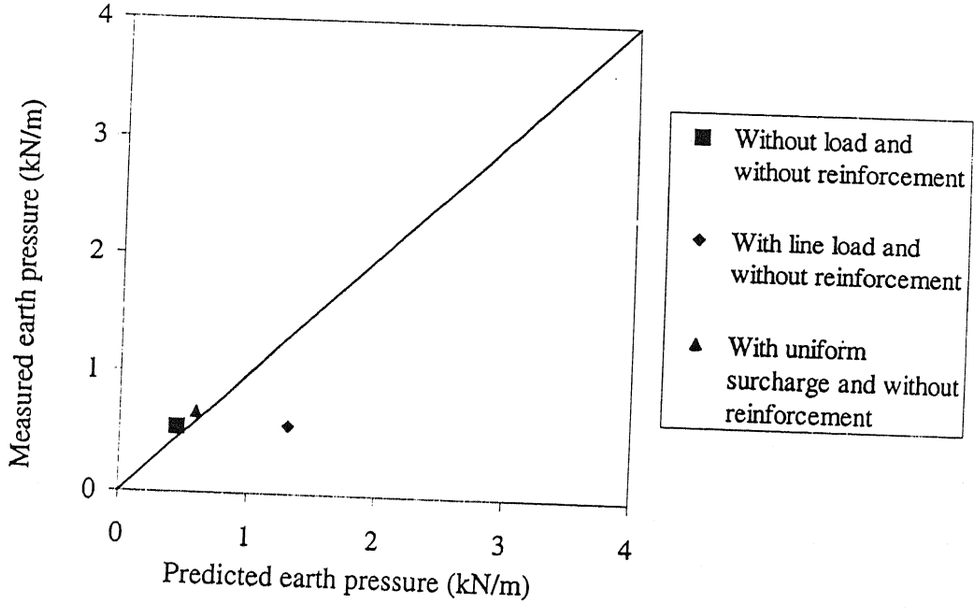

Figure 6.10: Comparison of measured and predicted values of earth pressures (counterfort retaining wall with shelves, fly ash backfill)

CHAPTER VII

Conclusions

7.1 General

Based on the present experimental and analytical study following conclusions are drawn:

7.2 Conclusions from experimental results

Experimental investigations on model cantilever, counterfort and counterfort with shelves retaining walls have been carried out to study the lateral movement of the wall and the nature of the failure modes. Based on the outcome of the experimental study, it can be concluded that the active earth pressure depends upon properties of backfill, type and amount of reinforcement used loading conditions and wedge angle of failure surface. Also with the increase in the lateral movement of the wall, overturning moment decreases and the minimum value of the overturning moment is taken as the limiting value.

The salient conclusions from the experimental results for cantilever, counterfort and counterfort with shelves retaining walls are given below:

7.2.1 Cantilever retaining wall

i. The overturning moments in the reinforced case are about 25% to 41% and 22% to 79% less than the unreinforced case for sand and fly ash backfill respectively. Hence the wall is more stable in case of the reinforced one.

ii. The failure surfaces obtained from experimental investigations are parabolic for all types of loading conditions and both types of the backfill materials.

7.2.2 Counterfort retaining wall

i. The overturning moments in the reinforced case are about 40% to 75% and 27% to 37%less than the unreinforced case for sand and fly ash backfill respectively. Hence, the wall is more stable in case of the reinforced one.

ii. The failure surfaces obtained from experimental investigation are parabolic in case of the retaining wall with fly ash backfill for all types of loading conditions and retaining wall with sand backfill for line load and uniform surcharge. The failure surfaces are linear in case of the retaining wall with sand backfill without any surcharge.

7.2.3 Counterfort retaining wall with shelves

Based on the outcome of the experimental study on the counterfort retaining wall with shelves it can be concluded that there are breakages in the failure surfaces corresponding to the position of the shelves along the height of the retaining wall. So, there are three parallel failure surfaces at 0.33m, 0.67m and 1.0m from the top of the retaining wall. The failure surfaces are linear in nature.

7.3 Conclusions from analytical investigations

Analytical methods, based on observed failure surfaces, have been proposed to predict lateral earth pressures and overturning moments on cantilever and counterfort retaining walls. Generally two types of failure surfaces are considered in the analysis i.e. parabolic and planar. These methods take into considerations the parameters such as loading conditions, ϕ, δ, θ, c, spacing of reinforcement etc. For the analytical method considering planar failure surfaces, the following conclusions can be made:

i. The resultant earth pressure is a function of length of reinforcement and non-dimensional parameter D_P. The resultant pressure decreases as the length of reinforcement and D_p increase.

ii. The resultant earth pressure and resulting overturning moment decrease with increase in the value of $c/\gamma H$ and ϕ.

iii. The resultant earth pressure and resulting overturning moment increase with increase in the value of $q/\gamma H$.

7.4 Conclusions from Comparative Study

7.4.1 Comparison of experimental overturning moments

The overturning moments of fly ash backfill are compared with sand backfill for different types of retaining wall. Based on this study following conclusions can be made:

i. The overturning moments for fly ash backfill are about 5 to 66% less than the sand backfill for cantilever retaining wall. Hence, it may be concluded that the retaining wall with fly ash backfill is more stable than the sand one.

ii. The overturning moments for fly ash backfill are about 55 to 93% less than the sand backfill for counterfort retaining wall.

iii. The overturning moments for fly ash backfill are about 3 to 28% less than the sand backfill for counterfort retaining wall with shelves.

Hence, it may be concluded that the retaining wall with fly ash backfill is more stable than the sand one.

7.4.2 Comparison of experimental and analytical study

Comparison has been made between predicated and observed values of resultant earth pressures and overturning moments for cantilever, counterfort and counterfort with shelves retaining walls.

7.4.2.1 Cantilever retaining wall

i. Observed values of the resultant earth pressure of the present model laboratory tests have been compared with the predictions from the proposed analysis in chapter V. The predicted values are about 41% and 44% more than the observed values for parabolic failure surface for sand and fly ash backfill respectively.

ii. The observed values of overturning moments have been compared with the predictions from the proposed analysis in chapter V. The observed value of the overturning moment is satisfactorily predicted by the theory for planar failure surface.

7.4.2.2 Counterfort retaining wall

i. Observed values of the resultant earth pressure of the present model laboratory tests have been compared with the predictions from the proposed analysis in chapter V. The predicted values are about -36 to 24% and 28% more than the observed values for parabolic failure surface for sand and fly ash backfill respectively.

ii. The observed values of overturning moments have been compared with the predictions from the proposed analysis in chapter V. The predicted values are about 30% more than the observed values for sand backfill. In case of fly ash backfill the observed value of the overturning moment is satisfactorily predicted by the theory for planar failure surface.

7.4.2.3 Counterfort retaining wall with shelves

The observed values of resultant earth pressures are compared with the predicted values. The observed values are satisfactorily predicted by the theory for planar failure surface.

7.4.3 Comparison between analytical investigations

The values of resultant earth pressures for counterfort retaining wall with shelves are compared with the values of resultant earth pressures for counterfort retaining wall without shelves. It is observed that the resultant earth pressure is reduced about 40 to 65% in case of counterfort retaining wall with shelves than the counterfort retaining wall without shelves for both the backfill material. So, by providing relief shelves retaining walls can be made more stable.

SCOPE OF THE FURTHER STUDY

1. The stability analysis of counterfort retaining wall with reinforced backfill carrying uniformly distributed load and line should be verified by prototype experiments which are suitably instrumented to monitor the variation of earth pressure distribution along the height of wall.
2. Experiments on wall with reinforced cohesive-frictional backfill should be performed under dynamic loading conditions. Horizontal and vertical earth pressures and tension in the strips should be measured.
3. Yielding of the wall at the bottom should be considered.

APPENDIX

Analysis of counterfort retaining wall with shelves

(uniform surcharge and unreinforced sand backfill)

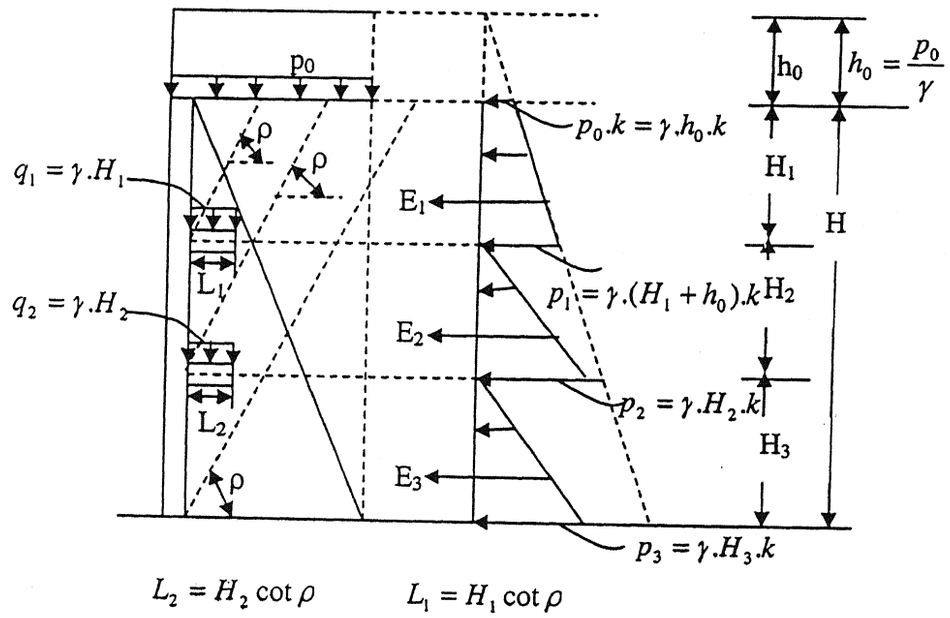

Figure A1: Counterforted wall with relief shelves (uniform surcharge and unreinforced sand backfill)

For the analysis, the required parameters taken are as follows:

i) H = 0.9m, ii) H_1 = 0.23m, iii) H_2 = 0.33m, iv) H_3 = 0.34m., v) $\phi = 38^0$, vi) γ=14.62 kN/m^2, vii) uniformly distributed surcharge load intensity = p_0 = 1.8kN/m^2.

$$k = \frac{1-\sin\phi}{1+\sin\phi} = 0.24.$$

$$h_0 = \frac{p_0}{\gamma} = \frac{1.8}{14.62} = 0.12\text{m}.$$

$p_o.k = 1.8 \times 0.24 = 0.432$

$p_1 = 14.62 \times (0.23+0.12) \times 0.24 = 1.228\ kN/m^2.$

$p_2 = 14.62 \times 0.33 \times 0.24 = 1.16\ kN/m^2.$

$p_3 = 14.62 \times 0.34 \times 0.24 = 1.193\ kN/m^2.$

$E_1 = 1/2 \times (0.432+1.228) \times 0.23 = 0.1909\ kN/m^2.$

Similarly,

$E_2 = 0.1914\ kN/m^2.$

$E_3 = 0.203\ kN/m^2.$

So, Resultant earth pressure = 0.5853 kN/m.

If there is no shelves, then,

Resultant earth pressure = $1/2 \times (0.9+0.12)^2 \times 14.62 \times 0.24$

$= 1.7544$ kN/m.

So, Reduction in the resultant earth pressure due to relief shelves = 66.6 %.

REFERENCES

1. Broms, B.B., (1977). "Polyester Fabrics as Reinforcement in Soils", *Proc. International Conference on the Use of Fabrics in Geotechnics*, Paris, France, Vol. III, pp.129-133.
2. Hausmann, M.R. and Lee, K.L., (1978). "Rigid Model Wall Soil Reinforcement", *Proc. Symposium on Earth Reinforcement, ASCE*, Pittsburgh, pp. 400-427.
3. Garg, K.G., (1988). "Earth Pressure behind Retaining Wall Reinforced Backfill", *Ph.D. Thesis*, University of Roorkee.
4. Garg, K.G., (1998). "Retaining Wall with Reinforced Backfill- A Case Study", *Geotextiles and Geomembranes*, Vol. 16, pp.135-149.
5. Garg, K. G., Chandra, Ramesh, Chand, Prakash and Ahmad, Zamir, (2002). "Performance of Instrumented Walls Retaining Reinforced Earth Fill", *Indian Geotechnical Journal*, Vol. 32, No.4, pp.364-381.
6. Helwany, S.M.B., Reardon, G. and Wu, J.T.H., (1999). "Effects of Backfill on the Performance of GRS Retaining Walls", *Geotextiles and Geomembranes*, Vol.17, pp.1-16.
7. Ho, S.K. and Rowe, R. Kerry, (1996). "Effect of Wall Geometry on the Behaviour of Reinforced Soil Walls", *Geotextiles and Geomembranes*, Vol.14, pp.521-541.
8. Jumikis, R.A., (1964). "Mechanics of Soils: Fundamentals for Advanced Study", *D. Van Nostrand Company*, INC, Princeton, New jersey.
9. Juran, I. and Christopher, B., (1992). "Laboratory Model Study on Geosynthetic Reinforced Soil retaining Walls", *Journal of Geotechnical Engineering, ASCE*, Vol.115, No. 7, pp.905-926.

10. Karpurapu, R., and Bathrust, R.J., (1992). "Numerical Investigation of Controlled Yielding of Soil-Retaining Wall Structures", *Geotextiles and Geomembranes*, Vol.11, pp.115-131.

11. Khan, I.N., (1991). "A study of Reinforced Earth Wall and Retaining Wall with Reinforced Backfil", *Ph.D. thesis*, University of Roorkee.

12. Ling, H.I., Cardany, C.P., Sun, L-X. and Hashimoto, H., (2000). "Finite Element Study of a Geosynthetic-Reinforced Soil Retaining Wall with Concrete-Block Facing", *Geosynthetics International*, Vol.7, No. 3, pp.163-188.

13. Mittal, Satyendra, Garg, K. G., Saran, Swami and Pathak, A.N., (2001). "Rigid Wall Retaining Bottom Ash Backfill with Geogrid Reinforcement", *Indian Geotechnical Journal*, Vol.31, No.1, pp. 89-102.

14. Palmeira, E.M. and Lanz, Daniela, (1994). "Stresses and Deformations in Geotextile Reinforced Model Walls", *Geotextiles and Geomembranes*, Vol.13, pp.331-348.

15. Patra, N. R., and Pise, P. J., (2001). "Ultimate Lateral Resistance of Pile Groups in Sand", *Journal of Geotechnical and Geoenvironmental Engineering*, Vol.127, No.6, pp.481–487.

16. Pinto, M.I.M. and Cousens, T.W., (1996). "Geotextile Reinforced Brick Faced Retaining Walls", *Geotextiles and Geomembranes*, Vol.14, No.9, pp.449-464.

17. Pinto, M.I.M. and Cousens, T.W., (2000). "Effect of the Foundation Quality on a Geotextile-Reinforced, Brick-Faced Soil Retaining Wall", *Geosynthetics International*, Vol.7, No. 3, pp.217-242.

18. Porbaha, A., (1996). "Geotextile Reinforced Lime Treated Cohesive Soil Retaining Wall", *Geosynthetics International*, Vol.3, No. 3, pp.393-405.

19. Saran, S., Garg, K.G. and Bhandari, R. K., (1992). "Retaining Wall with Reinforced Cohesionless Backfill", *Journal of Geotechnical. Engineering, ASCE,* Vol. 118, No.12, pp.1869-1888.

20. Sawicki, A., (1999). "Creep of Geosynthetic Reinforced Soil Retaining Walls", Geotextiles and Geomembranes, Vol. 17, pp.51-65.

21. Singh, D.N. and Basudhar, P.K., (1993). "Determination of the Optimal Lower-Bound-Bearing Capacity of Reinforced Soil-Retaining Walls by Using Finite Elements and Non-Linear Programming", *Geotextiles and Geomembranes,* Vol. 12, pp.665-686.

22. Talwar, D.V., (1981). Behaviour of Reinforced Earth in Retaining Structures and Shallow Foundations, Ph.D. Thesis, Department of Civil Engineering, University of Roorkee, Roorkee, India.

23. Tsukamoto, Y., Ishihara, K., Higuchi, T. and Aoki, H, (1999). "Influence of Geogrid Reinforcement on Lateral Earth Pressures against Model Retaining Walls", *Geosynthetics International*, Vol.6, No. 3, pp.195-218.

24. Vidal, H., (1969). "The principle of Reinforced Earth", *Highway Research Record* No. 282, USA.

25. Wong, K.S. and Broms, B.B., (1994). "Failure Modes at Model Tests of a Geotextile Reinforced Wall", *Geotextiles and Geomembranes*, Vol. 13, pp.475-493.